3 cys.

Gulf General Atomic
Incorporated

AEC RESEARCH AND
DEVELOPMENT REPORT

GA-6233

ADVANCED, GRAPHITE-MATRIX, DISPERSION-TYPE FUEL SYSTEMS AND RESEARCH ON GRAPHITE

ANNUAL REPORT

APRIL 1, 1964, THROUGH MARCH 31, 1965

Prepared under
Contract AT(04-3)-167
Project Agreement 12, Tasks I and II
for the
San Francisco Operations Office
U.S. Atomic Energy Commission

July 20, 1965

DISCLAIMER

GENERAL ATOMIC

DIVISION OF

GENERAL DYNAMICS

JOHN JAY HOPKINS LABORATORY FOR PURE AND APPLIED SCIENCE

P.O. BOX 608, SAN DIEGO, CALIFORNIA 92112

AEC RESEARCH AND DEVELOPMENT REPORT

GA-6233

ADVANCED, GRAPHITE-MATRIX, DISPERSION-TYPE FUEL SYSTEMS AND RESEARCH ON GRAPHITE

ANNUAL REPORT

APRIL 1, 1964, THROUGH MARCH 31, 1965

Prepared under
Contract AT(04-3)-167
Project Agreement 12, Tasks I and II
for the
San Francisco Operations Office
U.S. Atomic Energy Commission

Written by

J. C. Bokros, W. V. Goeddel, H. K. Lonsdale, R. J. Price,
G. R. Tully, Jr., J. L. White, L. R. Zumwalt

July 20, 1965

PREVIOUS REPORTS IN THIS SERIES

GA-5606—June, July, August, 1964
GA-5918—September, October, November, 1964
GA-6181—December, 1964; January, February, 1965

CONTENTS

I. INTRODUCTION

The purpose of the present program is to realize substantial improvements in the materials required for use in high-temperature, gas-cooled reactors of advanced design. The approach is based on gaining a more complete understanding of the properties and behavior of such materials in order to provide effective guidance for the development of improved materials. Two principal lines of effort have been pursued: Task I, "Advanced Graphite-Matrix Fuel Systems," is concerned with the various materials directly involved in the fuel systems of high-temperature reactors; Task II, "Research on Graphite," is concerned with the graphitic materials employed either in the fuel systems or in other structural components of such reactors. Because of the close relationship between the items of work in Task I and Task II of this program, the reports of progress have been combined into a single report.

In the period covered by the present report, April 1, 1964, through March 31, 1965, investigations have been conducted in the following areas:

1. Studies of Pyrolytic-carbon Coatings Deposited in Fluidized Beds. The structures of pyrolytic carbons deposited in a fluidized bed are being characterized in order to establish the relationships existing between bed deposition conditions, coating structure, and the physical and mechanical properties relevant to reactor performance. The earlier studies are being extended to deposition temperatures greater than 1900°C. The property studies include measurements of the effects of annealing and irradiation on pyrolytic carbons.

2. Diffusion of Thorium and Uranium in Pyrolytic Carbon. The rates of diffusion of thorium and uranium in pyrolytic carbons typical of those employed in graphite-matrix fuel systems are being determined. Particular emphasis is being given to determining the effect of coating structure on diffusion.

3. Fission-product Release from Carbide Fuel Systems. The release of fission products through pyrolytic-carbon coatings typical of those employed in graphite-matrix fuel systems is being determined in an effort to relate release rates to coating structure.

4. Characterization of Microstructure of Graphitic Materials. Methods of characterizing the degree of graphitization of carbons and graphitic materials are being investigated.

5. Relation of Physical Properties of Graphitic Materials to Microstructure. The relationship of certain physical properties, including Young's modulus and the dimensional changes under irradiation, to the preferred orientation of various graphitic materials is being studied.

6. Chemical and Metallurgical Processes for Modifying the Microstructure of Graphite. The process of hot-working graphitic materials is being investigated, with current emphasis on evaluating the variables of pitch content and additives in the graphite bodies.

II. SUMMARY

STUDIES OF PYROLYTIC-CARBON COATINGS DEPOSITED IN FLUIDIZED BEDS

Systematic investigations of the effect of deposition temperature, bed surface area, and methane concentration on the structure of carbons deposited in fluidized beds have shown that a wide variety of structures is possible. It was found that all the structures deposited could be divided into three broad groups according to whether their microstructures are laminar, isotropic, or granular. Each of the structures was characterized further by measuring its density, crystallite size, and degree of preferred orientation. The variation of structure with deposition conditions has been interpreted using current knowledge of carbon formation in the pyrolysis of gaseous hydrocarbons.

The structures of representative laminar, isotropic, and granular carbons were studied in more detail using diffuse X-ray scattering techniques. It was found that significant quantities of amorphous carbon can be present in carbons deposited at 1400°C and that the amount present increases with deposition rate. The concentration of misaligned single layers in the 1400°C deposits varied from 23% in low-density laminar carbon deposited from 5% methane to less than 2% in high-density laminar carbon deposited from 40% methane. Carbons deposited at 1650°C and above had no detectable (<1%) amorphous carbon in their structure. A low-density carbon deposited at a very high rate at 1650°C was found to contain 10% misaligned single layers as compared with 1% and 2% in carbons deposited at 2000° and 1900°C, respectively. A model of carbon formation consistent with the variations of structure with deposition conditions is presented in this report.

Absorption factors for a modified Bacon preferred-orientation technique used in structural studies of carbon films have been calculated for specimen sizes and densities encountered in practice.

The mechanical properties of the carbon structures encountered in the studies described above have been measured in bending tests. These studies have shown that the carbons deposited below about 1450°C have high elastic moduli, high fracture stresses, and low fracture strains. The isotropic carbons deposited above 1450°C have low elastic moduli, low fracture stresses, and relatively high fracture strains (~2%). A coarse-grained granular deposit was the weakest tested. Fracture appeared to be initiated in this carbon by separation of the layers within individual grains.

The carbons deposited below 1450°C were found to respond to annealing treatments in different ways. Annealing caused substantial structural and mechanical-property changes in the carbons deposited from high methane concentrations, but had little effect on the low-density carbons deposited from low methane concentrations. Annealing of isotropic carbons deposited above 1450°C caused only small structural and property changes.

Thermal-diffusivity measurements on representative carbon structures showed that carbons deposited at 1400°C have a thermal conductivity an order of magnitude lower than that of isotropic or granular carbons deposited at higher temperatures. Annealing for 96 hr at 1500°C caused substantial improvement (+100%) in the thermal diffusivity of carbons deposited from 40% methane but had only a small effect on the carbons deposited from 5% methane. These changes are discussed in terms of the structural changes that occurred due to the anneal.

Seven representative carbon structures are presently being exposed to a fast-neutron flux in the General Electric Test Reactor (GETR) at temperatures in the range 670° to 1075°C. After irradiation, the dimensional, structural, and property changes will be measured and compared with control specimens.

A study relating uranium migration in pyrolytic carbon to structure showed that high-density, oriented, laminar carbon deposited at low temperature from high methane concentrations was superior to isotropic and granular carbon in resisting uranium migration.

The structure and properties of pyrolytic carbon deposited in a fluidized bed between 1900° and 2400°C from a carrier gas containing between 1% and 15% methane have been studied. The carbons have either granular, isotropic, or transition microstructures. Granular microstructures are favored by high temperatures, low methane partial pressures, and low bed surface areas. For a given methane pressure, the density, apparent crystallite size, and degree of orientation of the granular carbons increase with increasing deposition temperature. The elastic moduli and fracture stresses of the granular carbons are in the ranges 1.5 to 1.8×10^6 psi and 15 to 35×10^3 psi, respectively. There is a trend toward higher elastic modulus and fracture stress parallel to the deposition plane with increasing deposition temperature, i.e., increasing anisotropy. The isotropic and "transition" carbons have elastic moduli of 1.5 to 2.2×10^6 psi and fracture stresses of about 30×10^3 psi. The modulus decreases with increasing deposition temperature, while the fracture stress remains approximately constant. The carbons have thermal conductivities perpendicular to the deposition plane lying in the range 1 to 4×10^2 cal/cm-sec-°C. The conductivities are highest for the isotropic carbons and lowest for the most highly oriented granular carbons.

DIFFUSION OF THORIUM IN PYROLYTIC CARBON

Tracer-level diffusion studies have been carried out in laboratory-prepared samples of pyrolytic carbons of widely divergent microstructure. These samples are well characterized and contain no exposed layer-plane edges. Using Th^{228} tracer, diffusion coefficients have been measured perpendicular to the plane of deposition, over the temperature range 1600° to 2000°C. The diffusion coefficients were found to have a significant dependence on microstructure, with the diffusion coefficient in the highly oriented, laminar pyrolytic carbon about an order of magnitude smaller than that in either the isotropic or granular carbons, both of which gave approximately the same results. The activation energy for tracer-level diffusion of thorium perpendicular to the plane of deposition in granular pyrolytic carbon was determined to be 152 kcal/mole.

FISSION-PRODUCT RELEASE FROM CARBIDE FUEL SYSTEMS

By means of a small graphite disk impregnated with U^{235} and coated with pyrolytic carbon, a diffusion coefficient of 1.0×10^{-9} cm^2/sec has been obtained for barium in granular-type pyrolytic carbon at 1400°C. This is in excellent agreement with earlier results obtained for the diffusion of Ba^{140} perpendicular to the layer planes in a large slab of pyrolytic carbon.

The steady-state release of short-lived fission gases between 1100° and 1700°C from high-density ThC_2 (150 to 250 μ) indicates that the release mechanism is similar to that of monogranular UC_2 (179 to 210 μ). The inclusion of about 5% UC_2 in the high-density ThC_2 improves the fission-gas retention by a factor of 2 to 10.

CHARACTERIZATION OF MICROSTRUCTURE OF GRAPHITIC MATERIALS

Methods for measuring the degree of graphitization of graphite materials are being developed for the purpose of following structural changes taking place in carbonaceous materials during heat treatment and in graphite materials during irradiation. A chemical method, in which the kinetics of oxidation by a hot dichromic acid solution are measured manometrically, has been set up and tested.

Electron replication micrography has been employed to study the five structures existing in graphitic materials. A cathodic etching device has been set up and used in this work. The micrographs have been used to study the differences in structure between a fuel-matrix graphite, a graphite

matrix hot-worked with a dispersed liquid-carbide phase, and graphitized pitch binder.

RELATION OF PHYSICAL PROPERTIES OF GRAPHITIC MATERIALS TO MICROSTRUCTURE

Equations have been derived which express physical properties such as the thermal expansion, radiation-induced length changes, and Young's modulus of polycrystalline graphite and carbon in terms of the single-crystal properties and functions of the preferred orientation. In the case of Young's modulus, the expressions are based on the assumption of either constant stress or constant strain through the aggregate. The expressions were tested by making measurements of static Young's modulus and preferred orientation on several kinds of pyrolytic carbon covering a wide range of anisotropies. It was found that the "constant stress" model fitted the observations well. In order to test the model for irradiation-induced length changes, samples cut from the wall of an extruded graphite tube where the radial, tangential, and longitudinal directions have different degrees of preferred orientation are being irradiated at temperatures between 650° and 1050°C. The length changes in the three directions will be measured and compared with the model. Experiments have been initiated to determine the role of binder and filler type and content on the structure and irradiation stability of polycrystalline graphite bodies.

CHEMICAL AND METALLURGICAL PROCESSES FOR MODIFYING THE MICROSTRUCTURE OF GRAPHITE

Investigations of processes aimed at improving the structure of graphites have been restricted to two aspects of the hot-working process: investigations of pitch content as a hot-working variable, and exploratory studies of the effects of various additives on hot-working behavior and on the properties of hot-worked graphitic materials. Relatively high pitch contents in the starting material have been found to lead to improved properties in the hot-worked graphite; the hot-working behavior is not sensitive to pitch content. These higher pitch contents have also been found favorable with respect to the properties of a hot-worked graphite matrix containing solid carbide particles.

Investigations of the hot-working of a graphite matrix containing a liquid-carbide phase have resulted in the development of unique graphite-carbide materials with significant improvements in the properties. During hot-working, the liquid carbide is progressively squeezed from the body, leaving a densified matrix containing a fine dispersion of carbide particles. The principal efforts have been placed on bodies containing either molybdenum

or zirconium carbide. This hot-working process has been applied successfully to extruded as well as hot-pressed starting materials.

The materials hot-worked with a liquid-carbide phase possess properties which approach those of pyrolytic carbons and graphites. The strong preferred orientations are reflected in the directional physical properties. Compressive strengths in excess of 30, 000 psi and moduli of rupture in excess of 15, 000 psi are observed for the favorable test orientations. The helium permeabilities are less than 10^{-6} cm^2/sec for only modest levels of hot-working. The materials show excellent thermal conductivity, and the thermal expansion can be varied within wide limits by controlling the hot-working strain and the carbide content.

III. STUDIES OF PYROLYTIC-CARBON COATINGS DEPOSITED IN FLUIDIZED BEDS

J. C. Bokros, R. J. Price, J. Chin, W. E. Ellis
K. Koyama, J. O. Gardner

STUDIES OF COATINGS DEPOSITED AT TEMPERATURES BELOW 1900°C

Effect of Coating Variables on the Structure of Pyrolytic Carbons

A survey of the structures of pyrolytic carbons deposited from methane in the temperature range 1350° to 1925°C has been completed, and the results have been presented in a topical report entitled "The Structures of Pyrolytic Carbons Deposited in a Fluidized Bed" by J. C. Bokros.[1]* Figure 1 summarizes the dependence of the various structural parameters of carbons deposited in a 2.5-cm-diameter coater on deposition conditions.

In work subsequent to this survey, it has been found that fractographs of pyrolytic carbon can reveal structural features not revealed by microscopy of polished surfaces or by X-ray scattering. Figure 2 shows a fractograph of a high-density, laminar carbon deposited at 1400°C in a 2.5-cm-diameter coater using 40% methane in helium. The initial charge area was 400 cm^2 and the total flow was 2750 cm^3/min. The fractograph shows that the dispersion in the pole figure of this structure is due to undulations in which appears to be a continuous layer structure, rather than to a dispersion of the c-axes of distinct "grain" or "growth cones" (see Fig. 3). This is consistent with the supposition that laminar structures such as that shown in Fig. 2 are built up from planar complexes that form in the gas phase, condense directly on the bed surface, and become aligned with it. It is thought that for large bed surface areas, only occasional gas-phase condensation to droplets occurs. Decreasing the surface area or increasing the contact time (decreasing the total flow rate) is thought to increase the frequency of gas-phase condensation to droplets. The incorporation of a high concentration of these droplets into the deposit decreases the degree of preferred orientation and the density. Figure 4 shows a fractograph of a carbon deposited using the same conditions as those given in Fig. 2 except that the total flow rate was reduced by 45% (i.e., the contact time was increased) and the initial bed surface area was reduced by ~50%. These changes in deposition conditions reduced the Bacon anisotropy factor

*References are listed at the end of each section.

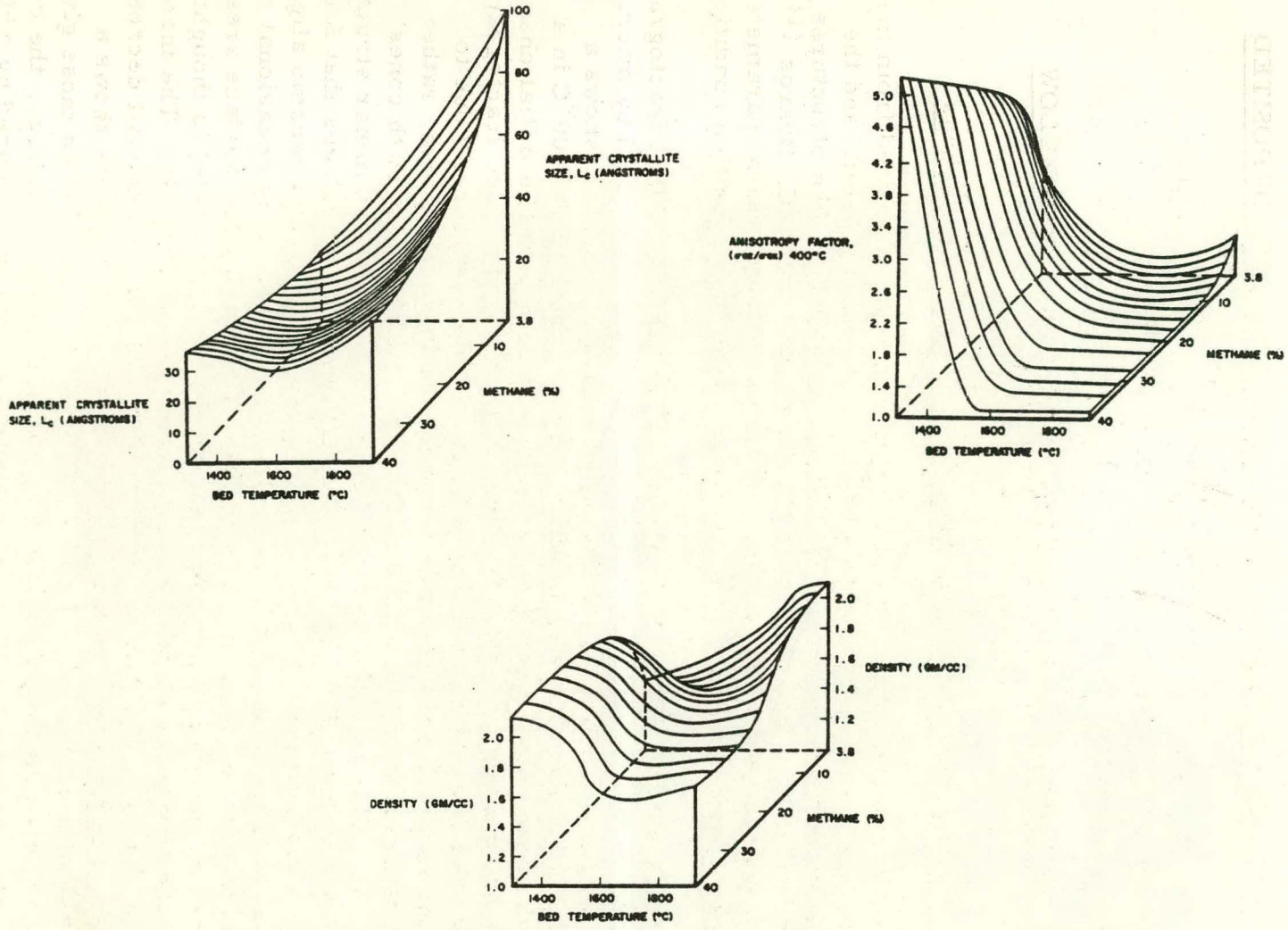

Fig. 1--Dependence of density, anisotropy, and crystallite size on the deposition conditions in the fluidized bed process.

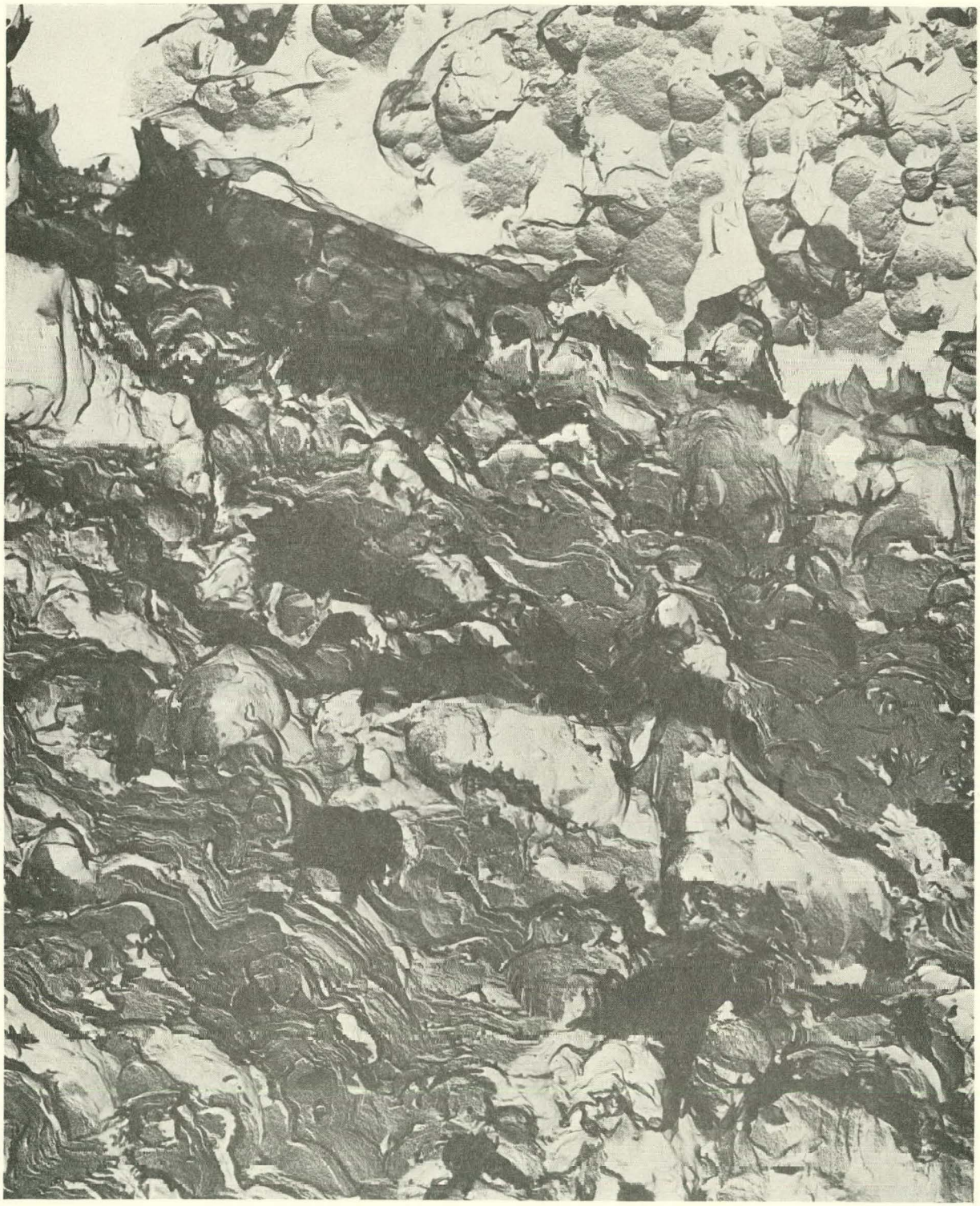

P-5321 (17,000×)

Fig. 2--Fractograph of a high-density, oriented, laminar carbon deposited from 40% methane at 1400°C in a 2.5-cm-diameter coater. The initial bed surface area was 400 cm^2 and the total flow (at 23°C and 1 atm) was 2750 cm^3/min.

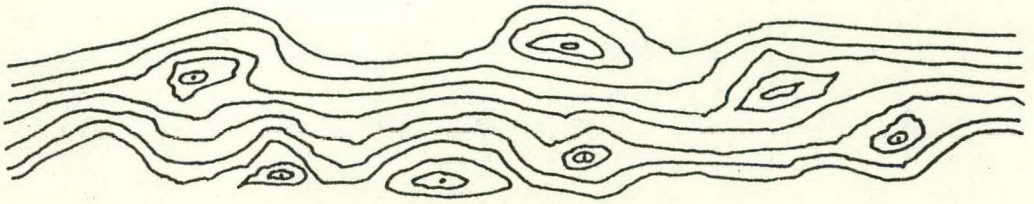

(a)

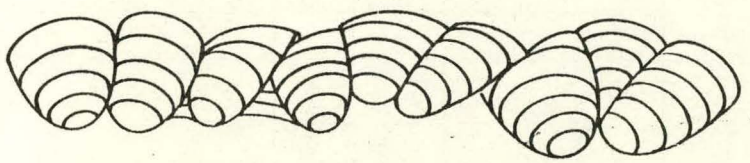

(b)

Fig. 3--Schematic diagrams contrasting an undulating layer structure with a structure made up of distinct grains or growth cones: (a) an undulating layer structure with gas-phase-nucleated particles incorporated in the deposits; (b) a structure made of "grains" or "growth cones."

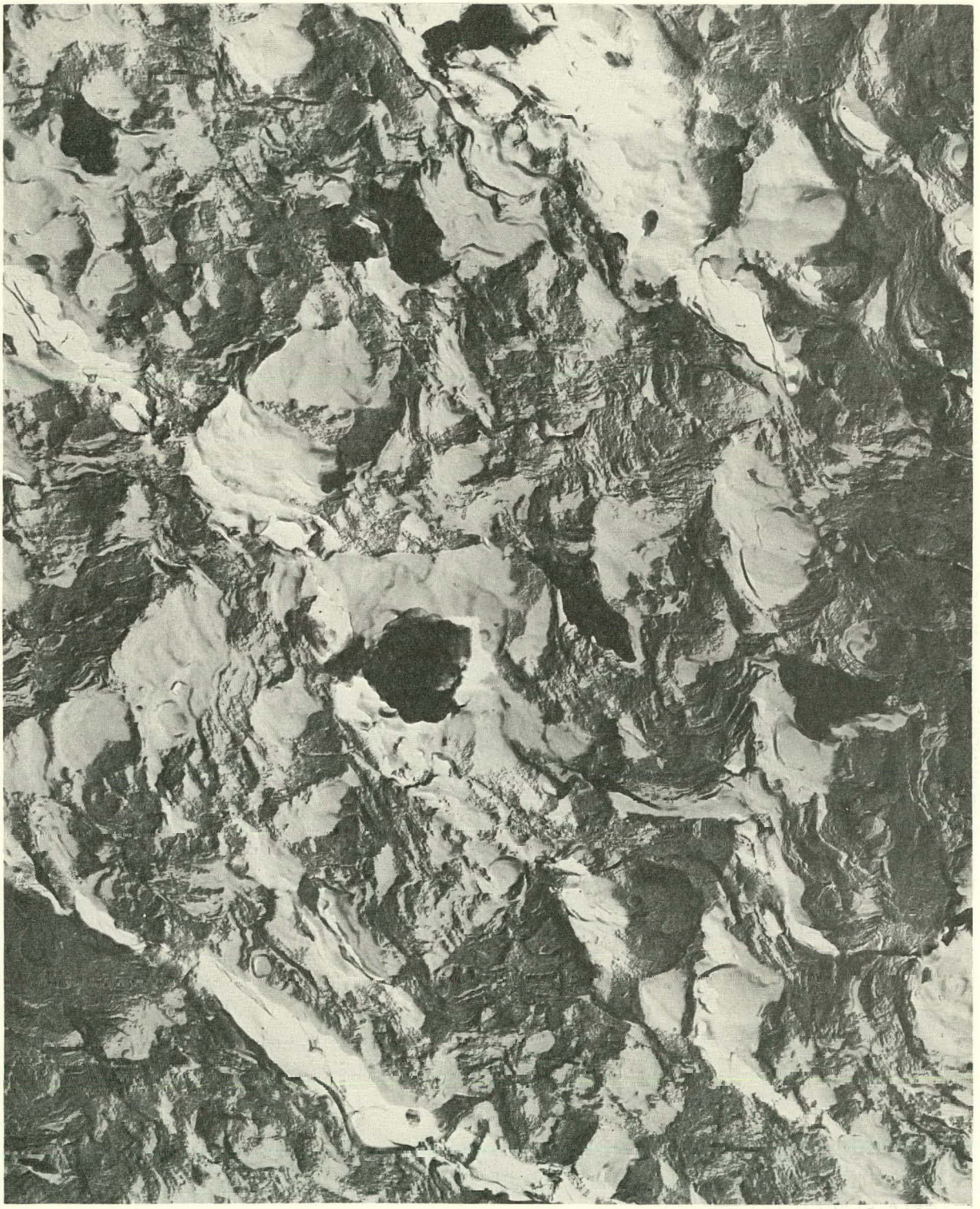

P-5664 (17,000×)

Fig. 4--Fractograph of a carbon deposited from 40% methane at 1400°C in a 2.5-cm-diameter coater. The initial bed surface area was 210 cm^2 and the total flow (at 23°C and 1 atm) was 1500 cm^3/min.

from 3.5 to near 1.0. The fractograph reflects the more isotropic texture of this deposit and reveals a higher concentration of features which might be gas-phase-nucleated particles that were incorporated into the deposit.

Decreasing the methane concentration at 1400°C from 40% to 5%, while keeping all the other coating parameters the same as those used to deposit the carbon shown in Fig. 2, reduced the degree of preferred orientation, the apparent crystallite size, and the density of the carbon deposited in spite of the concomitant decrease in deposition rate. A fractograph of the carbon deposited from 5% methane is shown in Fig. 5 and reveals a structure finer than that shown in Fig. 2. or 4 and a more poorly defined layered structure. Decreasing the methane concentration at 1400°C is thought to decrease the size of the planar complexes at the instant of deposition because of the reduced polymerization rate at lower methane partial pressures. The smaller complexes cannot align themselves with the deposition surface or with one another as well as the larger ones formed at higher methane concentrations. As a result, the deposits are less dense, less anisotropic, have smaller apparent crystallite sizes, and are more difficult to graphitize.

X-ray scattering data for carbon deposits made at 1400°C support the ideas expressed above. Using the approach described by Franklin,[2] the weight fractions of these deposits which are in the form of amorphous carbon, single unassociated layers, and associated layers have been measured. The results show that the carbons deposited from 5% methane (i.e., involving small planar complexes) contain 23% single unassociated layers and no amorphous carbon. On the other hand, the carbon deposited from 40% methane (i.e., involving larger planar complexes) contains only 1.7% single unassociated layers. The apparent crystallite size of the deposit from 40% methane was 43 Å as compared with 27 Å for the carbon deposited from 5% methane. Some of the X-ray scattering data are reported in Table 1.

Two topical reports entitled "Absorption Factors for a Modified Bacon Preferred Orientation Technique"[3] and "Variations in the Crystallinity of Carbons Deposited in Fluidized Beds"[4] by J. C. Bokros have been issued.

Mechanical Properties of Pyrolytic Carbons

The mechanical properties of pyrolytic-carbon coatings are important in determining the service behavior of coated-particle fuels. The present investigation is aimed at relating the mechanical properties of coatings to their structures, which in turn depend on the coating conditions and subsequent heat treatment.

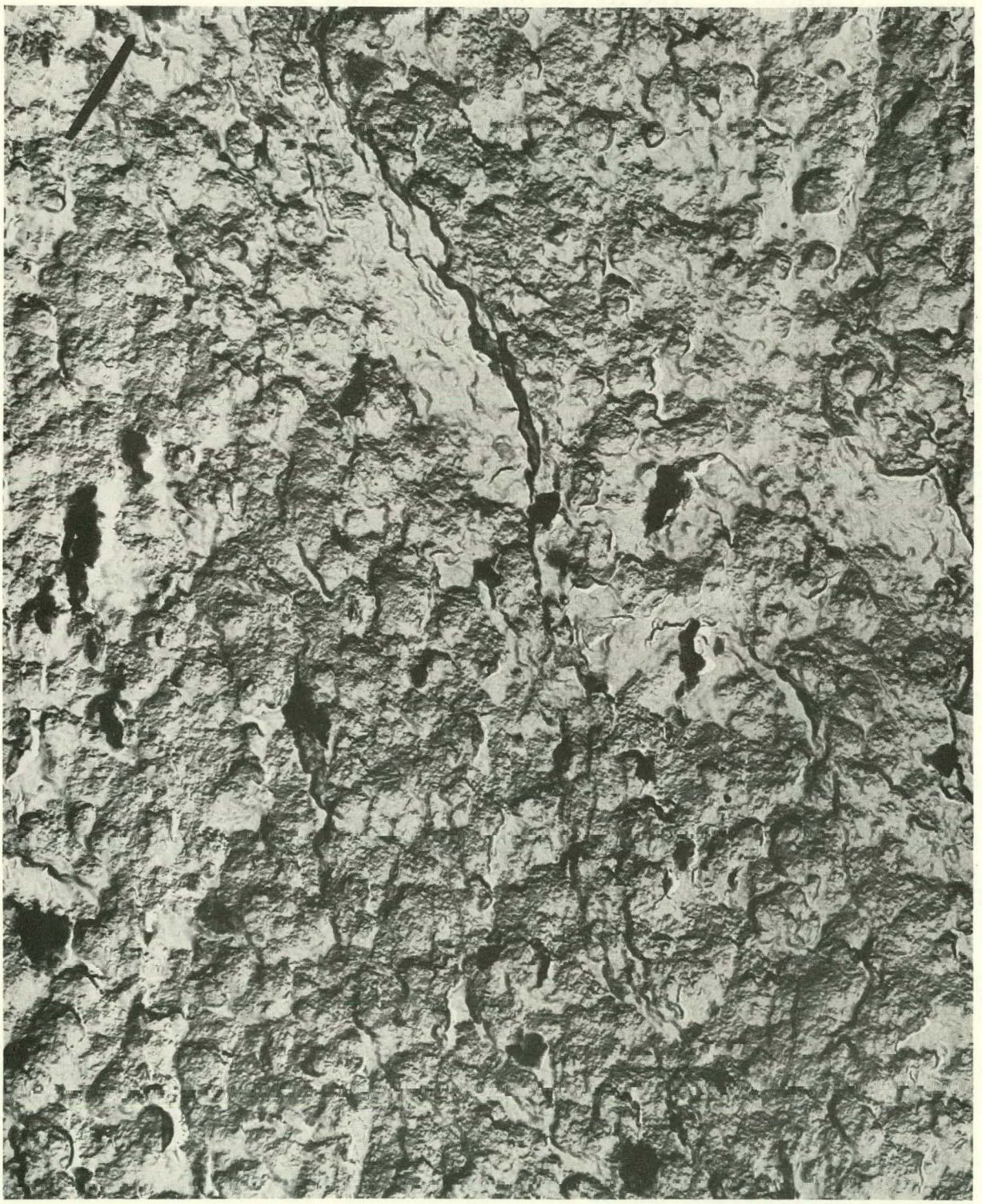

P-5452 (17,000×)

Fig. 5--Fractograph of a carbon deposited from 5% methane at 1400°C in a 2.5-cm-diameter coater. The initial bed surface area was 400 cm^2 and the total flow (at 23°C and 1 atm) was 2400 cm^3/min.

Table 1

STRUCTURAL DATA FOR CARBON DEPOSITS MADE FROM METHANE AT 1400°C IN A 2.5-CM-DIAMETER COATER

Methane Concentration (%)	Total Flow Rate (cm^3/min)	Initial Bed Surface Area (cm^2)	Density (g/cm^3)	Bacon Anisotropy Factor	L_c (Å)	Single Layers (%)	Amorphous Carbon (%)
5	2400	400	1.51	1.9	27	23	<1
28	2780	400	1.94	1.7	35	10	1
40	2750	400	2.11	3.5	43	2	3
40	1500	210	1.94	1.1	32	7	4

Mechanical properties were measured by performing three-point bend tests on planar samples approximately 0.250 in. by 0.040 in. by 0.004 in. cut parallel to the plane of the deposit. The technique of sample preparation has been reported previously.[5] The bending jig was used in conjunction with a table-model Instron testing machine which enabled plots of bending load versus deflection to be obtained automatically. The load and deflection were converted to maximum fiber stress and strain by using the usual bending-beam formulas. These formulas apply rigorously only to isotropic materials; therefore, the calculated stresses and strains are subject to some error in the case of the oriented carbons. The load-deflection curves were used to obtain values for the initial flexural modulus, the maximum fiber stress, the maximum fiber strain, and the mean elastic modulus (maximum fiber stress divided by maximum fiber strain). The initial modulus was always higher than the mean modulus because all the curves were concave toward the strain axis.

Measurements were made of the mechanical properties of carbon deposited under various conditions, corresponding roughly to the range of laminar and isotropic coatings and a typical granular coating.[1] Then a typical laminar deposit was annealed at a series of temperatures, and the mechanical properties of the annealed samples were measured. Finally, the effects of a standard annealing treatment (4 hr at 2300°C) on the mechanical properties of a series of deposits produced under different conditions were determined.

Effect of Deposition Conditions on Mechanical Properties

Measurements were made of the mechanical properties of two series of coatings deposited at various temperatures in a 2.5-cm-diameter coater. The methane concentration in the helium carrier gas was 11% in one series of runs and 40% in the other (total flow in both cases was 2600 cm^3/min at 23°C and 1 atm total pressure). In both cases, the initial total surface area of the particle charge was 400 cm^2 (15 g of 150 to 250 μ diameter UC_2 particles; see Table 2 for average deposition rates). The metallographic appearance of the coatings was laminar for deposition temperatures below 1500°C and isotropic for temperatures above 1500°C.

Figures 6 and 7 show the elastic modulus, maximum fiber stress, and maximum fiber strain of the deposits as a function of deposition temperature, together with their anisotropy factor, apparent crystallite size, and density. The definitions and methods of measuring these structural parameters appear in Ref. 1. For both series of tests, the modulus decreases with increasing deposition temperature, except for the unexpectedly high modulus of the deposit produced at 1835°C from 40% methane (Fig. 7c). The fracture stress also shows a general decrease with increasing deposition temperature, but since the fractional decrease in fracture stress is smaller than the decrease in elastic modulus, there is a net increase in the elastic strain at fracture.

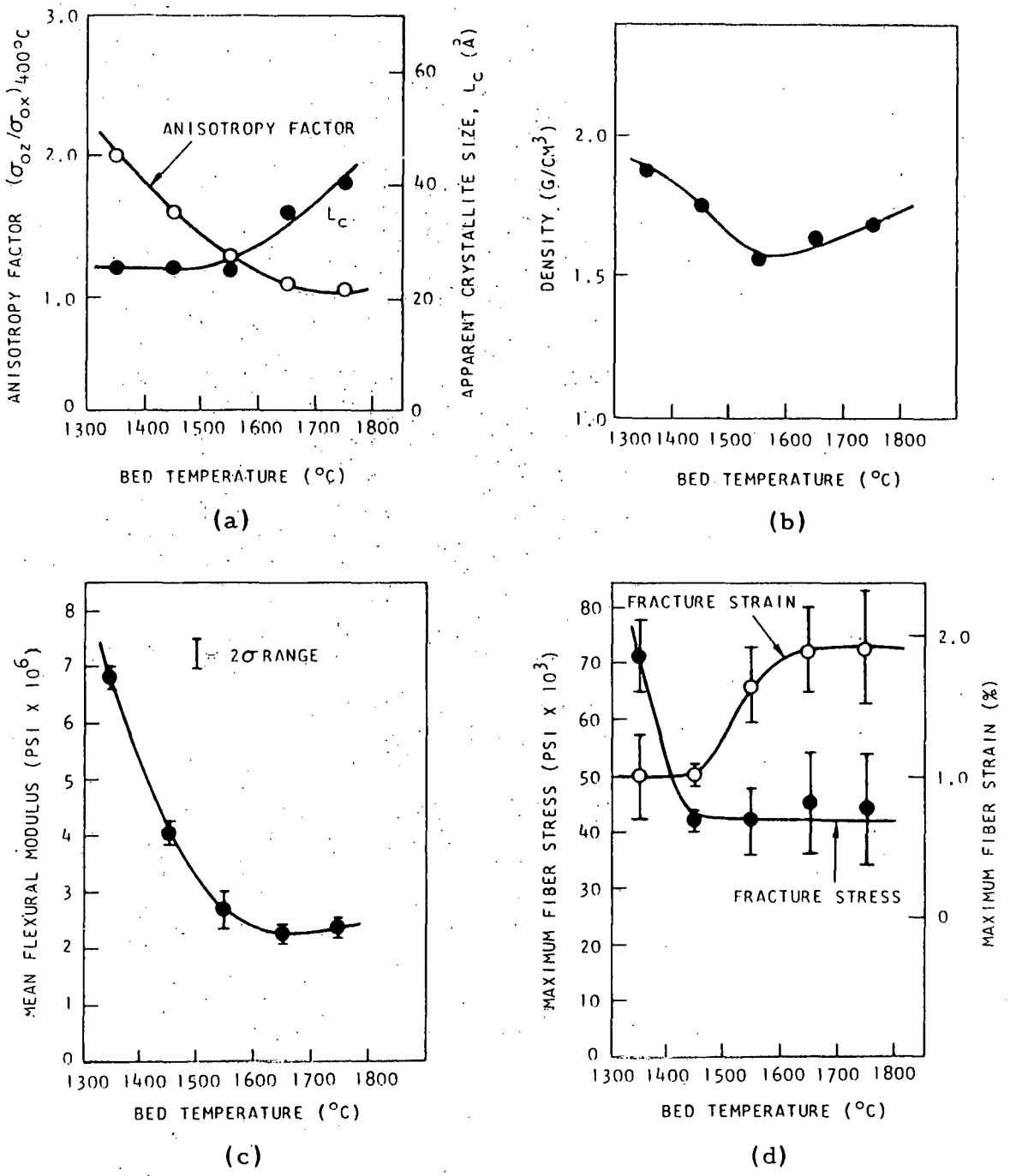

Fig. 6--Dependence of structural parameters and mechanical properties on deposition temperature for deposits produced in a 2.5-cm-diameter coater, using 11% methane in helium and 400-cm^2 (15-g) charge: (a) anisotropy factor and apparent crystallite size; (b) density; (c) room-temperature flexural modulus; (d) maximum fiber stress and strain at fracture.

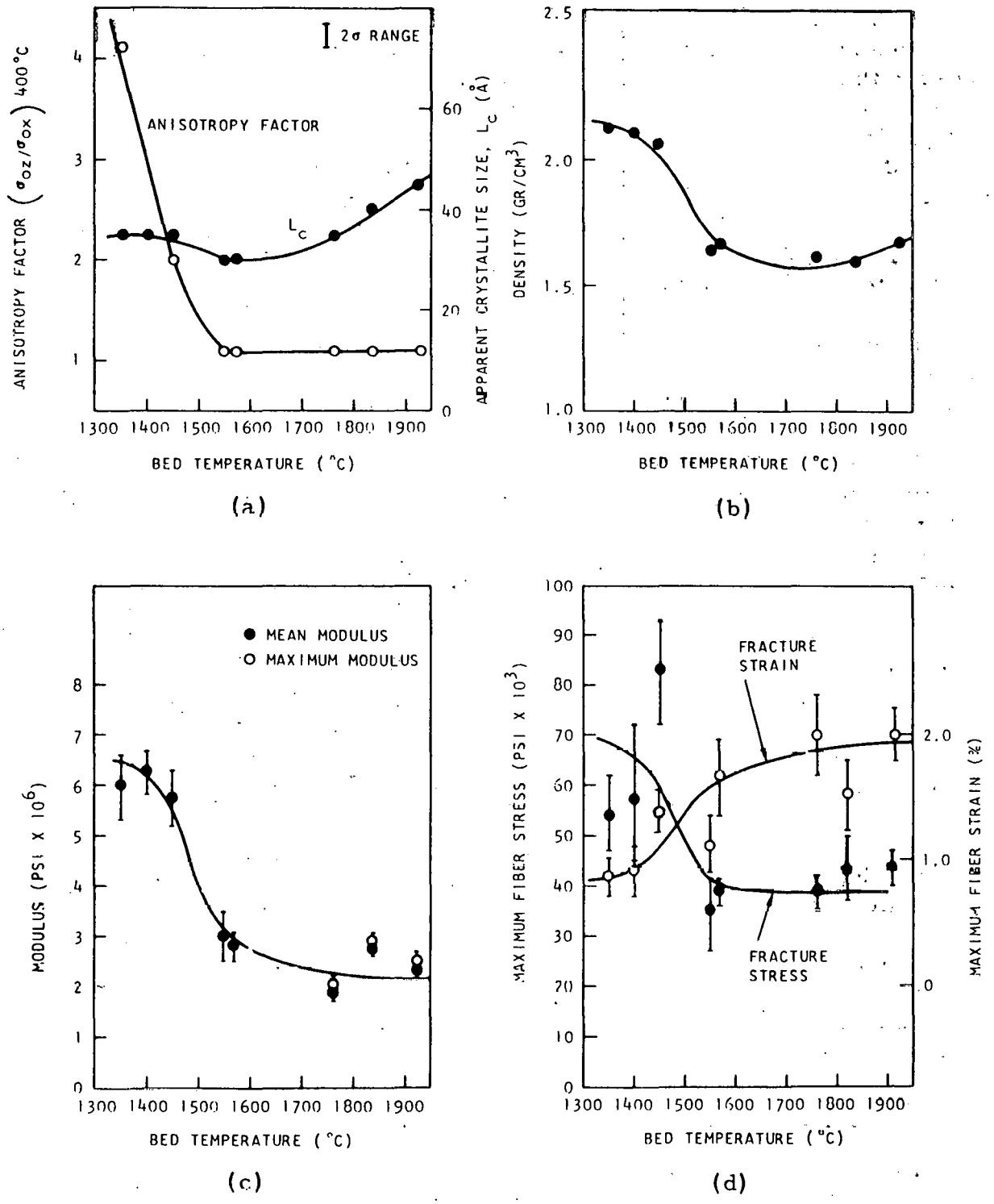

Fig. 7 -- Dependence of structural parameters and mechanical properties on deposition temperature for deposits produced in a 2.5-cm-diameter coater, using 40% methane in helium and a 400-cm^2 (15-g) initial charge.

The material deposited from 40% methane at the three highest temperatures showed a stress-strain curve that became increasingly nonlinear with increasing deposition temperature. This is shown by the increasing gap between the initial modulus and the mean modulus plotted in Fig. 7c. A similar effect was observed when a 1450°C deposit was annealed at a series of temperatures; details are reported in the following section.

The mechanical properties, anisotropy factor, density, and apparent crystallite size (L_c) of three laminar structures deposited at 1400°C are plotted in Fig. 8 as a function of the methane concentration from which the structures were deposited. The data show a rise in the moduli and fracture stress with methane concentration and a fairly constant fracture strain.

Table 3 shows the deposition conditions, mechanical properties, and structural parameters of a granular structure deposited at 1730°C from 3% methane. Of particular interest are the very low fracture stress and moduli observed for this structure. Metallographic examinations of specimens that were embedded in a pliable epoxy and stressed to incipient fracture provided some evidence as to the cause of the low strength of the granular structure. The photomicrographs in Fig. 9 show that large interlaminar cracks form in the individual grains and are undoubtedly the cause of the low fracture stresses that were observed.

All mechanical-property data obtained to date from as-deposited samples are summarized in Fig. 10, where Young's modulus, fracture stress, and fracture strain are plotted as functions of the bed temperature and methane partial pressure used in the preparation of the samples. Laminar deposits (corresponding to the low-temperature side of the plots) are typified by high moduli and fracture stresses but low fracture strains. Isotropic structures (the central region of the plots) have intermediate moduli and fracture stresses and can sustain high elastic strains before fracture. The granular deposits (corresponding to the high-temperature, low-methane-concentration corner of the surfaces) had the lowest moduli and fracture stresses of all the structures investigated.

Effect of Annealing on Mechanical Properties of Laminar Deposits

Pyrolytic-carbon samples deposited from 40% methane at 1450°C (see previous section for coating conditions) were annealed for 4 hr at 1700°, 1900°, 2100°, and 2300°C, and then bend tests were performed on the samples. The mechanical properties are shown in Fig. 11. There is a marked decrease in mean modulus and fracture stress with increasing annealing temperature, and a slight increase in fracture strain. The most remarkable effect of annealing is the increasing curvature of the stress-strain curve, shown in Fig. 12, which results in an increasingly large gap

Table 2

AVERAGE COATING RATES FOR A 2.5-CM-DIAMETER COATER (In μ/hr)

Bed Temp. (°C)	Coating Rate[a]	
	11% CH_4	40% CH_4
1200	--	--
1350	17	22
1450	20	30
1550	26	49
1650	29	57
1750	33	67
1850	44	76
1925	26	56

[a] The initial charge was 400 cm^2 for both series.

Table 3

STRUCTURAL PARAMETERS AND MECHANICAL PROPERTIES OF GRANULAR PYROLYTIC-CARBON STRUCTURE DEPOSITED AT 1730°C FROM 3% METHANE[a]

Density	2.00-2.02 g/cm^3
Bacon anisotropy factor	1.1
Apparent crystallite size, L_c	140 Å
Layer spacing	3.43 Å
Mean modulus[b]	1.21 ±0.11×10^6 psi[c]
Maximum modulus[b]	1.62 ±0.17×10^6 psi[c]
Fracture stress[b]	17.8 ±1.7×10^3 psi[c]
Fracture strain[b]	1.48 ±0.17%

[a] Deposited in a 2.5-cm-diameter coater using a 10-g charge of 420 to 495 μ (U, Th)C_2 particles (130 cm^2). The total flow rate was 3300 cm^3/min and the average deposition rate was 15 μ/hr.

[b] Average from ten specimens.

[c] The ± values are standard deviations of the determinations.

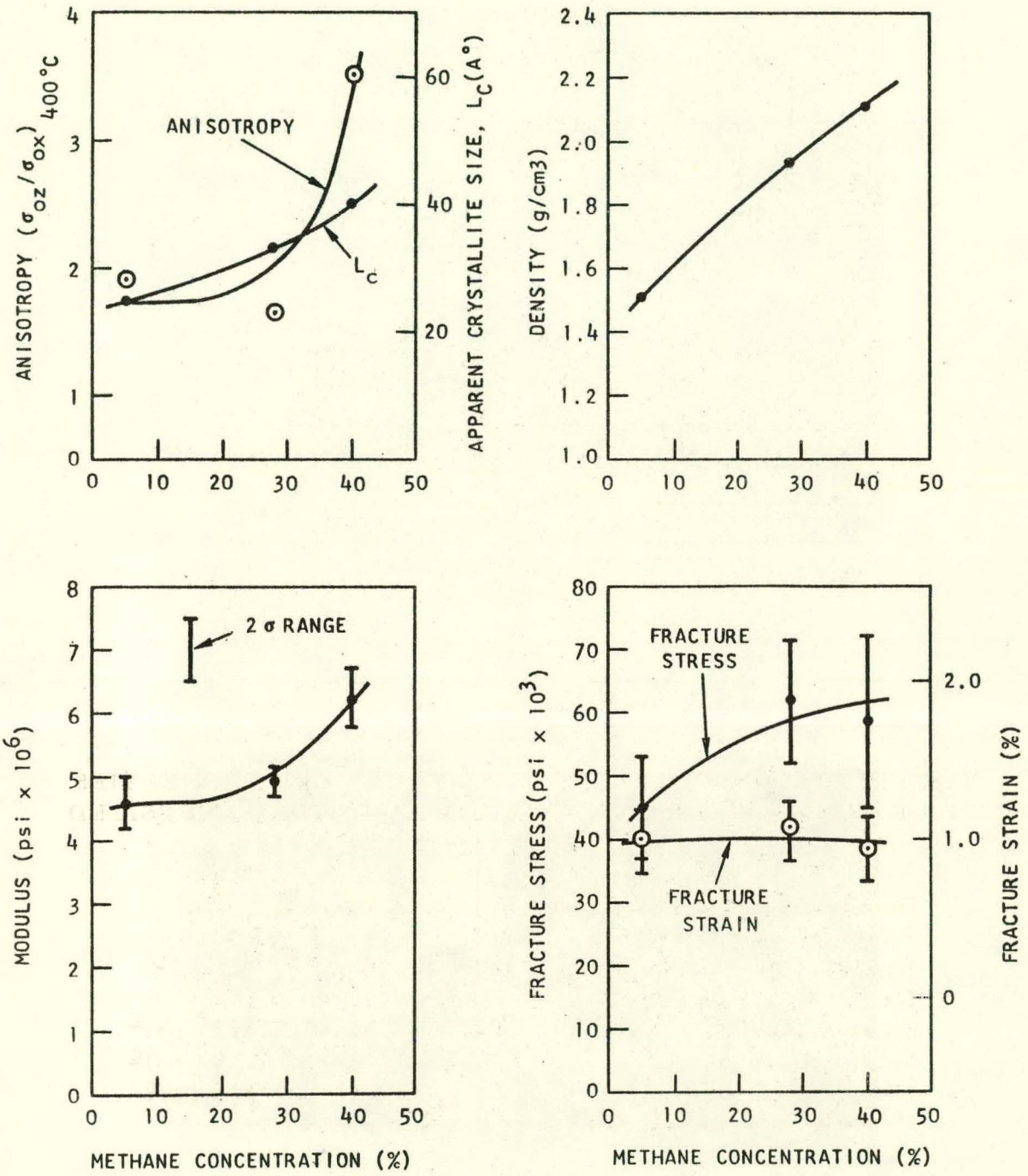

Fig. 8--Dependence of structural parameters and mechanical properties on methane concentration for pyrolytic carbon deposited at 1400°C (initial charge area, 400 cm^2).

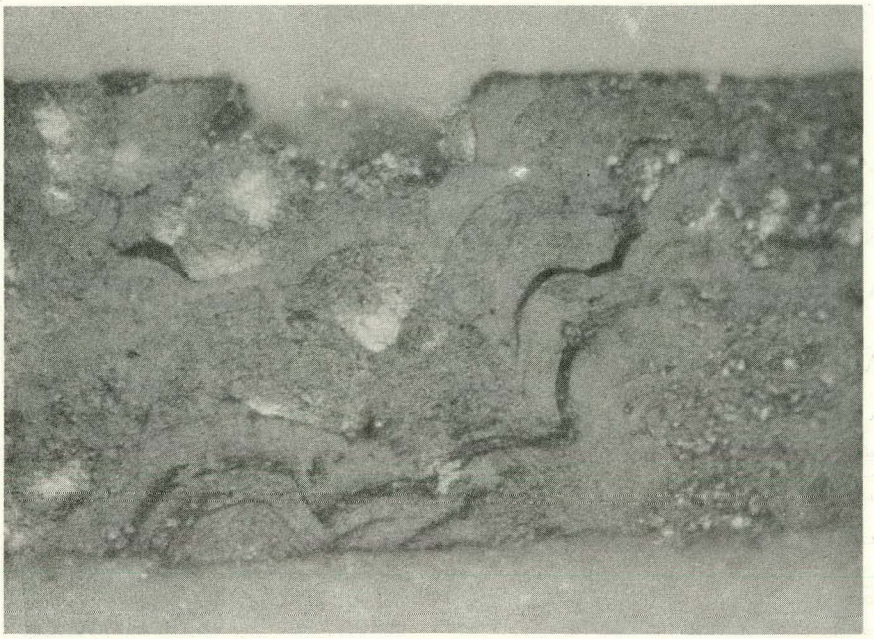

(a)

M-9405-4 1000×

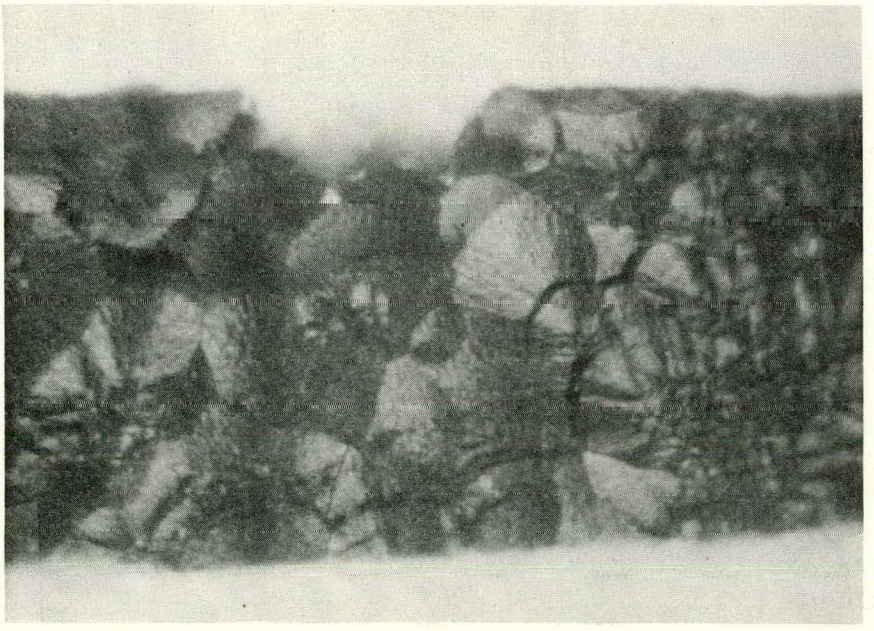

(b)

M-9405-3 1000×

Fig. 9--Photomicrographs showing interlaminar fracture in a granular pyrolytic-carbon deposit (see Table 3 for structural parameters): (a) bright field; (b) polarized light.

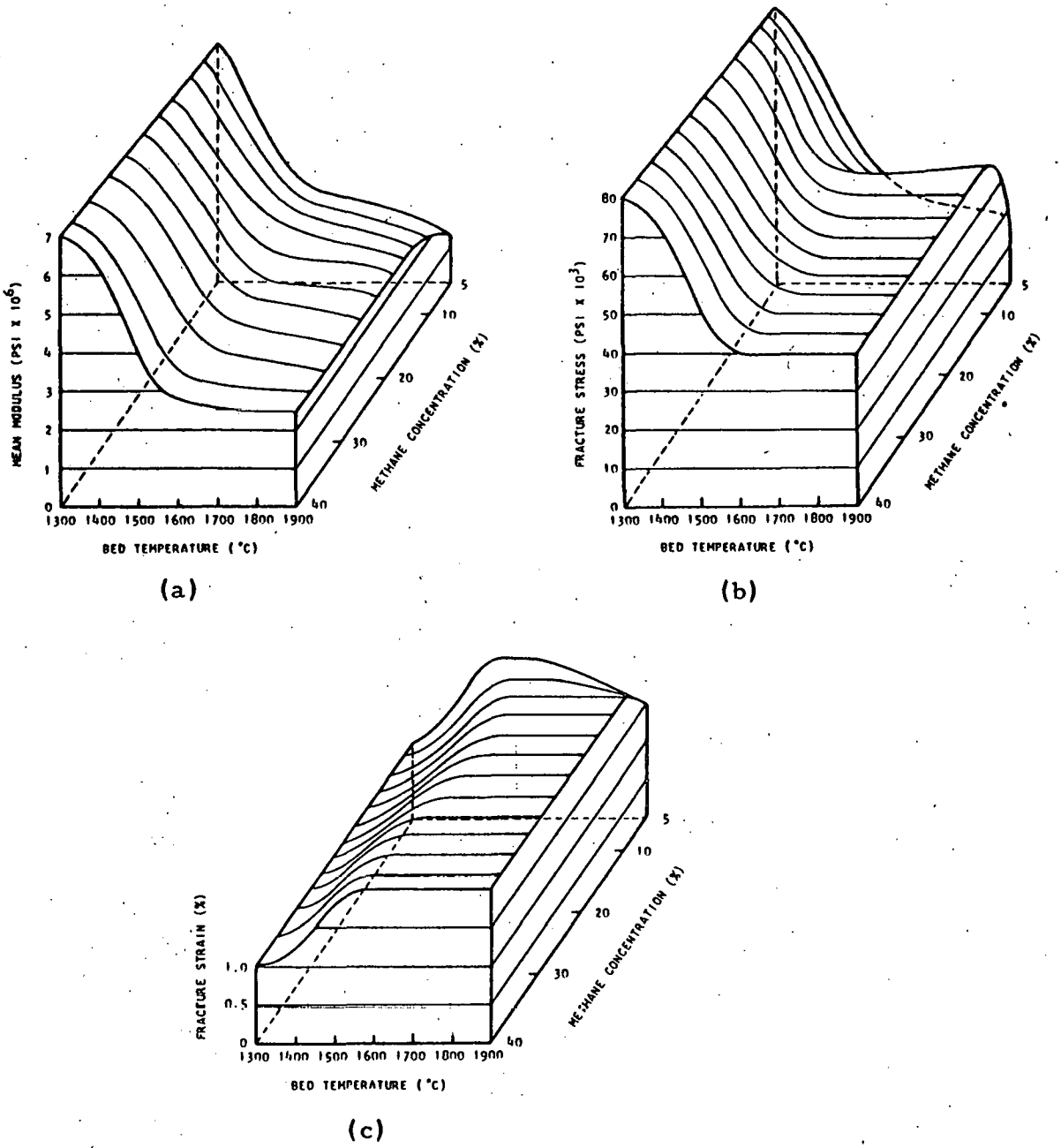

Fig. 10--Diagrams relating mechanical properties of pyrolytic-carbon deposits to deposition conditions; deposits were prepared in a 2.5-cm-diameter coater using a 400-cm^2 initial charge.

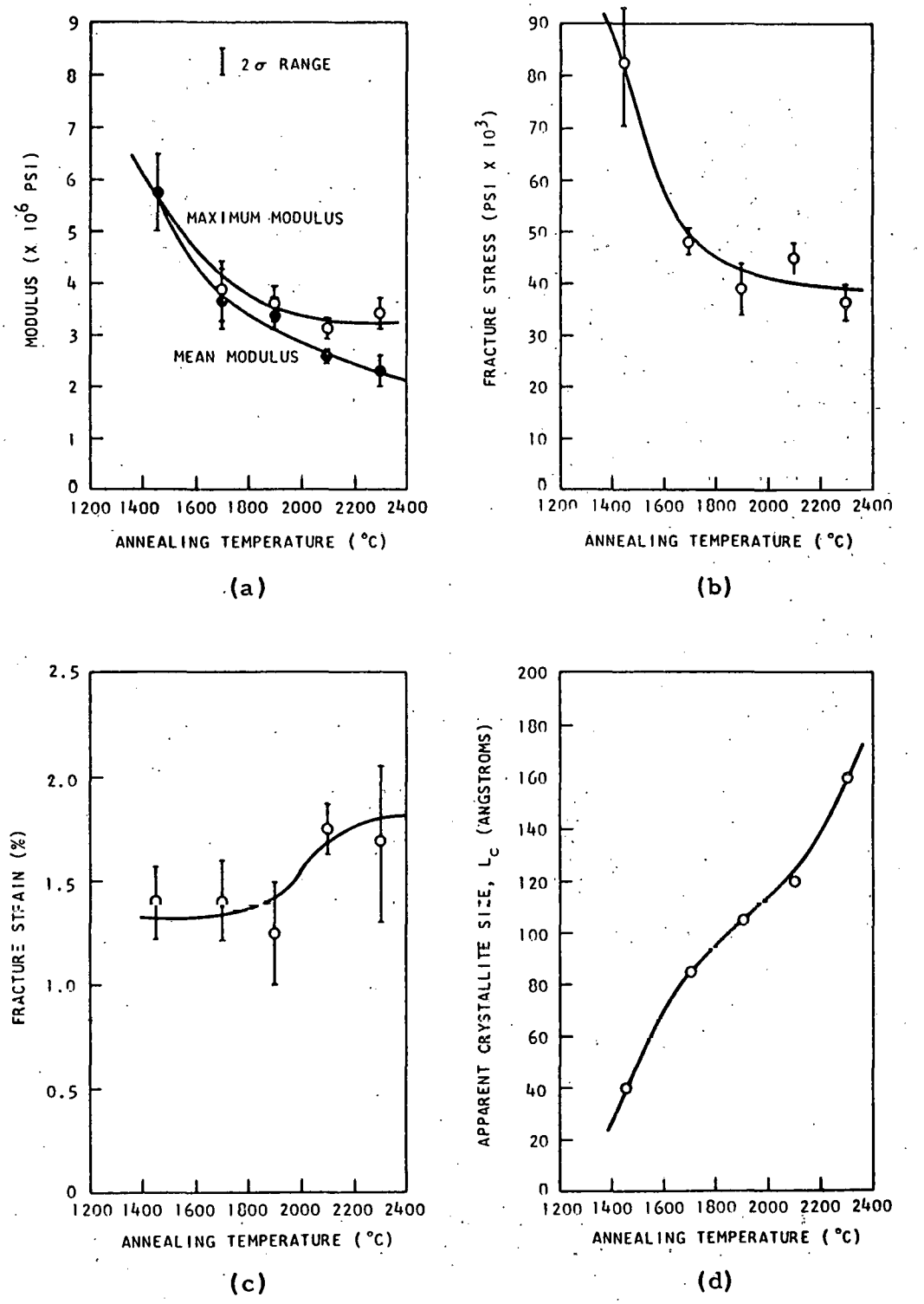

Fig. 11 --Dependence of mechanical properties and L_c on annealing temperature for a 1450°C laminar structure deposited from 40% methane (400-cm^2 charge); annealing time was 4 hr in each case.

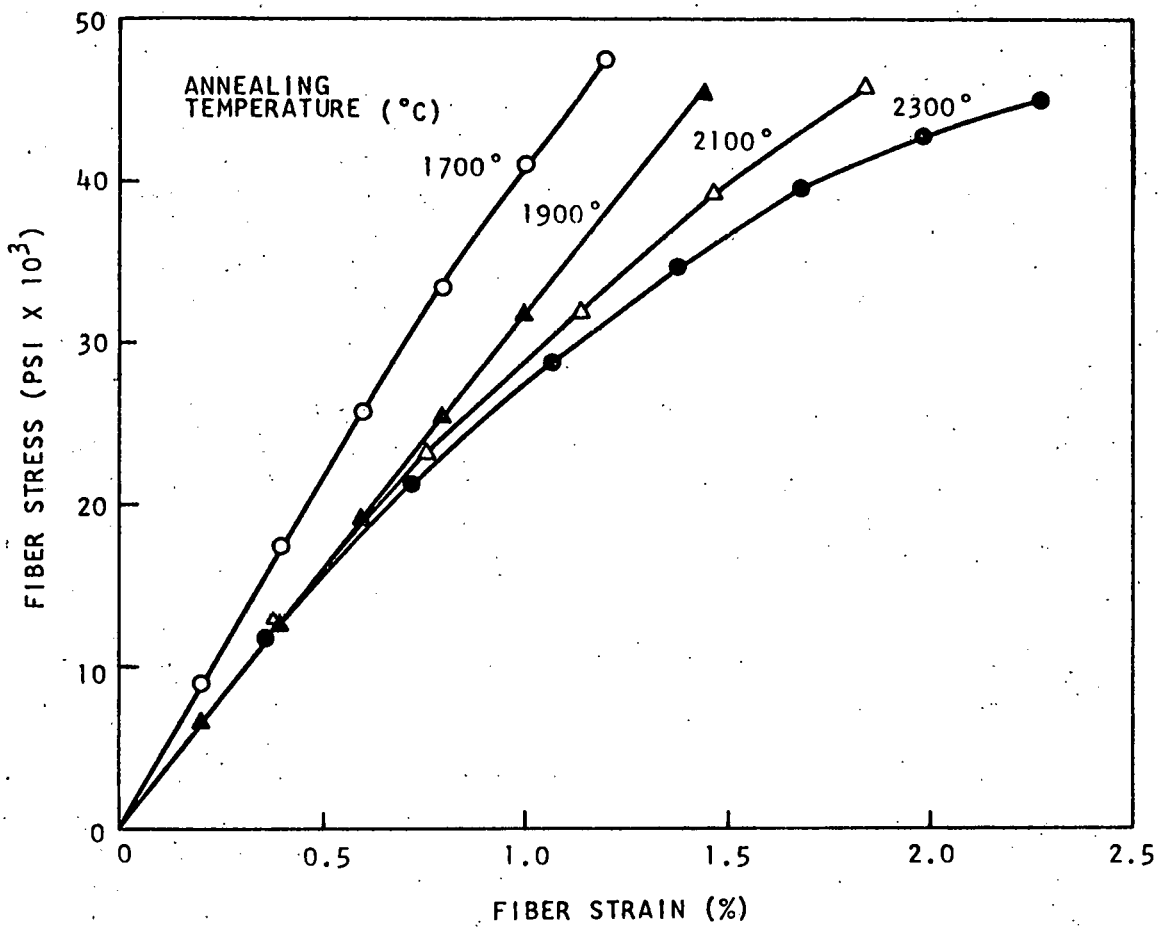

Fig. 12--Effect of annealing for 4 hr at various temperatures on the stress-strain relationship for pyrolytic carbon deposited at 1450°C from 40% methane; the charge area was 400 cm^2.

between the mean modulus and initial modulus of Fig. 11a. The decrease in maximum modulus on annealing is not accompanied by any change in preferred orientation, but there is a steady increase in apparent crystallite size with annealing temperature (see Fig. 11d). It is possible that this decrease is due to a reduction in the amount of cross-linking between layer planes, with a corresponding decrease in the effective shear modulus parallel to the planes.

Laminar deposits do not all respond to annealing treatments in the same way. The effect of annealing for 4 hr at 1900°C and 2 hr at 2800°C on three laminar structures deposited at 1400°C is shown in Fig. 13. Annealing increases the strain-to-fracture of laminar deposits, but reduces their strength. The "annealability" of these carbons depends on their structure. High-density deposits made from high methane concentrations are affected by annealing temperatures as low as 1900°C, but low-density carbons deposited from low methane concentrations are only slightly affected by annealing at temperatures as high as 2800°C. The largest changes in properties occurred in the structures in which the largest changes in crystallite size and layer spacing occurred. The anisotropy factor of these three laminar deposits was unaffected by the annealing treatments.

Effects of Annealing at 2300°C on Mechanical Properties of Isotropic Deposits

A number of isotropic deposits were annealed at 2300°C for 4 hr, and the mechanical properties were measured before and after annealing. The deposition conditions and mechanical-property changes are shown in Table 4. The structural parameters of the as-deposited material may be obtained from Figs. 6 and 7. In contrast to the large changes in mechanical properties observed in the laminar deposits on annealing (noted in the previous section), changes in the properties of the isotropic materials were small. There was, however, a significant increase in the elastic moduli of the structures deposited at 1650°C from 11% methane and at 1760°C from 40% methane, accompanied by a slight decrease in the fracture strain.

Effect of Structure on Mode of Fracture of Pyrolytic-carbon Deposits

The fracture mode of the carbons studied depended sensitively on structure. This was studied by nickel-plating the fractured samples and preparing metallographic sections. The fracture path in as-deposited laminar structures was predominantly perpendicular to the layer planes (Fig. 14a), but after annealing at either 1900° or 2800°C, the fracture path tended to follow the layer planes, resulting in delamination on planes perpendicular to the loading direction (Fig. 14b).

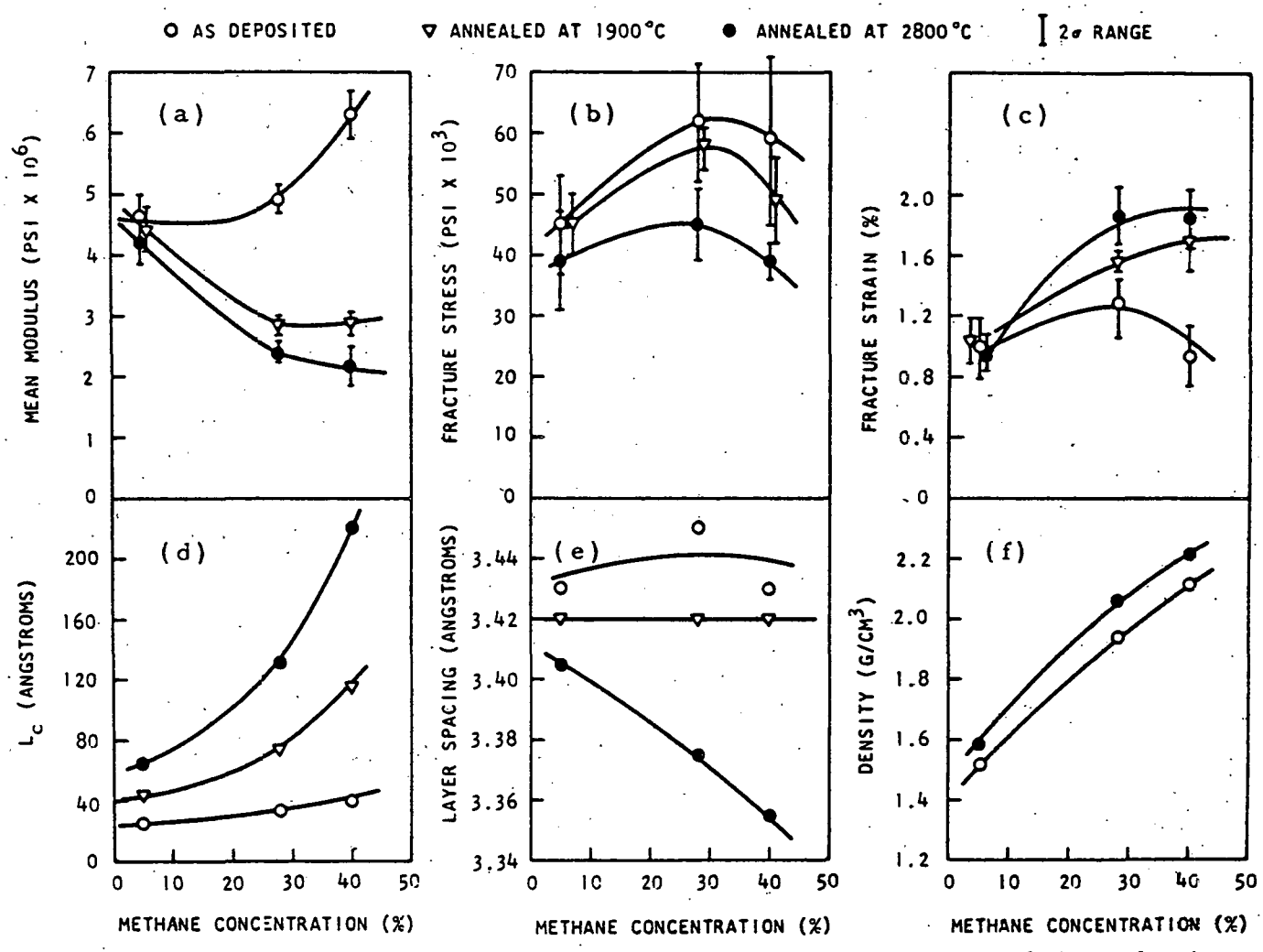

Fig. 13--Effect of annealing on structure and mechanical properties of three laminar pyrolytic-carbon structures deposited from various methane concentrations at 1400°C, in a 2.5-cm-diameter coater, using a 400-cm^2 initial charge.

Table 4

EFFECT OF ANNEALING FOR 4 HOURS AT 2300°C ON THE MECHANICAL PROPERTIES OF THREE ISOTROPIC PYROLYTIC-CARBON STRUCTURES DEPOSITED IN A 2.5-CM-DIAMETER COATER

(The initial charge area was 400 cm^2 and the total flow was 2600 cm^3/min.)

Specimen Number	Coating Conditions			Mechanical Properties[a]					
				As Deposited			After Annealing		
	Bed Temp. (°C)	Methane Conc. (%)	Coating Rate (μ/hr)	Mean Modulus (psi × 10^6)	Fracture Stress (psi × 10^3)	Fracture Strain (%)	Mean Modulus (psi × 10^6)	Fracture Stress (psi × 10^3)	Fracture Strain (%)
2359-57	1650	11	29	2.4 ± 0.1	44 ± 6	1.9 ± 0.3	2.8 ± 0.1	44 ± 2	1.6 ± 0.1
2511-17	1760	40	67	1.9 ± 0.1	39 ± 3	2.0 ± 0.4	2.5 ± 0.1	37 ± 1	1.5 ± 0.1
2511-23	1925	40	56	2.2 ± 0.1	44 ± 3	2.0 ± 0.2	2.0 ± 0.1	40 ± 3	2.0 ± 0.2

[a]The ± figures are the standard deviations of the determinations.

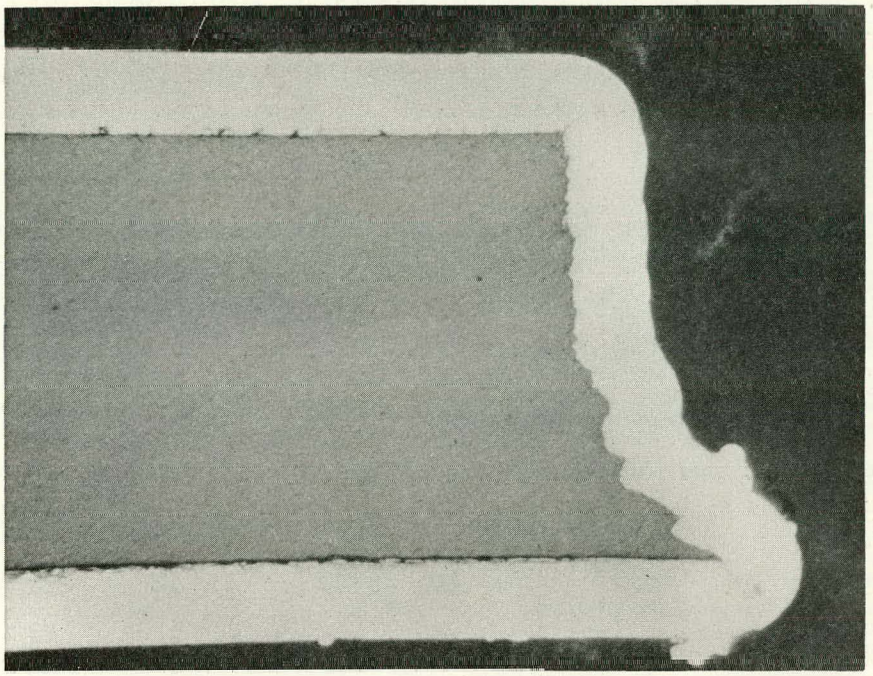

(a)

M-9317-1 500×

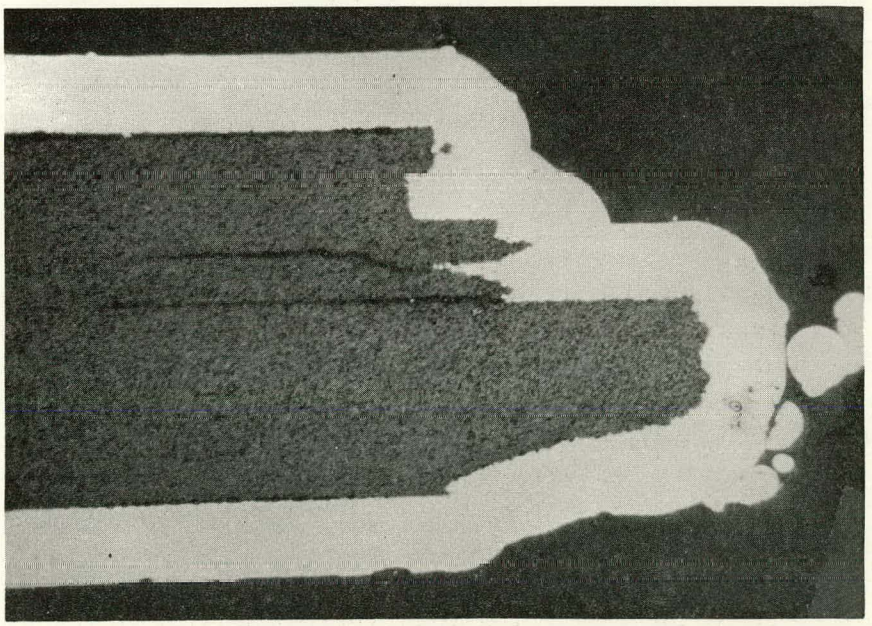

(b)

M-9315-1 500×

Fig. 14--Photomicrographs of fractured laminar deposits (a) fractured as-deposited; (b) fractured after annealing for 2 hr at 2800°C; carbon was deposited from 40% methane at 1400°C; anisotropy factor was 3.5 for both as-deposited and annealed samples (see Fig. 8 for other structural parameters).

An electron micrograph* of replicas taken from the fractured surface of an as-deposited, high-density, laminar structure is shown in Fig. 15. Fracture occurred predominantly perpendicular to the layer planes, revealing details of the layered structure. Several small areas where the fracture proceeded parallel to the layer planes are also visible. A similar electron micrograph of the fractured surface of the same laminar deposit, annealed for 2 hr at 2800°C before testing, is shown in Fig. 16. The fracture in this case proceeded predominantly parallel to the layer planes. The electron micrograph also shows that polygonization of the curvature of the as-deposited layer planes occurred during annealing.

The fracture surface of isotropic structures was characteristically conchoidal on a macroscale. Figure 17 shows a cross section of the fracture. The electron micrograph shown in Fig. 18, however, reveals many structural features that are probably caused by the incorporation of gas-phase-nucleated solid carbon into the structure during deposition. The electron micrograph suggests the presence of many particles of the order of 1 μ in diameter.

The interlaminar fracture in individual grains of the granular structure is shown in Fig. 9. The electron micrograph shown in Fig. 19 shows the details of the fracture surface. The relatively large regions, 5 to 10 μ across, that show circular symmetry are most likely the result of interlaminar fracture of individual grains.

A topical report entitled "Deformation and Fracture of Pyrolytic Carbons Deposited in a Fluidized Bed" by J. C. Bokros and R. J. Price[6] is in preparation. Full details of the current work on mechanical properties of coatings are included.

Annealing Behavior of Low-temperature Carbon Deposits

As noted earlier in this report, the effects of heat treatment on the properties of laminar pyrolytic carbons depend on the structure of the carbons. Low-density pyrolytic carbons deposited from gas containing low methane concentrations are almost unaffected by heat treatment, whereas high-density carbons deposited from gas containing high methane concentrations can have their structure and properties profoundly altered by annealing. This structure-dependence of the "annealability" is important because coated fuel particles may be exposed to temperatures higher than their deposition temperature during processing and while in service, and it is desirable to know the extent to which the properties of the coating may be altered. It is also of theoretical interest because of the relation between the "annealability" and the structure of the carbon. Consequently, a series of experiments has been initiated in which four laminar structures will be

*Electron micrographs were prepared by J. O. Gardner of General Atomic.

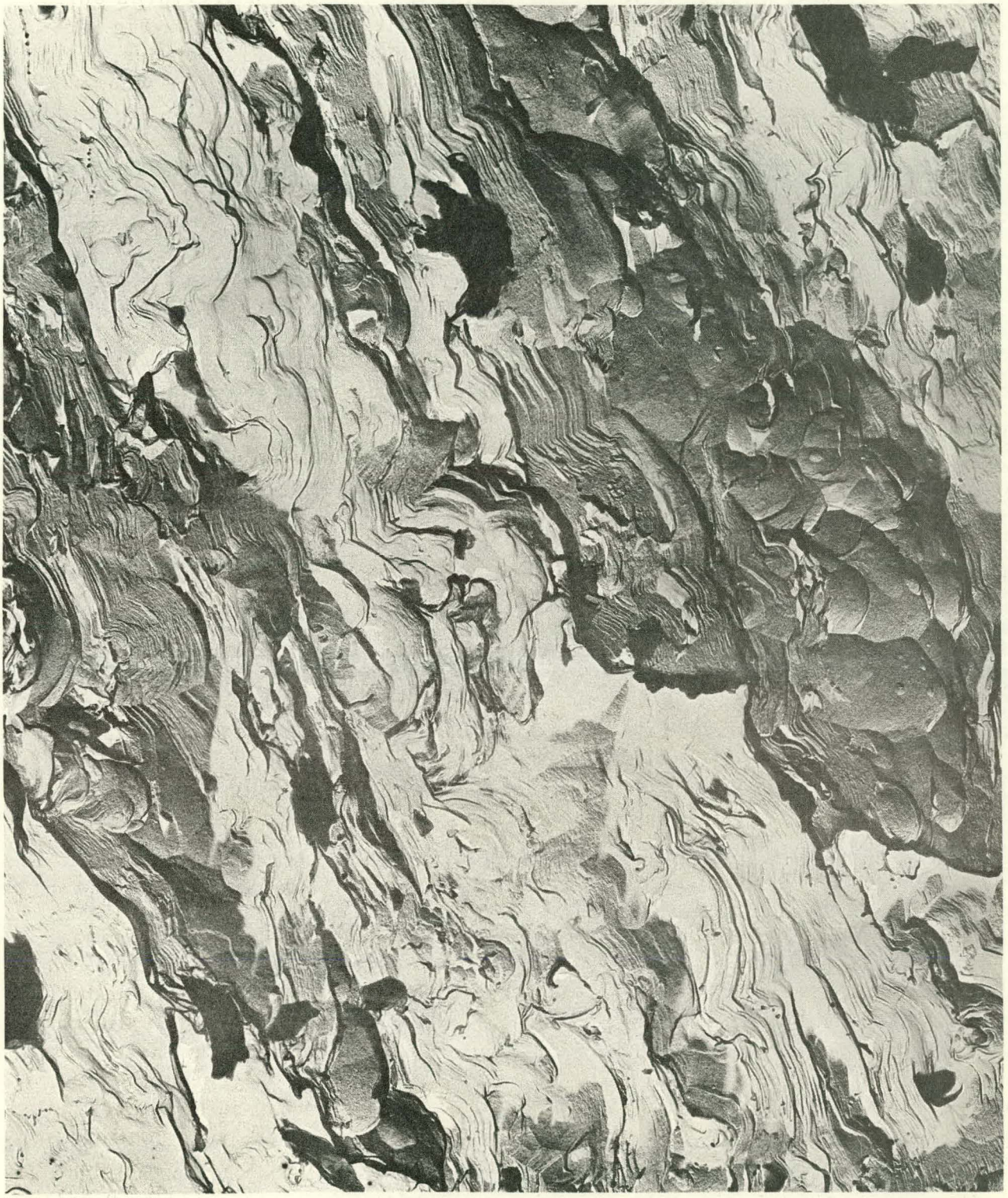

P-4835 (18,000×)

Fig. 15--Electron micrograph of laminar pyrolytic carbon deposited at 1400°C from 40% methane (see Fig. 8 for structural parameters).

P-4854 (18,000×)

Fig. 16--Electron micrograph of annealed (2 hr at 2800°C) laminar pyrolytic carbon deposited at 1400°C from 40% methane (see Fig. 8 for structural parameters).

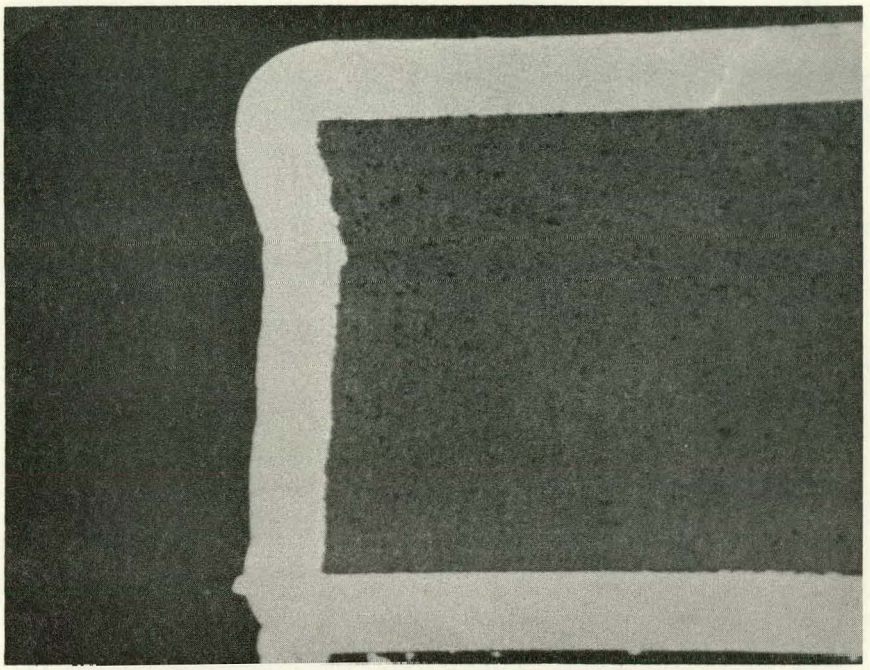

M-9322-1 500×

Fig. 17--Electron micrograph of fractured isotropic deposit; specimen was deposited at 1650°C from 15% methane; deposit had a density of 1.55 g/cm^3, an L_c of 49 Å, and an anisotropy factor of 1.05.

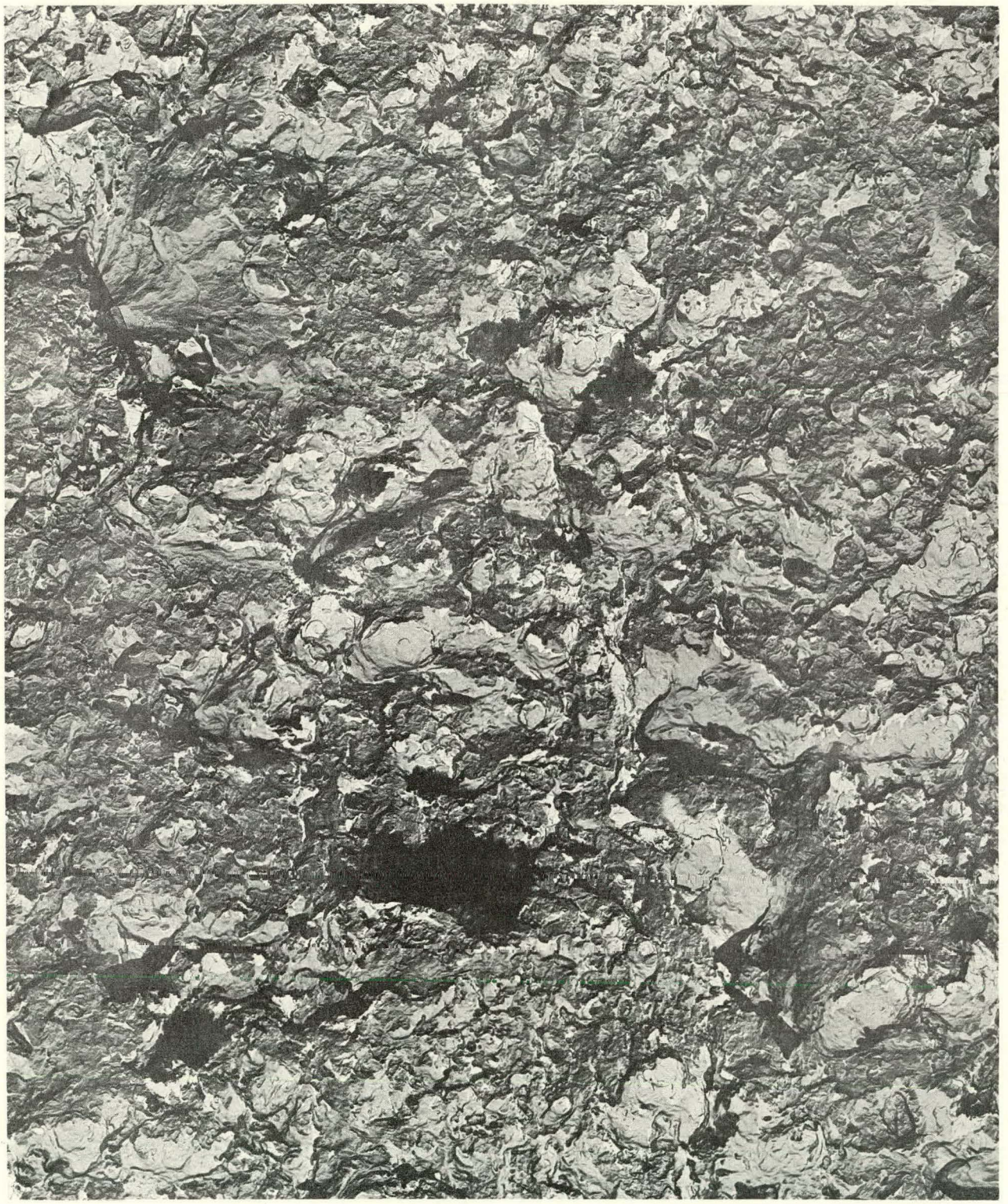

P-4759 (18,000×)

Fig. 18--Electron micrograph of isotropic carbon deposited at 1650°C from 15% methane; deposit had a density of 1.55 g/cm^3, an L_c of 49 Å, and an anisotropy factor of 1.05.

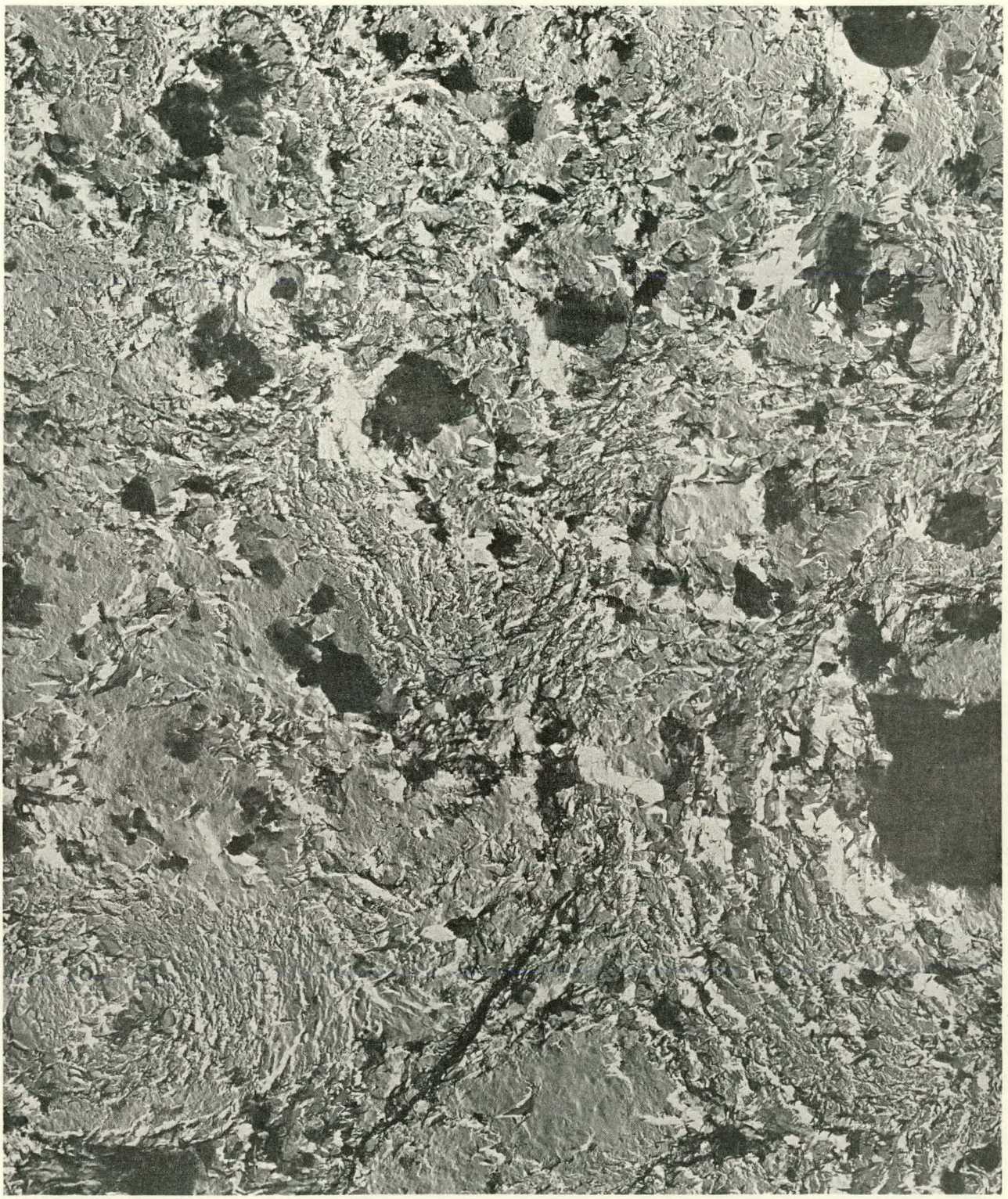

P-4710 (8000×)

Fig. 19--Electron micrograph of granular pyrolytic carbon (see Table 3 for structural details).

annealed at a constant temperature for successively increasing time periods. The changes in lattice spacing, crystallite size, density, Young's modulus, and electrical resistivity will be measured as a function of annealing time. Electrical resistivity is being used to follow the progress of the anneal because it is related to the presence of small defects such as regions of amorphous carbon and it is easy to measure with high precision.

The laminar carbons used include the three structures, designated numbers 1, 2, and 3, deposited at 1400°C from helium containing 40%, 28%, or 5% methane in a 2.5-cm-diameter coater. (The other structural and coating parameters are reported in the section on the effects of annealing on the mechanical properties of laminar deposits.) In addition, a deposit with very low preferred orientation was especially prepared at 1375°C in a 2.5-cm-diameter coater, using a methane partial pressure of 40% and an initial bed surface area of 210 cm^2 (15 g of 350 to 420 μ diameter UC_2 particles). The total gas flow was 1500 cm^3/min (measured at room temperature and pressure). The density of the deposit was 1.92 g/cm^3; the apparent crystallite size, L_c, was 32 Å; and the anisotropy factor was 1.1. This structure was designated number 8.

The first series of anneals has been completed. The annealing temperature was 1500°C and the annealing times were progressively increased from 30 min to 96 hr. Eight samples of each structure were used to measure the flexural modulus and electrical resistivity at each annealing stage, and pairs of samples from each structure were used to follow changes in density and L_c. In addition, the thermal diffusivity of pairs of samples of each structure was measured before and after the series of anneals, and finally the fracture stresses and strains after annealing were determined by bend tests on the elastic-modulus samples.

The fractional changes in the flexural modulus, electrical resistivity, and L_c during the course of the anneal are shown in Figs. 20 through 22. The error bands delineate the standard deviations of the measurements. The changes in the mean values of thermal diffusivity and fracture stress and strain are given in Tables 5 and 6. The densities of structures 2, 3, and 8 did not change significantly during the anneal, but structure 1 increased in density from 2.126 to 2.164 g/cm^3.

Annealing produced the largest changes in elastic modulus, electrical resistivity, L_c, and thermal diffusivity in structure 1. There were also substantial increases in the thermal diffusivity and L_c for structure 2 and in L_c for structure 8 (diffusivity measurements were not made for structure 8). The electrical resistivity was significantly reduced in all the carbons, but L_c for structure 3 and the elastic modulus in structures 2, 3, and 8 were not changed significantly. The apparent increase in the modulus of structure 3 (Fig. 20) is probably not significant and may have

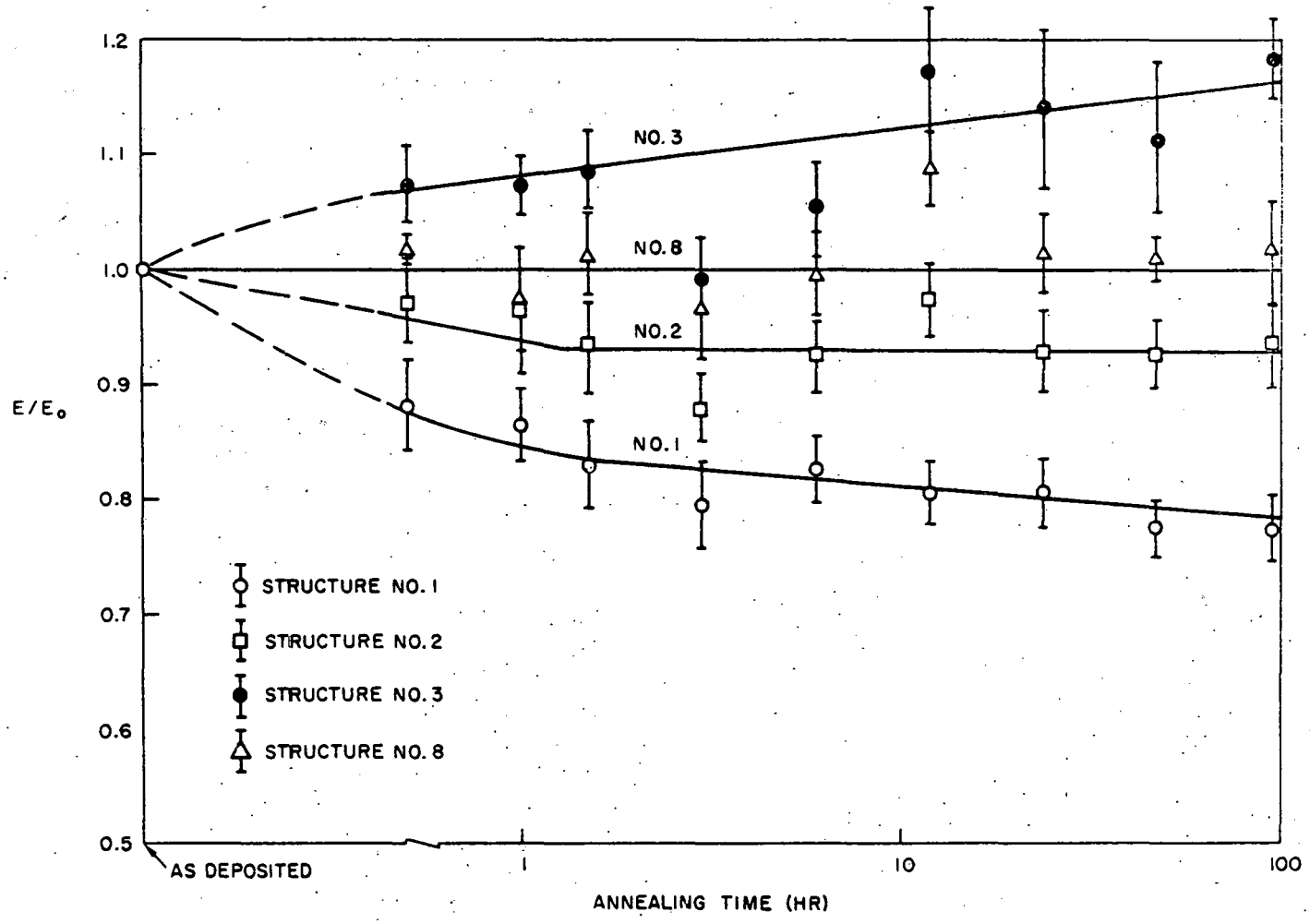

Fig. 20 - Fractional changes in flexural modulus as a function of annealing time at 1500°C for laminar pyrolytic carbons deposited at 1400°C. Details of each of the four structures are given in the text.

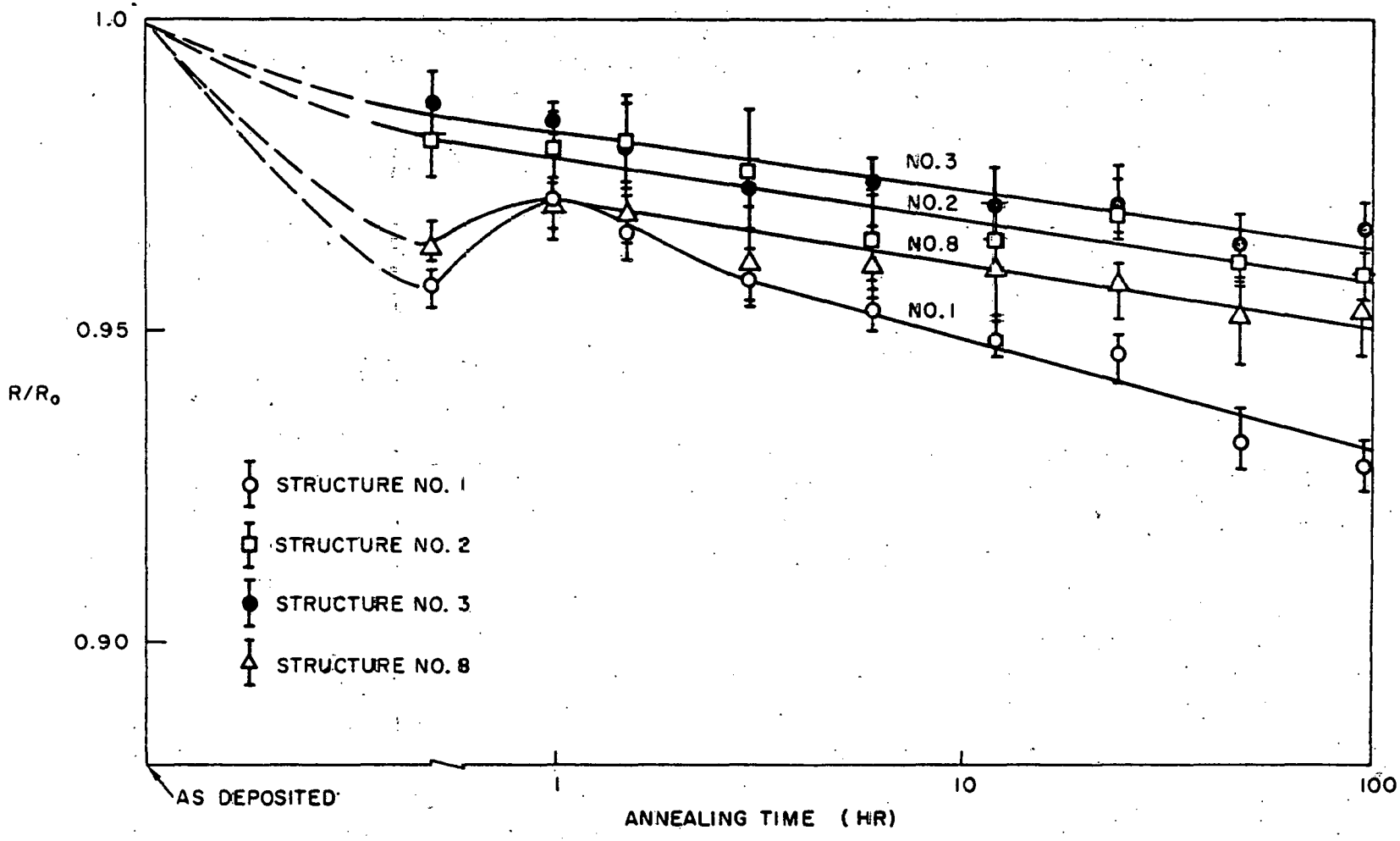

Fig. 21--Fractional changes in electrical resistivity as a function of annealing time at 1500°C for laminar pyrolytic carbons deposited at 1400°C. Details of each of the four structures are given in the text.

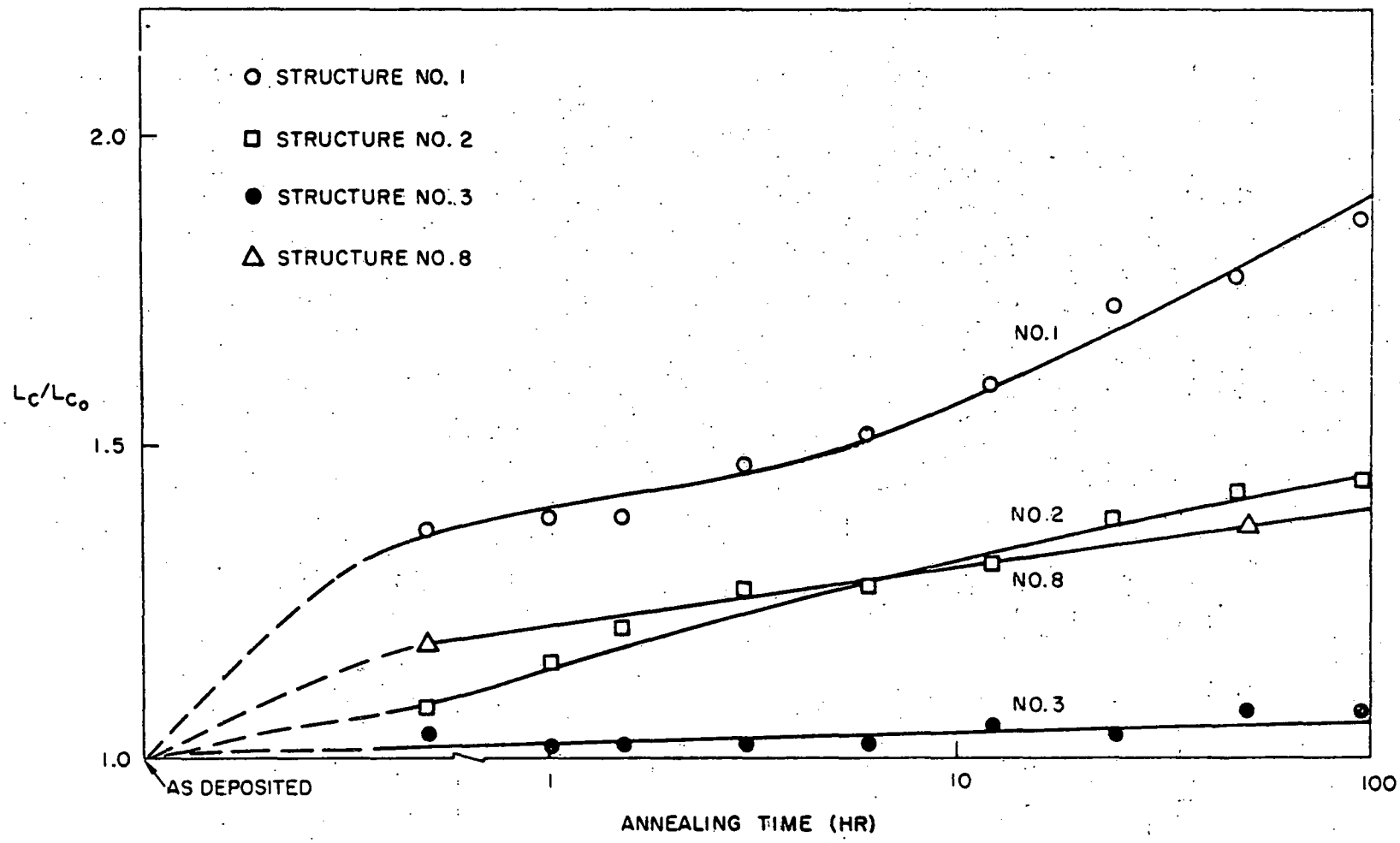

Fig. 22--Fractional changes in apparent crystallite size, L_c, as a function of annealing time at 1500°C for laminar pyrolytic carbons deposited at 1400°C. Details of each of the four structures are given in the text.

Table 5

EFFECT OF ANNEALING FOR 96 HR AT 1500°C ON THE ROOM-TEMPERATURE THERMAL CONDUCTIVITY OF THREE LAMINAR CARBONS DEPOSITED AT 1400°C IN A 2.5-CM-DIAMETER COATER

Deposit	Thermal Conductivity (cal/cm-sec-°C)		Change (%)
	Before Annealing	After Annealing	
Laminar I[a]	1.1×10^{-3}	2.2×10^{-3}	+100
Laminar II[b]	2.4×10^{-3}	4.7×10^{-3}	+96
Laminar III[a]	1.9×10^{-3}	2.1×10^{-3}	+11

[a] Average of two specimens.
[b] Average of three specimens.

Table 6

MEAN FRACTURE STRESSES AND STRAINS OF LAMINAR PYROLYTIC CARBONS DEPOSITED AT 1400°C AS-DEPOSITED AND AFTER ANNEALING AT 1500°C FOR 96 HR

Structure Number	Fracture Stress			Fracture Strain		
	As-deposited (10^3 psi)	Annealed (10^3 psi)	Change (%)	As-deposited (%)	Annealed (%)	Change (%)
1	58.9 ±13.9	59.1 ±10.6[a]	0	0.94 ±0.20	1.22 ±0.17	+30
2	62.3 ±10.4	61.8 ±17.6	-1	1.27 ±0.23	1.27 ±0.32	0
3	45.2 ±8.0	29.1 ±5.0	-36	0.98 ±0.21	0.66 ±0.12	-33
8	42.7 ±5.9	39.3 ±5.5	-8	1.11 ±0.14	1.07 ±0.17	-4

[a] The ± limits refer to the standard deviations of the determinations.

been due to errors in measuring the modulus of the as-deposited samples. The only changes in mechanical properties (Table 6) were the increase in the fracture strain of structure 1 associated with the decrease in elastic modulus, and decreases in the fracture stress and strain of structure 3, which were apparently caused by an unexplained surface cracking that developed during the final stages of the anneal.

The properties that were measured during the anneal are all sensitive to some type of structural imperfection in the carbon. It is evident from the results reported above that different properties respond to annealing to different extents, but the order of "annealability" between the four carbons remains the same: Structure 1 is readily annealable, but structure 3 is completely unaffected by treatment at 1500°C; structures 2 and 8 are intermediate in behavior. The "annealabilities" are in reverse order to the percentage of single layers in the structure as revealed by X-ray scattering measurements (see Table 1 in the section on the structure of carbons deposited below 1900°C).

The annealing of the same physical properties in the same carbon structures will be followed at higher temperatures so that a complete picture will be built up of the annealing kinetics of several different properties as a function of the structure of the pyrolytic carbon.

Effect of Structure on the Thermal Conductivity of Pyrolytic Carbons

Thermal-conductivity measurements have been made on representative pyrolytic-carbon structures using the flash technique. This method has the advantage of accommodating small, thin, disk samples 0.3 in. in diameter and <0.005 in. thick. The results of these measurements were used in calculating the thermal-conductivity values.

The flash method and its application in measurements on various materials have been described in the literature.[7, 8, 9] The method consists of the absorption of a very short pulse of radiant energy from a xenon flash lamp on the front surface of a specimen and the recording of the resultant temperature history of the back surface. The pulse of energy is short compared with the time required for the heat to flow through the specimen to the back surface.

For a perfectly insulated specimen with uniform absorptivity across its surface, the temperature of the back surface that results from a pulse of energy on the front surface is given by

$$\frac{T_{(L,t)}}{T_m} = 1 + 2\sum_{n=1}^{\infty} (-1)^n \exp\left(\frac{-n^2\pi^2\alpha t}{L^2}\right) \qquad (1)$$

where $T_{(L, t)}$ represents the instantaneous rise in temperature of the back surface at time t, T_m is the maximum rise in temperature of the back surface, α is the thermal diffusivity in cm^2/sec, L is the specimen thickness in centimeters, and n represents successive integers.

A plot of Eq. (1) is shown in Fig. 23, from which the thermal diffusivity α may be deduced. When $T_{(L, t)}/T_m$ is equal to 0.5, and $(\pi/L)^2\alpha t$ is equal to 1.37, then

$$\alpha = \frac{1.37\ L^2}{\pi^2 t_{1/2}} = \frac{0.139\ L^2}{t_{1/2}} \quad . \tag{2}$$

The thermal conductivity is then related to thermal diffusivity by the expression

$$K = \rho C \alpha \quad , \tag{3}$$

where K is the thermal conductivity in cal/cm-sec-$^{\circ}$C, ρ is the density in g/cm^3, C is the heat capacity in cal/g-$^{\circ}$C, and α is the thermal diffusivity in cm^2/sec.

The use of Eq. (2) is confined to measurements in which the duration of energy pulse τ is short compared with time $t_c = (L/\pi)^2\alpha^{-1}$, which is roughly the time required for the pulse to penetrate the thickness of the sample. Equation (2) is applicable when $\tau < 0.1\ t_c$. This requirement is usually met by the choice of an appropriate specimen thickness, L, and by the adjustment of the pulse length. For very thin samples, however, such as pyrolytic-carbon coatings, of $L < 0.005$ in., t_c becomes small, giving a $\tau > 0.1\ t_c$. In this case, a correction is applied according to the calculations reported by Cape and Lehman[10]. Figure 24 is a graph of this correction, showing how the factor $t_{1/2}/t_c$ of Eq. (2) increases as the pulse time increases.

The apparatus used is shown schematically in Fig. 25. It consists of a xenon flash lamp with a power supply, a sample holder, and an oscilloscope-camera combination to obtain the temperature history of the back surface. Up to several hundred joules are discharged in less than 500 μsec through the xenon flash lamp, which is placed approximately 3 cm in front of the specimen. The temperature rise at the back surface is sensed by a Chromel-Alumel thermocouple of 0.005-in.-diameter wire, with the junction made by the specimen.

In order to test the method, especially the method of correcting for the duration of the pulse, copper specimens of various thicknesses were measured using pulse durations varying from 130 to 230 μsec. These

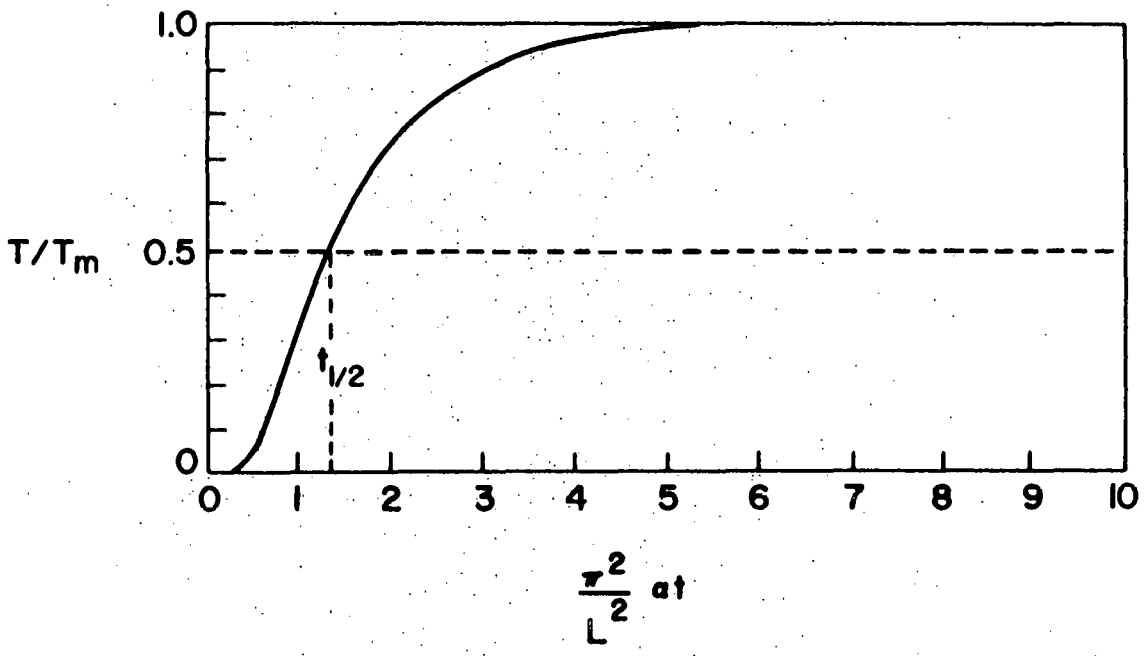

Fig. 23--Plot, predicted from Eq. (1), of the temperature history at the rear surface of the specimen.

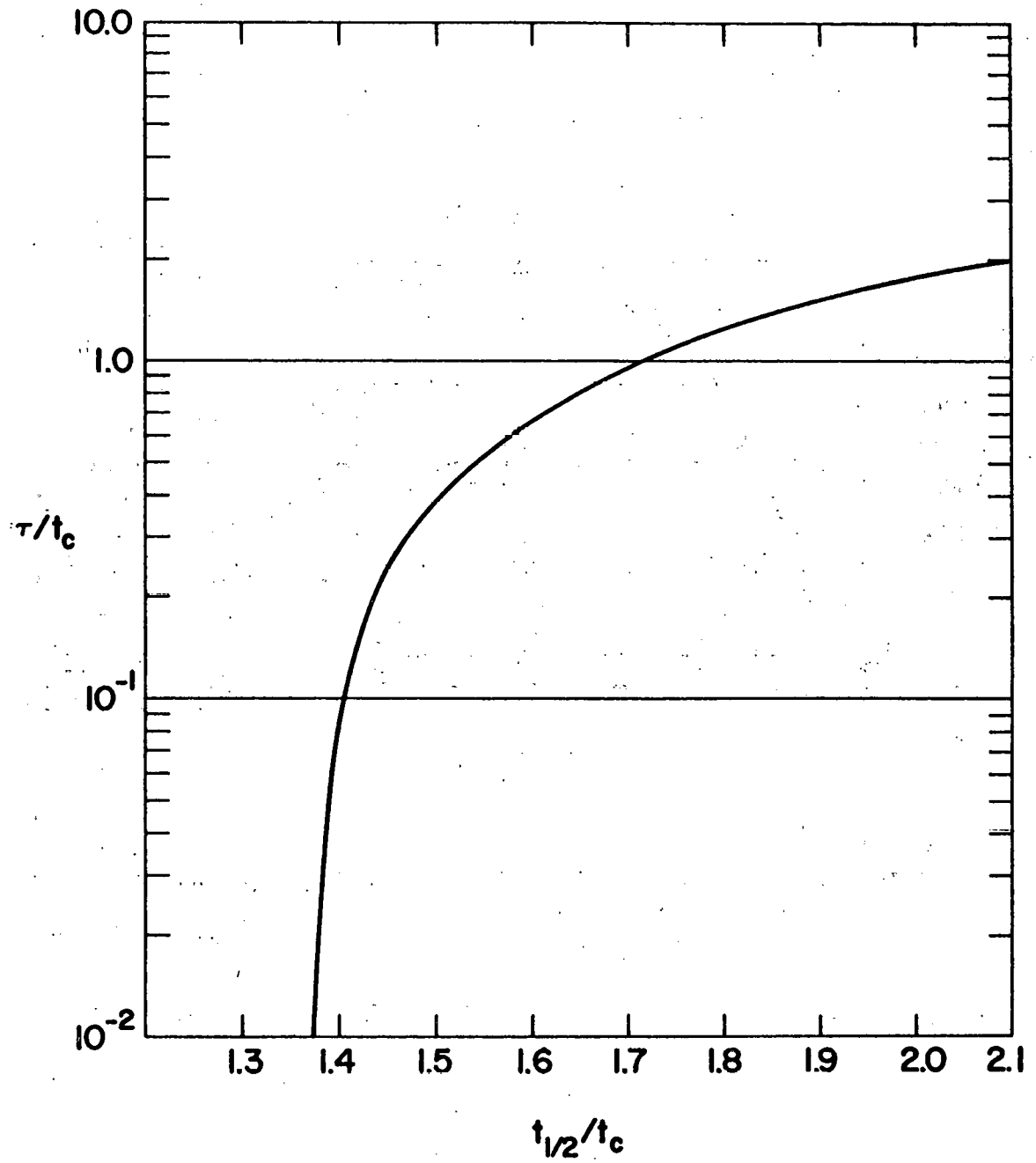

Fig. 24 -- A plot showing the increase in the factor of Eq. (2) with increase in pulse length

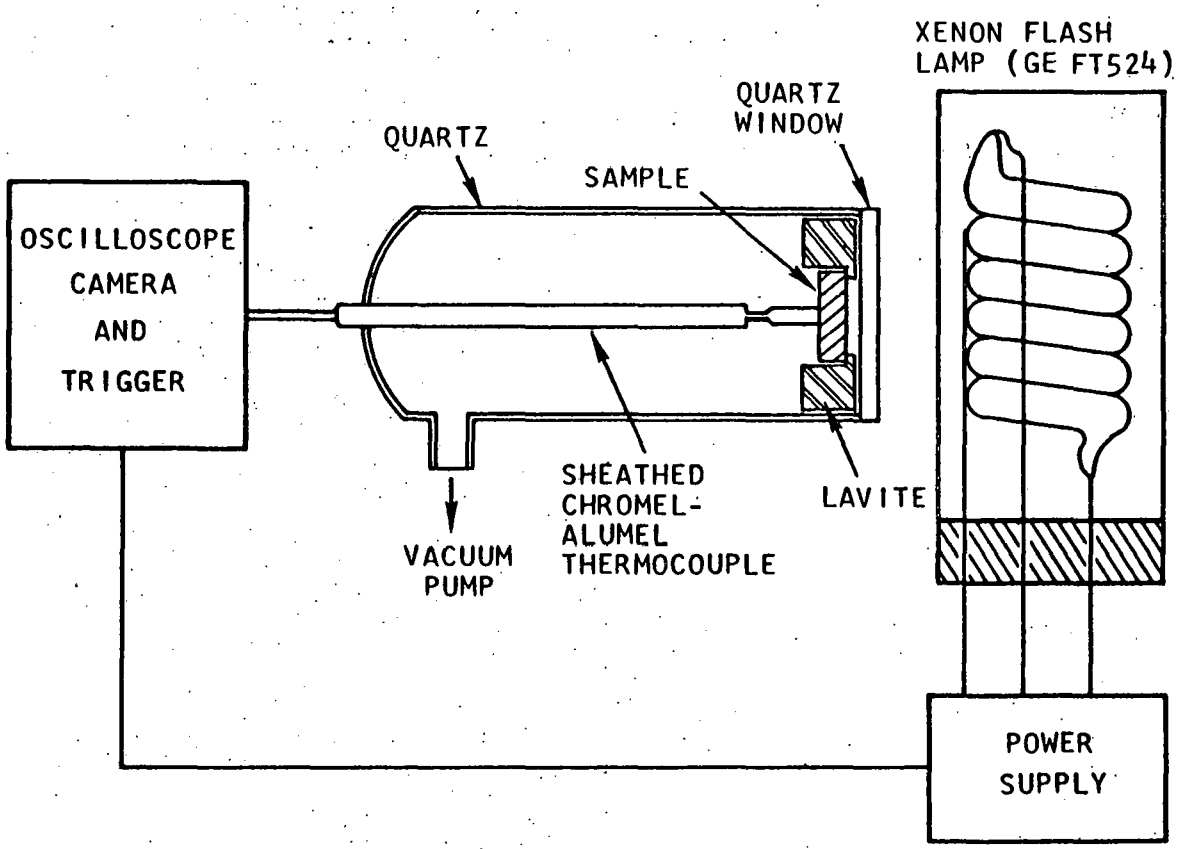

Fig. 25--Schematic diagram of the thermal-diffusivity apparatus

results are shown in Table 7. The corrected values were within 10% of the thermal diffusivity reported in the literature.[7] The thinnest specimen (the worst case) required a correction of about a factor of 2.

A photograph of the oscilloscope display showing the temperature history of the rear surface of a pyrolytic-carbon specimen is presented in Fig. 26. The shape of the curve is in good agreement with the theoretical curve of Fig. 23. The pip near the start of the trace is caused by noise from the trigger circuit and serves as a convenient time base, t = 0, from which $t_{1/2}$ can be measured.

Thermal-diffusivity measurements at room temperature were made perpendicular to the deposition plane on specimens of pyrolytic carbon with laminar, isotropic, and granular structures. The results are listed in Table 8 and are shown graphically in Fig. 27. The thermal-conductivity values were 0.0011 to 0.0024 cal/cm-sec-°C in the laminar region, 0.018 to 0.030 cal/cm-sec°C for the isotropic structures, and 0.021 cal/cm-sec-°C for the granular structure. The conductivity for the laminar coatings was about an order of magnitude lower than that for the isotropic or granular coatings.

The thermal-conductivity value listed in Table 8 for each structure represents the average of at least three measurements, except the value for structure VI, which is the average of nine determinations. The value of the specific heat used in calculating the thermal conductivities was 0.25 cal/g-°C, which represents the average of room-temperature values found in engineering handbooks on pyrolytic carbon.[11, 12]

The flash technique was found to be an effective method of obtaining thermal-diffusivity and thermal-conductivity values on very thin specimens of pyrolytic-carbon coatings. The method is rapid and is able to accommodate the paper-thin specimens with very little breakage. The standard deviation of the method on a single sample for a single measurement is better than ±5%.

Comparison of the structural parameters and conductivities given in Table 8 shows a correlation of the thermal conductivity with the degree of preferred orientation. The relatively low conductivities of the oriented laminar deposits are most likely a consequence of the low conductivity perpendicular to the layer planes of the individual crystallites. The variations of conductivity within the laminar set also correlate with the degree of preferred orientation, with the most highly oriented deposit having the lowest conductivity. In the isotropic region (structures V, VI, and VII) the lowest conductivity was observed for the deposit with a small amount of preferred orientation, i.e., structure VI of Table 8.

Table 7

TEST OF METHOD FOR PULSE-LENGTH CORRECTION WITH COPPER SPECIMENS OF VARIOUS THICKNESSES
(Pulse duration was 130 to 230 μsec)

Thickness (mils)	Thermal Diffusivity (cm^2/sec)		
	Uncorrected	Corrected	From Literature[a]
59.3	1.06	1.06	1.07
38.0	0.93	1.03	1.07
16.2	0.90	0.97	1.07
7.0	0.48	0.99	1.07

[a] From Reference 7.

Table 8

THERMAL DIFFUSIVITY AND CONDUCTIVITY OF VARIOUS PYROLYTIC-CARBON COATINGS[a]

Structure	Bed Temp. (°C)	Density, ρ (g/cm^3)	L_c (Å)	Anisotropy Factor	Thermal Diffusivity, α (cm^2/sec)	Thermal Conductivity, K (cal/cm-sec-°C)
Laminar (I)	1400	2.11	41	3.5	0.0021	0.0011
Laminar (II)	1400	1.95	33	1.7	0.0049	0.0024
Laminar (III)	1400	1.51	25	1.9	0.0050	0.0019
Granular (IV)	1750	2.00	140	1.1	0.042	0.021
Isotropic (V)	1650	1.55	49	1.05	0.060	0.023
Isotropic (VI)	2000	2.00	145	1.3	0.036	0.018
Isotropic (VII)	1800	1.81	105	1.1	0.066	0.030

[a] Figure 27 is a graphic presentation of these data.

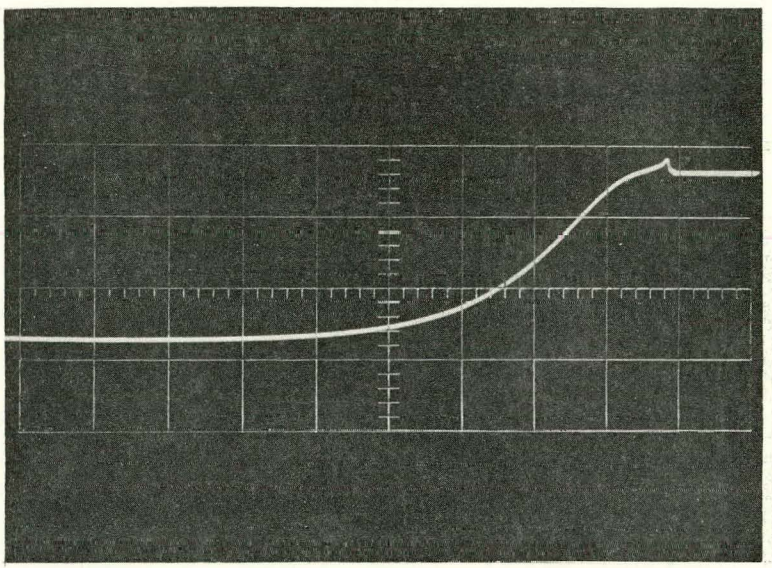

Fig. 26 -- Photographic trace of temperature rise on rear surface of a sample of pyrolytic carbon; reference baseline and trigger transient are left.

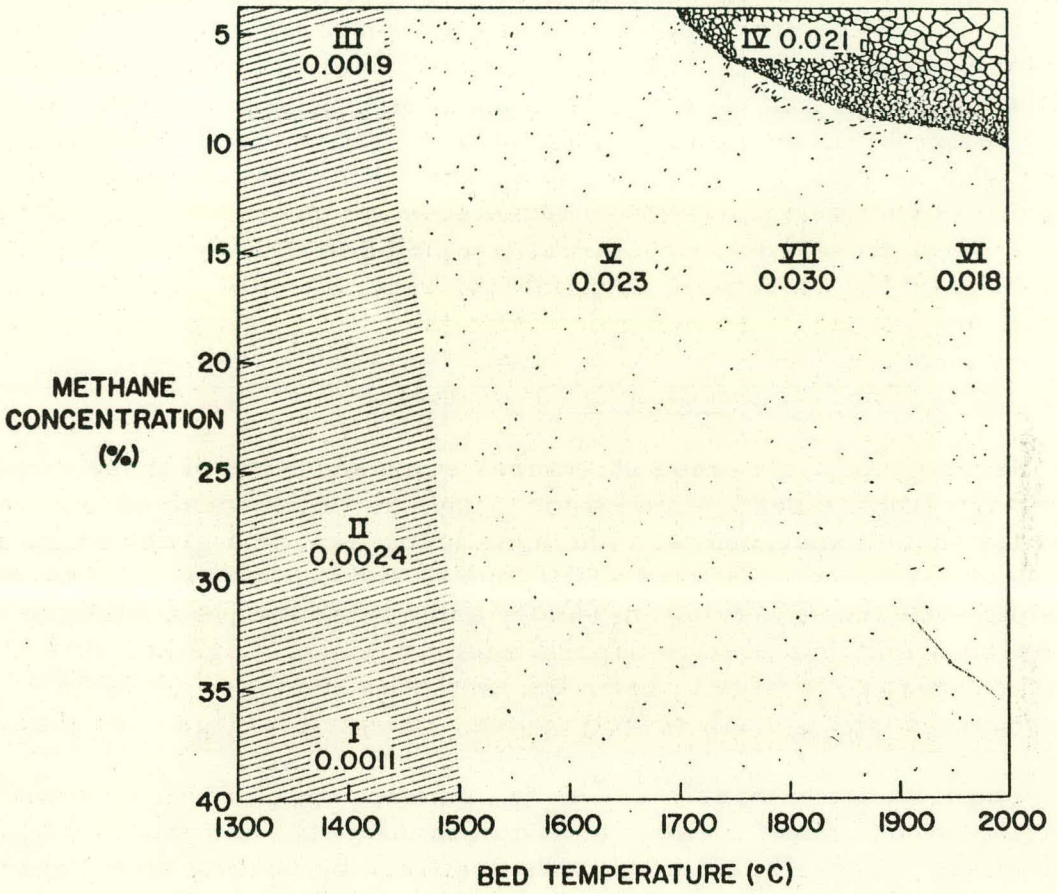

Fig. 27--Diagram showing thermal conductivity of various pyrolytic-carbon deposits; values measured at room temperature are in cal/cm-sec-^{o}C

Irradiation Effects in Pyrolytic Carbon

Previous work has shown that the structure of pyrolytic carbon can be varied over wide ranges of density, anisotropy, and apparent crystallite size.[1] These parameters depend on the mechanism by which the carbon is formed during pyrolysis and are determined by specific deposition conditions. Since the physical properties of pyrolytic-carbon deposits are structure-sensitive, the effects of fast-neutron irradiation may also be expected to be structure-sensitive; examination of irradiated coated fuel particles suggests that this is indeed the case. This portion of the work has therefore been devoted to a study of irradiation effects in pyrolytic carbon with specific reference to structure. Irradiation-induced dimensional changes, as well as the effects of irradiation on mechanical properties of various pyrolytic-carbon structures, are being measured. The effects of irradiation on the structural parameters, e.g., density and apparent crystallite size, are also being determined.

Irradiation-induced Dimensional Changes

Seven pyrolytic-carbon structures representative of those already characterized have been selected for study, and specimens have been prepared for these experiments. The structures include a granular structure, three laminar structures varying in density and anisotropy, and three isotropic structures varying in density and apparent crystallite size. The deposition conditions used to deposit each structure, together with the structural parameters that characterize them, are given in Table 9. Photomicrographs of each structure are presented in Figs. 28a through 28g.

The irradiation specimens were prepared in the form of small pyrolytic-carbon disks measuring 6 mm in diameter and from 60 to 130 μ in thickness. These specimens were prepared by coating small graphite disks in a fluidized bed together with the particle charge and then stripping the coatings from the disks. In all cases, the outer 25 to 35 μ of the coating surface was ground off in order to remove any surface inhomogeneity or roughness such at those visible in Figs. 28b or 28d. This technique has been described and discussed in Ref. 1.

In addition to unrestrained pyrolytic-carbon disks, graphite (HLM-85) disks coated with each structure were left intact for irradiation. Since the pyrolytic carbon is expected to shrink faster under irradiation than the graphite-disk substrate, the behavior of these "restrained" specimens should provide a measure of the ability of these structures to accommodate strain by means of irradiation-induced creep. Typical free and restrained specimens are shown in Fig. 29.

Table 9

DEPOSITION AND STRUCTURAL PARAMETERS OF SAMPLES PREPARED FOR CAPSULE IRRADIATION

		Deposition Conditions							As-deposited Structural Parameters		
Specimen Designation and Number	Bed Temp. (°C)	Methane Conc. (%)	Bed Surface Area (cm^2)	Charge Weight (g)	Particle Size (μ)	Total Flow (cm^3/min)	Average Deposition Rate (μ/hr)	Coater Diam. (cm)	Density (g/cm^3)	Bacon Anisotropy Factor	L_c (Å)
Laminar I	1,400	40	400	15	150-250	2,750	24	2.5	2.11-2.12	3.5	43
Laminar II	1,400	28	400	15	150-250	2,780	20	2.5	1.92-1.96	1.7	32
Laminar III	1,400	5	400	15	150-250	2,400	9.1	2.5	1.50-1.52	1.9	27
Granular IV	1,730	3.0	130	10	420-495	3,300	15	2.5	2.00-2.02	1.1	140
Isotropic V	1,650	15	400	34	420-495	4,600	89	2.5	1.54-1.56	1.05	49
Isotropic VI	2,000	14.7	2,600	186	350-420	13,500	25	6.3	1.99-2.01	1.3	145
Isotropic VII	1,800	14.7	2,600	186	350-420	13,500	22	6.3	1.81-1.82	1.1	105

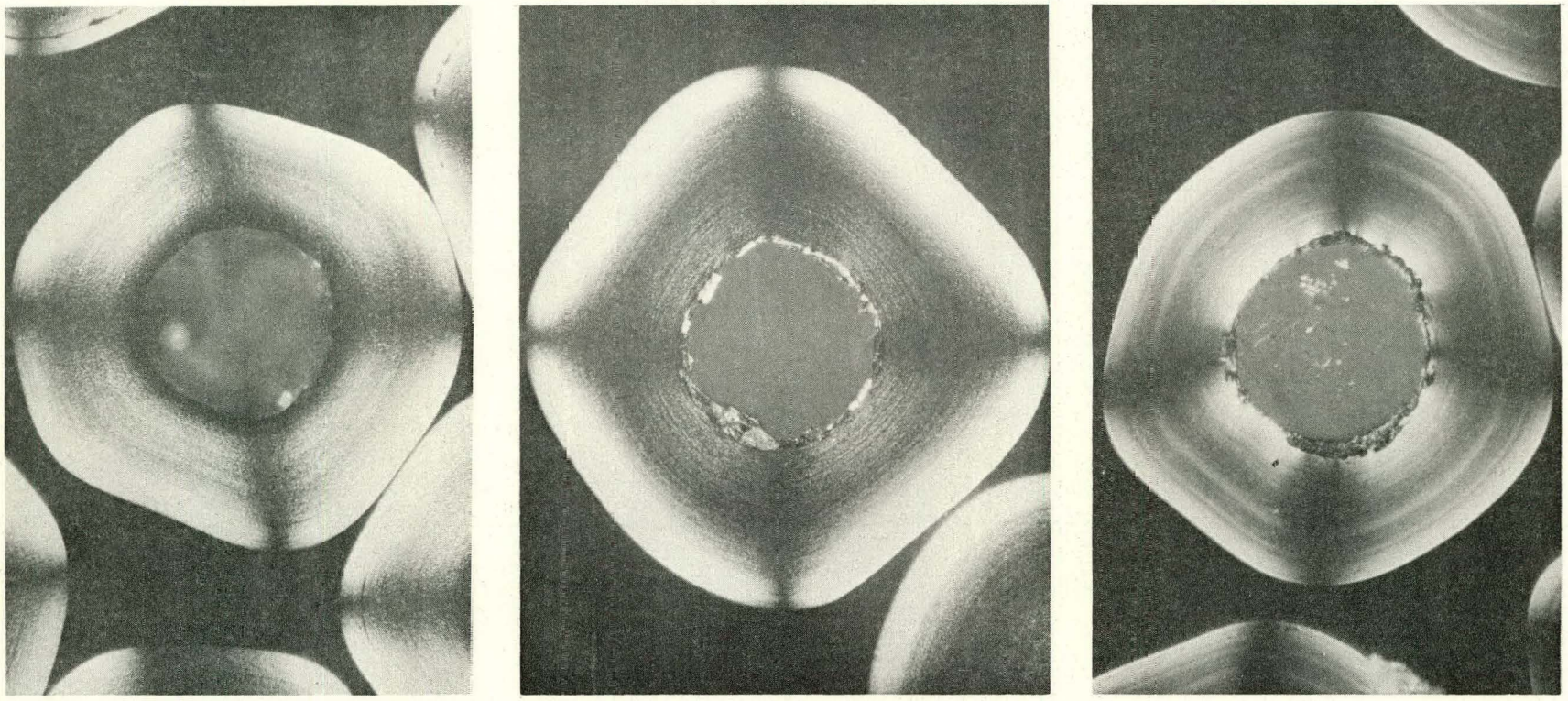

M-8980-3 (150×) M-8980-2 (150×) M-8980 (150×)

(a) Laminar I (b) Laminar II (c) Laminar III

Fig. 28--Photomicrographs of the seven structures selected for irradiation (polarized light)

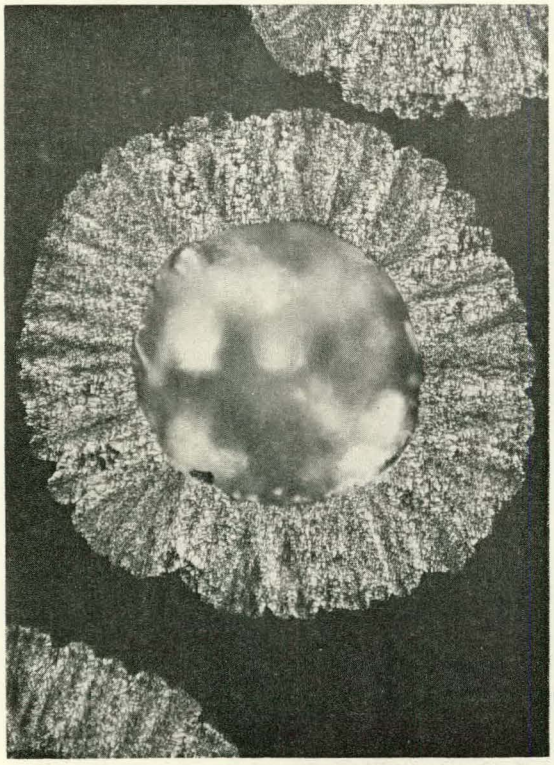

M-8980-4 (150×)

(d) Granular IV

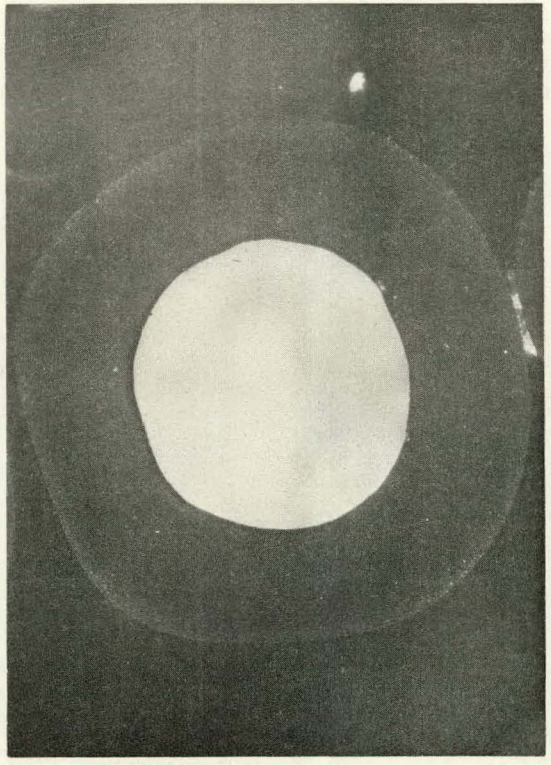

M-8980-6 (150×)

(e) Isotropic V

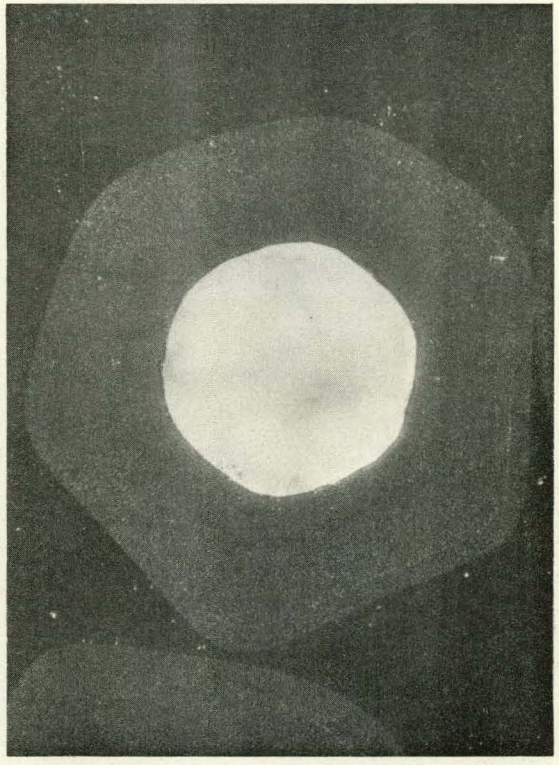

M-8980-7 (150×)

(f) Isotropic VI

Fig. 28(continued)

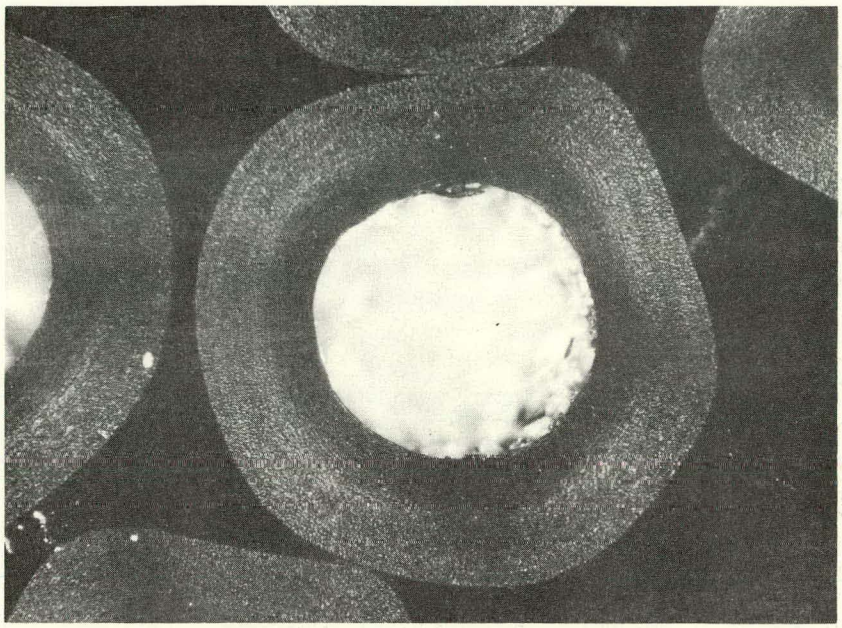

M-8980-5 (150×)

(g) Isotropic VII
Fig. 28 (continued)

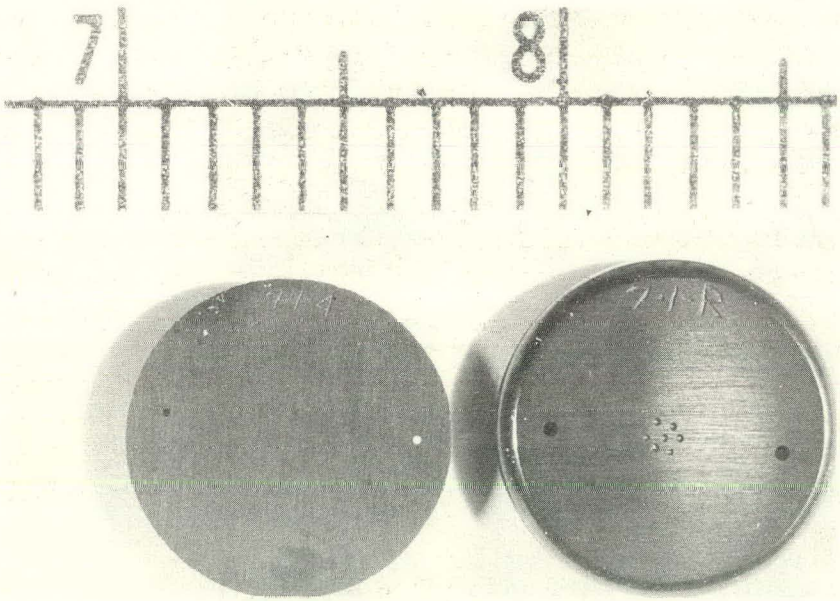

M-8616

Fig. 29--Typical pyrolytic-carbon irradiation specimens: left, free specimen; right, restrained specimen (scale in centimeters).

Since three of these structures (the laminar deposits) were deposited at temperatures below those commonly used for subsequent fuel-element processing, in practice they often are irradiated in an annealed condition. Exposure to temperatures usually encountered in processing is known to produce significant annealing effects, such as dimensional and mechanical-property changes;[5] therefore, the laminar structures in Table 9 have been prepared for irradiation in both the annealed (4 hr at 1900°C) and as-deposited conditions.

In order to explore the influence of graphitization on the irradiation-induced dimensional changes in pyrolytic carbon, specimens of four of the structures were annealed for 2 hr at 2800°C. The density and dimensional changes resulting from this anneal proved to be quite structure-sensitive, as did the degree of graphitization achieved. These data are summarized in Table 10. The layer spacing of all four structures was 3.44 Å or larger before the anneal; after the anneal the spacings varied from 3.35 to 3.40 Å. The degree of graphitization of the laminar structures deposited at 1400°C varies systematically with the methane concentration used in their preparation and consequently is correlated with the initial density and anisotropy. Further details are given in the section on the effects of annealing on the mechanical properties of laminar deposits.

The irradiation capsule* contains five separate cells, each of which contains two thermocouples. The measured temperatures and expected doses for each cell are shown in Table 11. Even though the temperatures of each cell will vary somewhat during the irradiations, all specimens, because of the small volume they occupy, will experience the same temperature history and will receive the same dose. This will allow direct comparison of all specimens exposed within a given cell.

The irradiation-induced dimensional changes in the plane of the disk-shaped specimens are to be determined by measuring the change in spacing of two 125-μ holes drilled near the ends of a diametral line (see Fig. 29). The spacing of these holes can be measured with a precision of 1 part in 10^4 with the aid of a toolmaker's microscope. These measurements, together with density measurements before and after irradiation (precise to 1 part in 2000), allow calculation of the dimensional changes perpendicular to the deposition surface. Since the density of a disk of thickness t and diameter d is

$$\rho = \frac{4\,(\text{mass})}{d^2 t \pi} \qquad (4)$$

or

$$\rho d^2 t = \text{constant}\,, \qquad (5)$$

*Irradiation of this capsule will be performed under Project Agreement No. 17 of Contract AT(04-3)-167.

Table 10

EFFECT OF 2-HR, 2800°C ANNEAL ON PYROLYTIC-CARBON STRUCTURES I, II, III, AND VI OF TABLE 9

Structure Designation	Specimen Number	Change in Diameter, Δd (%)	Change in Density, $\Delta\rho$ (%)	Change in Thickness [a] Δt	Initial C_o (Å)	Final C_o (Å)
Laminar I	1-1-1-G	+0.47	+4.33	-5.3	3.43	3.346
	1-1-2-G	+0.48	+4.18	-5.1	-----	-----
	1-1-4-G	+0.57	(b)	-----	-----	-----
Laminar II	2-1-1-G	+0.22	+6.33	-6.8	3.45	3.370
	2-1-2-G	-----	+6.32	-----	-----	-----
	2-1-3-G	+0.35	-----	-----	-----	-----
Laminar III	3-1-1-G	-----	+4.51	-----	3.43	3.398
	3-1-2-G	+1.28	+5.03	-7.6	-----	-----
	3-1-3-G	+1.48	-----	-----	-----	-----
Isotropic VI	6-1-1-G	+0.11	0.00	-0.22	3.43	3.404
	6-1-2-G	+0.14	0.00	-0.28	-----	-----
	6-1-3-G	+0.10	-----	-----	-----	-----
	6-1-4-G	+0.09	-----	-----	-----	-----

[a] Calculated from $(2\Delta d/d) + (\Delta t/t) + (\Delta\rho/\rho) = 0$.
[b] Not measured.

Table 11

IRRADIATION PARAMETERS AND SAMPLE DISTRIBUTION FOR IRRADIATION

Cell No.	Mean Measured Temp.[a] (°C)	Estimated Terminal Exposure (fast nvt $\times 10^{21}$)	Number of Specimens of Each Type in Each Cell				
			I-VII As-deposited		I-III Heat-treated		VI Graphitized
			Free	Restrained	2 Hr at 2800°C	4 Hr at 1900°C	
1	550	2.0	4 each	1 each	4 of Types I and III 3 of Type II	None	4 each
2	600	2.6	4 each	1 each	None	4 of each type	4 each
3	980	2.9	4 each	1 each	3 of Type I	None	4 each
4	1030	3.1	4 each	1 each	None	4 of each type	4 each
5	1030	3.5	4 each	1 each	3 of Types I and II 2 of Type III	None	4 each

[a] Mean temperature recorded by thermocouples over the first four irradiation cycles.

the changes in dimension and density due to irradiation are related by

$$\frac{\Delta t}{t} + \frac{\Delta \rho}{\rho} + \frac{2\Delta d}{d} = 0 \quad . \tag{6}$$

The values of $\Delta t/t$ and $\Delta d/d$ are expected to be of the order of 10^{-2}, so changes in $\Delta t/t$ can easily be measured with a precision of 5×10^{-4}.

The diametral changes of the disks for the various structures are of immediate interest to coating designers. In addition, however, considerable basic data that describe the average intrinsic distortion rates of the individual crystallites, β_a and β_c (see Ref. 13 for details of this analysis), may also be obtained if accurate thickness changes $\Delta t/t$ are available. The data obtained in these experiments should yield valuable information relating β_a and β_c to the structural parameters and should provide a test of the usefulness of the model (described in Ref. 13) for the rationalization of irradiation-induced dimensional changes in pyrolytic carbon and graphite.

The capsule has now successfully completed five cycles of a scheduled six-cycle irradiation and is due to be discharged in April.

Influence of Irradiation on Mechanical Properties

The mechanical properties of pyrolytic carbon are of considerable importance in fuel-element design. Work already described elsewhere in this report has shown that these properties are extremely structure-sensitive and, in some cases, respond significantly to heat treatment. It is expected, therefore, that the mechanical properties may be influenced by irradiation. In order to assess these effects, the pyrolytic-carbon disks, described in the previous section, will be cut into small strips and tested in bending. The data obtained from the irradiated specimens, when compared with those obtained from control specimens, will determine the magnitude of any irradiation effect.

Effect of Structure on Resistance to Uranium Migration Through Pyrolytic-carbon Coatings

A topical report entitled "Uranium Migration Through Pyrolytic Carbons Deposited in a Fluidized Bed" by J. C. Bokros and N. L. Sandefur[14] describes the dependence of uranium migration on structure. It was found that the high-density, oriented, laminar structures deposited at low temperatures from high methane concentrations were superior to all the rest in resisting uranium migration.

STUDIES OF COATINGS DEPOSITED AT TEMPERATURES ABOVE 1900°C

Effect of Coating Variables on the Structure of Pyrolytic Carbons

Experiments have been carried out to determine the structure of pyrolytic carbons deposited above 1900°C in a 3.5-cm-diameter coater. Three series of experiments have been completed, using 3%, 7%, and 15% methane in helium and making a run every 100°C in the range 1900° to 2400°C. The total flow was held constant at 18,000 cm^3/min (measured at 296°K and 1 atm), and the initial bed surface area in all cases was 1140 cm^2 (70 g of 300 to 420 μ UC_2 particles containing 10.1 to 10.5 wt-% carbon). The average coating rates are summarized in Table 12 and the coating efficiencies are given in Table 13.

Metallographic examination of these deposits revealed that the structures were either isotropic or granular. Formation of the granular structures occurred at low methane concentrations, high temperatures, and low bed surface areas. The bed areas at which the transition from granular to isotropic occurred are shown in Table 14.

The variation of layer spacing with deposition conditions (methane concentration and bed temperature) is shown in Table 15.

The densities of these carbons are reported in Table 16 and are plotted in Fig. 30 as a function of the bed temperature and methane concentration used in their preparation. Comparison of these data with the density data reported previously for deposits prepared in a 2.5-cm-diameter coater[1] shows good agreement at 1900°C. This good agreement is probably fortuitous, since it is known that structural data for carbons deposited in different coaters are, in general, not directly comparable. The intermediate "shoulder" in Fig. 30 is undoubtedly a consequence of the transition from a high-density granular structure to a lower-density isotropic structure during the coating run in this region of temperature, methane concentration, and bed surface areas.

The apparent crystallite sizes, L_c, of these carbons are given in Table 17 and are plotted in Fig. 31 as a function of the bed temperature and methane concentration used in their preparation. These data also show good agreement with those reported previously for carbons deposited in a 2.5-cm-diameter coater.[1]

Because of the large particle size of the charge used in these studies (70 g of 300 to 420 μ UC_2 particles), the bed surface area changes rather slowly with coating thickness and, as a result, the influence of the bed surface area on the formation of the granular deposits is clearly defined. Table 14 shows the bed surface areas at which the transition from a granular

Table 12

AVERAGE COATING RATE OF PYROLYTIC CARBONS DEPOSITED IN 3.5-CM-DIAMETER COATER

Bed Temp. (°C)	Average Coating Rate (μ/hr) for Carbon Deposits		
	From 3% CH_4	From 7% CH_4	From 15% CH_4
1900	36, 37, 34, 35[a]	55	79
2000	38	72	86
2100	31, 36, 37, 32, 36[a]	73	99
2200	36	71	---
2300	36	71	115
2400	51	93	110

[a] Results from duplicated runs.

Table 13

COATING EFFICIENCY DATA FOR 3.5-CM-DIAMETER COATER USING 1140-CM^2 INITIAL BED AREA AND TOTAL FLOW RATE OF 18,000 CM^3/MIN (AT 296°K AND 1 ATM)

Bed Temp. (°C)	Coating Efficiency (%)[a]		
	For 3% CH_4	For 7% CH_4	For 15% CH_4
1900	84, 85[b]	58	38
2000	----	77	45
2100	90	79	56
2200	----	81	--
2300	94	79	61
2400	95	82	60

[a] Coating efficiency is defined as the proportion of carbon originally present in the hydrocarbon gas that is deposited as coating on the fuel particles.

[b] Duplicated runs.

Table 14

BED SURFACE AREA AT WHICH TRANSITION FROM GRANULAR TO ISOTROPIC STRUCTURES OCCURRED
(Data are for 3.5-cm-diameter coater, using 18,000 cm^3/min total flow rate)

Bed Temp. (°C)	Bed Area (cm^2) at Transition		
	For 3% CH_4	For 7% CH_4	For 15% CH_4
1900	>5200	1900	<1140
2000	>4000	2600	1300
2100	>4400	2600	2200
2200	>4300	2900	----
2300	>4100	2800	2600
2400	>3900	>3100	3200

Table 15

LAYER SPACING OF PYROLYTIC CARBONS DEPOSITED IN 3.5-CM-DIAMETER COATER
(Measurements from (002) reflection (CuK_α))

Bed Temp. (°C)	Layer Spacing (Å) for Carbon Deposits		
	From 3% CH_4	From 7% CH_4	From 15% CH_4
1900	3.42	3.43	3.42
2000	3.43	3.43	3.43
2100	3.42	3.42	3.43
2200	3.42	3.42	----
2300	3.42	3.42	3.42
2400	3.43	3.42	3.42

Table 16

DENSITIES OF CARBONS DEPOSITED AT 1900° TO 2400°C FROM METHANE IN A 3.5-CM-DIAMETER COATER

Temperature of Bed (°C)	Density (g/cm^3) of Carbon Deposited		
	From 3% CH_4	From 7% CH_4	From 15% CH_4
1900	1.97, 1.97[a]	1.68	1.61
2000	2.02, 2.02[a]	1.78	1.67
2100	2.02, 2.03[a]	1.91	1.79
2200	2.06	1.93	----
2300	2.08	1.90	1.77
2400	2.09	2.12	1.89

[a] Duplicate runs.

Table 17

APPARENT CRYSTALLITE SIZE, L_c, FOR PYROLYTIC CARBONS DEPOSITED FROM 3%, 7%, AND 15% METHANE AT 1900° TO 2400°C IN A 3.5-CM-DIAMETER COATER

Temperature of Bed (°C)	L_c (Å) of Carbon Deposited		
	From 3% CH_4	From 7% CH_4	From 15% CH_4
1900	102, 115, 103[a]	64	54
2000	124	76	54
2100	134, 128[a]	102	80
2200	154	107	---
2300	135	118	100
2400	168	161	115

[a] Duplicate runs.

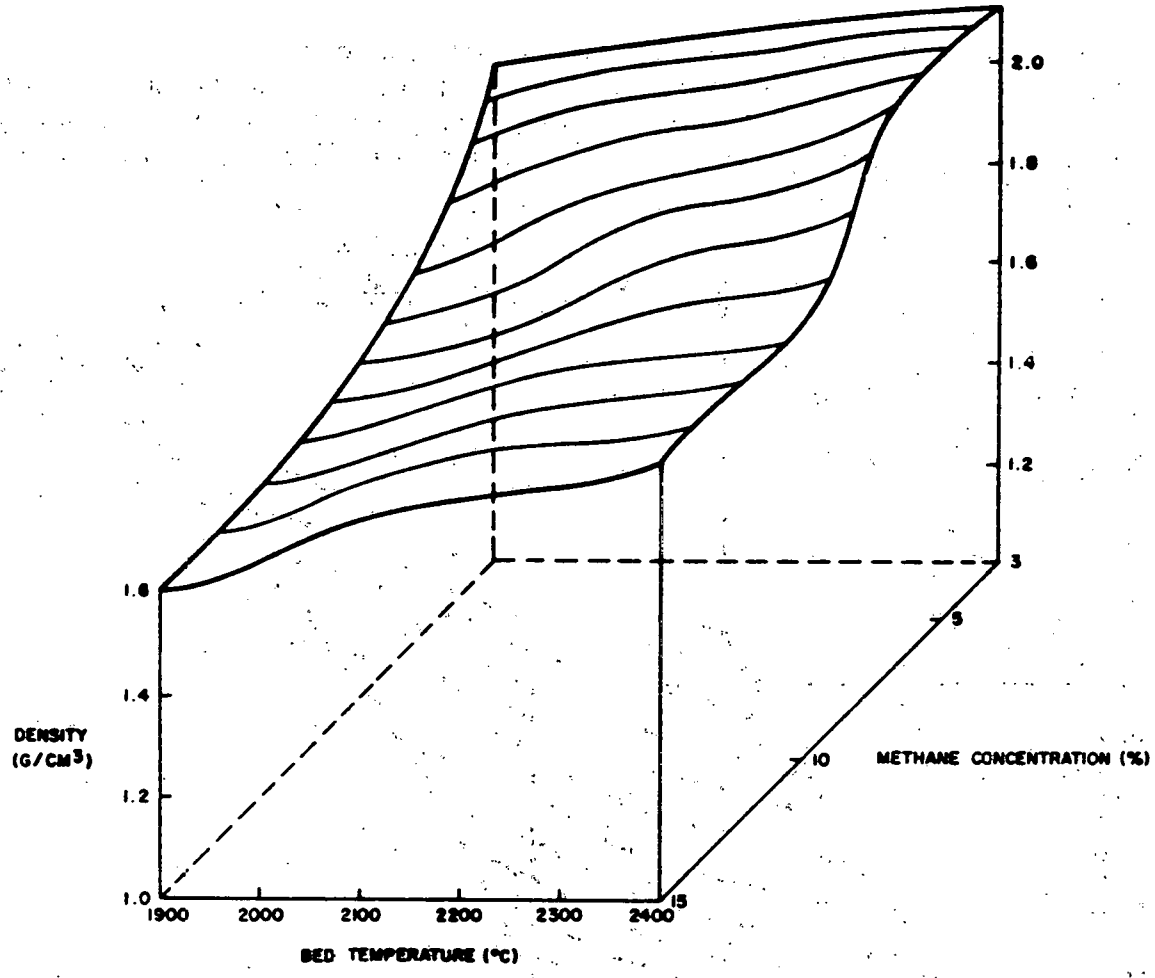

Fig. 30--Density of carbons deposited in a 3.5-cm-diameter coater plotted as a function of the bed temperature and methane concentration used in their preparation. Total flow was 18,000 cm^3/min (at 23°C and 1 atm) and the initial bed surface area was 1140 cm^2.

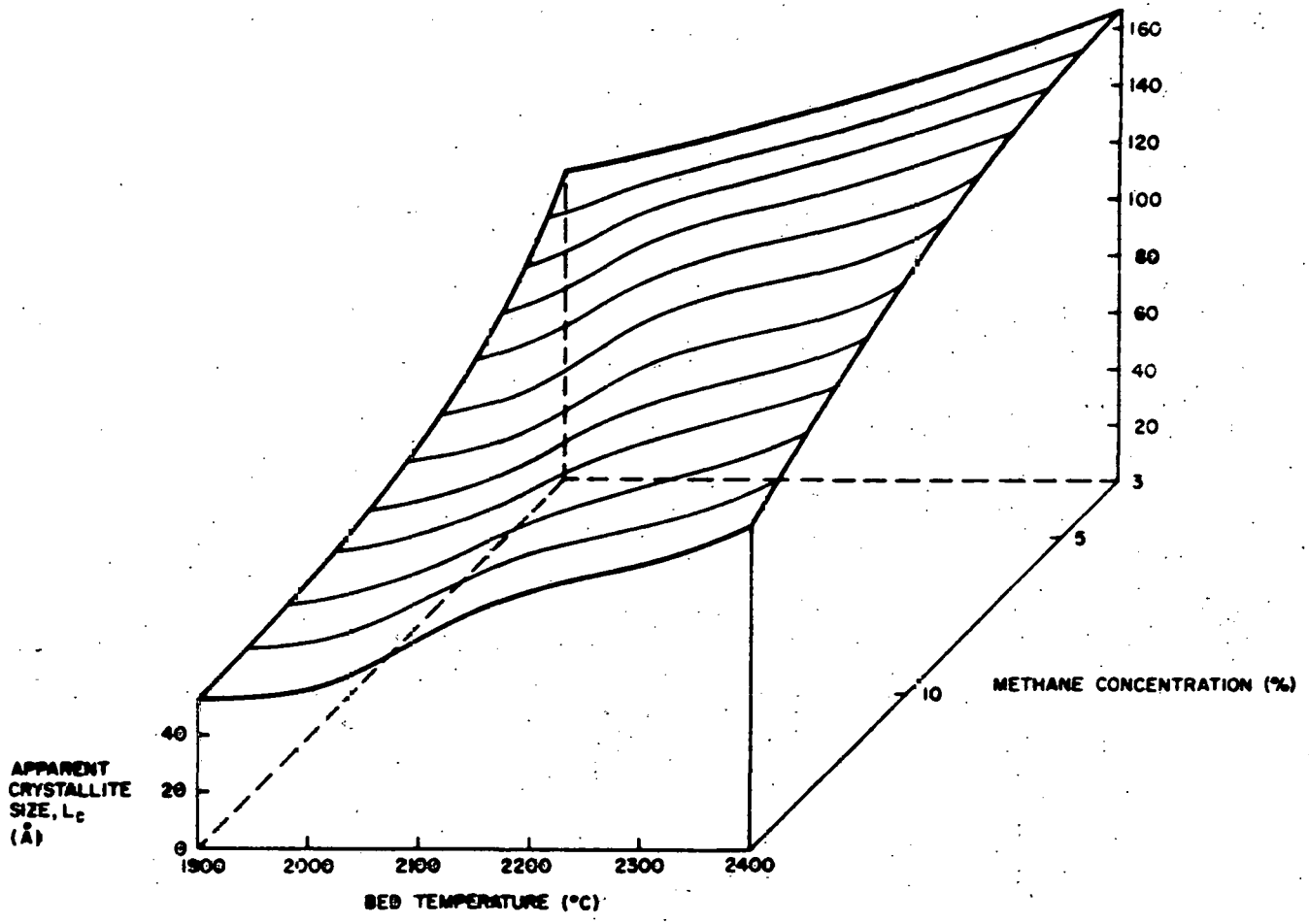

Fig. 31--Apparent crystallite sizes, L_c, of carbons deposited in a 3.5-cm-diameter coater plotted as a function of the bed temperature and methane concentration used in their preparation. The total flow was 18,000 cm^3/min (at 23°C and 1 atm) and the initial bed surface area was 1140 cm^2.

to isotropic structure occurs for various combinations of bed temperature and methane concentration. These data, together with metallographic results, were used to construct the schematic diagram shown in Fig. 32. This diagram shows that low methane concentrations and high temperatures favor the granular deposits and that for a given methane concentration and bed temperature, the granular deposits are most likely to form when small surface areas are used. These results are consistent with results previously reported for a 2.5-cm-diameter coater and lower deposition temperatures.

Metallographic examination of the carbons deposited from 3% methane shows a decrease in grain size* with increasing temperature and a gradual increase in anisotropy (Fig. 33). As the anisotropy increases (with deposition temperature), the granular structure becomes obscure and the deposits take on a laminar appearance. Distinctly laminar structures deposited at 2000°C from 2.7% methane in a 6.3-cm-diameter coater were observed in earlier work. (1)

Mechanical Properties of Pyrolytic Carbons

Measurements have been made of the mechanical properties of pyrolytic carbon deposited in a 3.5-cm-diameter coater between 1900° and 2400°C from helium containing 3%, 7%, and 15% methane, using a charge of 70 g of 300 to 420 μ diameter UC_2 particles (initial surface area 1140 cm^2) and a total flow rate of 18,000 cm^3/min. Coating rates and efficiencies are reported in Tables 12 and 13. The samples had microstructures that cover the transition from isotropic to granular and included a range of granular structures of different densities and anisotropies. In several samples, the microstructure was granular at the start of the coating run but turned to isotropic before the end of the run. In such cases, extra sets of mechanical-property samples were made and a series of bend tests was made with either the granular or the isotropic face of the sample in tension.

All the samples deposited from 3% methane had fully granular structures. The densities and anisotropies increased steadily with deposition temperature (see the section on the structure of pyrolytic carbons deposited above 1900°C). The mechanical properties (mean and maximum flexural elastic modulus, fracture stress, and fracture strain) are plotted in Fig. 34. The error bands on the figure refer to the standard deviation of the determinations. There were no significant differences between the properties of samples tested with the inside of the deposit in tension and those tested with the outside in tension. There is a systematic

*These grains are those visible metallographically using polarized light and should not be confused with the apparent crystallite size measured by X-ray diffraction.

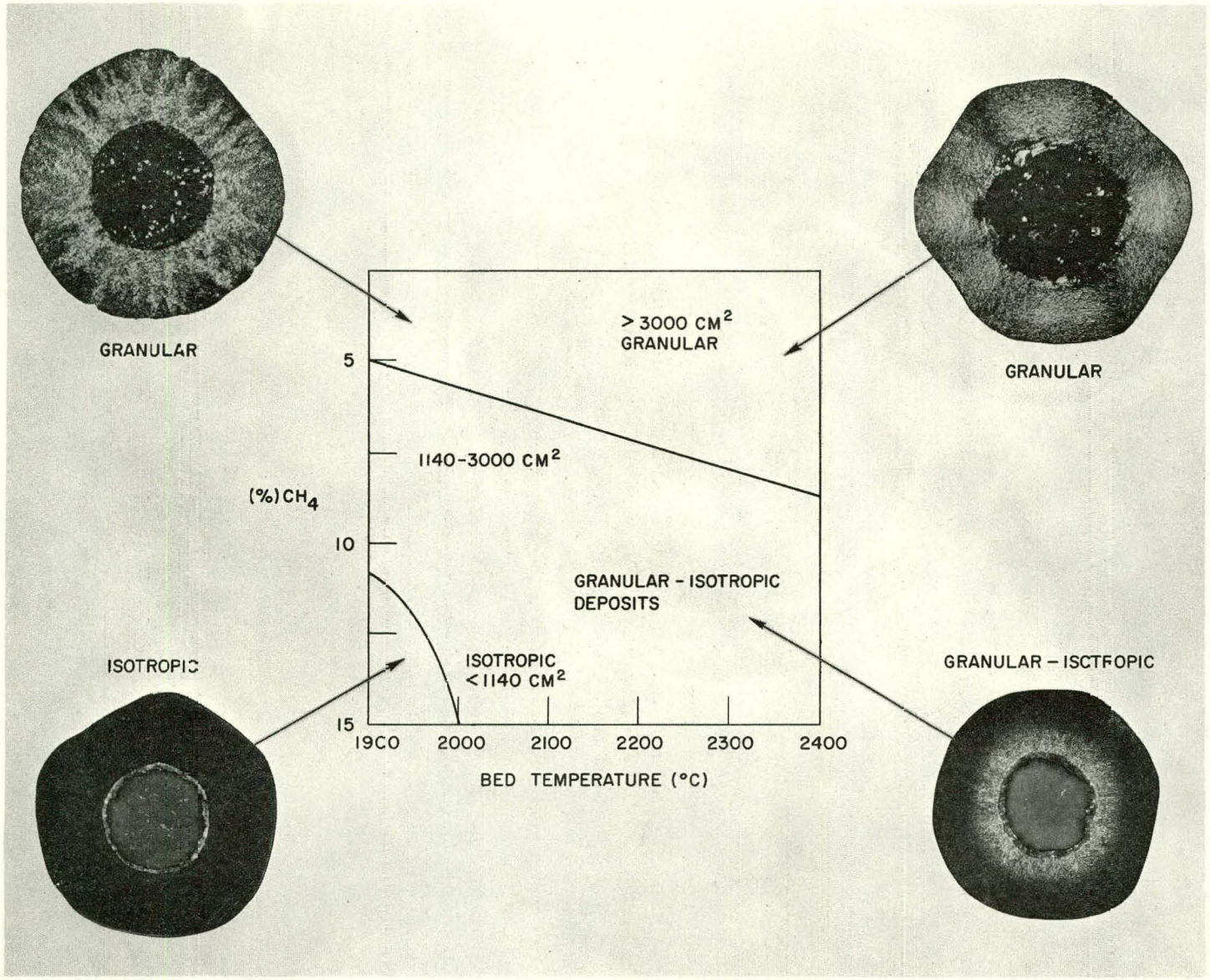

Fig. 32--Schematic representation of the metallographic appearance of carbons deposited in a 3.5-cm-diameter coater using a total flow of 18,000 cm^3/min (at 23°C and 1 atm) and an initial bed surface area at which the transition from a granular to an isotropic structure occurs.

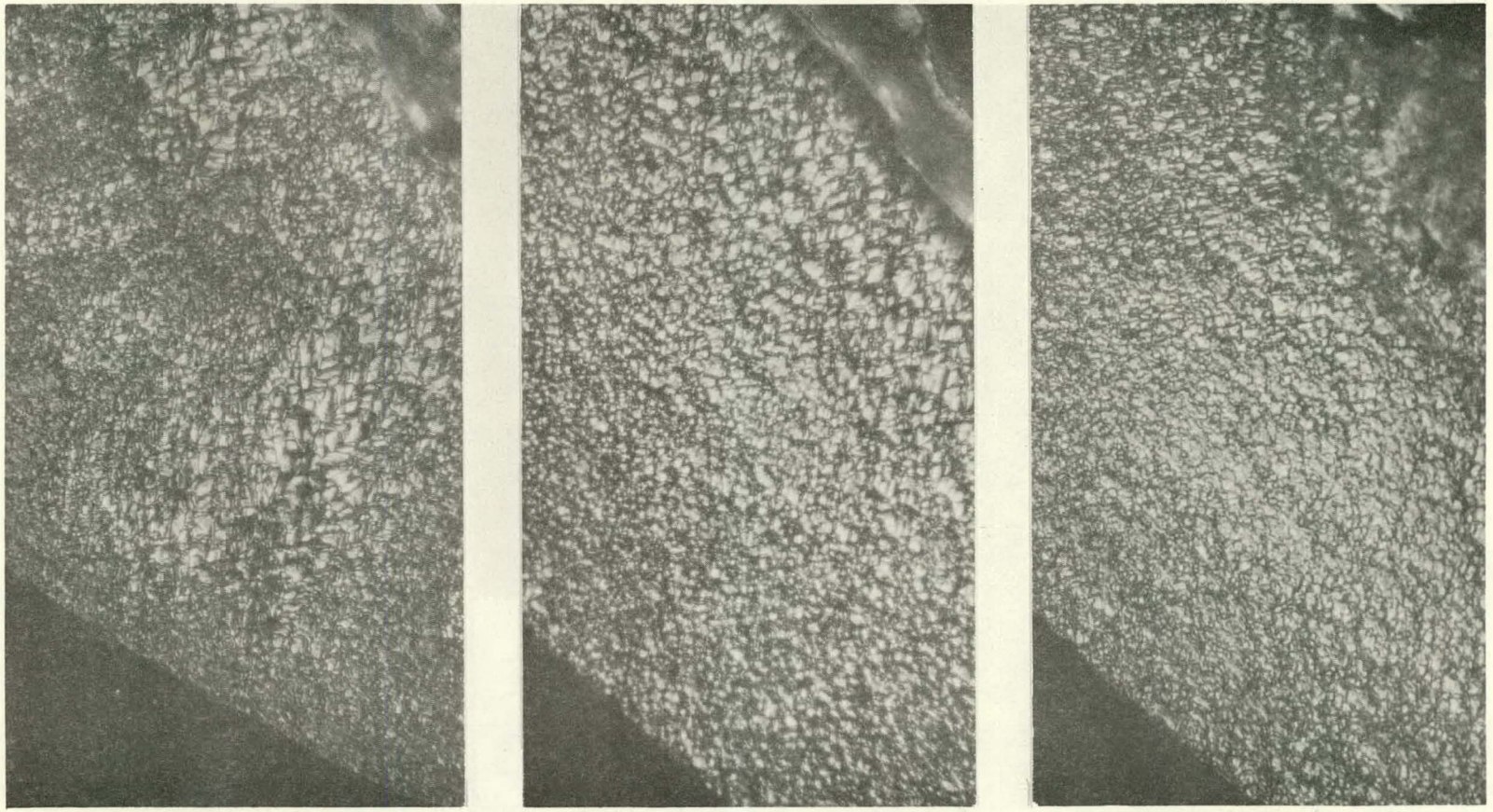

M-10904-1 (500x) (a)

M-10900-1 (500x) (b)

M-10903-1 (500x) (c)

Fig. 33--Photomicrographs of carbons deposited from 3% methane in a 3.5-cm-diameter coater at (a) 1900°C, (b) 2200°C, and (c) 2400°C. The total flow rate was 18,000 cm^3/min (at 23°C and 1 atm) and the initial charge area was 1140 cm^2.

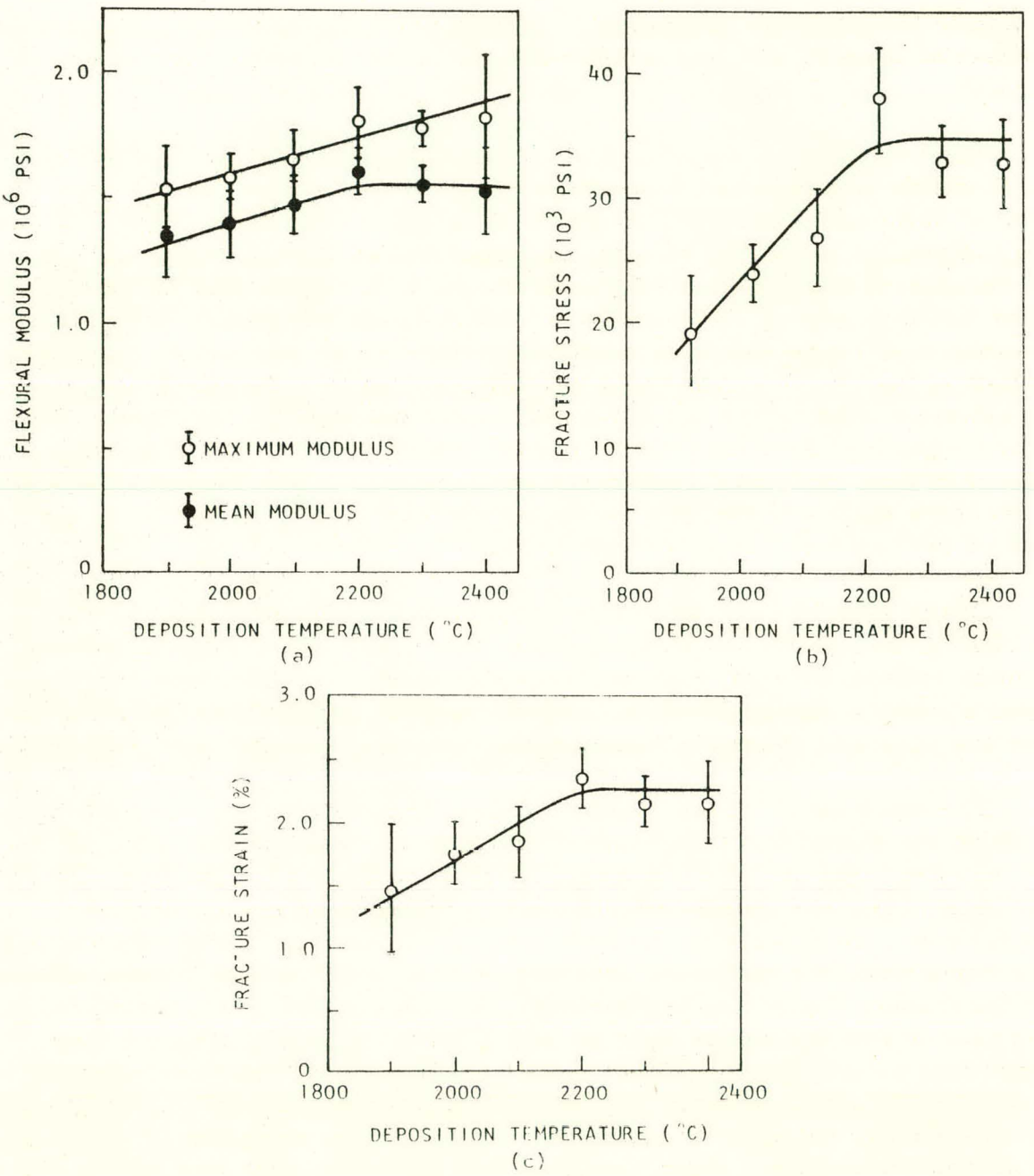

Fig. 34--Dependence of mechanical properties on deposition temperature for deposits produced in a 3.5-cm-diameter coater, using 3% methane in helium and a 1140-cm^2 (70-g) charge of UC_2 particles: (a) room-temperature flexural modulus; (b) maximum fiber stress at fracture; (c) maximum fiber strain at fracture.

increase in elastic modulus, fracture stress, and fracture strain as the deposition temperature increases. This is probably caused by the parallel increase in density and anisotropy over the same deposition temperature range.

The mechanical properties of carbons deposited from 7% methane are shown as a function of deposition temperature in Fig. 35. Of this group of samples, the microstructure of samples deposited at 1900°C was fully isotropic, while that of samples deposited at 2400°C was fully granular. The remainder had a mixed microstructure, with a granular microstructure on the inside changing to an isotropic structure at the outside of the deposit. Nevertheless, there was no systematic difference in properties according to whether the inside or the outside of the deposit was stressed in tension. The elastic moduli of the samples with isotropic or mixed microstructures showed a gradual decrease with increasing temperature, whereas the fracture stress remained approximately constant. Both the modulus and the fracture stress of the fully granular structure were much lower than those of the isotropic or mixed structures.

Of the samples prepared from 15% methane, those made at 1900° and 2000°C were fully isotropic and the rest contained a transition from granular to isotropic microstructure. The elastic modulus and fracture stress showed a steady decrease with increasing deposition temperature, while the fracture strain remained approximately constant (see Fig. 36).

The dependence of the mean modulus, fracture stress, and fracture strain on the deposition temperature and methane partial pressure is shown in the form of three-dimensional plots in Fig. 37, together with an indication of the microstructure of each of the sample groups tested. Several conclusions may be drawn. Among samples with a purely granular microstructure, the modulus, fracture stress, and fracture strain increase with increasing deposition temperature, the increase corresponding to increases in density and anisotropy and a decrease in grain size. The occurrence of very low moduli (1 to 1.3×10^6 psi) and fracture stresses (15 to 20×10^3 psi) seems to be limited to a narrow band of coarse-grained, low-anisotropy, granular structures. The fine-grained granular material that forms immediately after the transition from the isotropic microstructure has the same strength (30×10^3 psi) as the isotropic structures, as shown by tests where samples with a transition microstructure were tested with either the inside or the outside of the deposit in tension. Among the isotropic and transition structures there is a slight decrease in modulus and fracture stress with increasing deposition temperature. It is interesting to note that the surfaces representing mechanical properties versus deposition temperature and methane pressure (Fig. 37) form almost continuous extensions of the surfaces based on samples made at lower temperatures in a different (2.5-cm-diameter) coater.

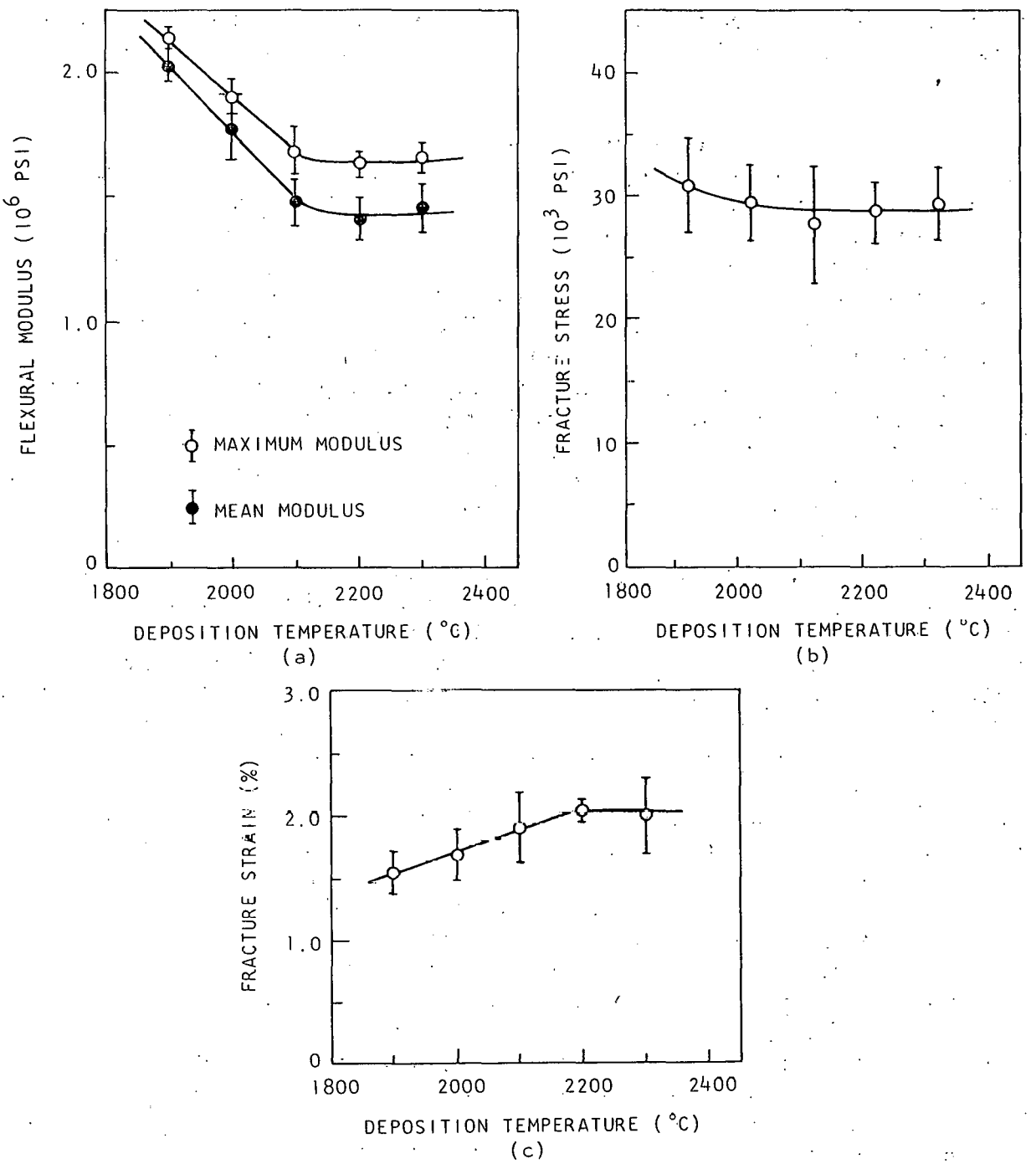

Fig. 35--Dependence of mechanical properties on deposition temperature for deposits produced in a 3.5-cm-diameter coater, using 7% methane in helium and a 1140-cm^2 (70-g) charge of UC^2 particles: (a) room-temperature flexural modulus; (b) maximum fiber stress at fracture; (c) maximum fiber strain at fracture.

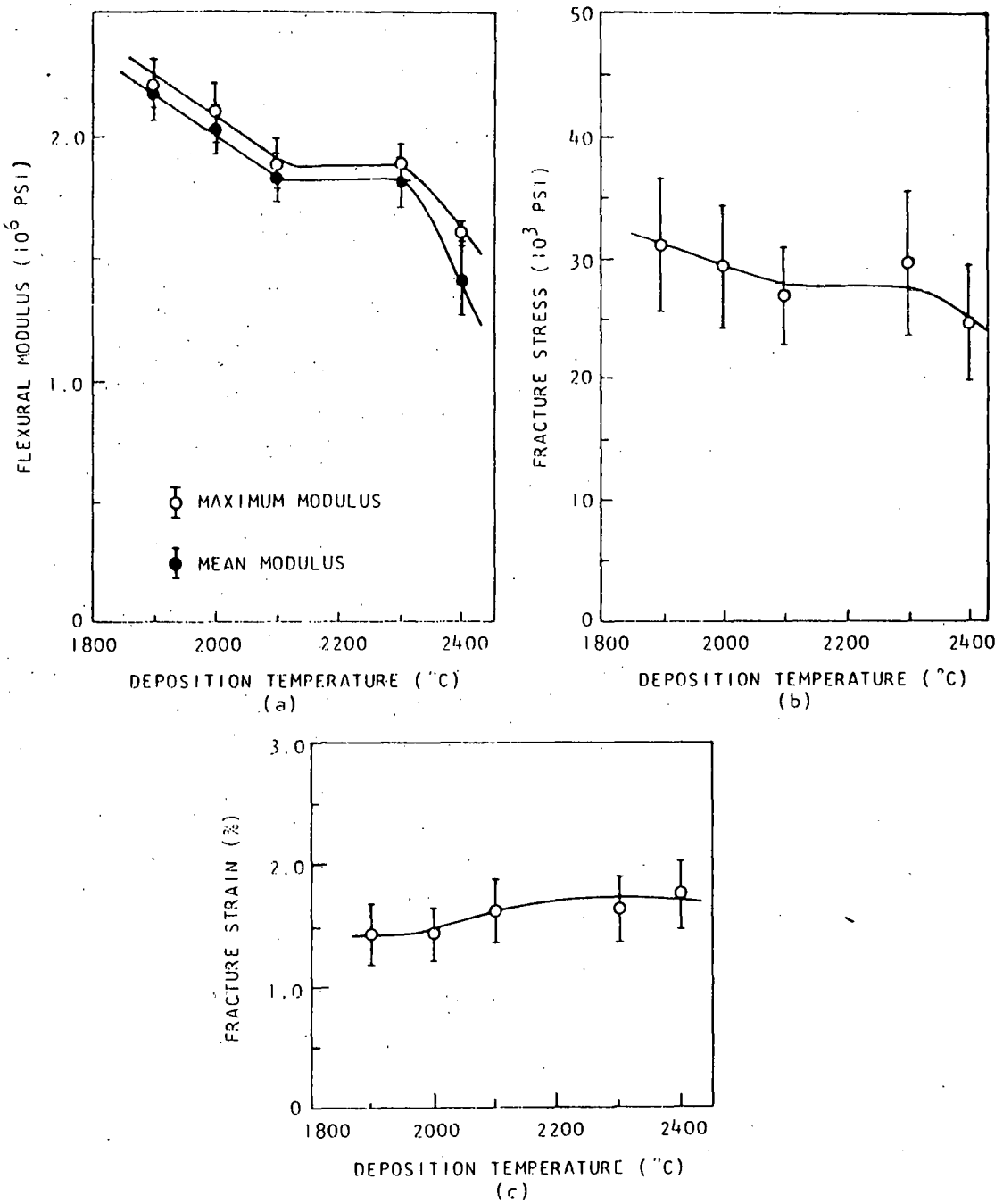

Fig. 36--Dependence of mechanical properties on deposition temperature for deposits produced in a 3.5-cm-diameter coater, using 15% methane in helium and a 1140-cm^2 (70-g) charge of UC_2 particles; (a) room-temperature flexural modulus; (b) maximum fiber stress at fracture; (c) maximum fiber strain at fracture.

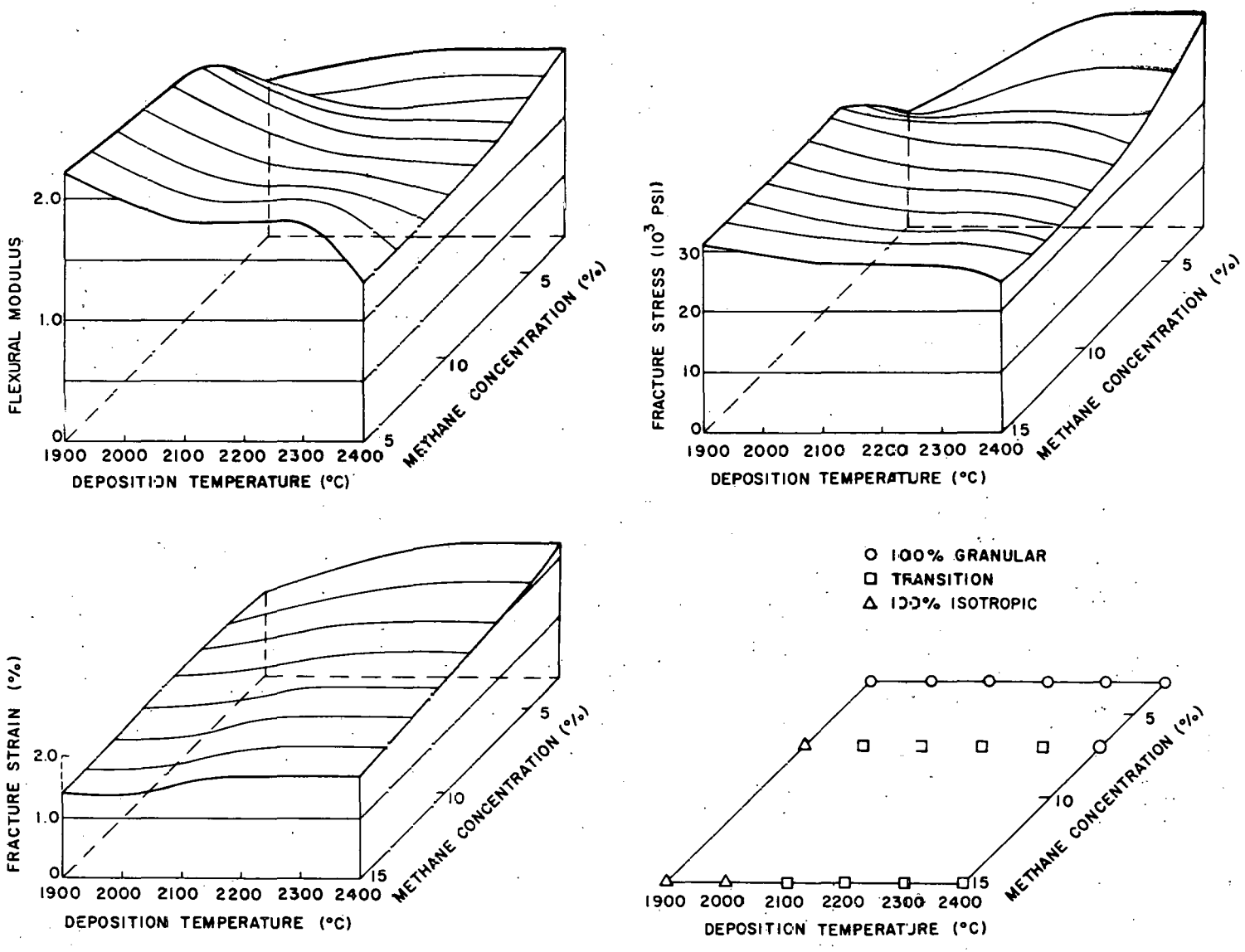

Fig. 37--Diagrams relating mechanical properties of pyrolytic-carbon deposits to deposition conditions; deposits were prepared in a 3.5-cm-diameter coater using 1140-cm^2 initial charge surface area: (a) mean flexural modulus; (b) fracture stress; (c) fracture strain; (d) microstructural type of deposits tested.

This work has been summarized in a topical report entitled "Structure and Properties of Pyrolytic Carbon Prepared in a Fluidized Bed Between 1900°C, and 2400°C."(15)

Effect of Structure on the Thermal Conductivity of Pyrolytic Carbons

The thermal diffusivities of the carbons described in the preceding section have been measured in a direction perpendicular to the deposition plane using the flash technique described in an earlier section of this report. From these data, the thermal conductivities were calculated using measured densities and a specific heat of 0.25 cal/g-°C. These results, which are presented in Table 18, show that the carbons deposited from 15% methane have higher thermal conductivities than the granular deposits formed from 3% methane. The gradual decrease in thermal conductivity with increasing deposition temperature for the carbons deposited from 3% methane is most likely due to the increase in anisotropy in this series.

Table 18

ROOM-TEMPERATURE THERMAL CONDUCTIVITY[a] (CAL/CM-SEC-°C) OF CARBONS DEPOSITED AT 1900° TO 2400°C FROM METHANE IN A 3.5-CM-DIAMETER COATER

Temperature of Bed (°C)	Thermal Conductivities for Carbon Deposited		
	From 3% CH_4	From 7% CH_4	From 15% CH_4
1900	1.7×10^{-2}	2.1×10^{-2}	3.0×10^{-2}
2000	1.6×10^{-2}	2.6×10^{-2}	2.4×10^{-2}
2100	1.6×10^{-2}	2.4×10^{-2}	4.1×10^{-2}
2200	1.2×10^{-2}	3.3×10^{-2}	----
2300	1.4×10^{-2}	2.2×10^{-2}	3.0×10^{-2}
2400	1.4×10^{-2}	1.6×10^{-2}	3.4×10^{-2}

[a] Calculated from the thermal diffusivity using a specific heat of 0.25 cal/g-°C.

REFERENCES

1. Bokros, J. C., "The Structure of Pyrolytic Carbons Deposited in a Fluidized Bed," to be published in Carbon (General Atomic Report GA-5163, June, 1964).

2. Franklin, R., "The Interpretation of Diffuse X-ray Diagrams of Carbon," Acta. Cryst. 3, 107 (1950).

3. Bokros, J. C., "Absorption Factors for a Modified Bacon Preferred Orientation Technique," submitted to Carbon (General Atomic Report GA-6031, January, 1965).

4. Bokros, J. C., "Variations in the Crystallinity of Carbons Deposited in Fluidized Beds," submitted to Carbon (General Atomic Report GA-6050, April 1, 1965).

5. Bokros, J. C., et al.,"Advanced, Graphite-Matrix, Dispersion-Type Fuel Systems. Annual Report, April 1, 1963, Through March 31, 1964," USAEC Report GA-5016 (Part I), General Atomic Division of General Dynamics Corporation.

6. Bokros, J. C., and R. J. Price, "Deformation and Fracture of Pyrolytic Carbons Deposited in Fluidized Beds," General Atomic Report GA-6332 (in preparation).

7. Parker, W. J., et al., "Flash Method of Determining Thermal Diffusivity, Heat Capacity, and Thermal Conductivity," J. Appl. Phys. 32, 1679 (1961).

8. Rudkins, R. L., R. J. Jenkins, and W. J. Parker, "Thermal Diffusivity Measurements on Metals at High Temperatures," Rev. Sci. Instr. 33, 21 (1962).

9. Deems, H. W., and W. D. Wood, "Flash Thermal Diffusivity Measurements Using a Laser," Rev. Sci. Instr. 33, 1107, (1962).

10. Cape, J. A., and G. W. Lehman, "Temperature and Finite Pulse-Time Effects in the Flash Method for Measuring Thermal Diffusivity," J. Appl. Phys. 34, 1909 (1963).

11. General Electric Company, Pyrolytic Graphite Engineering Handbook, Detroit, Michigan, 1963.

12. High Temperature Materials, Inc., Data Sheet on Pyrolytic Graphite, Brighton, Massachusetts, 1961.

13. Price, R. J., and J. C. Bokros, "Analysis of the Thermal Expansion and Radiation-Induced Length Changes in Graphite in Terms of Preferred Orientation," submitted to J. Appl. Phys. (General Atomic Report GA-5571, August, 1964).

14. Bokros, J. C., and N. L. Sandefur, "Uranium Migration Through Pyrolytic Carbons Deposited in a Fluidized Bed (U)," (General Atomic Report GA-5793 (C/RD), November, 1964.

15. Price, R. J., J. C. Bokros, K. Koyama, and J. Chin, "Structure and Properties of Pyrolytic Carbon Prepared in a Fluidized Bed Between 1900°C and 2400°C," General Atomic Report GA-6506 (to be issued).

IV. DIFFUSION OF THORIUM IN PYROLYTIC CARBON

H. K. Lonsdale, J. Graves

INTRODUCTION

The study of the diffusion and solubility of the actinide metals in various forms of carbon was begun in earnest over a decade ago,[1] and in the intervening period a number of additional studies, both direct and indirect, have been made.[2-7] A detailed comparison of the early researches of Loftness[1] and of Loch, Gambino, and Duckworth[2] on the diffusion of uranium in polycrystalline graphites shows that while the calculated diffusion coefficients are in qualitative agreement, the activation energies for diffusion differ by a sizeable amount. Furthermore, the concentration levels expressed in units of weight of uranium per unit volume of graphite are grossly different, even though uranium dicarbide was used as the uranium source in both studies. From these studies, as well as from experiments involving diffusion of thorium and uranium through pyrolytic carbons,[6][7] it would appear that one or more important experimental parameters have not been defined or controlled, and that diffusion in these materials is a rather complex phenomenon, being at least as dependent on details of microstructure as other transport properties such as electrical and thermal conductivity.

Wolfe, McKenzie, and Borg[3] (referred to henceforth as WMB) were apparently the first to reduce the number of variables in the diffusion experiments involving metals in carbon by using a pyrolytic carbon of well-defined microstructure and performing tracer-level experiments. Their work demonstrated that the extreme anisotropy of one type of pyrolytic carbon--columnar pyrolytic carbon--is manifested in the rate of diffusion of metal atoms parallel as compared with perpendicular to the plane of deposition. They also demonstrated that thorium and uranium have measurably different diffusion coefficients in this material.

A number of questions remain to be answered, however, before one can predict metal diffusion coefficients in a given carbon with any confidence. Among the important variables are the nature and concentration of the metal species or the presence of other species; the microstructure of the carbon or graphite, including specifically the degree of orientation and average crystallite size; the time of observation, if the structure tends to change with time; the presence of neutron or fission-fragment flux; the orientation of the layer planes with respect to the source of the diffusion species; and temperature. Evans, Stiegler, and Truitt[4] (referred to henceforth as EST) have addressed themselves to some of these problems, including the importance of the concentration of the diffusing species.

The present study is aimed at determining the effect of the structure of pyrolytic carbon on the diffusion rates of thorium. This portion of the general problem has particular practical significance in that pyrolytic-carbon-coated uranium/thorium carbide fuels as prepared in this and other laboratories have shown wide variations in their resistance to the migration of fuel through their coatings, and these variations have been traced to the nature of the coating and ultimately to its microstructure. Furthermore, the effects of irradiation are also microstructural in nature, and the study of the dependence of diffusion coefficients on structure may have relevance to the problem of the irradiation stability of pyrolytic-carbon coatings.

EXPERIMENTAL

All experiments were carried out with thorium at a very low concentration level, and diffusion coefficients were measured only perpendicular to the plane of deposition. The important differences between this study and previous studies are that the pyrolytic-carbon diffusion samples have been well characterized microstructurally, and that the samples contained no exposed edges of layer planes. In previous diffusion studies on pyrolytic carbons (excluding studies with coated particles), the carbon specimens have been machined from a flat or nearly flat plate of commercially deposited carbon. In the study of diffusion perpendicular to the plane of deposition, these measurements suffered from the fact that the rapid diffusion of the impurity atoms over the surface of the specimens[8] served to create a source for diffusion parallel to the layer planes, which are generally aligned with the plane of deposition, in the early stages of the diffusion anneal.

As WMB have pointed out, the diffusion coefficient parallel to the layer planes is two to three orders of magnitude greater than that perpendicular to the planes, depending on the temperature and the nature of the diffusing species, so it is difficult to carry out a diffusion anneal in which the diffusion "parallel" does not interfere with or completely mask the diffusion "perpendicular."

The specimens used in the present study were prepared by applying a pyrolytic-carbon deposit under well-defined conditions to graphite disks, nominally 1/16 in. thick by 5/16 in. in diameter, in a fluidized bed.* Normally, 12 to 20 such disks were coated in a single run; then the properties of the set were determined from a representative sample, and the remainder were used for diffusion anneals. There was a small amount of

*Uranium dicarbide microspheres were coated simultaneously and the diffusion specimens may have contained a trace of uranium; none was detected by α-counting, however.

non-uniformity in the structure of the specimens prepared by this procedure. This non-uniformity was present across the thickness of the deposit on each specimen and was caused by the dependence of carbon structure on the size of the charge in the fluidized bed, as has been discussed previously by Bokros and others.[9] On the basis of these previous studies, the effect is believed to be small.

A total of three different types of pyrolytic-carbon coatings were studied. In the terminology of the present report, they are known as granular, isotropic or random, and laminar pyrolytic carbons. A summary of the coating variables which have been found to be important in determining the structure, along with certain physical properties of these materials, is given in Table 1. The variables used in this table and the relationships between coating conditions and the microstructure of the deposits are discussed elsewhere in this annual report and in the previous annual report in this series.[9] All deposits were made from methane gas in a helium stream at 1 atm pressure. In all instances, the carbon deposits were not absolutely flat, but were enlarged at the edges so that the thickness of the specimens at their axial center was uniformly less than that at the edges. All specimens were therefore polished flat and with the faces plane-parallel to $\pm 3\ \mu$ before the diffusion anneals. In the process, a secondary carbon deposit, which was present on the periphery of some of the specimens, was removed. In the case of the granular and isotropic carbons, the diffusion anneals were carried out at temperatures not exceeding the deposition temperature, and there was no change in physical properties brought about by the diffusion anneals. This was not the case for the laminar pyrolytic carbons, which can only be prepared at relatively low temperatures. These samples were therefore preannealed (in the absence of any thorium) at a temperature in excess of any of the subsequent diffusion anneals. The preannealing conditions and the effect on the apparent crystallite size, L_c, are given in Table 1.

Photomicrographs of cross sections of coated disks and particles prepared in the fluidized bed are shown in Fig. 1. The samples shown are typical of the three kinds of carbon used, but they are not among the actual samples used in this study. All the carbon deposits were approximately 100 μ thick.

Except for the method of preparing samples, the experimental technique was quite similar to that developed by WMB, who generously communicated the procedure to us before publishing it. Th^{228} was used as the tracer in all experiments. This nuclide has a half life of 1.91 yr and is normally in secular equilibrium with four α-emitting daughters. The decay chain is indicated below. The material was procured from the Radiochemical Centre at Amersham, England, in the form of an HCl solution containing approximately 7 μg of thorium (Th^{232}) as a carrier for approximately 2 mc of Th^{228}.

Table 1

SUMMARY OF DEPOSITION CONDITIONS AND PROPERTIES OF PYROLYTIC CARBONS USED IN STUDY[a]

Graphite Type	Sample Number	Deposition Temp. (°C)	Charge Size (cm^2)	CH_4 (%)	Coating Rate (μ/cm)	Contact Time (sec)	Density (g/cm^3)	Anisotropy Factor	L_c (Å)	Preanneal Temp. (°C)	Preanneal Time (hr)	L_c After Preanneal (Å)
Granular	2812-9N	1900	1140	3	37	0.06	1.98	1.3	110	----	----	--
Isotropic	2703-47N	2000	800	15	63	0.15	1.94	1.0	125	----	----	--
Isotropic	3023-37N	2000	800	15	60	0.15	2.12	1.3-1.4	170	----	----	--
Laminar	2511-107N	1350	400	28	21	0.2	1.91	1.6	37	1970	16	76
Laminar	2701-13N	1350	400	28	14	0.2	1.96	2.0	39	1985	5.3	98
Laminar	2701-103N	1400	400	40	23	0.2	2.12	1.9	43	2000	24	76

[a] Specimens were prepared by J. Chin and the physical properties of the pyrolytic carbons were measured by J. Bokros and W. Ellis, all of this Laboratory. The isotropic carbon 3023-37N appears to have properties which are rather similar to those of granular carbon. However, as viewed in the microscope it had a clearly different microstructure, typical of those referred to as isotropic.

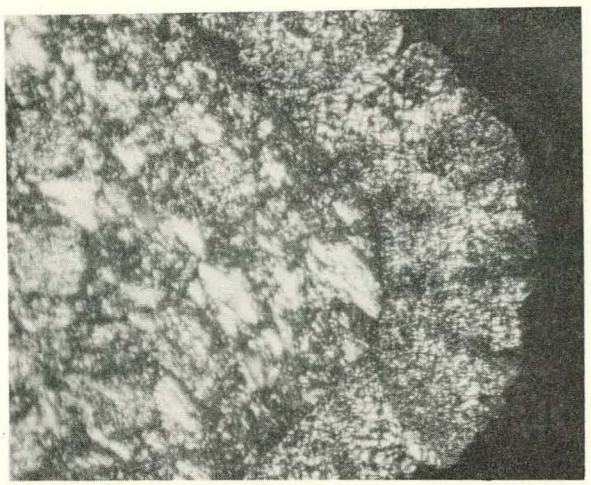

M-6970 200×

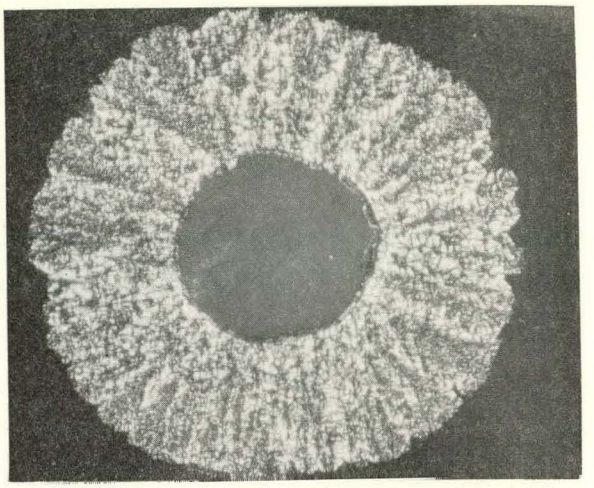

M-6969 200×

(a)

M-6262 200×

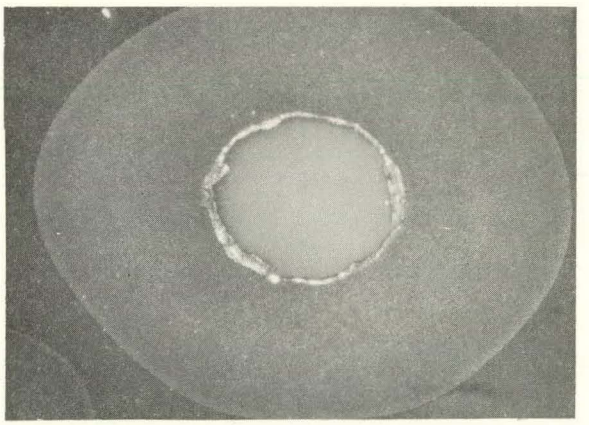

M-6337 200×

(b)

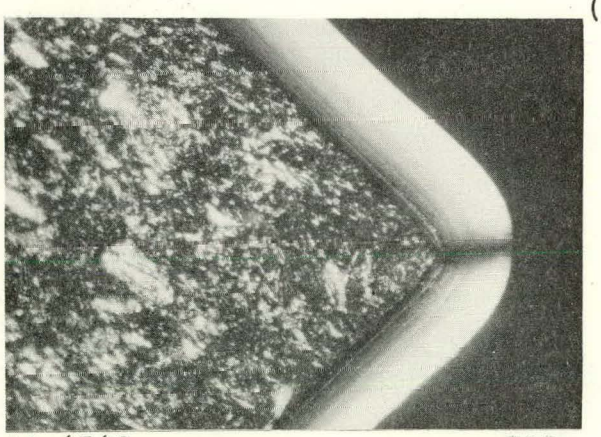

M-6763 200×

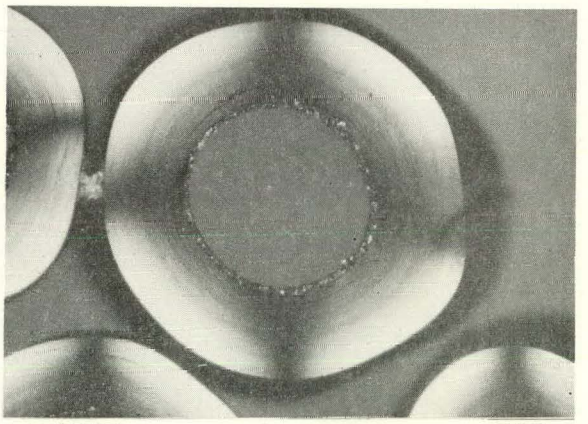

M-6764 200×

(c)

Fig. 1--Typical microstructures deposited on particles and disks in a 2.5-cm-diameter coater: (a) granular structure deposited from 3.8% CH_4 at 1700°C with initial charge of 130 cm^2; (b) isotropic structure deposited from 40% CH_4 at 1925°C with initial charge of 400 cm^2; (c) laminar structure deposited from 11% CH_4 at 1350°C with initial charge of 2000 cm^2.

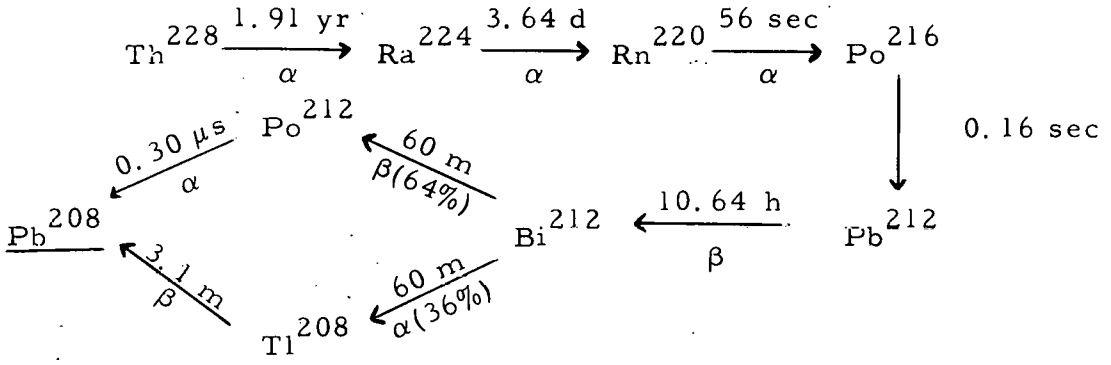

The diffusion samples were prepared by evaporating a very small amount of the Th^{228} solution onto one face of a polished carbon disk. About 0.01 to 0.02 μc of Th^{228} was deposited on each specimen, which amounted to approximately 50,000 cpm in a 2π α-counter. On the basis of 1 μg of thorium carrier in the Th^{228} solution and the assumption that the thorium was uniformly distributed in the pyrolytic carbon of the specimen, the atom fraction of thorium was less than 10^{-10}. Following a diffusion anneal, the atom fraction probably never exceeded 10^{-8} in any portion of the specimen; this is discussed in more detail below.

The diffusion anneals were carried out in pairs in a vacuum resistance-heated furnace. A drawing of the furnace is shown in Fig. 2. The residual pressure in the furnace during the anneal was $\sim 2 \times 10^{-5}$ mm Hg. Heat-up and cool-down times were usually quite short in comparison with the annealing time; the shortest anneals were 4 hr in duration. The temperature was sensed with a Radiamatic radiation pyrometer (Minneapolis Honeywell Type RI-3), which was focused on the graphite container holding the samples and not directly on the samples themselves. The temperature of the samples was read through an opening in the lid of the sample container which was an effective hohlraum and through a Pyrex window with a Leeds and Northrop Model 8622-C optical pyrometer. The optical pyrometer and window were calibrated periodically against a National Bureau of Standards secondary standard (tungsten filament lamp). In every case but one (a diffusion measurement in porous graphite discussed below), the calibration did not change significantly with time, indicating that darkening of the window due to graphite vaporization during the anneals was not a problem. After bringing the sample to temperature with manual increase in the power settings, the temperature was read with the optical pyrometer, the radiation pyrometer was put in position, and the power supply to the furnace was switched to automatic control.

A Barber-Coleman MMC controller was used, and temperature cycling during an anneal was less than $\pm 2^{\circ}$C. At the end of each anneal the furnace was switched back to manual operation, and the temperature was again read with the optical pyrometer. In almost all cases the initial and final readings

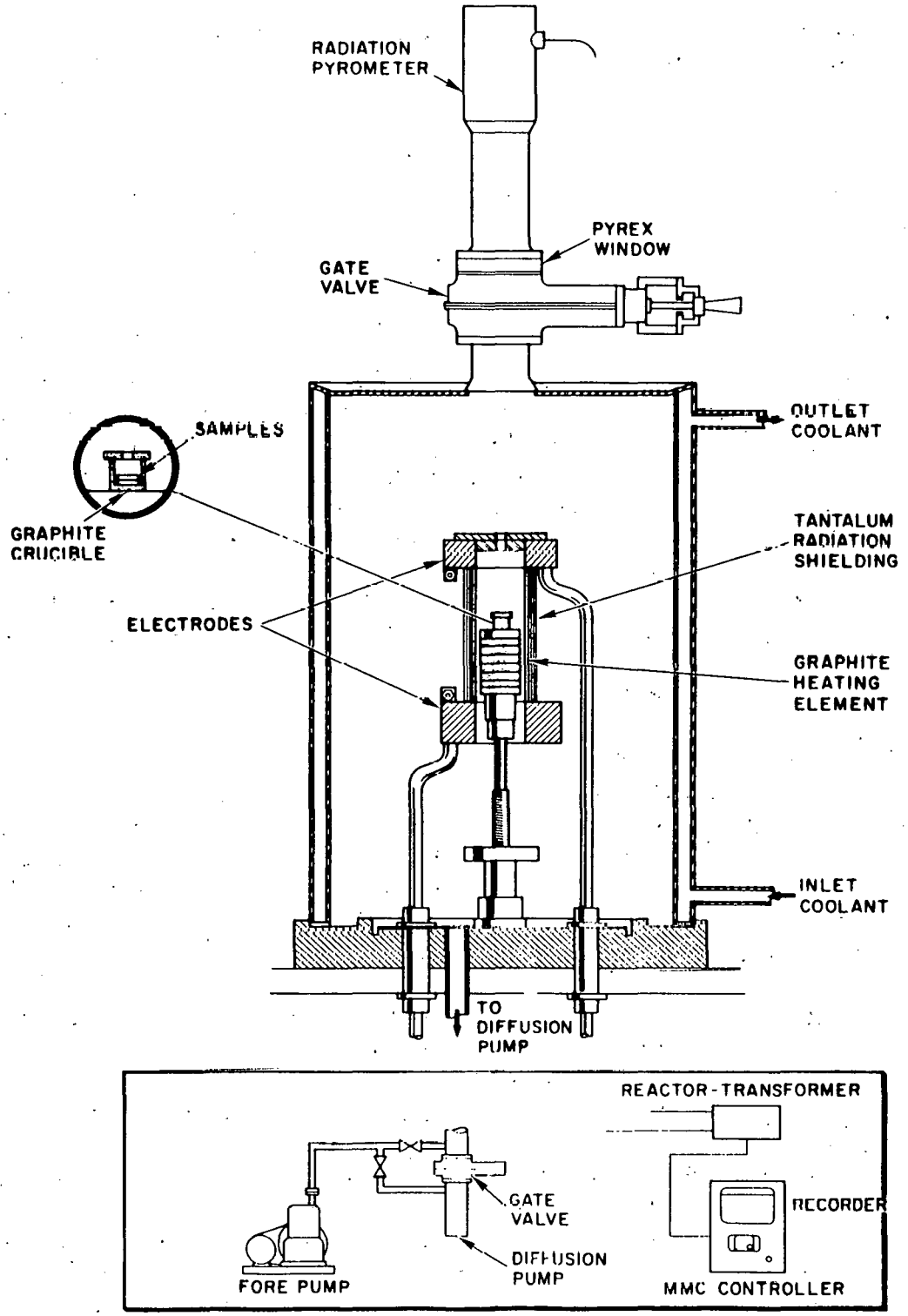

Fig. 2--Diffusion annealing furnace showing a pair of samples in position.

did not differ significantly. The accuracy of the temperature assignment is estimated to be $\pm 5^{\circ}$ to 10°C, with the uncertainty increasing with increasing temperature.

Following an anneal, a sample was prepared for sectioning by gluing it to a piston and turning off the pyrolytic carbon on the sample edge with a lathe. The purpose of this step was to eliminate Th^{228} from the sample edges, the presence of which would provide a spurious background as the sample was sectioned. The steps taken to prepare the sample for annealing and later for sectioning are indicated in Fig. 3.

The samples were stored for 2 to 3 weeks between annealing and sectioning in order to restore secular equilibrium in the decay chain. During the diffusion anneal the radium and radon daughters were undoubtedly volatilized to some extent from the specimen, and there may well have been diffusion of radium and other daughters into the carbon specimen in advance of the thorium diffusion, as was found by WMB. After a period of several half-lives of 3.6-day Ra^{224}, the total activity in the sample increased approximately fivefold as the equilibrium was re-established and the daughters present before and immediately after the anneal completely decayed away.

Samples were sectioned by abrasion on fine (4/o) emery paper which was supported by a granite flat as depicted in Fig. 4. The piston with the sample to be sectioned was placed in the lapping jig, which was inverted with respect to its orientation in the photograph. A lead weight was added to the piston to supply a constant loading on the sample as the sample was pushed across the emery paper. Pressures of approximately 80 to 200 psi were applied to the sample, depending on the hardness of the pyrolytic carbon and on the thickness of cut desired.

The length of the carbon strip formed by abrasion of the carbon section on the emery paper was made uniform with "stops" on the granite flat. In a 9-in. strip, on the order of 1 μ of carbon was removed from the sample. To prevent smearing, a portion of the base of the lapping device was machined off so that the base did not pass indirectly over the carbon strip. Only the sample touched the emery paper along the line of sectioning.

Before each sectioning step, the relative sample thickness was measured with a Mauser dial indicator (Model No. 658) calibrated in 0.00005 in. (1.27 μ) which could be read to ± 0.00001 in. (0.25 μ) with interpolation. However, the reproducibility of successive readings was probably not better than 0.5 μ.

After the sample was sectioned, the emery paper was cut up to divide the carbon strips into six segments of equal length. These segments

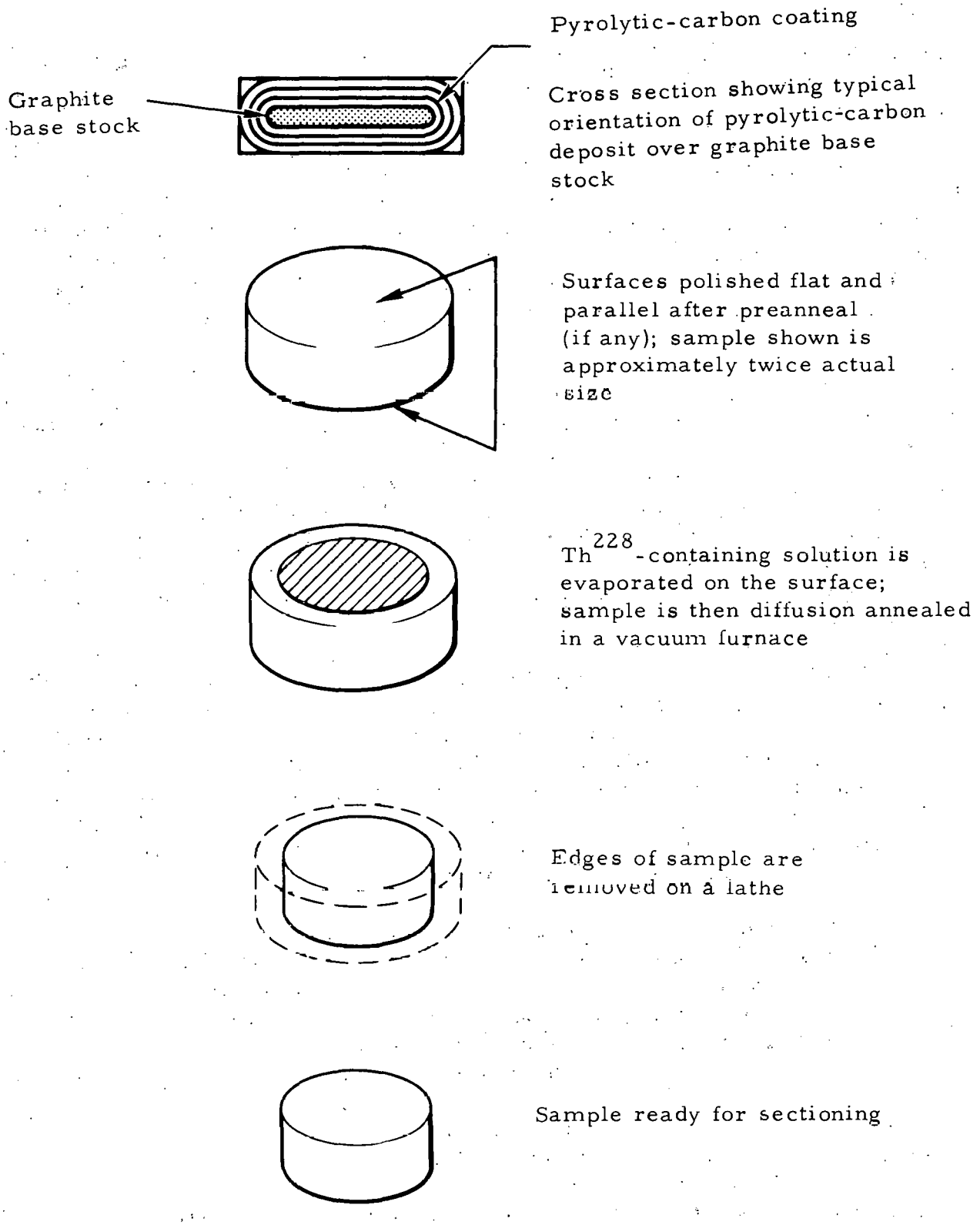

Fig. 3--Preparation of pyrolytic-carbon-coated samples for diffusion annealing and sectioning.

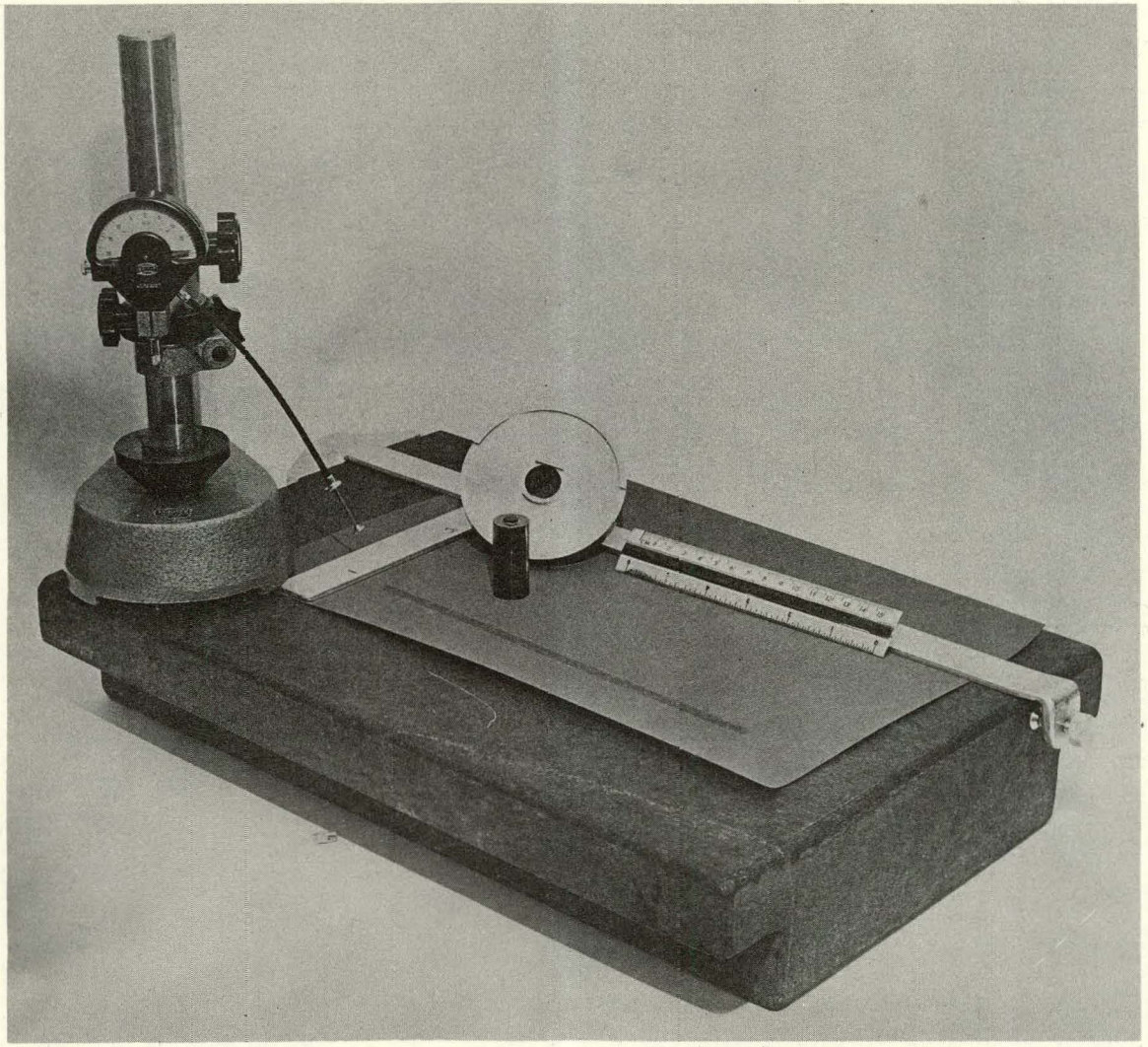

Fig. 4--Photograph of the lapping device used for sectioning samples; a strip of pyrolytic carbon has been removed from the sample

of paper were then counted directly in an α-counter (Nuclear Measurements Corporation Model PC-3B). A counting plateau for the α particles in the Th^{228} decay chain was found to extend from 1000 to 1300 v; all counting was done at a potential of 1150 v.

During the course of counting these emery paper samples, the background in the α-counting chamber increased, presumably owing to the release of a small amount of Rn^{220} from the samples and the deposition of Pb^{212} on the chamber walls. This problem was circumvented by purging the chamber at a high rate, by checking the background often, and by counting the least concentrated samples first. Following a series of counts, the excess background was observed to decay with approximately the 10.6-hr half-life of Pb^{212}. Samples were generally counted until at least 1000 total counts were recorded. Count rates of 10 cpm above background were considered significant for calculational purposes.

The technique of counting the Th^{228} in the pyrolytic carbon while it is embedded within the emery paper does not lead to a significant error in the calculated diffusion coefficients. The several α particles in the Th^{228} decay chain vary in energy from about 5.4 to 8.8 Mev. The range of these α particles in the emery paper particulate matter (Al_2O_3) is 5.4 to 12 mg/cm^2, or 14 to 30 μ; however, the face of the paper contains perhaps 50% voids, so this range should be nearly doubled. Even if one assumes that the pores are completely filled with carbon of density 2.0, this calculated range should be increased. The maximum particle diameter in this paper is 12 μ, so except for the lowest energy α particles emitted at large angles from the vertical, the attenuation is not severe. More important, the attenuation should be nearly the same on a relative basis for all specimens.

The raw counting data were converted to units proportional to concentration by dividing by the thickness of the sample represented by the carbon strip. For a given sample the diameter is the same for all specimens (carbon strips), and a uniform rate of removal of carbon along the emery paper has been assumed. Thus, relative concentrations are expressed in terms of net cpm/μ. All the data reduction was carried out on the IBM-7044 computer.

RESULTS AND DISCUSSION

Diffusion in Pyrolytic Carbons

Concentration Profiles and Diffusion Coefficients

Because of the uncertainty in the expected diffusion coefficients, it was impossible to preselect the annealing conditions which would result

in a penetration distance comparable in magnitude to, but never exceeding, the coating thickness. Thus, all the experiments with the isotropic and laminar samples were carried out twice. In the first attempt, the annealing conditions were conservative and the penetration distances were generally too small to give accurate results. Since some of the initial results obtained with these two pyrolytic carbons have been reported previously[10] and the data are less reliable than subsequent results reported below, they are not repeated here.

There are, however, no inconsistencies of a qualitative nature between the initial measurements and the later, more refined measurements. Therefore, in the discussion to follow, only three sets of pyrolytic-carbon samples will be included: the granular carbon 2812-9N; the isotropic carbon 3023-37N; and the laminar carbon 2701-103N (see Table 1).

Some typical relative concentration plots are presented in Figs. 5, 6, and 7. Concentrations are expressed in units of net counts-per-minute per micron of thickness. The solution to Fick's law for an instantaneous plane source diffusing into a semi-infinite slab is given by[11]

$$C = \frac{S}{2(\pi Dt)^{\frac{1}{2}}} \exp\left(\frac{-x^2}{4Dt}\right), \qquad (1)$$

where C is the concentration of the impurity species at distance x, and S is the source strength, i.e., the total amount of impurity species deposited per cm^2. One can calculate the diffusion coefficient, D, from the slope of these curves and the annealing time, t. An effect which was observed in a number of the concentration profiles was a surface concentration which was anomalously high relative to the intercept value. The high-surface-concentration data points were not used in calculating the diffusion coefficients.

A summary of the annealing conditions and the calculated diffusion coefficients is given in Table 2. Runs 22-27 were carried out with the granular pyrolytic carbon, runs 28-32 with the isotropic carbon, and runs 33-37 with the laminar carbon.

These results are plotted in typical Arrhenius fashion in Figs. 8, 9, and 10, and a summary of D_o and Q values, computed by fitting the diffusion coefficient data to the phenomenological equation

$$D = D_o \exp\left(\frac{-Q}{RT}\right) \qquad (2)$$

is presented in Table 3. Two points, runs 29-2 and 36-1, have been omitted from the figures and from the least-squares fit to the data because they

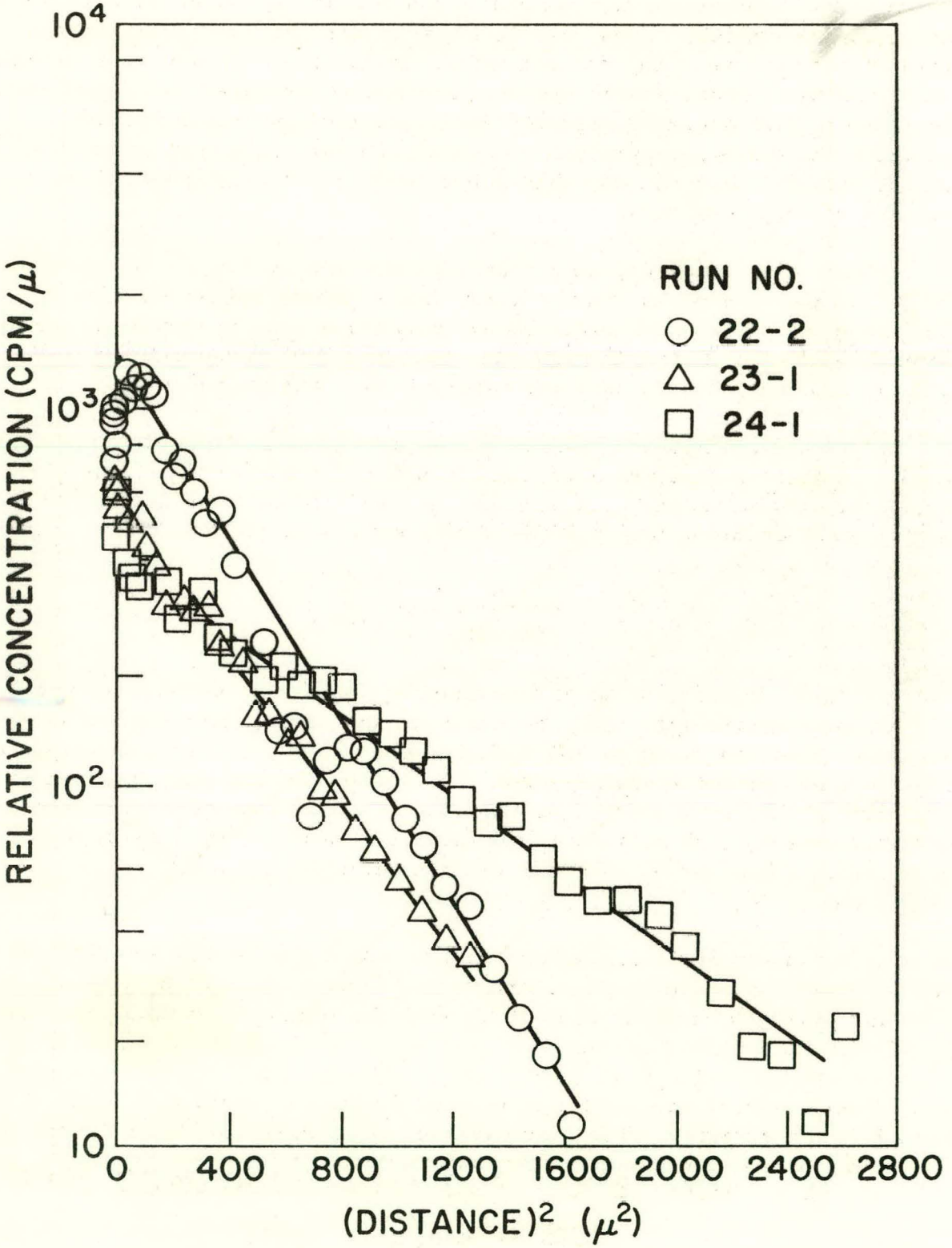

Fig. 5--Concentration profiles for three Th^{228} diffusion anneals in granular pyrolytic carbon, Lot No. 2812-9N

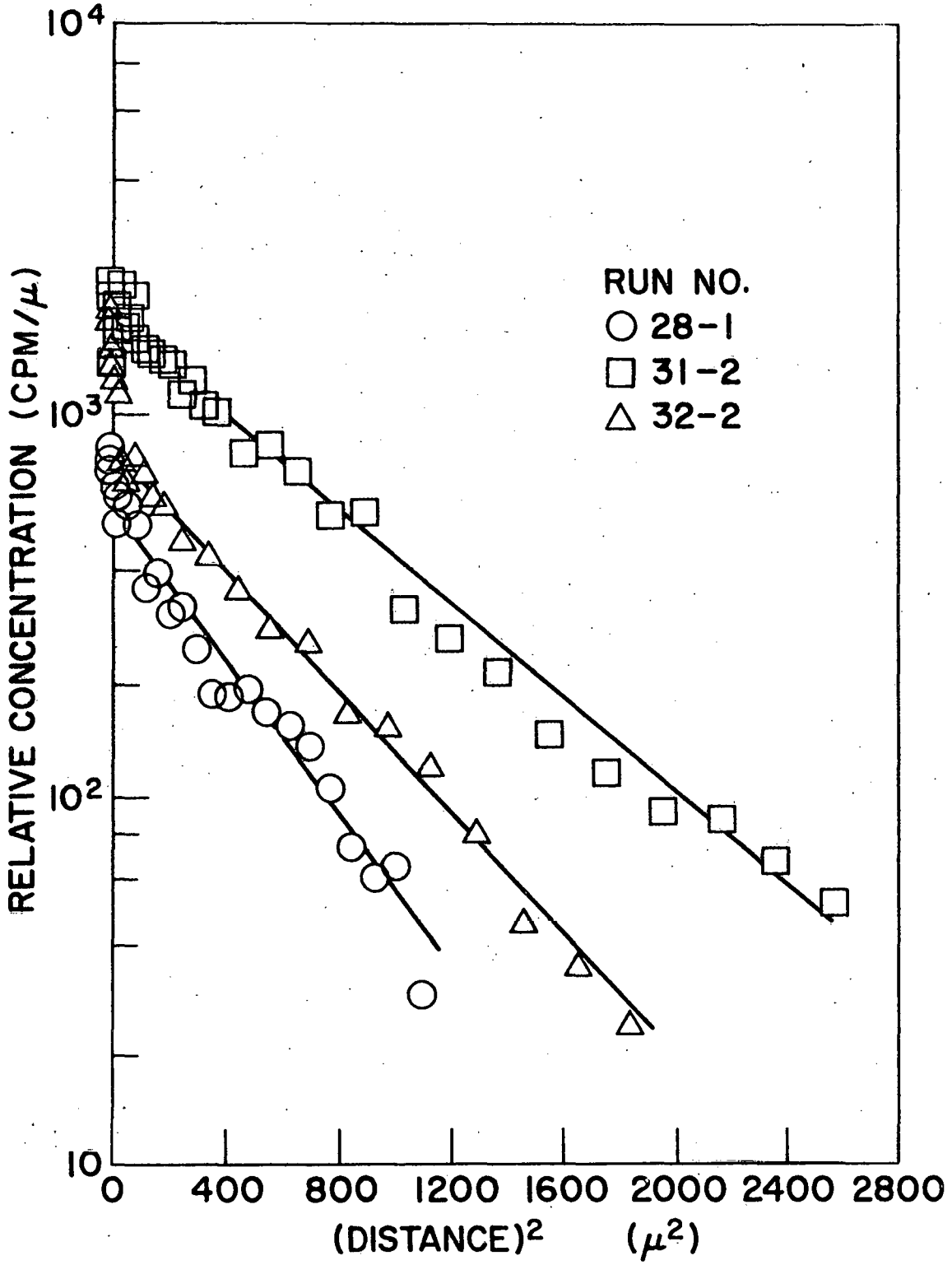

Fig. 6--Concentration profiles for three Th^{228} diffusion anneals in isotropic pyrolytic carbon, Lot No. 3023-37N

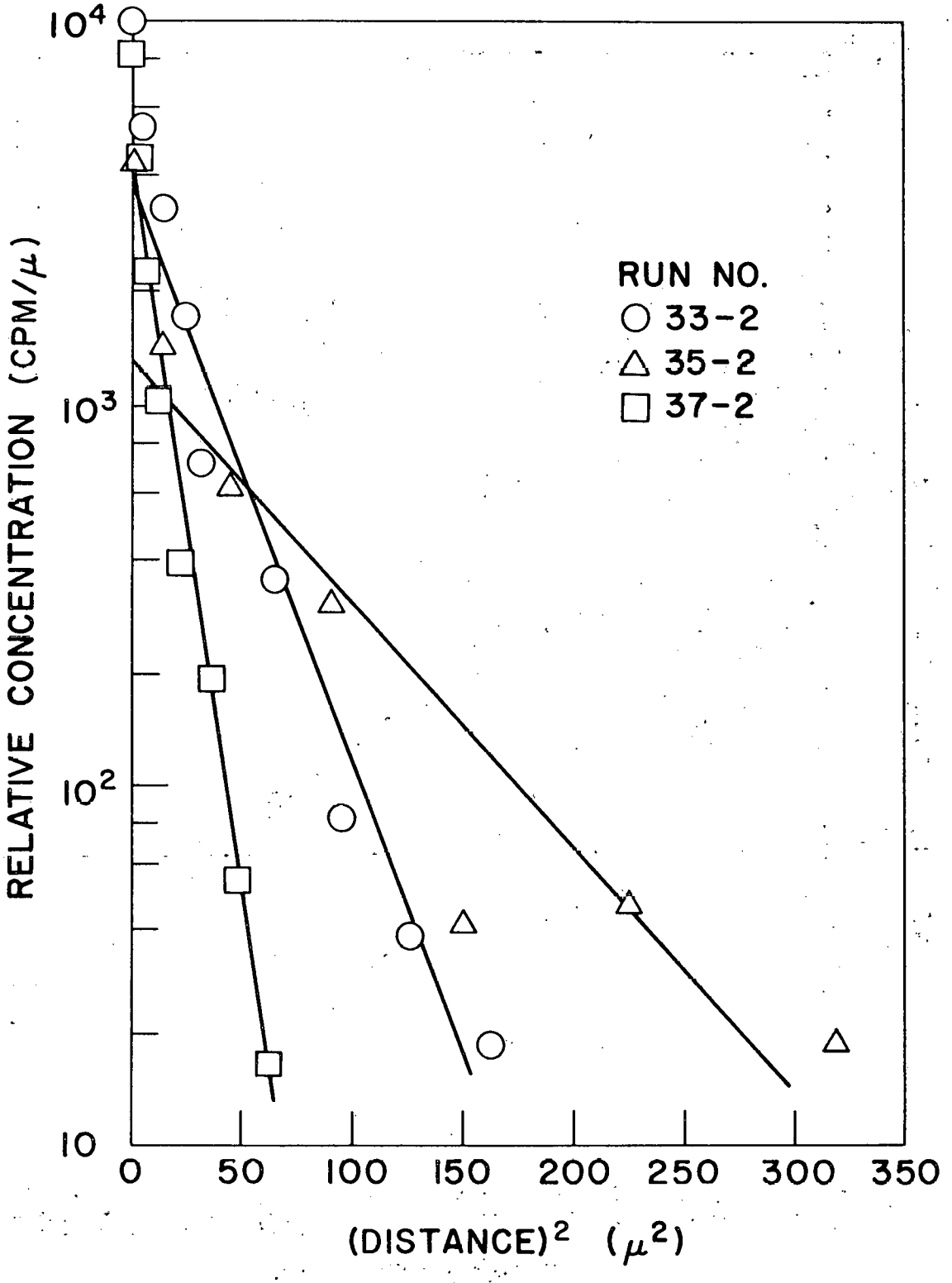

Fig. 7--Concentration profiles for three Th^{228} diffusion anneals in laminar pyrolytic carbon, Lot No. 2701-103N

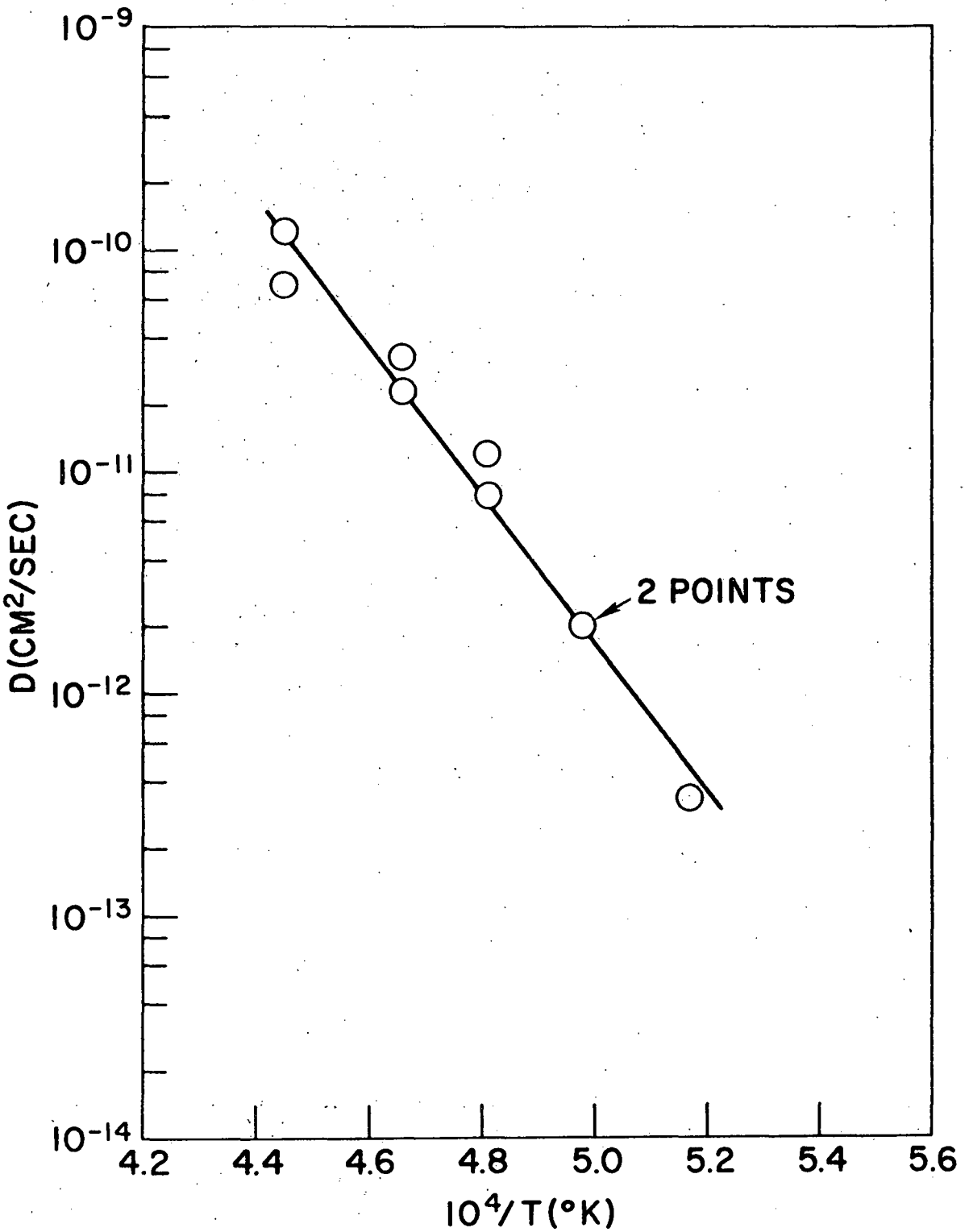

Fig. 8--Tracer diffusion coefficients of thorium in granular pyrolytic carbon

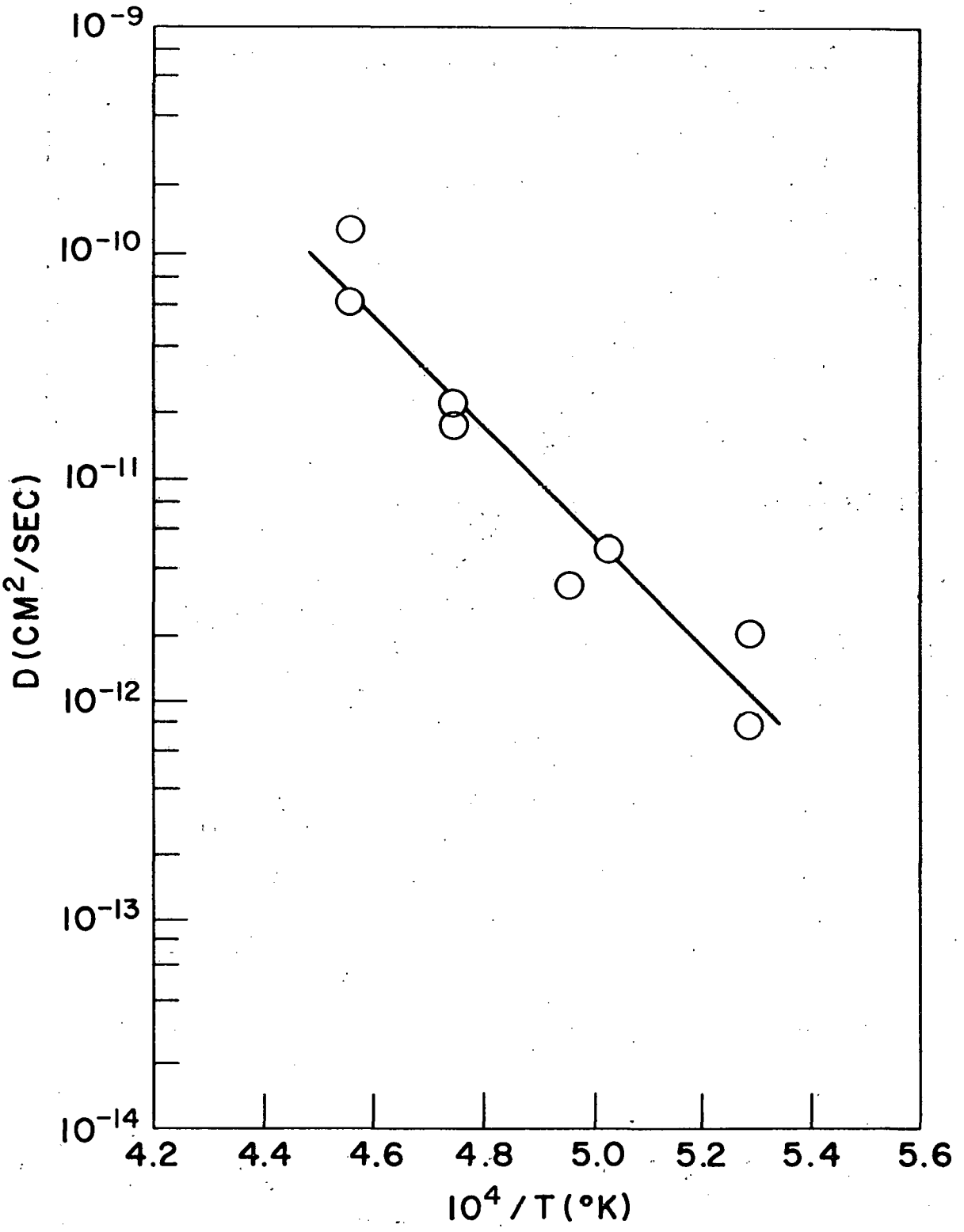

Fig. 9--Tracer diffusion coefficients of thorium in isotropic pyrolytic carbon

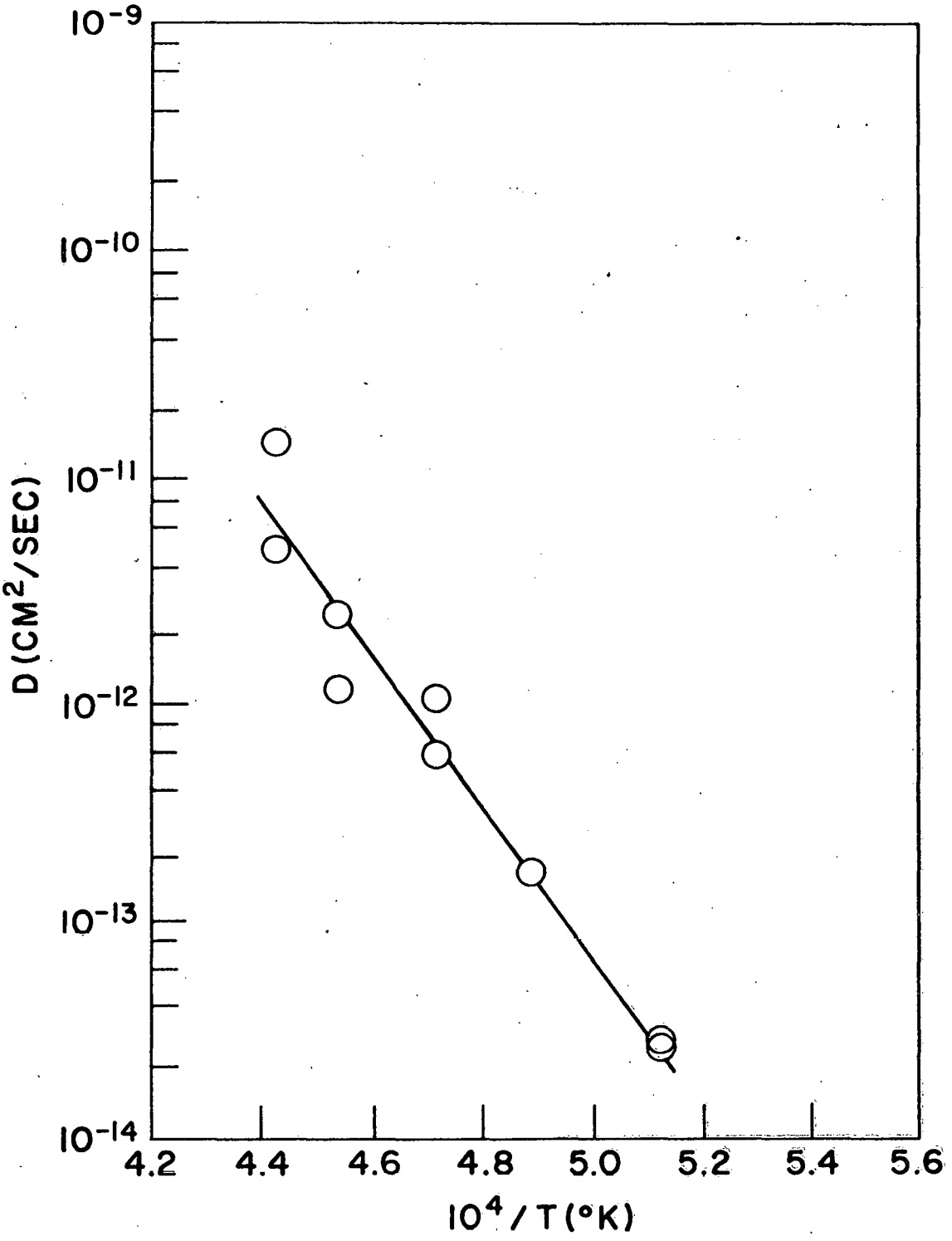

Fig. 10--Tracer diffusion coefficients of thorium in laminar pyrolytic carbon

Table 2

ANNEALING CONDITIONS AND THORIUM TRACER DIFFUSION COEFFICIENTS IN PYROLYTIC CARBON

Sample No.	Annealing Temp. (^{o}C)	Annealing Time (hr)	$10^4/T$ (^{o}K)	$D_\perp$ (cm^2/sec)
22-1	1734	121.4	4.98	2.0×10^{-12}
22-2	1734	121.4	4.98	2.0×10^{-12}
23-1	1804	24.0	4.81	1.2×10^{-11}
23-2	1804	24.0	4.81	7.7×10^{-12}
24-1	1875	17.0	4.66	3.3×10^{-11}
24-2	1875	17.0	4.66	2.3×10^{-11}
26-1	1975	16.0	4.45	1.2×10^{-10}
26-2	1975	16.0	4.45	6.8×10^{-11}
27-2	1660	262	5.17	3.3×10^{-13}
28-1	1840	16.6	4.73	1.8×10^{-11}
28-2	1840	16.6	4.73	2.3×10^{-11}
29-1	1750	24.0	4.94	3.6×10^{-12}
29-2	1750	24.0	4.94	8.8×10^{-13}
30-1	1925	6.4	4.55	1.3×10^{-10}
30-2	1925	6.4	4.55	6.3×10^{-11}
31-1	1630	240.2	5.26	8.5×10^{-13}
31-2	1630	240.2	5.26	2.2×10^{-12}
32-1	1715	72.0	5.03	5.1×10^{-12}
32-2	1715	72.0	5.03	5.2×10^{-12}
33-1	1930	16.0	4.54	2.6×10^{-12}
33-2	1930	16.0	4.54	1.2×10^{-12}
34-1	1850	42.1	4.71	6.2×10^{-13}
34-2	1850	42.1	4.71	1.1×10^{-12}
35-1	1985	4.0	4.43	5.0×10^{-12}
35-2	1985	4.0	4.43	1.5×10^{-11}
36-1	1770	93.0	4.88	2.0×10^{-12}
36-2	1770	93.0	4.88	1.8×10^{-13}
37-1	1680	263.6	5.12	2.8×10^{-14}
37-2	1680	263.6	5.12	2.9×10^{-14}

Table 3

Q AND D_o VALUES FOR THORIUM DIFFUSION IN PYROLYTIC CARBONS

Material/Reference	ρ (g/cm^3)	L_c (Å)	Anisotropy Factor	Q (kcal/mole)	D_o (cm^2/sec)	D at 2000°K (cm^2/sec)	Percent Error
Columnar ⟨c⟩, WMB	2.20	150	6-7[a]	114.7 ±3	2.5	7.2×10^{-13}	5
Columnar ⟨c⟩, EST	2.20	150	6-7[a]	60.8	3.2×10^{-5}	7.5×10^{-12}	Not reported
Granular/present study (2812-9N)	1.98	110	1.3	152 ±8	7.1×10^{4}	1.7×10^{-12}	21
Isotropic/present study (3023-37N)	2.12	170	1.3-1.4	114 ±11	15.5	5.3×10^{-12}	36
Laminar/present study (2701-103N)	2.12	76	1.9	157 ±11	1.2×10^{4}	7.0×10^{-14}	33
Columnar ⟨a⟩, WMB	2.20	150	6-7[a]	145 ±3	1.3×10^{5}	1.7×10^{-11}	11

[a] Estimated by J. Bokros of this Laboratory from a sample of the WMB material.

deviate markedly from the remainder of the results. Also presented in Table 3 are results reported by WMB and by EST on thorium diffusion in commercially prepared samples of columnar pyrolytic carbon. The last entry in Table 3 refers to the work of WMB on the diffusion parallel to the plane of deposition, i. e., D <a>, while all the other entries refer to diffusion perpendicular to the plane of deposition, i. e., D <c>. The uncertainties presented for the present Q results represent standard deviations. Also, the diffusion coefficient is presented at an arbitrarily selected temperature of 2000°C from these several studies. The final column in Table 3 refers to the average of the absolute deviations of the observed diffusion coefficients from the least-squares fit to the data.

The study carried out by EST was at low, but not tracer-level, thorium concentrations. The discrepancy between the EST and the WMB results on presumably similar pyrolytic carbons has not yet been completely resolved, but it has been suggested[12] that the large difference in concentrations in the two sets of experiments is responsible.

The scatter in the present results is significantly greater than that found by WMB for thorium diffusion. However, their uranium diffusion results have an error of 25% associated with them and uncertainties of this magnitude for diffusion coefficients are not alarming. On the other hand, the large range of values found for Q and D_o is surprising.

The results of these several investigations are plotted in Fig. 11 for purposes of comparison. Taking into account the uncertainties in the present results, one can conclude that tracer-level thorium diffusion in the isotropic carbon is significantly higher, at least below 2000°K, than that in the granular carbon. The activation energy is also significantly different, but in the opposite sense, so at approximately 2000°C the diffusion coefficients in these two materials could be expected to be the same. The most striking differences, however, exist between the granular or isotropic carbons and the laminar carbon. Over the temperature range studied, the diffusion coefficient in the laminar carbon was a relatively constant factor of 25 smaller than that in the granular carbons and was 30 to 100 times smaller than the diffusion coefficient in the isotropic carbon.

Surface Concentrations and "Solubilities"

The high surface concentrations found on some of the specimens deserve further comment. For those specimens in which this effect was observed, the assumption of an instantaneous source of thorium is clearly not justified if, as seems probable, the high surface α-activity is due to Th^{228} and its daughters. In some of these cases, the true thorium source was probably time-dependent owing to losses due to surface diffusion and the diffusion within the sample. However, in some of the samples, the

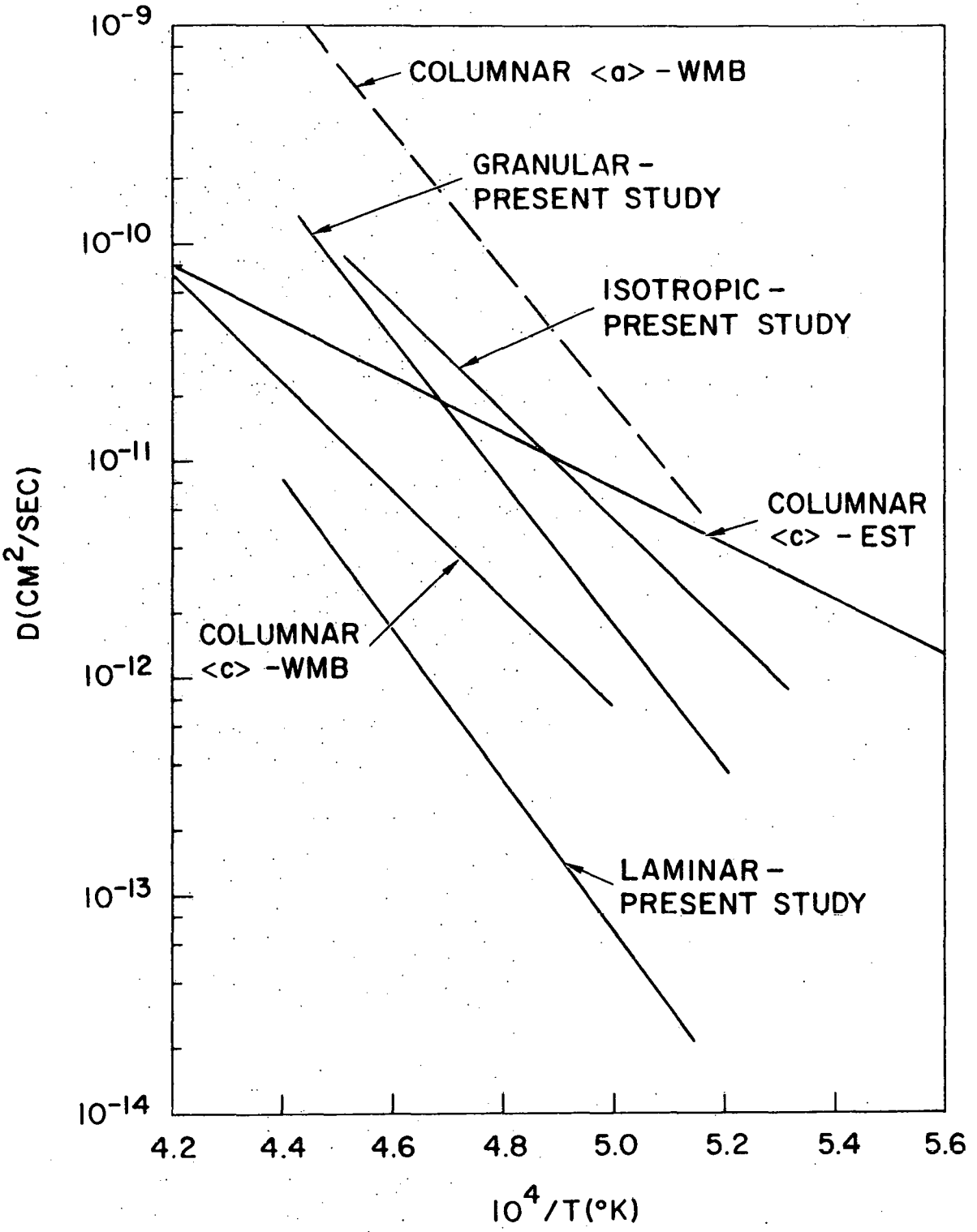

Fig. 11--Summary of several studies of thorium diffusion in pyrolytic carbon

surface concentration always exceeded that in the interior of the sample, and the constant-source solution to the diffusion problem applies:[11]

$$\frac{C}{C_0} = \text{erfc}\ \frac{x}{2\sqrt{Dt}} \quad . \tag{3}$$

In this expression C_0 is the constant concentration of impurity species in the sample at the boundary. One can only speculate about the time-dependence of the thorium source in those samples which did not show high surface concentrations. Perhaps in those samples also the surface concentration initially exceeded the "limiting" concentration within the sample but at the conclusion of those diffusion anneals the strength of the source had decayed via diffusion below this concentration. For those cases in which the surface concentration exceeded the value of the intercept on a concentration versus distance plot, the diffusion coefficients should have been derived by solving the complementary-error-function solution. When plotted against the square of the penetration distance on semilogarithm paper, this function gives a curve which is concave when viewed from the high concentration side. Our results did not, in general, have this shape, so our treatment of the results in terms of Eq. (1) is at least partly justified. Furthermore, given the same set of experimental concentrations versus distance data, the diffusion coefficients calculated by forcing a fit to either the exponential or the error function solutions do not differ greatly in the concentration range $0.01 < C/C_0 < 1$.

It is interesting to note at this point that WMB also found anomalously high surface concentrations following their diffusion anneals with Ni^{63} and Ag^{110m} tracers. Neither of these nuclides is available in carrier-free form, and WMB conclude that their samples were saturated with nickel or silver in these experiments by the small amount of carrier. (The experiments of WMB with Th^{228} and U^{232} were carried out with carrier-free sources and in those specimens they found no surface anomalies.) A further parallel between the WMB nickel and silver experiments and the present thorium experiments is that the WMB concentration profiles did not have the expected shape of the complementary-error-function solution to the constant potential diffusion problem (in fact, any deviations in their data are in the opposite sense) and they treated their data with the instantaneous source solution.

In a recent publication, Hennig[13] reports some diffusion experiments involving boron in single crystals of graphite. At relatively high concentrations (10^{-2} to 1 atom-%), he also finds an excessively high concentration of boron "within a few microns of the crystal edge," which apparently did not occur at lower concentrations. Hennig attributed this result to "abnormal diffusion."

We believe that there is some significance to these high surface concentrations which appear in diffusion experiments with carbons and graphite. One can estimate the surface concentrations of nickel and silver in the experiments of WMB from the data in their report. Making some reasonable assumptions about β- and γ-counting efficiencies, knowing the range of the respective β and γ rays, using the reported sample dimensions reduced somewhat for the removal of edges, and taking the specific activity of Ni^{63} and Ag^{110m} from the ORNL Catalog of Radio and Stable Isotopes distributed by the Isotopes Development Center, we calculate a concentration of approximately 4×10^{14} and 2×10^{14} atoms of nickel and silver, respectively, per cm^3 of carbon. These are the intercept or "saturation" concentrations, and they correspond to atom fractions of 4 and 2×10^{-9}, respectively.

In our experiments with Th^{228}, the thorium source contained a small amount of carrier, and we have estimated the intercept values of thorium concentration, C_s, in our specimens. The numbers show some trends with annealing conditions (higher Dt values are associated with lower C_s values) and with carbon type (the laminar carbons had the highest C_s and they did not, in general, appear to be saturated with thorium). However, most of the data fell in the range 1 to 4×10^{14} atoms/cm^3, about the same values we have calculated from the WMB data for nickel and silver. There is no good reason why these two sets of values should agree in view of the difference in the carbons and in the impurity species.

One can only speculate as to the nature of this "solubility." It is generally believed that only boron dissolves in carbon substitutionally and, according to theoretical calculations,[14, 15] it appears very unlikely that other atoms will dissolve even interstitially. We believe that the small, observed limiting concentration values represent some accessible defect concentration. This concentration is much lower than that which would be calculated by assuming that the impurity species filled all the free volume in the carbon or that the impurity species was adsorbed in a monolayer on all the crystallites if they were assumed to be 100-Å cubes. For example, a defect density of 10^{-9} corresponds roughly to the density represented by the surface area of the cone boundaries in the columnar pyrolytic carbons. These boundaries are spaced on the order of a millimeter apart. This observation may not be superfluous since both WMB and EST report finding, by autoradiography, the diffused species concentrated along the cone boundaries.

The high levels of metal atoms at the surface can be attributed to a surface effect such as chemisorption. All the experiments of EST were carried out with relatively strong thorium and uranium sources, and from their tabulations one may calculate that they find impurity concentrations on the order of 1 mg/cm^3 ($\sim 2.6 \times 10^{18}$ atoms/cm^3)--orders of magnitude

larger than the limiting concentrations estimated above. EST also found that their calculated diffusion coefficients were time dependent. Assuming that the microcracks found in the carbon specimens were not significant sinks for diffusion, these several observations can be reconciled by further assuming that the carbon structure is also time dependent in the presence of large concentrations of a metal impurity. The catalytic recrystallization of graphite with nickel, boron, and uranium has been suggested, * as has, recently, [6, 7] the crystallization of pyrolytic carbon into graphite in the presence of uranium or thorium. It is possible that in the presence of a strong source of uranium or thorium, the carbons in the EST study underwent at least a partial solid-state transformation to graphite and that the high concentrations they observed were due to chemisorption on crystallite surfaces or a real, low-level, substitutional solubility in graphite at high temperatures. In the absence of a strong source, no transformation occurs in the carbons and the observed limiting solubilities represent accessible defect concentrations.

Both EST and WMB report that on annealing their carbons at temperatures above 3000°C, the microstructure virtually disappeared and the diffusion coefficient for impurity atoms dropped precipitously. From Fig. 28 of Ref. 3 (by WMB), it appears that the "solubility" of nickel in the annealed carbon also decreased, although not to the same extent. These observations are compatible with the assumed model of a defect-type solubility.

Comparison With the Model of WMB

WMB have discussed in some detail the pre-exponential factor D_o in terms of the diffusion mechanism in columnar pyrolytic carbon. According to the absolute reaction-rate theory, † D_o in Eq. (2) is given by

$$D_o = a_o^2 \nu \exp\left(\frac{\Delta S}{R}\right) , \qquad (4)$$

where a_o is the atomic jump distance, ν is the jump frequency, and ΔS can be considered the entropy of activation for the diffusion process. WMB have observed that the values of both D_o and D for diffusion of several kinds

*This phenomenon seems to be generally accepted, but it is only vaguely described in the literature. See, for example, A. C. Titus, Proceedings of the Fourth Conference on Carbon, Pergamon Press, New York, 1960, p. 703; and W. P. Eatherly, et al., in Second International Conference on the Peaceful Uses of Atomic Energy, Vol. 15, 1958, p. 389.

†See, for example, P. G. Shewmon, Diffusion in Solids, McGraw-Hill Book Company, New York, 1963, Chapter 2.

of impurity atoms parallel to the layer planes (actually, parallel to the plane of deposition) are two to three orders of magnitude greater than those for diffusion perpendicular to the planes, while the activation energies are less variable; in fact, for thorium the activation energy for diffusion parallel to the planes is less than that for diffusion perpendicular to the planes (see Table 3). Hennig[13] also finds $Q(||) \cong Q(\perp)$ and $D_o(||) >> D_o(\perp)$ for the diffusion of boron in graphite single crystals. WMB argue that the large D_o implies a large jump distance which is of the order of the crystallite diameter, 150 Å. On this basis, the jump distance perpendicular to the planes is like the diameter of a carbon atom. This model does not adequately describe the present set of results for diffusion perpendicular to the planes, wherein the D_o values cover a wide range (16 to 7×10^4) and all the values are greater than those reported by WMB for columnar pyrolytic carbon. The variation in D_o with the type of carbon cannot be explained on the basis of differing apparent crystallite sizes, L_c, because the range in L_c values was not nearly great enough and the values are not in the right order (see Tables 1 and 3).

The lower activation energy for diffusion in the isotropic carbon and the similarity between this value and the Q reported by WMB for diffusion in columnar pyrolytic carbon in the <c> direction suggest that diffusion in these two materials occurs along similar, relatively high conductivity paths, i.e., grain or cone boundaries. The relatively high Q values for the granular and laminar carbons suggest that the differences in the details of microstructure, which are not particularly evident from the parameters in Tables 1 and 3, play a dominant role.

We have concluded that the parameters listed do not indicate the differences in microstructure which are important to diffusion. The anisotropy factor, for example, gives only the number of crystallites aligned at a given angle with respect to the plane of deposition; it says nothing about how these crystallites are aligned with respect to one another. Further evidence for this conclusion is derived from the fact that the diffusion coefficients in the laminar samples are even smaller than those observed by WMB and by EST on columnar carbons which have both a higher density, 2.20 g/cm^3, and a higher degree of preferred orientation (Bacon anisotropy factor estimated to be 6 to 7). Thus, cone boundaries are important structural imperfections which can effectively provide short-circuit paths for diffusion in the columnar carbons.

In the carbons of the present study, diffusion again must have occurred along grain boundaries of some sort (assuming no substitutional or interstitial solubility), and yet, from the range of D_o and Q values, it is apparent that these grain boundaries (or the bridges between boundaries) vary widely as conductivity paths as the carbon microstructure is changed. This is discussed further below.

Grain-boundary Diffusion Treatment

In view of the fact that a good deal of evidence points to a grain-boundary diffusion mechanism in pyrolytic carbons, it is reasonable to inspect the solutions to the grain-boundary diffusion problem which have been developed in the past fifteen years. * According to these treatments, for diffusion in a polycrystalline matrix in which the diffusion coefficient within the grain boundary is much larger than that within the grain, the logarithm of the relative concentration may be expected to be linear in the penetration distance raised to the first power† instead of the second power. However, the results of the present study, as well as those of WMB, fit the "X^2-solution" distinctly better than they fit the "X^1-solution" or "$X^{6/5}$-solution." A suggested reason for this is derived from an inspection of the grain-boundary diffusion equation. The statement of the grain-boundary diffusion problem is usually given as

$$\frac{\partial C'}{\partial t} = D' \frac{\partial^2 C'}{\partial y^2} + \frac{2D}{w} \left(\frac{\partial C}{\partial X} \right)_{X=0} , \qquad (5)$$

where C' is the concentration at any point y along the grain boundary, C is the concentration within a grain, X is the distance from the grain boundary into the grain itself, w is the width of the grain boundary, and D' and D are the grain boundary and lattice diffusion coefficients.

According to this model, the equilibrium concentration of the diffusing substance in the grain boundary is assumed to be the same as that in the grains; thus, the grain boundaries act as high conductivity paths which supply the diffusing substance to the grains, which are effectively very large sinks. The amount of diffusing material contained within the grain boundaries is thus small compared with that within the grains.

In the case of metal diffusion in pyrolytic carbons, however, we believe that C and D in Eq. (5) both effectively vanish and the equation reduces to the simple statement of Fick's second law, the solution to which is contained in Eq. (1) for the present boundary conditions. Stated somewhat differently, the high conductivity paths in pyrolytic carbons do not feed the sinks represented by the bulk of the material, and the diffusion occurs in a straightforward manner along the two-dimensional planes which constitute the grain boundaries and not within the three-dimensional lattice. The

---

*A concise review of these treatments through 1955 is given by D. McLean in Chapter 3 of Grain Boundaries in Metals (Oxford University Press, New York, 1957), and the discussion which follows is based on this chapter.

†According to the later treatment of H. S. Levine and C. J. MacCallum (J. Appl. Phys. 31, 595 (1960), the proper exponent is 6/5 over a large portion of the concentration range.

solution to this problem is the same as the solution to the surface-diffusion problem and is given essentially by Eq. (1), i. e., the logarithm of the concentration is linear in the square of the penetration distance.

The large activation energies reported herein and by WMB are not necessarily inconsistent with a grain-boundary diffusion mechanism. McLean reports the work of Clausing[16] and that of Langmuir[17] for the grain-boundary diffusion of thorium in tungsten in which Q (grain boundary) = 90 kcal/mole and Q (lattice) = 120 kcal/mole.

Previous studies of the effect of grain-boundary misorientation may have relevance to the observed large divergence in the diffusion coefficient of thorium perpendicular to the plane of deposition in the several pyrolytic-carbon structures, as well as to the extreme anisotropy of diffusion observed by WMB and EST for diffusion in columnar pyrolytic carbon. Turnbull and Hoffman[18] have found in their experiments on self-diffusion in polycrystalline silver that the rate of diffusion along a "tilt" boundary depends on the direction of the boundary with respect to the crystal orientations. It has also been reported[19] that the diffusion rates may be different in different directions along a given boundary. Furthermore, Turnbull and Hoffman[18] have analyzed the data of Achter and Smoluchowski[20] for the diffusion of silver along grain boundaries in copper, and have found that the ratio of grain-boundary diffusion coefficients for misorientations of 45° and 18° was 35.

Taken collectively, these results imply that the arrangement of the defects within a pyrolytic-carbon specimen with respect to one other is likely to be the dominant factor in determining impurity metal diffusion rates. Therefore, it does not appear that one can expect a quantitative microscopic understanding of the diffusion in these carbons either in terms of D_o and Q values or in terms of density, apparent crystallite size, and anisotropy factor. Data on the anisotropy of the thermal conductivity in these materials would probably not be of particular relevance because heat is not transported exclusively in the grain boundaries, and therefore the conductivity is less sensitive to the detailed arrangement of defects. Perhaps the best one can hope for is a corroboration of the present results with results for another diffusing species.

Extension of These Results to Other Pyrolytic Carbons

The present diffusion results are consistent with the data reported by Bokros and Sandefur on the resistance to "fuel migration" in pyrolytic-carbon coatings,[6,7] namely, that mobility is the smallest in the laminar carbons. In this regard one might reasonably ask about the ultimate limits which might be attained. It is possible to deposit laminar pyrolytic carbons with considerably higher degrees of preferred orientation. However,

because of the gross differences in the circumferential and radial thermal expansion coefficients, these materials tend to delaminate and crack readily, so they are not very interesting in practice.[6, 7] At the other extreme, the isotropic and granular carbons studied in the present research were relatively isotropic and the diffusion rates would therefore be expected to be close to upper limits. These diffusion coefficients are still smaller than those reported by WMB for the diffusion of thorium in polycrystalline graphites or for the diffusion of thorium parallel to the plane of deposition in columnar pyrolytic carbon. The anisotropy in diffusion coefficients in the relatively isotropic carbons of the present study has not yet been measured.

Diffusion in Porous Graphite

Although it was not originally intended as a part of this study, the diffusion of Th^{228} in porous graphite was observed in a cursory fashion. For three samples, the pyrolytic-carbon deposit was completely removed before depositing the thorium tracer and diffusion annealing. A summary of the results is presented in Table 4, along with some data reported by EST. Very little is known about the structure of these porous graphites. The material used in the present studies was National Carbon Company Grade ATJ graphite, a fine-grained material with a density of 1.73 g/cm^3; the graphite used in the EST studies was not specified. The data are interesting mostly because they are in qualitative agreement even though the two sets of experiments were carried out at grossly different thorium source strengths, and because the diffusion coefficients are larger by about an order of magnitude than those found in the isotropic and granular pyrolytic carbons.

Table 4

SUMMARY OF THORIUM DIFFUSION COEFFICIENTS IN POROUS GRAPHITES

Sample No.	Annealing Temp. (°C)	Annealing Time (hr)	D (cm^2/sec)
1-1	1950 ±50	64	6.1×10^{-10}
4-2	1950 ±50	64	2.8×10^{-10}
5-1	1790	8.1	6.4×10^{-11}
EST	1950	--	5.4×10^{-10}[a]
EST	1790	--	1.8×10^{-10}[a]

[a] Calculated from Eq. (9) of Ref. 4.

DISCUSSION OF ERRORS

Of the several contributory errors in the present experiments, the most serious was in the measurement of the amount of sample removed during sectioning. This number was used not only in determining the depth of penetration, but also in calculating the concentration at a given depth as expressed in the relative concentration parameter, cpm/μ. A very significant factor in the thickness measurement was the temperature of the piston on which the sample was mounted. The piston changed in length by 0.7 μ with each ^{o}C temperature change, and the temperature variations brought about by handling the piston undoubtedly led to incorrect measurements. About midway through the experiments the procedure was changed in that the piston was manipulated with tongs in order to reduce temperature and thereby length variations. Nevertheless, we believe that errors in this measurement were the most serious errors in the procedure.

For each of the materials under study, one or more "blanks" were run. In the blank runs the Th^{228} solution was deposited on one surface and the sample was then sectioned without any annealing. The tracer penetration was about the same for all blank runs--3 to 5 μ. This penetration is probably a measure of the surface roughness of the samples, which was on too fine a scale to detect with the dial indicator, and/or the smearing which occurs along the emery paper during sectioning. As such, it represents a trivial correction to the penetration via diffusion for the granular and isotropic carbon samples. However, in some of the laminar samples the total penetration distance observed after annealing was on the order of 10 μ, and it would appear that a correction might be in order. However, none of the concentration profiles for the laminar samples are anomalously high at small distances, and we have chosen to use the uncorrected data for calculating the diffusion coefficients.

SUMMARY AND CONCLUSIONS

Using a tracer technique, it has been demonstrated that the diffusion of thorium and probably, therefore, of other metal impurity atoms in pyrolytic carbons is strongly structure dependent. The diffusion coefficients in a laminar pyrolytic carbon perpendicular to the plane of deposition are about a factor of 25 smaller than those in a granular pyrolytic carbon in the temperature range 1600^{o} to 2000^{o}C. The results of this study may be summarized as follows:

$$D\ (\text{granular}) = 7.1 \times 10^{4} \exp(-152,000/RT),$$
$$D\ (\text{isotropic}) = 15.5 \exp(-114,000/RT),$$
$$D\ (\text{laminar}) = 1.2 \times 10^{4} \exp(-157,000/RT).$$

The diffusion coefficients in the present type of laminar pyrolytic carbon are even smaller than those reported by Wolfe, McKenzie, and Borg[3] and by Evans, Stiegler, and Truitt[4] for thorium diffusion in columnar pyrolytic carbons, even though the columnar material is considerably more anisotropic. It is therefore concluded that other structural parameters, particularly grain boundaries and their arrangement with respect to one another, play an important role in determining the mobility of foreign atoms.

Some of the questions remaining to be answered in the field of transport of actinides and other metallic impurities in pyrolytic carbons concern the effects of the nature and concentration of the impurity atom, the variation in diffusion coefficient parallel to the plane of deposition with structure, the effects of irradiation, the "solubility" of impurity atoms as a function of structure, the microscopic nature of the "solid solution" of impurity atoms, and the details of the transport mechanism in these materials.

REFERENCES

1. Loftness, R. L., "The Diffusion of Uranium Carbide in Graphite," North American Aviation Company Report NAA SR-64, August 2, 1950.

2. Loch, L. D., J. R. Gambino, and W. H. Duckworth, A. I. Ch. E. J. 2, 195 (1956).

3. Wolfe, J. R., D. R. McKenzie, and R. J. Borg, "The Diffusion of Non-volatile Metallic Elements in Graphite," Lawrence Radiation Laboratory Report UCRL-7324, April 29, 1964.

4. Evans, R. B., III, J. O. Stiegler, and J. Truitt, "Actinide Diffusion in Pyrocarbons and Graphite (A Summary Report on Thin-Layer Experiments)," Oak Ridge National Laboratory Report ORNL-3711, December, 1964.

5. Lonsdale, H. K., and J. N. Graves, in "Advanced, Graphite Matrix, Dispersion-Type Fuel Systems. Annual Report, April 1, 1962, to March 31, 1963," USAEC Report GA-4022 (Part I), General Atomic Division, General Dynamics Corporation, May 1, 1963, pp. 75-84.

6. Bokros, J. C., and N. L. Sandefur, "Uranium Migration Through Pyrolytic Carbons Deposited in a Fluidized Bed (U)," General Atomic Report GA-5793, October, 1964 (C/RD).

7. Bokros, J. C., et al., "Advanced, Graphite-Matrix, Dispersion-Type Fuel Systems, Annual Report, April 1, 1963, through March 31, 1964." (U) USAEC Report GA-5016 (Part II), General Atomic Division, General Dynamics Corporation, pp. 5-45. (C/RD).

8. Lonsdale, H. K., and J. N. Graves, in "Advanced, Graphite-Matrix, Dispersion-Type Fuel Systems. Annual Report, April 1, 1963, through March 31, 1964," USAEC Report GA-5016 (Part I), General Atomic Division, General Dynamics Corporation, pp. 61-63.

9. Bokros, J. C., et al., "Advanced, Graphite-Matrix, Dispersion-Type Fuel Systems. Annual Report, April 1, 1963, through March 31, 1964," USAEC Report GA-5016 (Part I), General Atomic Division, General Dynamics Corporation, pp. 7-37.

10. Lonsdale, H. K., and J. N. Graves, in "Advanced, Graphite-Matrix, Dispersion-Type Fuel Systems and Research on Graphite. Quarterly Progress Report for the Period Ending February 14, 1965," USAEC Report GA-6181, General Atomic Division, General Dynamics Corporation, February 15, 1965, pp. 30, 31.

11. Crank, J., Mathematics of Diffusion, Clarendon Press, Oxford, 1956.

12. Evans, R. B., III, Oak Ridge National Laboratory, private communication.

13. Hennig, G., J. Chem. Phys. 42, 1167 (1965).

14. Dienes, G. J., J. Appl. Phys. 23, 1194 (1952).

15. Iwata, T., F. E. Fujita, and H. Suzuki, J. Phys. Soc. Japan 16, 197 (1961).

16. Clausing, P., Physica 7, 193 (1927).

17. Langmuir, I., J. Franklin Inst. 217, 543 (1934).

18. Turnbull, D., and R. E. Hoffman, Acta Met. 2, 419 (1954).

19. Couling, S. R. L., and R. Smoluchowski, J. Appl. Phys. 25, 1538 (1954).

20. Achter, M. R., and R. Smoluchowski, J. Appl. Phys. 22, 1260 (1951).

V. FISSION-PRODUCT RELEASE FROM CARBIDE FUEL SYSTEMS

P. Gethard, C. Adams, R. Precourt, L. Zumwalt

EFFECT OF COATING STRUCTURE ON DIFFUSION OF URANIUM AND METALLIC FISSION PRODUCTS THROUGH PYROLYTIC CARBON

In order to obtain information which will help elucidate the mechanism by which uranium and metallic fission products diffuse in pyrolytic carbon, disks of U^{235}-impregnated ATJ graphite were coated with several types of pyrolytic carbon for use in fission-product release studies. The procedure is to produce fission products in the disks by neutron irradiation. The concentration gradient of metallic fission products through the coatings is then measured as a function of annealing time and temperature.

The diffusion of uranium is measured by first annealing the samples and then irradiating them. Measuring the concentration gradient of the La^{140} fission product then gives the distribution of uranium in the coating caused by the anneal.

Since earlier experiments indicated the need for assuring parallel surfaces,[1] the ATJ graphite disks were machined parallel (±1.25 μ) prior to impregnation with U^{235}. After coating the impregnated disks, the flat surfaces were again machined parallel (±1.25 μ), since the pyrolytic carbon tends to build up on edges even though they are beveled as they were in this case.

The disks (5/16 in. in diameter, 1/16 in. thick) were impregnated by placing them in a concentrated solution of uranyl nitrate plus nitric acid and then placing the system under vacuum. About 7% volume impregnation is accomplished this way, and thus the amount of U^{235} ending up in the graphite is determined by its concentration in the solution. The impregnated disks, each containing 0.1 mg of U^{235}, were dried at 110°C and finally baked in vacuo at 1015°C for 1 hr to eliminate all traces of nitrate.

Three types of pyrolytic coatings were deposited on the impregnated disks (see Table 1). Using the TRIGA reactor King furnace, the steady-state release of fission gases was measured from one disk at 1200°C. The data obtained are shown in Table 2. As in the preliminary experiments, the release is relatively high in comparison with the release measured for coated fuel particles. This is indicative of a significant level of fuel in the coating itself.

Table 1

PYROLYTIC-CARBON COATINGS DEPOSITED ON U^{235}-IMPREGNATED GRAPHITE DISKS

Type	Deposition Temperature (°C)	CH_4 Concentration (%)	Coating Thickness (μ)
1. Isotropic[a]	1650	15	150
2. Grainy-isotropic[b]	2000	15	110
3. Granular[c]	1900	3	150

[a] Coatings were deposited in a 2.5-cm-diameter coater using an initial charge of 400 cm^2 (15 g of 150- to 250-μ (Th, U)C_2 particles together with graphite disks). Total gas flow was 4,500 cm^3/min and average deposition rate was 75 μ/hr.

[b] Coatings were deposited in a 3.5-cm-diameter coater using an initial charge of 800 cm^2 (48 g of 295- to 350-μ UC_2 particles together with graphite disks). Total gas flow was 7,325 cm^3/min and average deposition rate was 85 μ/hr.

[c] Coatings were deposited in a 3.5-cm-diameter coater using an initial charge of 970 cm^2 (70 g of 350- to 420-μ (Th, U)C_2 particles together with graphite disks). Total gas flow was 18,300 cm^3/min and average deposition rate was 25 μ/hr.

Table 2

STEADY-STATE RELEASE AT 1200°C OF FISSION GASES FROM A U^{235}-IMPREGNATED GRAPHITE DISK COATED WITH PYROLYTIC CARBON[a]

Isotope	Half-life (hr)	Fractional Release
Kr^{85m}	4.4	2.1×10^{-3}
Kr^{88}	2.8	1.9×10^{-3}
Kr^{87}	1.3	1.9×10^{-3}
Kr^{89}	0.053	9.8×10^{-4}
Xe^{138}	0.28	4.4×10^{-4}
Xe^{139}	0.011	1.6×10^{-3}

[a] Type 2 in Table 1.

Procedure

Each sample was lightly irradiated to about 10^{13} fissions. The concentration gradient through these flat specimens was measured by carefully removing graphite by a precision lapping procedure in which graphite is removed at about 6 μ at a time with an accuracy of $\pm 1\,\mu$. The sample is carefully mounted in a holder, and each layer is removed by a single pass over a sheet of fine (4/o emery) abrasive paper. Since all the carbon removed in each pass adheres to the paper, the Ba^{140} Removed is determined by γ-spectrometry on the paper itself. Ba^{140} is measured, of course, by means of the 1.60-Mev γ-ray of its La^{140} daughter.

Results

Measurements made of the distribution of uranium in the coatings, simply as a result of the coating process itself, show a surprisingly high level of uranium relative to that in impregnated disks. Figure 1 shows the concentration of fission-product barium (Ba^{138} and Ba^{140}) in an uncoated disk. From these data and the known irradiation conditions, the concentration and thus the distribution of U^{235} were determined. Figures 2, 3, and 4 show the distribution of U^{235} in the three types of coatings described in Table 1. It is interesting to note that for only one type of coating, isotropic-deposited at 1650°C, there was no peak concentration of U^{235} at the boundary between the fueled graphite and its coating. For the other two types, it has dropped off from the level in the unfueled wafer, but the boundary level is still higher than that either in the fueled graphite or in the coating. These high levels of fuel in the coatings complicate the intended studies of fission-product diffusion, but on the other hand the techniques used here can help to develop coatings in which the levels of uranium can be reduced to a minimum.

Included in Fig. 4 is the effect of a 1-hr anneal at 1400°C on the diffusion of barium in the granular type of pyrolytic carbon deposited at 1900°C. Except for a higher peak value at the boundary for the annealed sample, the distribution is not much different than for the unannealed control. Electron microprobe studies show that the concentration of fuel at the boundaries is associated with the bonding of the coating to the fueled ATJ graphite, the concentration being higher for a tight bond and non-existent for a poor bond. Therefore, the differences observed in these peak values at the boundaries may all be experimental. The only way to resolve this is to obtain microprobe data from a cross section of a disk prior to sectioning and to see if the correlation holds.

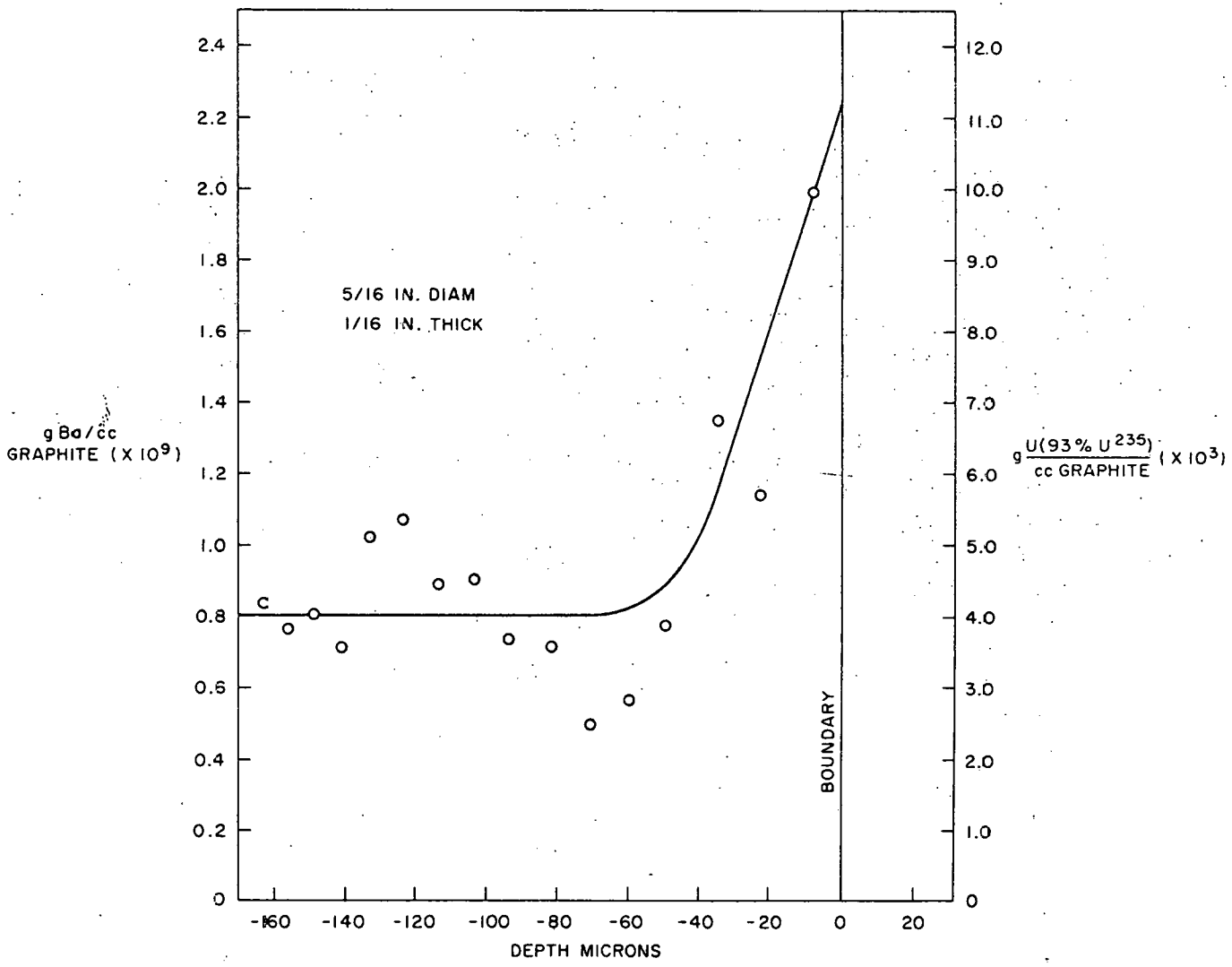

Fig. 1--Distribution of Ba^{140} and U^{235} in an uncoated graphite wafer impregnated with uranyl nitrate and baked 1 hr at 1015°C

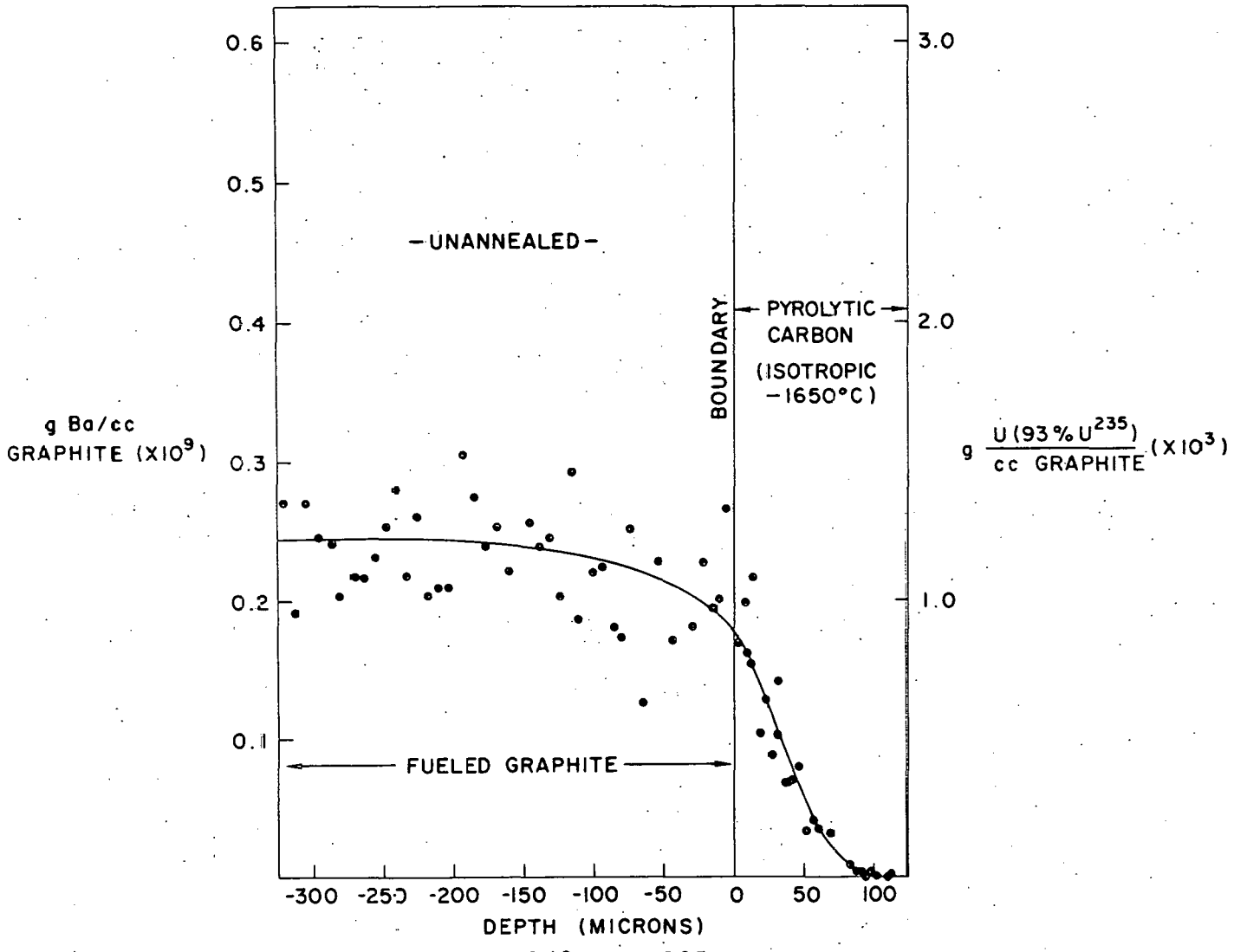

Fig. 2--Distribution of Ba^{140} and U^{235} in a fueled graphite wafer coated with pyrolytic carbon

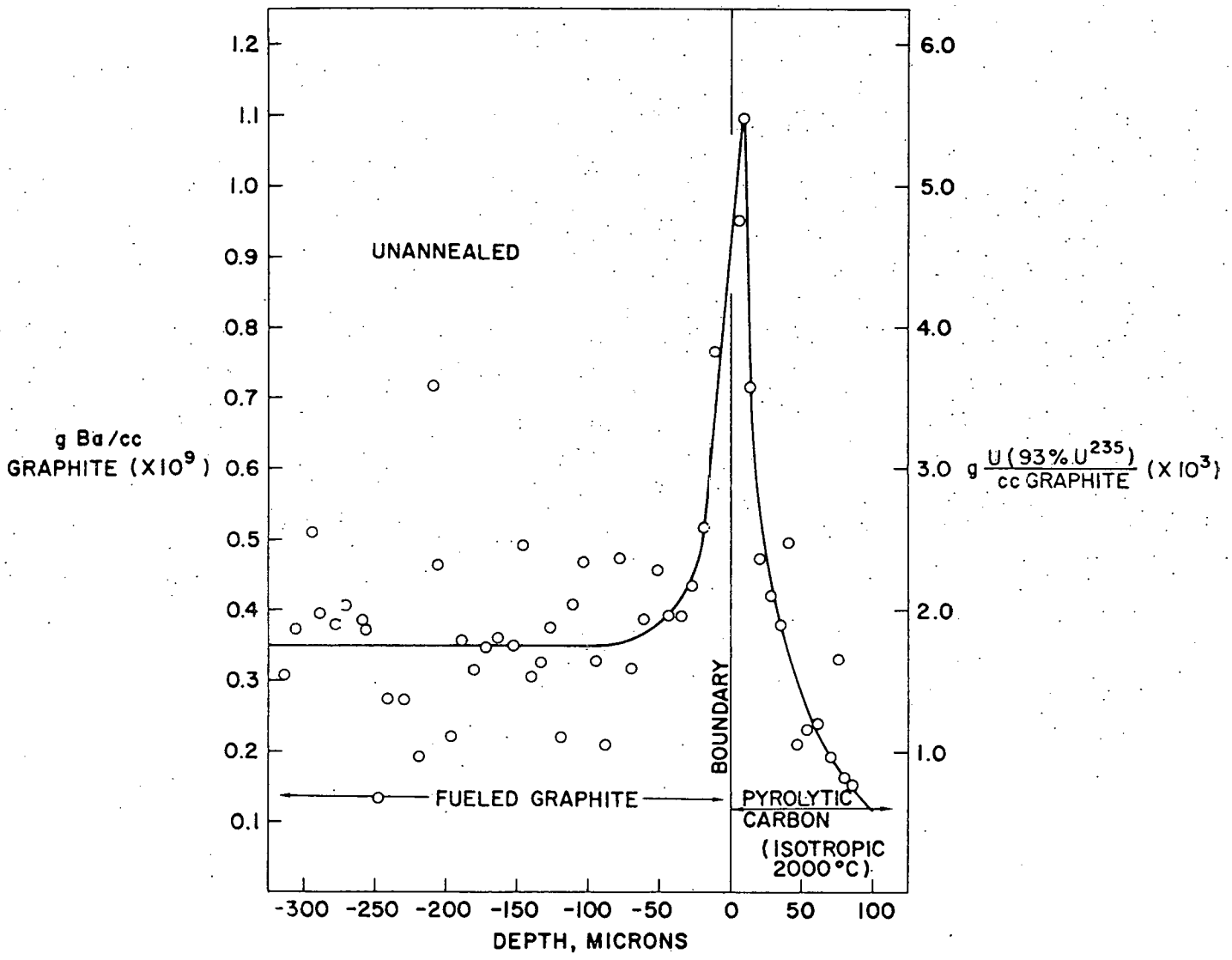

Fig. 3--Distribution of Ba^{140} and U^{235} in a fueled graphite wafer coated with pyrolytic carbon

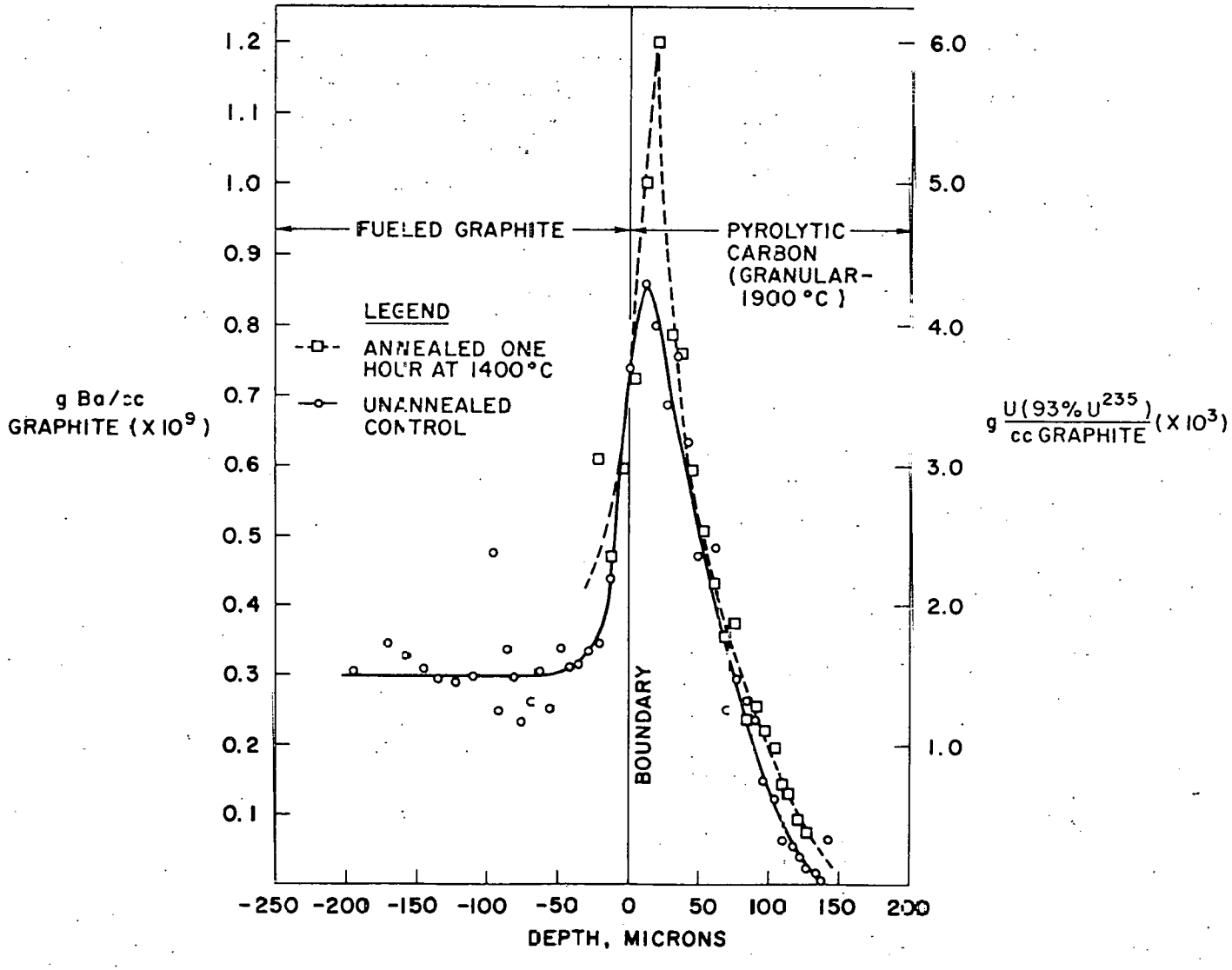

Fig. 4--Distribution of Ba^{140} and U^{235} in fueled graphite wafers coated with pyrolytic carbon

FISSION-GAS RELEASE FROM DENSE ThC_2

The steady-state release of short-lived fission gases from dense ThC_2 and $(Th, U)C_2$ containing a small amount of uranium (Th:U ratio, 21:1) was studied over the temperature range 1100° to 1700°C. Both types of particles were of the size range 150 to 250 μ.

The release data are shown in Table 3, along with release data obtained previously for monogranular UC_2 (179 to 210 μ) at 1400° and 1600°C. Note the similar fractional releases for dense ThC_2 and monogranular UC_2. This is taken to indicate that release is by a similar diffusion process (through krypton or xenon occupied lattice vacancy motion) in crystal structures (of ThC_2 and UC_2) which are quite similar.

It is also interesting to note that the inclusion of about 5% UC_2 along with ThC_2 in the dense material improves the fission-gas retention by a factor of 2 to 10.

The data were obtained by heating the samples to the desired temperature and then photofissioning them with X-rays generated with the General Atomic linear accelerator. Observed release fractions (F_t) were corrected to true steady-state release fractions (F_∞) as described in an earlier report.[2] As a test of the validity of this correction, a sample of ThC_2 was run for 3 hr at 1300°C and compared with data obtained for two 1-hr runs at the same temperature. As seen by the data in Table 4, which gives the observed steady-state release for a short-lived isotope (such as Kr^{89}, which attains equilibrium during a 1-hr irradiation), there is no difference. For isotopes such as Kr^{85m} (4.4 hr = $t_{1/2}$) which have not achieved equilibrium even after 3 hr, the apparent steady-state release increases with irradiation time, verifying, if in an approximate way, the validity of the correction.

REFERENCES

1. Bokros, J. C., et al., "Advanced, Graphite-Matrix, Dispersion-Type Fuel Systems and Research on Graphite, Quarterly Progress Report for the Period Ending November 14, 1964," USAEC Report GA-5918 (Part I), General Atomic Division, General Dynamics Corporation, December 1, 1964.

2. Anderson, E. E., et al., "Advanced, Graphite-Matrix, Dispersion-Type Fuel Systems, Annual Report, April 1, 1962, Through March 31, 1963," USAEC Report GA-4022 (Part 1), General Atomic Division, General Dynamics Corporation, April 1, 1962.

Table 3

STEADY-STATE FISSION-GAS RELEASE FROM WELL-DEFINED FUEL PARTICLES

Sample Description	Temp. (°C)	Fractional Release (F_∞ = R/B)					
		Kr^{85m}	Kr^{88}	Kr^{87}	Kr^{89}	Xe^{138}	Xe^{139}
High-density ThC_2 (150-250μ)	1100	3.5×10^{-2}	3.6×10^{-2}	3.2×10^{-2}	6.6×10^{-3}	9.5×10^{-3}	2.2×10^{-3}
	1300	6.0×10^{-2}	4.4×10^{-2}	5.2×10^{-2}	1.6×10^{-2}	1.0×10^{-2}	---
	1300	7.0×10^{-2}	6.8×10^{-2}	5.2×10^{-2}	1.2×10^{-2}	1.3×10^{-2}	5.3×10^{-3}
	1500	1.1×10^{-1}	2.6×10^{-2}	8.5×10^{-2}	2.0×10^{-2}	2.0×10^{-2}	---
	1700	1.1×10^{-1}	7.1×10^{-2}	6.0×10^{-2}	2.5×10^{-2}	3.1×10^{-2}	2.0×10^{-2}
Monogranular UC_2 (179-210μ)	1400	1.6×10^{-1}	9.7×10^{-2}	8.5×10^{-2}	1.9×10^{-2}	2.2×10^{-2}	---
	1600	1.1×10^{-1}	7.7×10^{-2}	7.0×10^{-2}	1.8×10^{-2}	2.5×10^{-2}	2.0×10^{-2}
High-density $(Th,U)C_2$ Th:U ratio 21:1 (150-250μ)	1100	1.4×10^{-2}	1.0×10^{-2}	7.8×10^{-3}	2.1×10^{-3}	1.9×10^{-3}	1.6×10^{-3}
	1300	4.0×10^{-2}	3.5×10^{-2}	2.7×10^{-2}	6.0×10^{-3}	2.6×10^{-3}	1.0×10^{-2}
	1500	6.7×10^{-2}	5.4×10^{-2}	3.9×10^{-2}	3.1×10^{-3}	2.7×10^{-3}	3.1×10^{-2}

Table 4

EFFECT OF IRRADIATION TIME ON OBSERVED STEADY-STATE RELEASE VALUES
(HIGH-DENSITY ThC_2 AT 1300°C)

Irradiation Time (hr)	Observed Fractional Release (F_t)					
	Kr^{85m}	Kr^{88}	Kr^{87}	Kr^{89}	Xe^{138}	Xe^{139}
1	1.7×10^{-2}	1.5×10^{-2}	2.4×10^{-2}	1.6×10^{-2}	6.5×10^{-3}	---
1	2.0×10^{-2}	2.3×10^{-2}	2.4×10^{-2}	1.2×10^{-2}	8.3×10^{-3}	5.3×10^{-3}
3	3.1×10^{-2}	2.9×10^{-2}	3.4×10^{-2}	1.0×10^{-2}	8.7×10^{-3}	---

VI. CHARACTERIZATION OF MICROSTRUCTURE OF GRAPHITIC MATERIALS

J. L. White, A. S. Schwartz, G. R. Tully, Jr.,
J. O. Gardner, E. A. Taylor, D. E. Davis

ELECTRON MICROGRAPHY

Work on this program using optical micrography, including the recent work illustrated in the section on carbide-graphite materials prepared by hot-working, has indicated the existence of important structural detail at magnifications at or beyond the resolution of optical microscopy. Attempts to apply replication electron micrography to polished graphite surfaces have been of limited value owing to smearing, microcracking, and deposition of debris in pores even with the most careful polishing procedures.[1] Therefore, an apparatus for etching by argon-ion bombardment has been set up, and some results on materials of interest to the present program are described here.

The cathodic etcher is similar in principle to that employed by other workers.[2-4] The work illustrated in this section employed etching conditions of 2 to 3 kv with approximately 10 μ argon pressure. This produced a discharge current of approximately 1 ma. It was found that specimens prepared by different polishing procedures, which produce somewhat different structures as observed optically, were brought to essentially equivalent structures after sufficient cathodic etching.

Structure of Fuel-matrix Graphite

The initial work with the cathodic etcher was done with a hot-pressed fuel-matrix graphite prepared with 25 wt-% Barrett No. 30 pitch binder and 75 wt-% GP-38 graphitized petroleum coke. This specimen was annealed at 2800°C. The bulk density of this specimen was 1.76 g/cm^3, and the porosity was 16%, measured by mercury porosimetry for pores with diameters greater than 0.085 μ. The micrographic sections were longitudinal, i.e., the plane of the section was parallel to the hot-pressing direction and therefore perpendicular to the preferred orientation of the graphite layer planes.

The effective action of cathodic etching in removing debris and in revealing the accommodation microcrack patterns may be seen by comparing

the etched structures of Figs. 1 and 2 with the as-polished structure of Fig. 3. The microcrack patterns, occurring in both linear and curved regions, are similar to those observed by other workers,[3][5] in conventional graphites and in pyrolytic graphite. The microcracks, which presumably run parallel to the graphite layer planes, appear to be made up of connected etch pits. Regions showing a stepped structure are believed to be areas where the layer planes are sectioned at a low angle. It is difficult to identify clearly any region as originally pitch binder. However, it is not clear at this point whether the etching conditions have been optimized with respect to removal of all effects of polishing, and further work will be done on this problem.

Structure of Hot-worked Graphite Containing Molybdenum Carbide

The cathodic etching technique is currently being applied to study the fine structure of the carbide-graphite materials prepared by hot-working at temperatures such that the dispersed carbide phase is in the liquid state. Figures 4 through 7 are electron micrographs prepared from cathodically etched surfaces of graphite-molybdenum carbide bodies hot-worked at 2720°C to a true strain of 56%. This specimen has a measured porosity ($d > 0.085\ \mu$) of approximately 1% and analyzes at 3.2 at.-% molybdenum. (Optical photomicrographs of this specimen are shown in Fig. 22, Section VIII, of this report.)

The photomicrograph of Fig. 4 was taken from a lightly etched region where the etching is inadequate to remove the graphite debris but is adequate to reveal structure in the molybdenum carbide particles. The photomicrographs of Figs. 5 through 7 were taken from somewhat more heavily etched regions; the fine structure of the carbide particles has disappeared, but the microcrack patterns of the graphite matrix are more clearly evident.

Several tentative observations may be drawn from these initial studies. The hot-worked carbide-graphite material does not show curved microcracks to the degree observed with the annealed matrix graphite, although the general appearance and spacing of the microcracks is approximately the same. Rather well-defined grain boundaries are also evident in the carbide-graphite material, and there appears to be good contact between the carbide particles and the graphite matrix.

In Figs. 5 and 6, the preferred orientation of the graphite layer planes is from upper left to lower right, as indicated by the delamination microcracks in the majority of the fields of view. These microcracks are most dense in the neighborhood of the carbide particles or in areas where the graphite is misoriented relative to the preferred orientation.

P-5608 (5,000×)

Fig. 1--Electron micrograph of an annealed fuel-matrix graphite. Cathodically etched. Carbon replica, negatively shadowed with Pd. Longitudinal section.

P-5611 (~14, 000x)

Fig. 2--Electron micrograph of an annealed fuel-matrix graphite. Cathodically etched. Carbon replica, negatively shadowed with Pd. Longitudinal section.

P-5620 (~14,000x)

Fig. 3--Electron micrograph of an annealed fuel-matrix graphite. No cathodic etching. Carbon replica, negatively shadowed with Pd. Longitudinal section.

P-5636

(5, 000×)

Fig. 4--Electron micrograph of a hot-worked graphite matrix containing molybdenum carbide particles. Lightly cathodically etched. Carbon replica, negatively shadowed with Pd. Longitudinal section.

P-5785 6300x

Fig. 5--Electron micrograph of a hot-worked graphite matrix containing molybdenum carbide particles. Moderately cathodically etched. Carbon replica, negatively shadowed with Pd. Longitudinal section.

P-5796 6300x

Fig. 6--Electron micrograph of a hot-worked graphite matrix containing molybdenum carbide particles. Moderately cathodically etched. Carbon replica, negatively shadowed with Pd. Longitudinal section.

P-5792 17,000x

Fig. 7--Electron micrograph of a hot-worked graphite matrix containing molybdenum carbide particles. Moderately cathodically etched. Carbon replica, negatively shadowed with Pd. Longitudinal section.

Several types of cracks may be distinguished. The delamination cracks appear as connected rows of pits, as grooves of relatively constant depth, or as intermediate forms of these two types. A few cracks perpendicular to the general delamination microcracks were found, as shown in Fig. 7; their appearance suggests a structure of aligned pits.

Although the majority of the carbide particles were rough in shape, some of the smaller particles, e.g., those appearing near the center in Fig. 6, have sides aligned with the graphite matrix. Few or no delamination microcracks appear to be associated with these particles.

Structure of Graphitized Pitch

In previous work with both optical and electron micrography, it has been found difficult to identify, with certainty, those regions of a manufactured graphite which were originally pitch binder. To simplify this problem, pure binder material (Barrett No. 30 pitch) has been pyrolyzed and finally heat-treated to 2800°C for 50 min, and the resulting porous body is being studied by optical and electron microscopy.

For the purpose of cathodic etching, the specimen was impregnated with Wood's metal. The optical photomicrograph of Fig. 8a displays a structure not unlike a very fine-grained graphite. Observation by sensitive-tint microscopy reveals that some regions of this material possess a preferred orientation. The electron micrograph shown in Fig. 8b displays a markedly different structure from those observed in the previous electron micrographs. Etch pits of approximately the same size as found in the commercial graphite are distributed in a much more random manner over the majority of the specimen, and few, if any, are aligned to form the microcrack pattern typical of a manufactured graphite.

KINETICS OF OXIDATION OF GRAPHITIC BODIES IN LIQUID MEDIA

It is well known that bodies containing a high percentage of a nongraphitizing carbon, such as lampblack, contract more during high-temperature irradiation than do bodies made from predominantly graphitizing carbon sources and heat-treated to graphitizing temperatures. Commercial graphites, and, indeed, graphites especially designed for nuclear reactor use, often contain small amounts of nongraphitizing carbon as binders, fillers, or impregnants. Often the formulation is not available, but of more importance is the fact that it is not known exactly where, and in what structure, these materials finally locate in a finished graphite body. Also, it is not known whether the graphitizing binder or filler does indeed graphitize fully during heat treatments. Furthermore, the effect of small amounts of carbon on irradiation contraction is not clear. As the designs

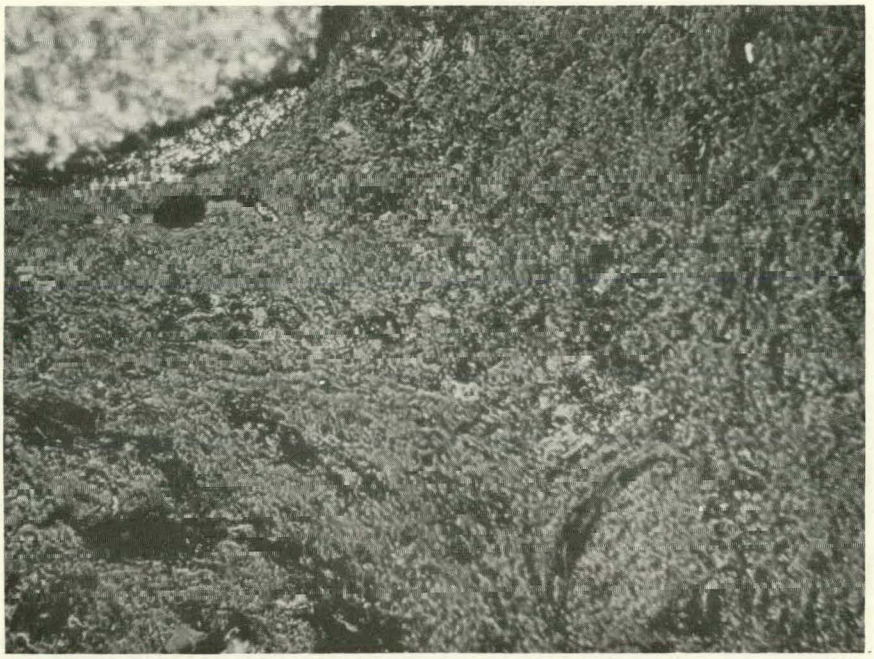

M-10411-7 500x

(a)

P-5913 6300x

(b)

Fig. 8--Optical and electron micrographs of graphitized pitch, impregnated with Wood's metal and moderately cathodically etched: (a) optical micrograph, bright field, (b) electron micrograph, carbon replica, negatively shadowed with Pd

of graphite-moderated reactors become more advanced, it becomes necessary to minimize the graphite contraction so that longer reflector and fuel-element life may be obtained.

In view of the above, it is thought that a method of determining small amounts of ungraphitized carbon in graphite bodies could be used to give a characterization factor that, together with an anisotropy relationship, would correlate with irradiation behavior and serve to point the way to improved formulations and fabrication methods.

A technique for the measurement of the graphitic and nongraphitic components has been developed and described in the literature by Oberlin and Mering.[6] The method involves manometric measurements of the rates of oxidation of graphitic materials in a chromic acid medium. Oberlin, Rappeneau, and Yvars[7] have shown that the method can be used to follow the structural effects during graphitization or irradiation.

The chemical principle of the technique is that all carbons are oxidized to CO_2 by a hot mixture of H_2SO_4 and $Ag_2Cr_2O_7$; however, the rate of oxidation varies a thousandfold, depending on the state of graphitization. Highest reaction rates are found for natural graphites or fully graphitized manufactured graphites. Lowest reaction rates are found for soft carbons heat-treated at temperatures of less than 1200°C. Oberlin, et al., have identified three characteristic levels of reaction rates, which are presumed to define three constituents: F_1, F_2, and F_3. The F_1 fraction corresponds to amorphous carbon and oxidizes at the lowest rate. Their published work does not indicate that they have attempted to detect small amounts of the F_1 fraction.

An apparatus has been built to apply the oxidation technique to graphites under study in this program. It is patterned after that of Oberlin and Mering[6] and is shown schematically in Fig. 9. Fifty milligrams of finely ground samples are placed in the bottom of a reaction flask, and the side arm of the reaction flask is filled with 25 cm^3 of reactant made up from 5 g of $Ag_2Cr_2O_7$ dissolved in 25 cm^3 of H_2SO_4. The reaction flask is connected to the rest of the apparatus through a pivoting joint, and it is immersed in a water bath maintained at 80°C. When the contents of the flask have equilibrated at 80°C, the flask is pivoted so that the dichromate solution empties into the body of the flask, starting the oxidation reaction. The gaseous product then passes through a reduction tube heated to 400°C; this tube is filled with active copper and a small amount of silver wool, and any free oxygen or halogens liberated by the oxidation reaction are trapped in the reduction tube. The gas is then passed through a water cooler into a large flask filled with silver wool and immersed in a constant-temperature bath at 25°C. This flask is also connected to an oil manometer that indicates the system pressure. This pressure rise can be directly correlated with the extent of reaction after the apparatus is calibrated.

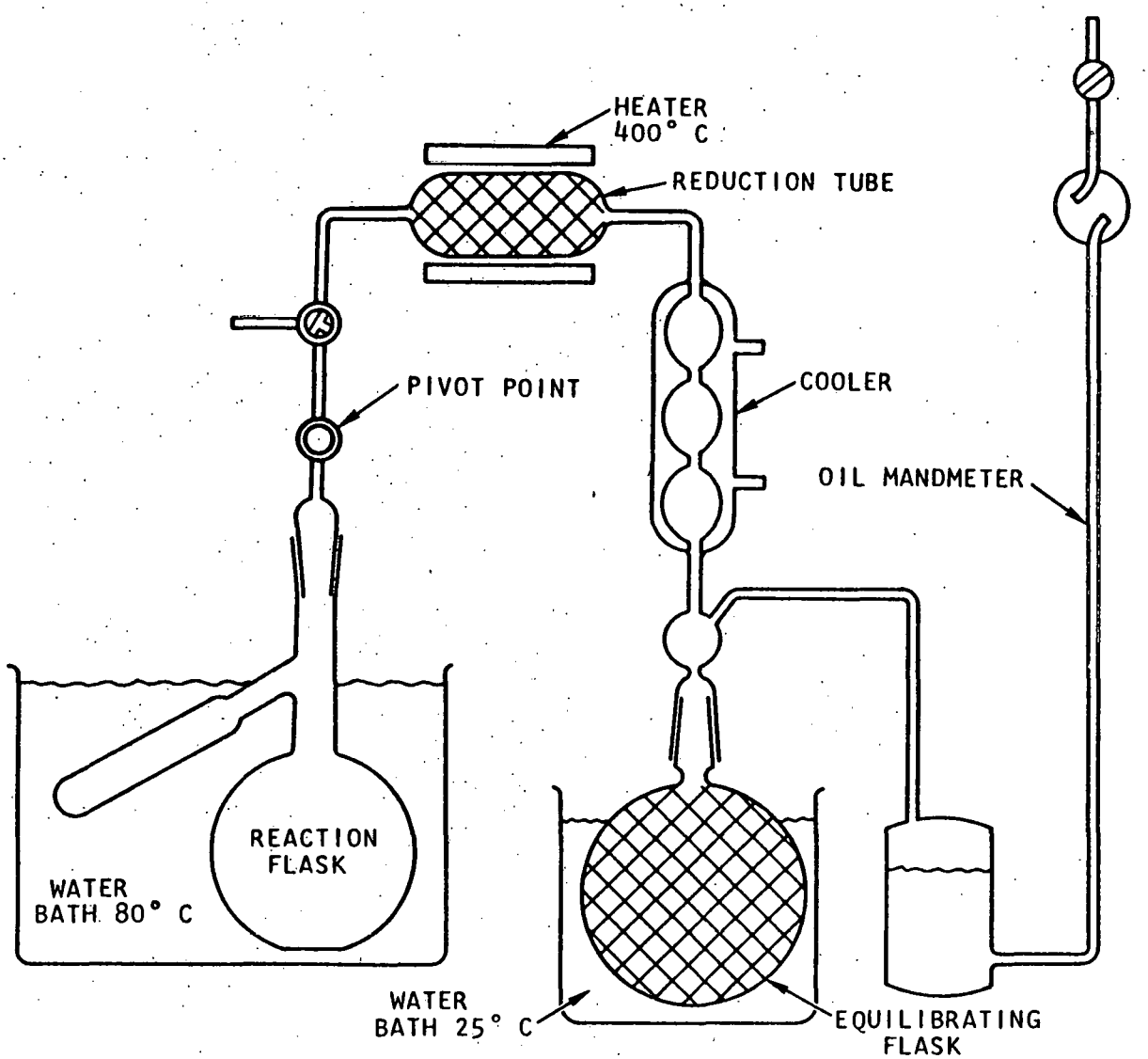

Fig. 9--Apparatus for determining the degree of graphitization using Oberlin technique

Two experimental runs have been made with this apparatus. The first run was made on unground natural flake graphite. Because of the large size of the graphite flakes used, the reaction rate in this case was so slow that no useful data were obtained. A run on natural flake graphite will be repeated with ground flakes. The second run was made on a commercial grade of finely ground graphite flour. Data were taken for the first 3 hr of the run, then the run was continued for another 16 hr to allow the reaction to proceed essentially to completion. At the end of this reaction period, calculations showed approximately 3% of the graphite unaccounted for. Inspection of the reaction vessel showed that foaming during the initial vigorous reaction between the graphite and the dichromate reagent had deposited small amounts of unreacted carbon on the sides of the reaction vessel above the liquid level. This carbon could account for the 3% difference between the measured amount of graphite sample and the calculated amount reacted.

Figure 10 is a plot of the logarithm of the amount of unreacted carbon versus time for the second run. The amount of carbon unreacted was corrected for the carbon deposited on the reaction vessel wall by assuming that all the carbon in contact with the reagent had reacted after 20 hr. With the nomenclature of Oberlin,[6] the data show two slopes, labeled f_3 and f_2. Slope f_2 represents partially graphitized carbon, and it indicates that 8.5% of the original sample of carbon was less than fully graphitized. Slope f_3 represents fully graphitized carbon, and it indicates that 91.5% of the original sample of carbon was fully graphitized. The reaction rate constants obtained from the data are shown in Table 1. These values agree well with those obtained by Oberlin, et al.[6][7] The reaction rate constants are defined by the equation

$$A_t = A_1 e^{-f_1 t} + A_2 e^{-f_2 t} + A_3 e^{-f_3 t}, \qquad (1)$$

where A_t is the fraction of the initial amount of carbon which is unreacted at time t, and A_1, A_2, and A_3 are the fractions of the three carbonaceous constituents F_1, F_2, and F_3.

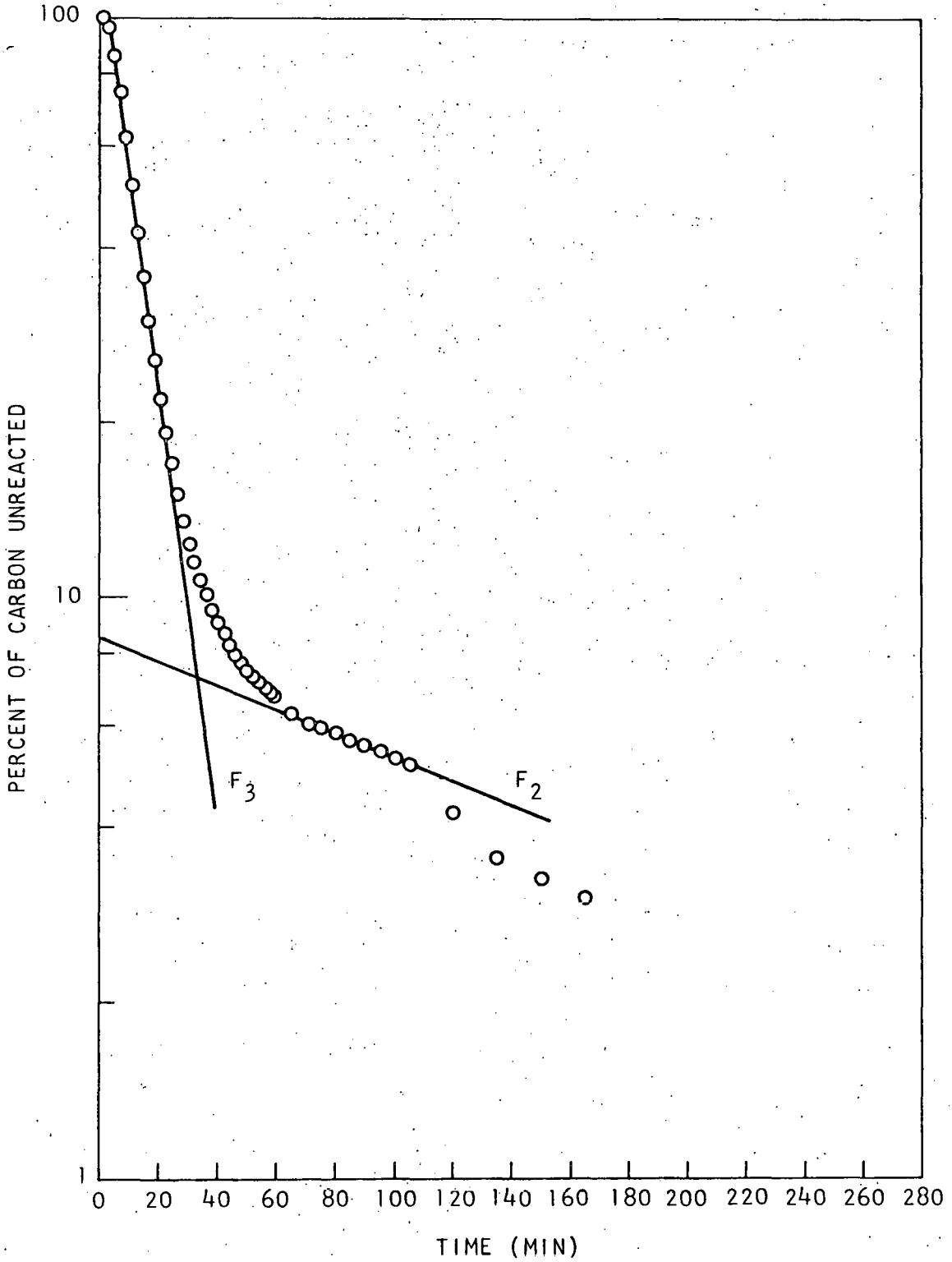

Fig. 10--Oxidation rate of finely ground graphite flour

Table 1

REACTION RATE CONSTANTS FOR THE OXIDATION OF GRAPHITE FLOUR BY SILVER DICHROMATE

Temperature (°C)	Components	Reaction Rate Constants, f_2 and f_3	
		Experimental Results (min^{-1})	Oberlin's Results (min^{-1})
80	f_2	4.8×10^{-3}	3 to 30×10^{-3}
80	f_3	8.5×10^{-2}	6 to 13×10^{-2}

REFERENCES

1. Hales, R. L., and E. M. Woodruff, "Technique for Microscopic Studies of Graphite," Proc. Fifth Carbon Conf. 1, 456 (1962).

2. Tarpinian, A., "Crystallographic and Microstructural Changes Occurring during the Graphitization of a Petroleum Coke," Watertown Arsenal Laboratory Report WAL-TR-825.5/1, January, 1960.

3. Thrower, P. A., and W. N. Reynolds, "Microstructural Changes in Neutron-irradiated Graphite," J. Nucl. Mater. 8, 221 (1963).

4. Bierlein, T. K., H. W. Newkirk, Jr., and B. Mastel, "Etching of Refractories and Cermets by Ion Bombardment," J. Am. Ceram. Soc. 41, 196 (1958).

5. Tarpinian, A., "Electrochemical and Ion Bombardment Etching of Pyrolytic Graphite," J. Am. Ceram. Soc. 47, 532 (1964).

6. Oberlin, M., and J. Mering, "Kinetic Studies of the Oxidation of Graphitizable Carbons by Liquid Media," Carbon 1, 471 (1964); available in free translation as General Atomic Report GA-tr-6049.

7. Oberlin, M., J. Rappeneau, and M. Yvars, "Kinetics of Oxidation by a Liquid Solution of Unirradiated and Irradiated Nuclear Graphites," Carbon 1, 481 (1964); available in free translation as General Atomic Report GA-tr-5174.

VII. RELATION OF PHYSICAL PROPERTIES OF GRAPHITIC MATERIALS TO MICROSTRUCTURE

R. J. Price, J. C. Bokros, G. B. Engle, W. E. Ellis

THERMAL EXPANSION AND PREFERRED ORIENTATION

The work on this subject is described in a topical report entitled "Relationship Between Preferred Orientation, Thermal Expansion, and Radiation-induced Length Changes in Graphite," by R. J. Price and J. C. Bokros,[1] and is summarized as follows.

Expressions may be derived for the thermal expansion coefficient of polycrystalline graphite in terms of the single-crystal coefficients and the preferred orientation of the sample. Thermal expansion and preferred orientation measurements were performed on pyrolytic, molded, hot-worked, extruded-rod and extruded-tube graphites in order to test the validity of this model. These results showed that such expressions adequately represent the behavior of several different graphites over a range of temperatures, provided that the "accommodation" of a part of the c-direction crystallite expansion by microcracks is taken into account. The amount of c-direction accommodation is a function of preferred orientation and the direction of measurement. It is small for the principal c-direction in a highly oriented body and large for a random aggregate of crystallites and is probably controlled by the number of microcracks which form when cooling from the graphitization temperature.

YOUNG'S MODULUS AND PREFERRED ORIENTATION

A topical report entitled "Young's Modulus of Pyrolytic Carbon in Relation to Preferred Orientation," by R. J. Price,[2] describing the theoretical and experimental work on this subject, has been prepared. In this report, expressions are derived which express Young's modulus of an anisotropic aggregate of hexagonal crystallites in terms of the single-crystal elastic constants and functions of the preferred orientation, assuming either a constant tensile strain or a constant tensile stress throughout the aggregate. Measurements of Young's modulus and preferred orientation on a number of pyrolytic carbons with different anisotropies show that the "constant stress" model represents the behavior of these materials to a good approximation. Young's modulus of polycrystalline nuclear graphite whose dislocations have been pinned by a low-temperature neutron irradiation agrees with the same model.

To obtain the data on Young's modulus of massive pyrolytic carbon and polycrystalline nuclear graphite, cylindrical samples having a 5-mm gauge diameter were tested in tension in an Instron testing machine. The specimens were cemented into gimbal-type grips with epoxy cement. The use of gimbals eliminates bending stresses in the gauge length. Strain was measured by pairs of metal-foil strain gauges glued onto opposite sides of the gauge length. The outputs of the two gauges were monitored separately, and final centering of the specimen in the gimbals was achieved by making adjustments until the two gauges recorded the same strain. Figure 1 shows one sample mounted in the gimbals ready for testing. Young's modulus was obtained from the initial slope of the loading curve.

RADIATION-INDUCED LENGTH CHANGES AND PREFERRED ORIENTATION

An analysis of radiation-induced dimensional changes in terms of preferred orientation is described in Ref. 1. A model similar to that used for thermal expansion may be used to express the irradiation-induced dimensional changes in polycrystalline graphite in terms of the preferred orientation of the sample, a contraction in the crystallite a-direction, and an expansion in the crystallite c-direction, which is partially accommodated by microcracks. The model was found to be in reasonable agreement with published irradiation data for a number of graphites. A rigorous test of the analysis is difficult to derive from existing data for two reasons: First, it is difficult to compare observations on different grades of graphite irradiated in different reactors at temperatures that frequently changed during the irradiation; second, nearly all the reliable measurements under well-controlled conditions have used nuclear graphite extruded as logs, the preferred orientation of which is very similar in all cases. Since the intrinsic distortion rates of individual crystallites have not been measured directly but must be deduced from a set of data on extruded polycrystalline graphite that is treated as a standard, application of the equations to data from graphite having a preferred orientation similar to that of the standard involves a built-in self-consistency, which greatly reduces the value of the test. A more satisfactory test would be to irradiate samples of graphite made from identical starting materials, but having different degrees of preferred orientation, under identical conditions of temperature and flux. It would then be possible to observe whether the dimensional changes have the predicted relationship to preferred orientation.

It is planned to make a test of this type, using samples cut from the wall of an extruded graphite tube whose texture is such that the radial, tangential, and longitudinal directions have different and well-defined degrees of crystalline alignment.[3] Preferred-orientation and thermal-expansion measurements have already been reported for this material.[1-3]

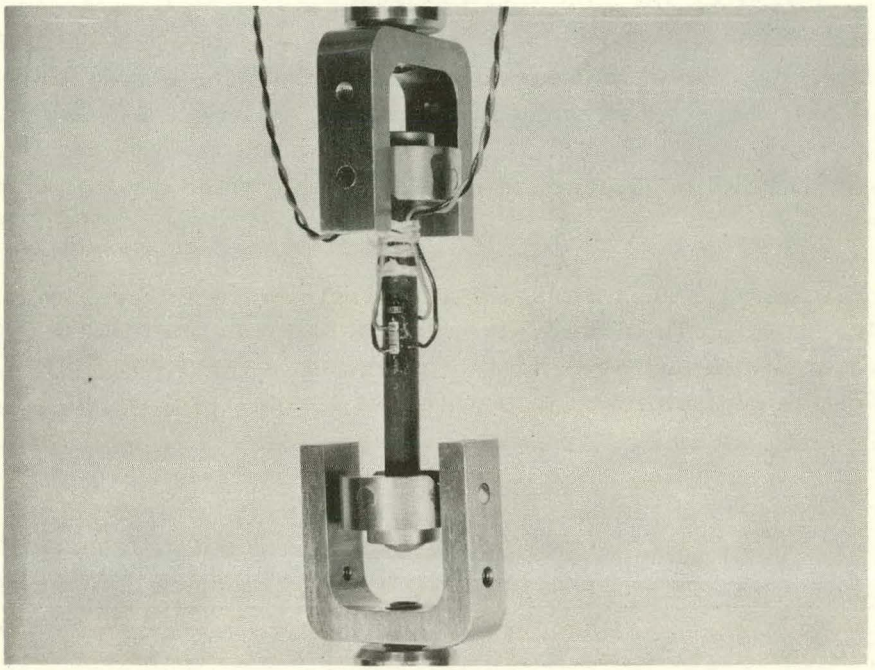

Fig. 1--Tensile sample of polycrystalline nuclear graphite mounted in gimbal grips for measurement of Young's modulus.

The starting materials for the tube were GP-38 coke and Barrett No. 30 pitch. A section of the tube was given a final graphitization heat treatment of 2 hr at 2800°C, and five pairs of samples, measuring approximately 0.500 in. by 0.375 in. by 0.045 in., were cut in the two orientations shown in Fig. 2. Fiducial holes 0.013 in. in diameter were drilled in the samples, as shown in Fig. 3. The spacing of the holes gives three length measurements in the longitudinal and tangential directions and four measurements in the radial direction for each pair of samples.

The spacings were measured with a toolmaker's microscope. Ten sets of readings were taken for each spacing, giving a ±0.01% standard error of the mean. After irradiation, the spacings will be remeasured and the dimensional changes in the three directions will be compared with the predictions.

The five pairs of samples are currently being irradiated in the GETR.* Each pair of samples is in a different cell of the capsule with a different irradiation temperature. The capsule is now in the fifth cycle of a scheduled six-cycle irradiation and is due for discharge in April. The mean operating temperatures of the five cells during the first four cycles lie in the range 600° to 1030°C.

INFLUENCE OF FILLER AND BINDER COMPOSITION ON STRUCTURE AND PROPERTIES

An experiment has been initiated to determine the role of pitch binder and binder content (binder film thickness) on the preferred orientation, microstructure, physical properties, and subsequently neutron-induced dimensional changes in graphitic bodies. Various techniques being developed in other phases of the current graphite research will be used to characterize the samples.

A series of molded samples were prepared with the following filler materials: (1) uncalcined needle coke, (2) calcined needle coke, (3) natural flake graphite, and (4) Gilsocarbon coke (isotropic). The binder (coal-tar pitch) content was varied in order to observe, if possible, the effect of binder film thickness on the various fillers and, in particular, the regions of binder-filler interface.

The samples were heated slowly to 900°C to carbonize the binder and subsequently heated to 2600°C to graphitize the binder and filler. The samples formed with Gilsonite carbon had poor physical integrity and cannot be machined. The others were satisfactory.

---

*This irradiation is being performed under Project Agreement No. 17 of Contract AT(04-3)-167.

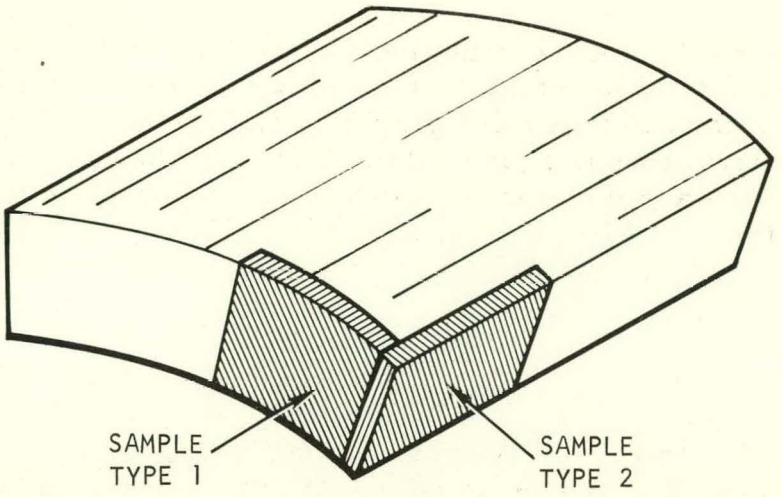

Fig. 2--Procedure for cutting samples from wall of an extruded graphite tube for measuring irradiation-induced length changes; Type 1 radial and tangential directions; Type 2 radial and longitudinal directions.

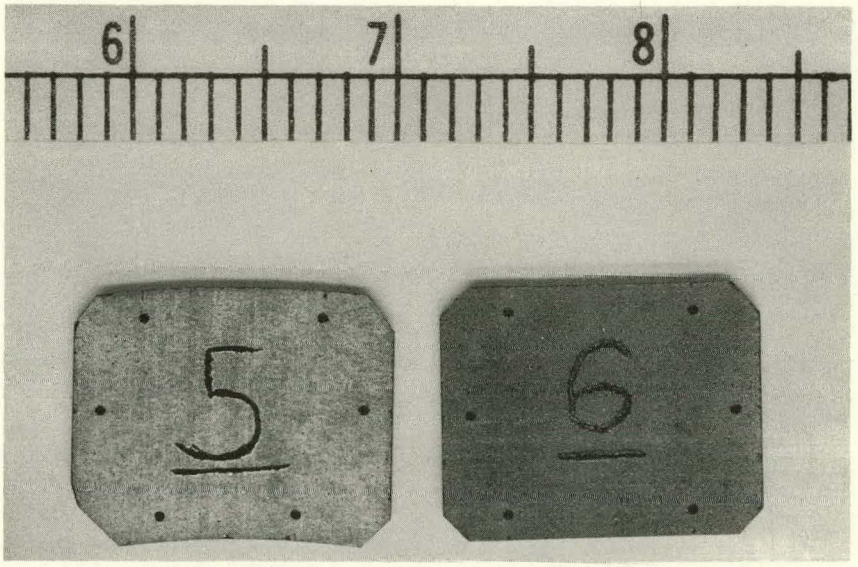

Fig. 3--Samples for measuring radiation-induced length changes in graphite; left, Type 1; right, Type 2 (see Fig. 2); scale is in centimeters.

In future work, special attention will be directed toward observation of the uncalcined coke materials and how the microstructure and orientation are affected by carbonization and graphitization of the binder. Later irradiation experiments are planned to determine the effect of fast neutron flux on properties and dimensional change and to correlate the effect of binder content.

REFERENCES

1. Price, R. J., and J. C. Bokros, "Relationship Between Preferred Orientation, Thermal Expansion, and Radiation-induced Length Changes in Graphite," submitted to J. Appl. Phys. (General Atomic Report GA-5571, August, 1964).

2. Price, R. J., "Young's Modulus of Pyrolytic Carbon in Relation to Preferred Orientation," to be submitted to Phil. Mag.

3. Bokros, J. C., R. J. Price, and G. R. Tully, Jr., "The Anisotropy of Extruded Graphite Tubes," J. Nucl. Mater., in press (General Atomic Report GA-5102, April, 1964).

VIII. CHEMICAL AND METALLURGICAL PROCESSES FOR MODIFYING THE MICROSTRUCTURE OF GRAPHITE

J. L. White, J. M. Pontelandolfo, L. C. Foster

During the period covered by this report, the investigation of processes for the modification of the microstructure of graphite has been directed toward two aspects of hot-working: (1) pitch content as a hot-working variable, and (2) the effects of additives on the hot-working process and on the properties of the resulting materials. In the latter case, particularly promising results have been obtained in hot-working carbide-containing bodies at temperatures such that a portion of the body is in the liquid state. Results presently available are given below for this work, which is currently in progress.

Details concerning the device and methods applied to hot-working graphitic bodies in compression at temperatures from 2250° to 3000°C are given in Refs. 1 through 3.

PITCH CONTENT AS A HOT-WORKING VARIABLE

The results of previous work[2] suggest that the pitch content of a fuel-matrix graphite is an important variable with respect to hot-working. Two studies have been undertaken to define how the properties of a hot-worked fuel-matrix graphite vary with the pitch content. In the first study, the amount of pitch binder is varied by using a standard graphitized petroleum coke as the filler. In the second study, various proportions of the standard filler are replaced by pitch-binder coke. In both cases the conventional hot-pressing process for fuel-matrix graphites[4] is used to prepare the compacts to be hot-worked. In the work reported below, emphasis has been given to defining the properties of a fuel-matrix graphite prepared with 20 wt-% pitch binder, since this is the same matrix used for the carbide-graphite bodies.

Fuel-matrix Graphite Prepared with 20 Wt-% Pitch Binder

Standard specimens of fuel-matrix graphite were prepared by hot-pressing cylinders 2 in. long by 1 in. in diameter. These bodies were prepared with 20 wt-% Barrett No. 30 pitch as the binder and 80 wt-% GP-38 graphitized petroleum coke as the filler. The hot-working conditions involved temperatures of 2400° to 2800°C and loads of 5000 to 10,000 lb, the more intensive conditions generally being employed to reach the higher strain levels. Representative microstructures of these bodies are shown

in Fig. 1 and compared with similar micrographs on bodies prepared with 10 wt-% pitch.

The data on compressive strength are summarized in Fig. 2. The compressive strengths were measured on cylindrical specimens, 0.25 in. in diameter by 0.375 in. high, cut with the cylinder axis either parallel or perpendicular to the direction of hot-working in compression. Data for hot-pressed fuel-matrix graphite prepared with 10 wt-% pitch binder are included to demonstrate the favorable effect of using greater pitch contents in specimens to be hot-worked than are used in conventional graphite-matrix fuel bodies. It is clear that pitch contents of the order of 20 wt-% or greater are necessary in order to obtain beneficial effects by hot-working and that these beneficial effects cannot be obtained at high strain levels.

The effective action of hot-working in reducing the gross porosity and in increasing the bulk density of fuel-matrix graphite is illustrated in Figs. 3 and 4. Bodies of higher pitch content are clearly superior in reaching higher densities and lower porosities. The scatter in the data is believed to be due in large part to the variations in density of the hot-pressed starting material.

The reduced porosity of the hot-worked graphite is expected to be reflected in the permeability. Some measurements of the helium permeability of the hot-worked fuel-matrix graphite are shown in Fig. 5. Although these measurements also show appreciable scatter, the superiority of higher pitch contents is again evident.

Fuel-matrix Graphite Prepared with Various Proportions of Pitch-coke Filler

The conventional hot-pressing process used to prepare compacts of fuel-matrix graphite is not readily adaptable to a raw-pitch content in excess of 30 wt-%. Therefore, in order to prepare graphite bodies with pitch-binder contents as high as 100 wt-%, the filler was prepared by mixing various fractions of pitch coke and graphitized petroleum coke, and the hot-pressed compacts were prepared with a pitch-binder content of 20 wt-%. The pitch coke was prepared by calcining Barrett No. 30 pitch and grinding the residue. After mixing with appropriate amounts of GP 38 graphite powder, the mixture was given a graphitization anneal at 2650°C for 1 hr. The compacts were then prepared by the conventional hot-pressing techniques, using Barrett No. 30 pitch as the binder.

The specimens were hot-worked in compression at temperatures in the neighborhood of 2700°C, using applied stresses as high as 10,000 psi. Annealed specimens were prepared for purposes of comparison. The physical-property measurements available at this time are summarized

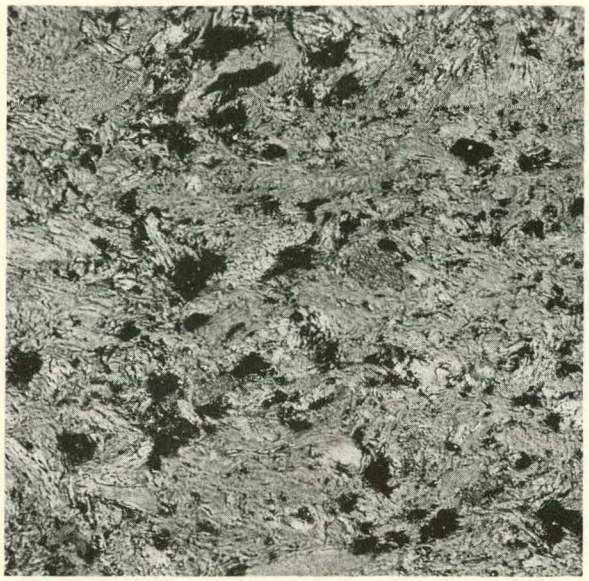

M-2501-2-1 150x

(a)

M-2502-2-3 150x

(b)

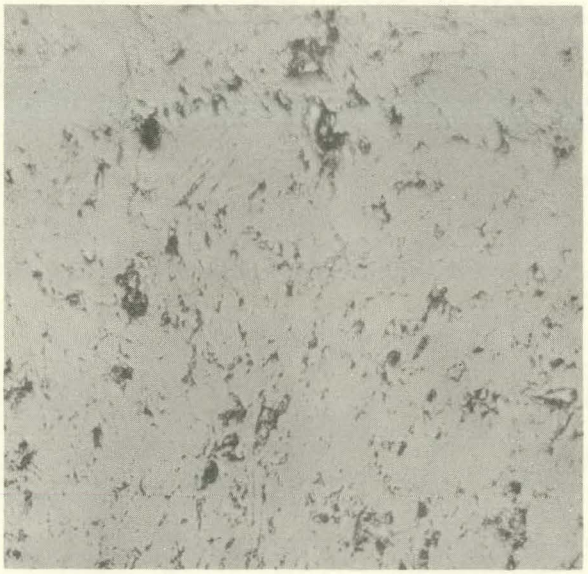

M-10363-1 200x

(c)

M-10365-1 200x

(d)

Fig. 1--The microstructures of fuel-matrix graphites as a function of pitch content and hot-working: (a) 10 wt-% pitch binder, no hot work, (b) 10 wt-% pitch binder, 38% true strain in hot-working, (c) 20 wt-% pitch binder, no hot work, (d) 20 wt-% pitch binder, 36% true strain in hot-working.

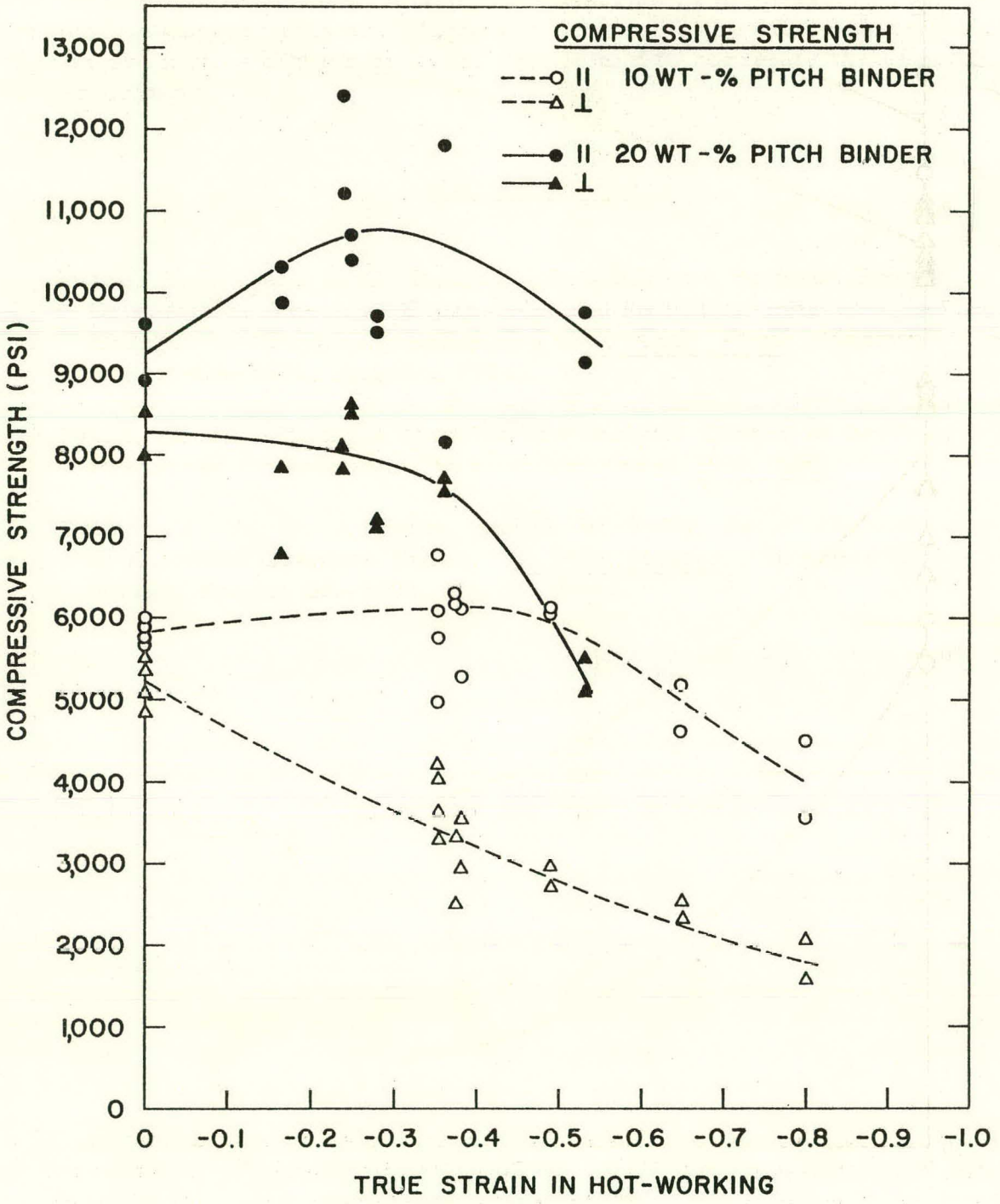

Fig. 2--The compressive strength of fuel-matrix graphites hot-worked in compression.

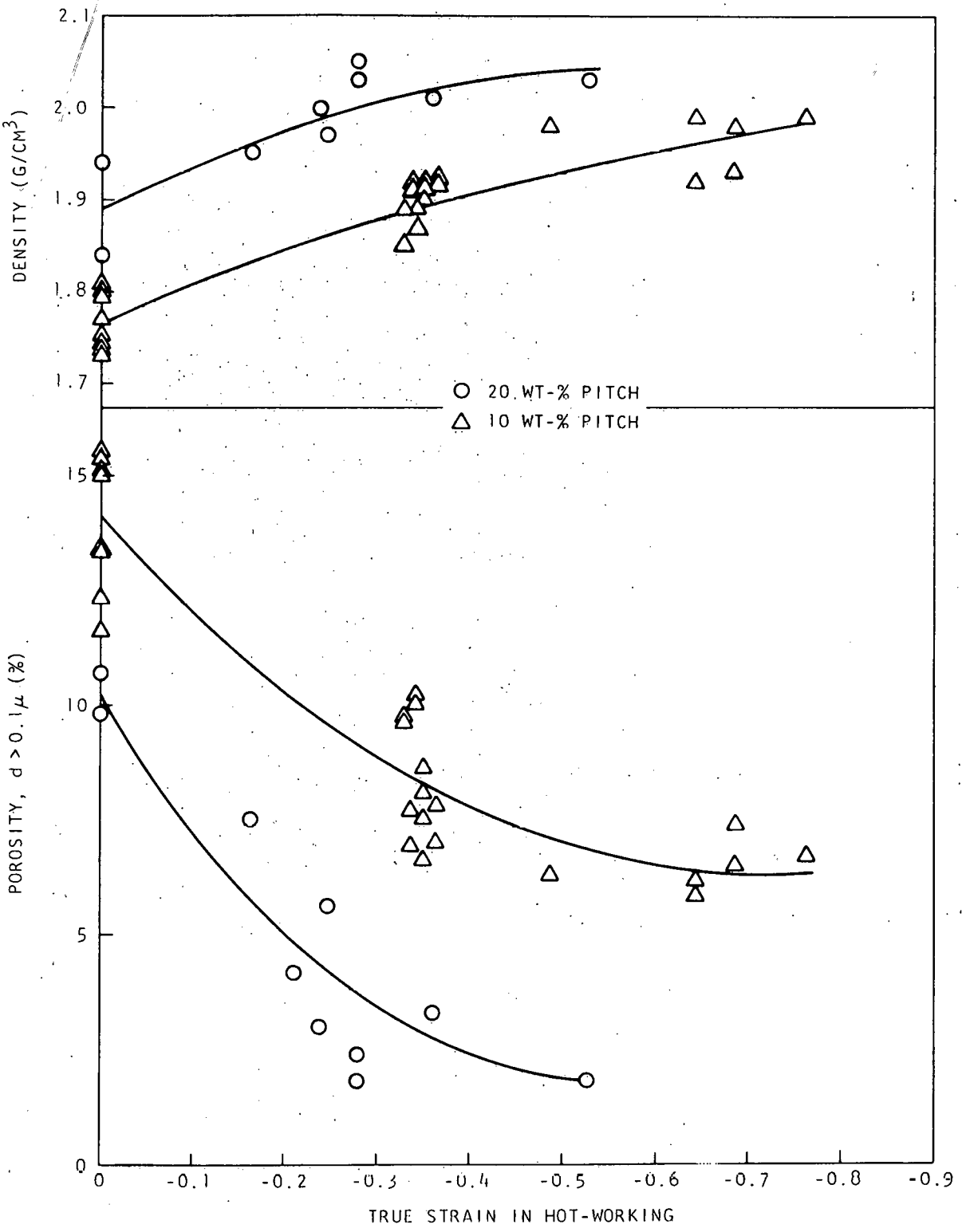

Fig. 3--Density and porosity (pores theoretically greater than 0.1 micron in diameter) of fuel-matrix graphites prepared with two levels of pitch content.

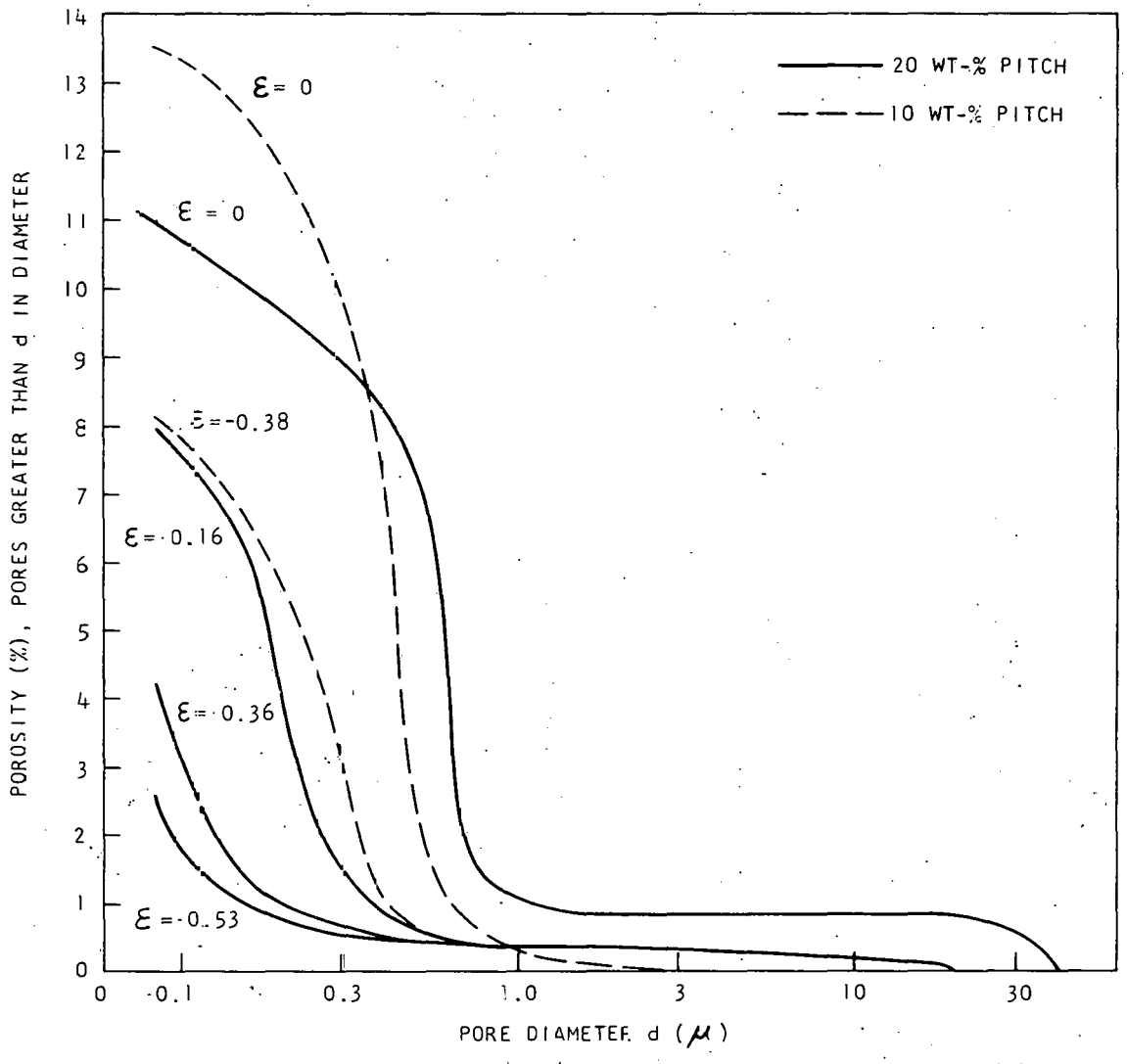

Fig. 4--Typical pore spectra of fuel-matrix graphite as a function of hot-working strain.

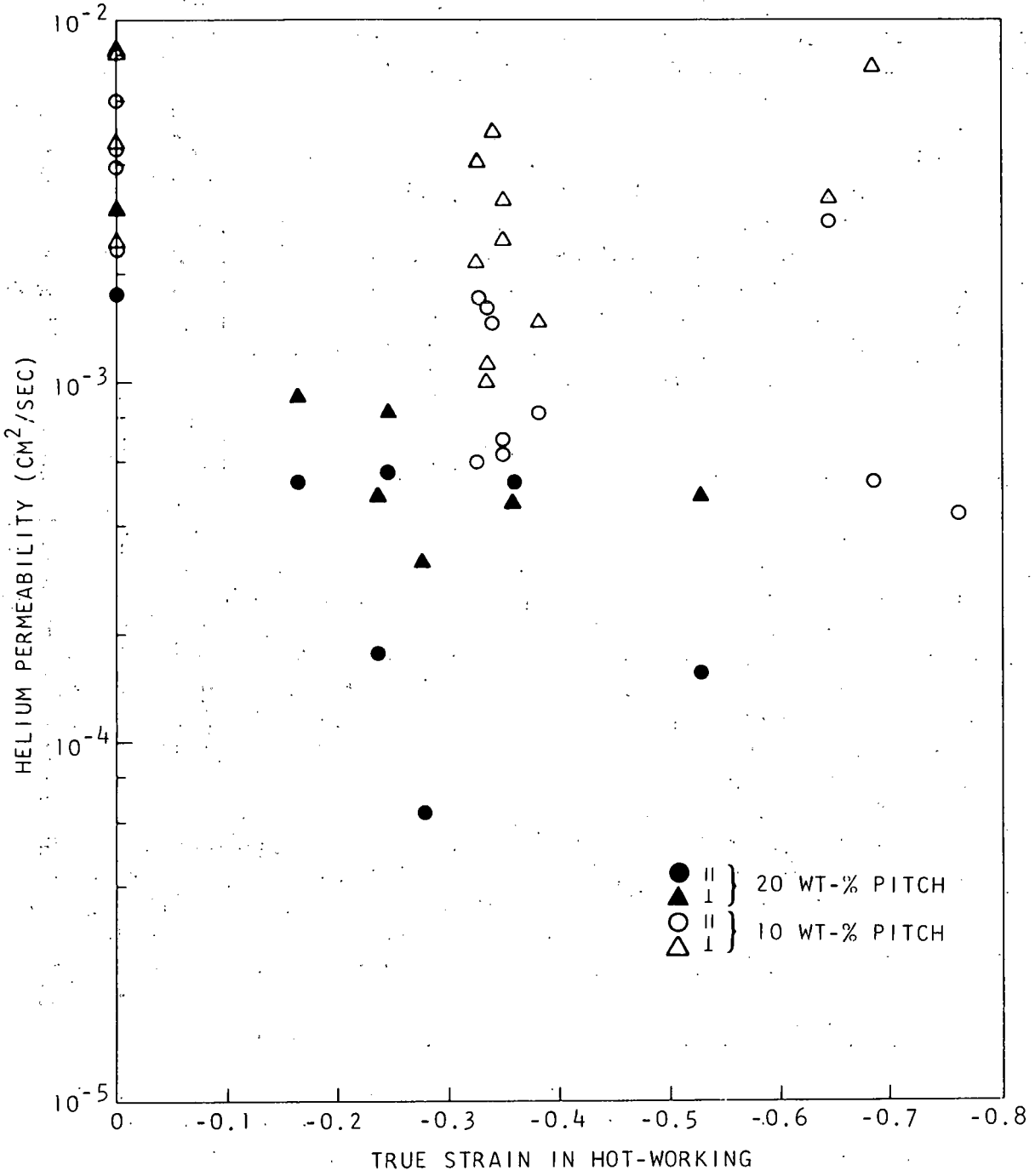

Fig. 5--Helium permeability of fuel-matrix graphites as a function of true strain in hot-working.

in Table 1. These data show appreciable scatter and inconsistency, particularly with respect to porosity and permeability. Although hot-working usually effected appreciable reductions in the values of these properties, there was no systematic pattern in the property data for the annealed specimens.

Micrographic studies provided several significant reasons for the scatter in the properties. By visual comparison of the photomicrographs of the various materials, it was possible to rank the specimens in an order consistent with the porosity values given in Table 1. Inhomogeneous regions and large shrinkage cracks, such as those shown in Fig. 6a, were also found and were attributed to the segregation of pitch coke. Observations by the sensitive-tint technique suggested that some of these pitch-coke regions were not fully graphitized.

HOT-WORKING GRAPHITE WITH ADDITIVES

In previous work,[1-3] an apparent enhancement in the plasticity of graphite during hot-working has been observed for two conditions: (1) hot-working a low-pitch fuel-matrix graphite containing 23 vol-% ZrC particles, and (2) hot-working a fuel-matrix containing 12 vol-% UC_2 particles at temperatures such that the carbide was in the liquid state. The microstructure of this latter body indicated good densification and low porosity. Thus, the purpose of the present investigation is to explore further the effects of various additives on the hot-working process and on the properties of the hot-worked bodies.

Although this work was begun by studying the properties and high-temperature behavior of bodies containing solid carbides, the emphasis during the period covered by this report has been shifted to investigation of graphite-carbide bodies hot-worked with the carbide-bearing phase in the liquid state. The initial results of this latter work are given in Ref. 5.

Graphite Bodies Hot-worked with Carbides in the Solid State

Hot-working runs were conducted on graphite bodies containing carbide particles (ZrC or NbC) at 12 vol-% loading. The graphite matrix was prepared with a pitch content of 20 wt-%, and the bodies were formed by hot-pressing. The particle sizes were 125 to 175 μ ZrC and 125 to 250 μ NbC. The cylindrical bodies (1 in. in diameter by 2 in. long) were hot-worked at approximately 2600°C to true strains of the order of 25% with a load of 6000 lb. Reference specimens containing no carbide particles were hot-worked under similar conditions. A comparison of the hot-working curves (ram displacement versus time) showed no significant differences in plasticity.

Table 1

PROPERTIES OF HOT-WORKED FUEL-MATRIX GRAPHITES
PREPARED WITH VARIOUS PITCH CONTENTS

Pitch Content in Filler (%)	Hot-working True Strain (%)	Density (g/cm^3)	Porosity, $d > 0.1\ \mu$ (%)	Helium Permeability[a] $[(cm^2/sec) \times 10^3]$		Compressive Strength[a] (psi)	
				Parallel	Perpendicular	Parallel	Perpendicular
40	0	1.69	18.6	39.2	56.2	6,120	5630
40	-0.43	1.93	5.8	2.9	2.2	10,510	6880
50	0	1.86	10.7	----	26.7	8,130	6340
50	0	1.78	12.2	4.7	7.5	8,880	8280
50	-0.34	1.97	1.4	0.022	0.24	12,600	6400
50	-0.36	1.92	1.9	1.00	1.43	11,480	6600
50	-0.41	1.96	7.4	2.0	5.1	10,180	6400
50	-0.63	2.03	6.8	----	3.3	10,600	4670
100	0	1.85	8.3	5.8	7.8	10,660	9780
100	-0.23	2.00	9.1	9.6	9.9	11,250	7500
100	-0.34	1.94	4.6	3.1	5.9	12,060	7220

[a] Measured parallel and perpendicular to the direction of hot-working in compression.

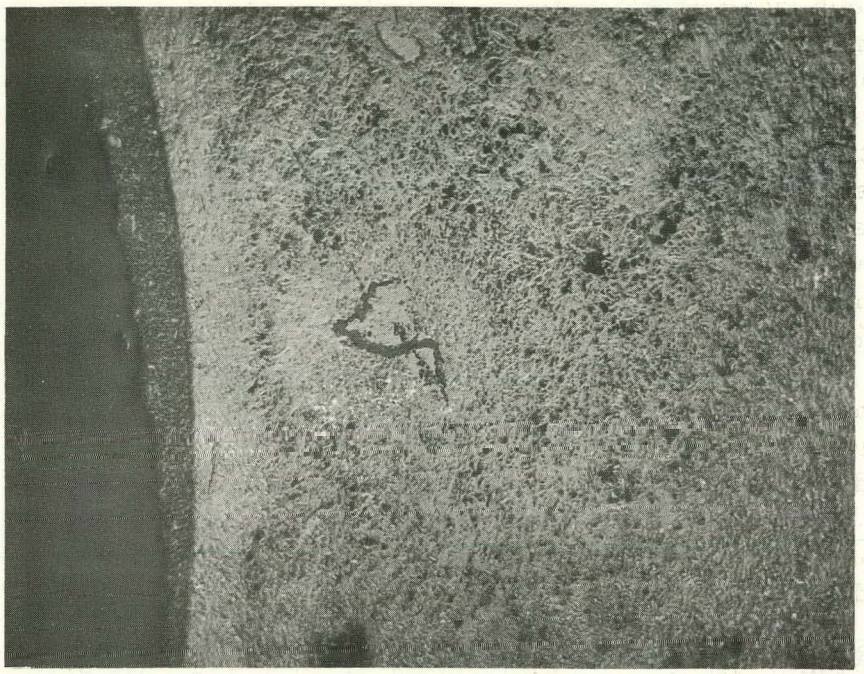

M-7588-1 (50×)

(a)

M-7589-1 (50×)

(b)

Fig. 6--Microstructure of matrix graphite with 50 wt-% pitch coke in filler, longitudinal section: (a) annealed, note regions of shrinkage cracks and penetration of mounting medium into various regions of specimen; (b) hot-worked to true strain of 36%.

In view of the fact that an apparently enhanced plasticity was observed in previous work with a matrix graphite prepared with 10 wt-% pitch and containing 23 vol-% ZrC particles, [3] a series of differential deformation experiments was undertaken on the graphite bodies containing NbC or ZrC particles at 12 vol-% loading. These differential deformation experiments[3] reduce the uncertainties of loading and temperature distribution present in the usual hot-working runs. The results of these experiments confirmed that (1) a significantly enhanced plasticity in hot-working is not observed with 20 wt-% pitch bodies containing 12 vol-% NbC or ZrC particles, and (2) an enhanced plasticity is observed with 10 wt-% pitch bodies containing 23 vol-% ZrC particles.

The microstructures of hot-worked bodies containing ZrC particles are compared in Fig. 7. The matrix of higher pitch content is apparently denser despite the lower hot-working strain.

Some properties are compared in Table 2 for bodies hot-worked or annealed at 2600°C. These results indicate that bodies prepared with 10 wt-% pitch are adversely affected by the presence of ZrC particles, whereas the superior strength of bodies prepared with 20 wt-% pitch is not appreciably affected by the presence of either ZrC or NbC particles. These observations lead to the speculation that the mechanism by which carbide particles impart an enhanced plasticity to a low-pitch matrix graphite during hot-working also leads to relatively poor mechanical properties in the hot-worked body.

Graphite Bodies Containing Nickel

The effect of nickel on the hot-working characteristics of graphite is of interest because no carbides are expected to be formed and because a liquid phase will be present in the body at temperatures above the eutectic, 1318°C. [6]

Differential deformation experiments were conducted at temperatures of 2600° and 2300°C, using a nickel-bearing graphite matrix prepared with 20 wt-% pitch and an additive of 1 at. -% nickel. The experiment at 2600°C showed a greater plasticity, of the order of 20%, in the nickel-bearing specimen despite the fact that the nickel was vaporized before the conclusion of the deformation run. A substantial loss of nickel was also observed in the subsequent differential deformation experiment at 2300°C; in this case, the deformation of the nickel-bearing specimens was approximately 35% greater than that of the nickel-free specimens.

Hot-working runs have been made on graphite bodies containing approximately 12 vol-% nickel in order to learn if appreciable strain can be attained before the nickel is lost by evaporation and to determine the

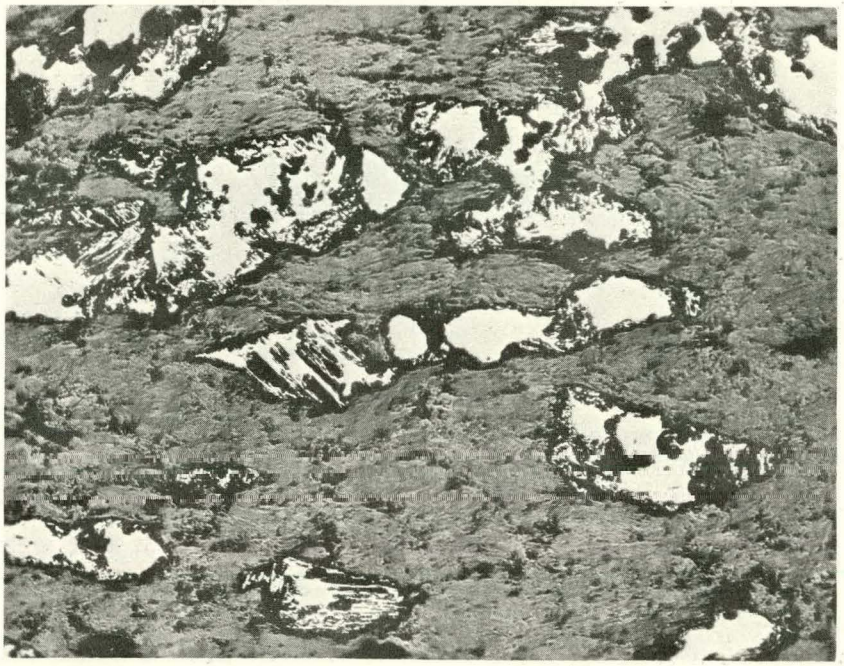

M-2505-2-2 (150×)

(a)

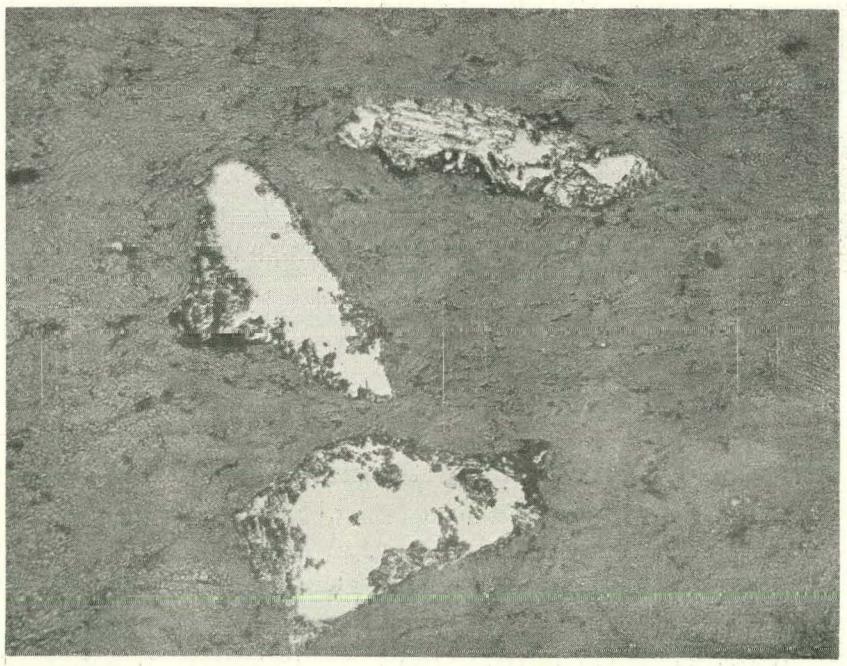

M-9914-1 (200×)

(b)

Fig. 7--Microstructure of hot-worked graphite bodies containing ZrC particles; longitudinal sections: (a) hot-worked at 2575°C to a true strain of 37%, 23 vol-% ZrC initial loading; (b) hot-worked at 2605°C to a true strain of 24%, 12 vol-% ZrC initial loadings.

Table 2

PROPERTIES OF HOT-WORKED GRAPHITE BODIES CONTAINING SOLID CARBIDES

Additive and Initial Loading (vol-%)	Pitch Content of Matrix (wt-%)	True Strain in Hot-working	Porosity, $d > 0.1\ \mu$ (%)	Compressive Strength (psi)		Helium Permeability [$(cm^2/sec) \times 10^3$]	
				Parallel	Perpendicular	Parallel	Perpendicular
None	10	0	14.1	6,230	5370	4.2	5.8
None	10	-0.36	8.3	6,510	3710	1.2	2.4
ZrC, 23%	10	0	14.6	5,280	4610	49.0	72.0
ZrC, 23%	10	-0.35	10.1	4,010	3070	41.0	69.0
None	20	0	10.2	9,250	8250	1.75	3.0
None	20	-0.24	4.3	11,180	8250	0.36	0.65
ZrC, 12%	20	-0.21	4.2	10,450	8100	0.54	1.5
NbC, 12%	20	-0.25	----	10,800	7200	2.6	2.6

NOTE: The values of compressive strength are averages of two or more tests for each condition. Hot-working temperatures were in the neighborhood of 2600°C.

properties of the hot-worked nickel-bearing body. These runs were made at 2500°C, and it was found necessary to use initial hot-working loads (for a 1-in.-diameter specimen) of less than 3000 lb to avoid fracture. In the course of hot-working, the excess liquid nickel is squeezed from the specimen, forming droplets on the surface. Evaporation of nickel from the droplets appears to be restrained by a graphite coating precipitated on the surface of the liquid.

The photomicrographs of Fig. 8 indicate appreciable densification of the nickel-bearing body when hot-worked to a true strain of 26%. Some properties of this hot-worked body have been measured and are given in Table 3. The compressive strengths are inferior to those of the other hot-worked graphites. The values of permeability are generally lower than obtained with matrix graphite, suggesting that the liquid nickel tends to close the pores, which contributes to the helium permeability.

Table 3

PROPERTIES OF HOT-WORKED GRAPHITE CONTAINING NICKEL

Hot-working strain (at 2525°C)	-0.26
Porosity, $d > 0.1\ \mu$	3.4%
Compressive strength:	
Parallel	9150 psi
Perpendicular	6050 psi
Helium permeability:	
Parallel	5.6×10^{-5} cm^2/sec
Perpendicular	3.8×10^{-4} cm^2/sec

Graphite Bodies Hot-worked with Liquid Zirconium Carbide

The initial investigations of graphite bodies hot-worked with a dispersion of liquid carbide particles were done with zirconium carbide, for which the eutectic with graphite occurs at 2850°C.[6] In view of the substantial improvements in the properties of graphite obtained by means of this modified hot-working process, the work was extended to include molybdenum carbide as an additive, and the present investigation is directed to a full characterization of these promising materials.

The results described here have been obtained with two characteristic sizes of zirconium carbide particles, coarse-grained particles screened to 125 to 175 μ (as used in the hot-working runs on solid carbide additives) and fine-grained particles screened to less than 38 μ. The carbide-bearing bodies were prepared by hot-pressing a dispersion of fine carbide particles in a graphite matrix comprised of 20 wt-% binder (Barrett No. 30 pitch)

M-9771-2 (200×)

(a)

M-9879-1 (200×)

(b)

Fig. 8--Microstructures of nickel-bearing matrix graphite before and after hot-working; longitudinal sections: (a) annealed at 1600°C; (b) hot-worked at 2500°C to true strain of 26%.

and 80 wt-% filler (GP-38 graphitized petroleum coke). The nominal carbide content before hot-working was approximately 10 vol-%. The bodies were hot-worked in compression to strain levels as high as 60% true strain. The hot-working temperatures were in the neighborhood of 2900°C, and the hot-working loads were moderate, generally less than 3000 lb except for the highest strain levels.

During the hot-working process, the carbon-saturated liquid carbide tends to be squeezed out of the graphite matrix, and carbide droplets are formed on the surface of the specimen during hot-working. The results of chemical analysis for zirconium as a function of hot-working strain are given in Fig. 9, which shows that the zirconium content is sharply reduced in the early stages of hot-working. In terms of atom fraction, these materials are relatively dilute mixtures of carbide in the graphite; hot-working to a true strain of 40% reduces the zirconium content from about 4 at. -% to 2 at. -%. The carbide beads appear to be coated with graphite precipitated from the liquid phase, and they can be readily removed from the hot-worked body if care is taken to keep the cutting edge of the lathe tool below the beads and in the graphite substrate.

Photomicrographs of the structure of these bodies are given in Fig. 10. The microstructures are dense, and the carbide phase is finely divided, with most of the particles less than 4 μ in size. The distribution of fine particles is more uniform for bodies prepared with finer-grained carbide particles.

Measurements of the bulk density were made by weighing machined cylinders, and the results are shown in Fig. 11. By using these data together with the chemical analyses and the reported lattice parameter for zirconium carbide saturated with graphite,[6] calculated values for the density of the graphite phase of the two-phase body were derived.

The sharp reduction in porosity caused by hot-working is shown in Fig. 12. The porosity was measured by conventional mercury porosimetry. Values for the theoretical porosity are also given in Fig. 12 and are calculated from the density of the graphite phase, assuming that no zirconium is present in the graphite phase. It will be noted that in bodies prepared with fine-grained ZrC, the porosity ($d > 0.1\ \mu$) is reduced to less than 1% in the first stages of hot-working. The higher porosity of the material prepared with coarse-grained ZrC is believed to be due to inadequate saturation of the body with the liquid carbide, leaving some regions of the body relatively unimpregnated with carbide.

Measurements of the helium permeability are shown in Fig. 13. Owing to the small size of the specimens and to the fact that the apparatus employed was designed primarily for measurements on more permeable graphites,

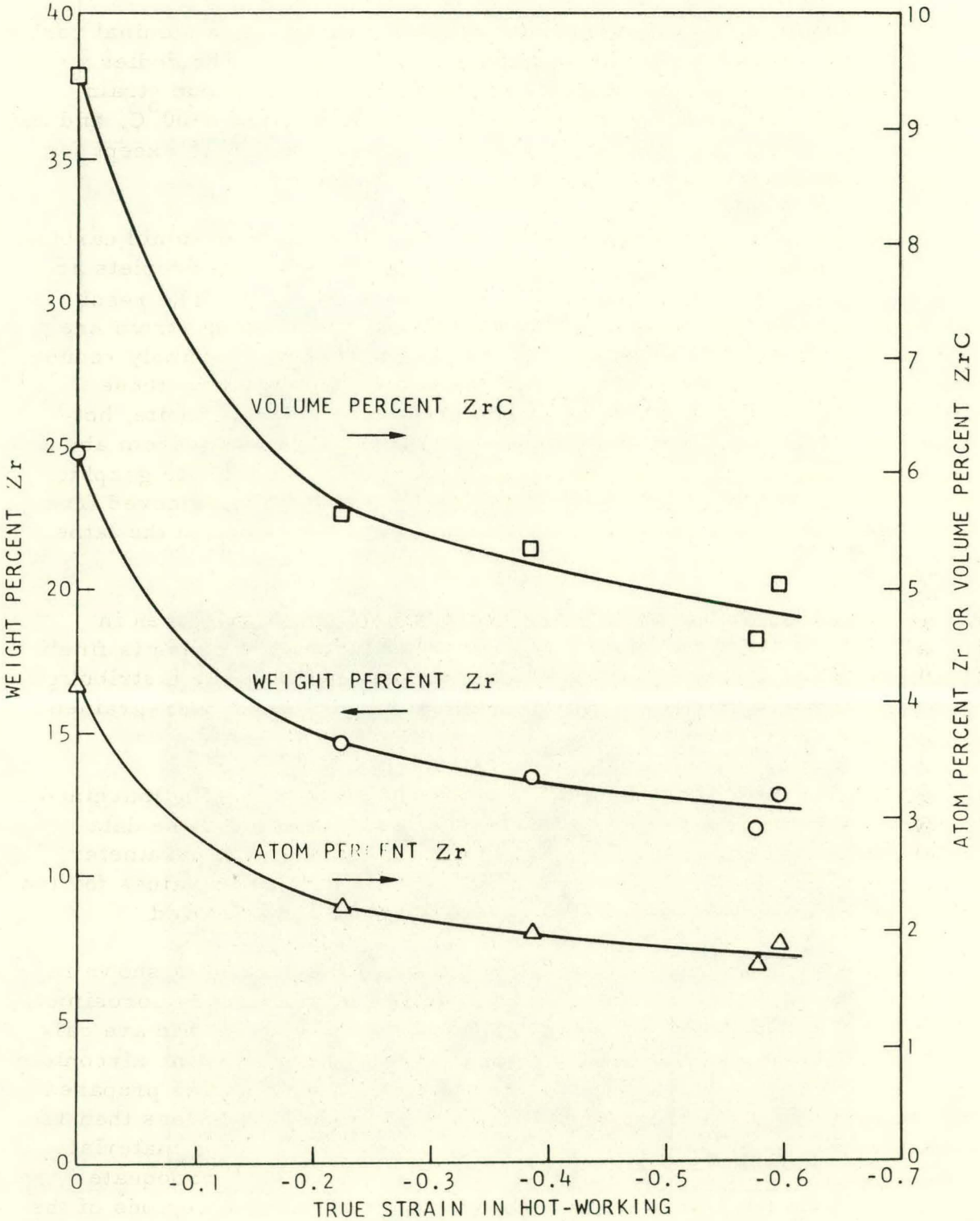

Fig. 9--Results of chemical analysis of hot-worked matrix graphite containing zirconium carbide.

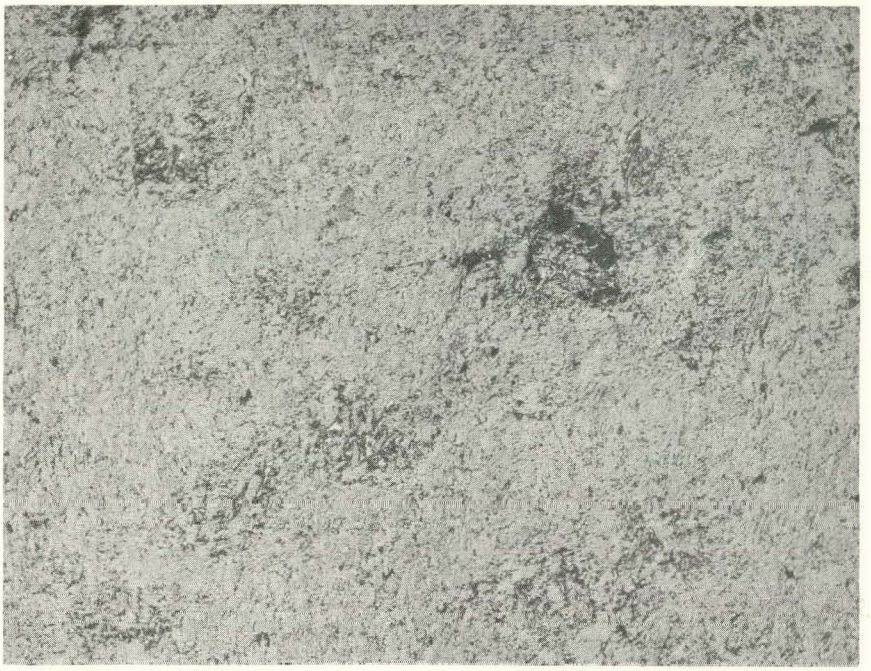

M-9640-5 (75×)

(a)

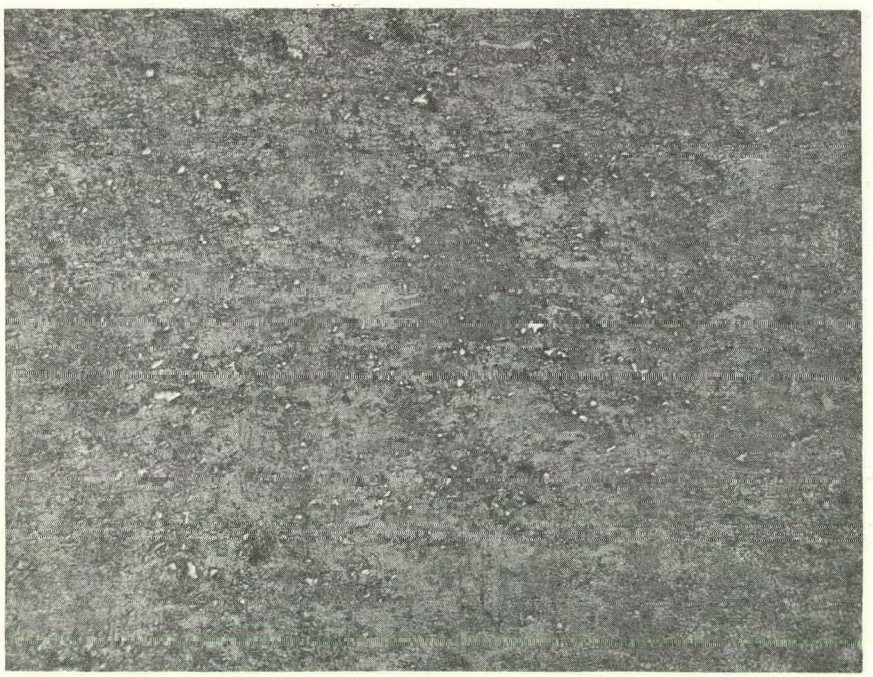

M-9880-1 (200×)

(b)

Fig. 10--Microstructures of ZrC-bearing graphite bodies hot-worked above eutectic temperature; longitudinal sections: (a) ZrC-graphite prepared with coarse-grained ZrC, hot-worked at 2960°C to true strain of 44%; (b) ZrC-graphite prepared with fine-grained ZrC, hot-worked at 2920°C to true strain of 39%.

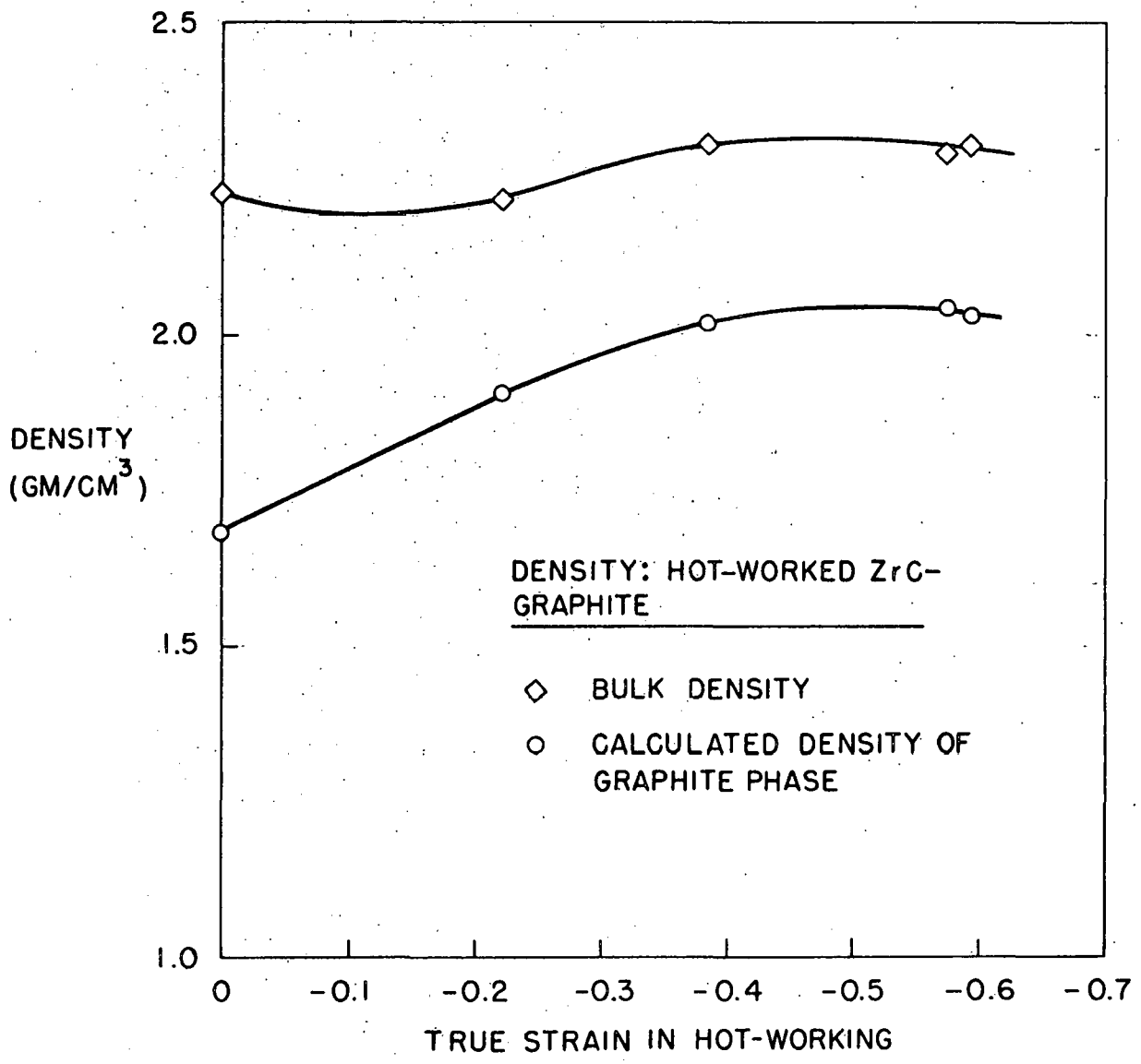

Fig. 11--Bulk density of hot-worked ZrC-graphite bodies; calculated values of the density of the graphite phase

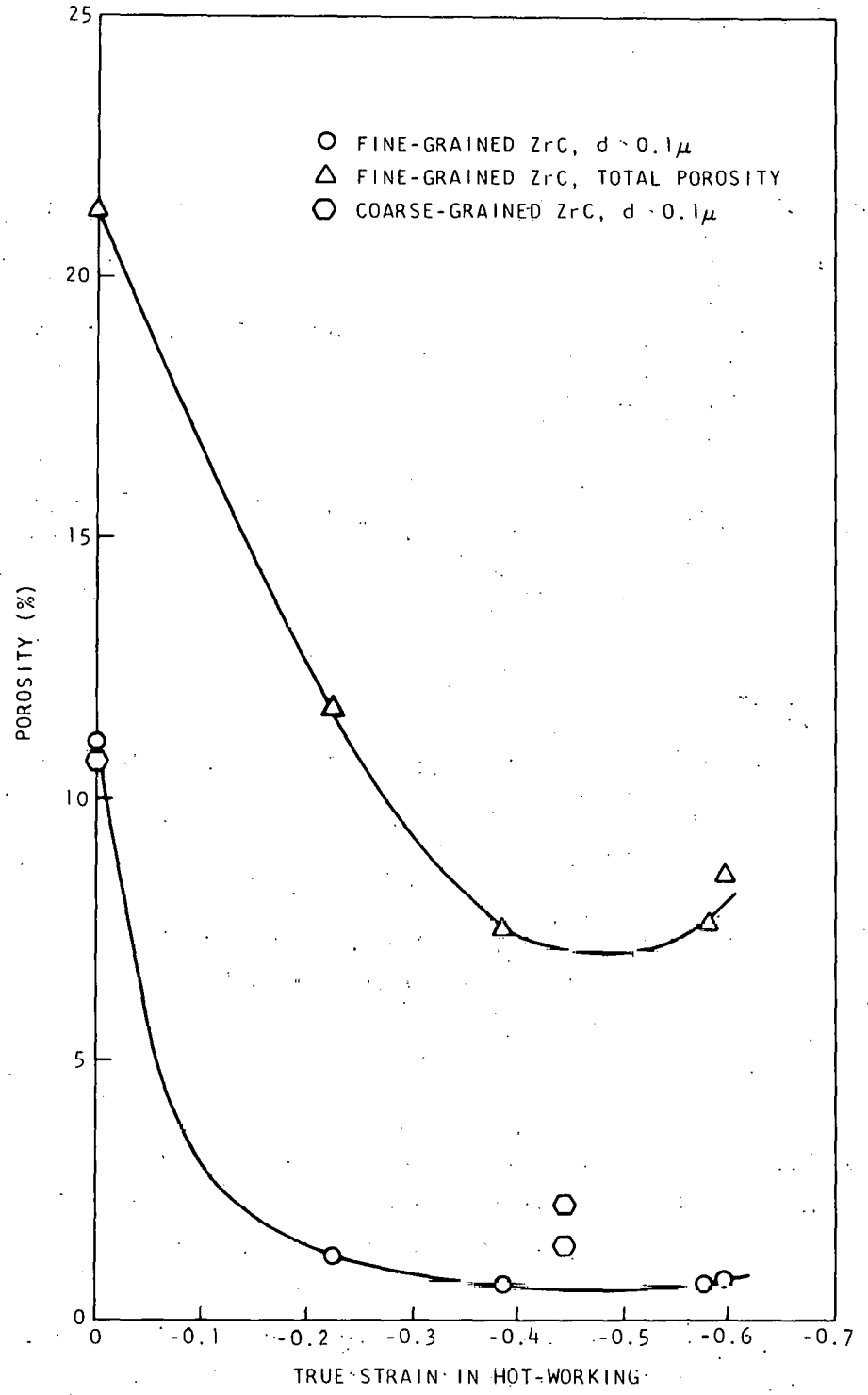

Fig. 12--Porosity of hot-worked ZrC-graphite bodies as measured by mercury porosimetry and as calculated from the density of the graphite phase.

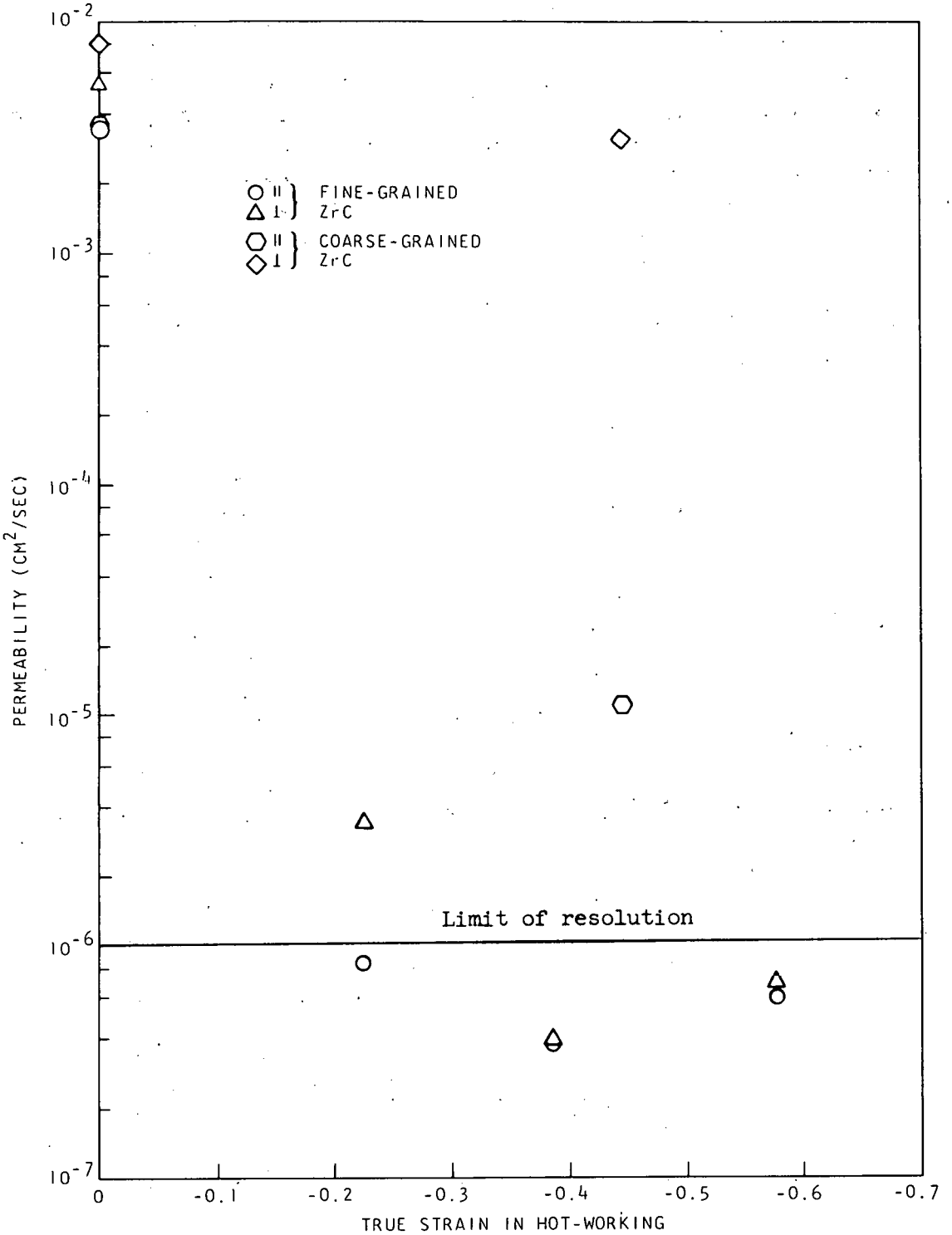

Fig. 13--Helium permeability of hot-worked graphite containing zirconium carbide.

the values below approximately 10^{-6} cm^2/sec must be considered as upper limits for the permeability.

Measurements of the compressive strength and modulus of rupture are shown in Figs. 14 and 15. The tests for compressive strength were made on cylindrical specimens, 0.25 in. in diameter and 0.375 in. high, cut with the cylinder axis either parallel or perpendicular to the direction of compression during hot-working. The flexure tests were made with a four-point loading jig, using specimens of approximately square cross section no larger than 0.1 in. on a side and approximately 0.6 in. long. Specimens were tested in the three orientations, relative to the preferred orientation imparted by hot-working (see Fig. 15). In contrast to the strength of graphites hot-worked without liquid additives,[3][7] these materials show a large increase in strength in one direction without sacrificing strength in the other directions.

In considering possible mechanisms whereby sharp improvement in strength is obtained for bodies hot-worked with a liquid carbide phase, it should be noted that the strength increases with increasing hot-working strain while the concentration of carbide is decreasing. Furthermore, the volume fraction of carbide is low, and the micrographic studies indicate that the graphite matrix is the continuous phase. Consequently, the effective strengthening would not appear to be attributable to the mere presence of a strong carbide phase, and the mechanism of strengthening would appear to be due to an interaction of the carbide phase with the graphite matrix.

Measurements of the thermal diffusivity at room temperature have been made using a flash method (see Section III). These data have been employed, together with the chemical analysis and the heat capacity of graphite[8] and zirconium carbide,[9] to calculate the thermal conductivities. It will be noted that the conductivity in the direction perpendicular to the direction of compression during hot-working is of the same order as that of copper. The thermal diffusivities and thermal conductivities are given in Fig. 16.

Graphite Bodies Hot-worked with Liquid Molybdenum Carbide

Molybdenum carbide offers two advantages as a liquid carbide additive for the hot-working of graphite; the eutectic with graphite is relatively low, approximately 2590°C,[10] and the carbide is nonvolatile. Accordingly, a series of hot-working runs has been made on graphite-matrix bodies containing a dispersion of fine molybdenum carbide particles, and the properties of the hot-worked bodies are being characterized.

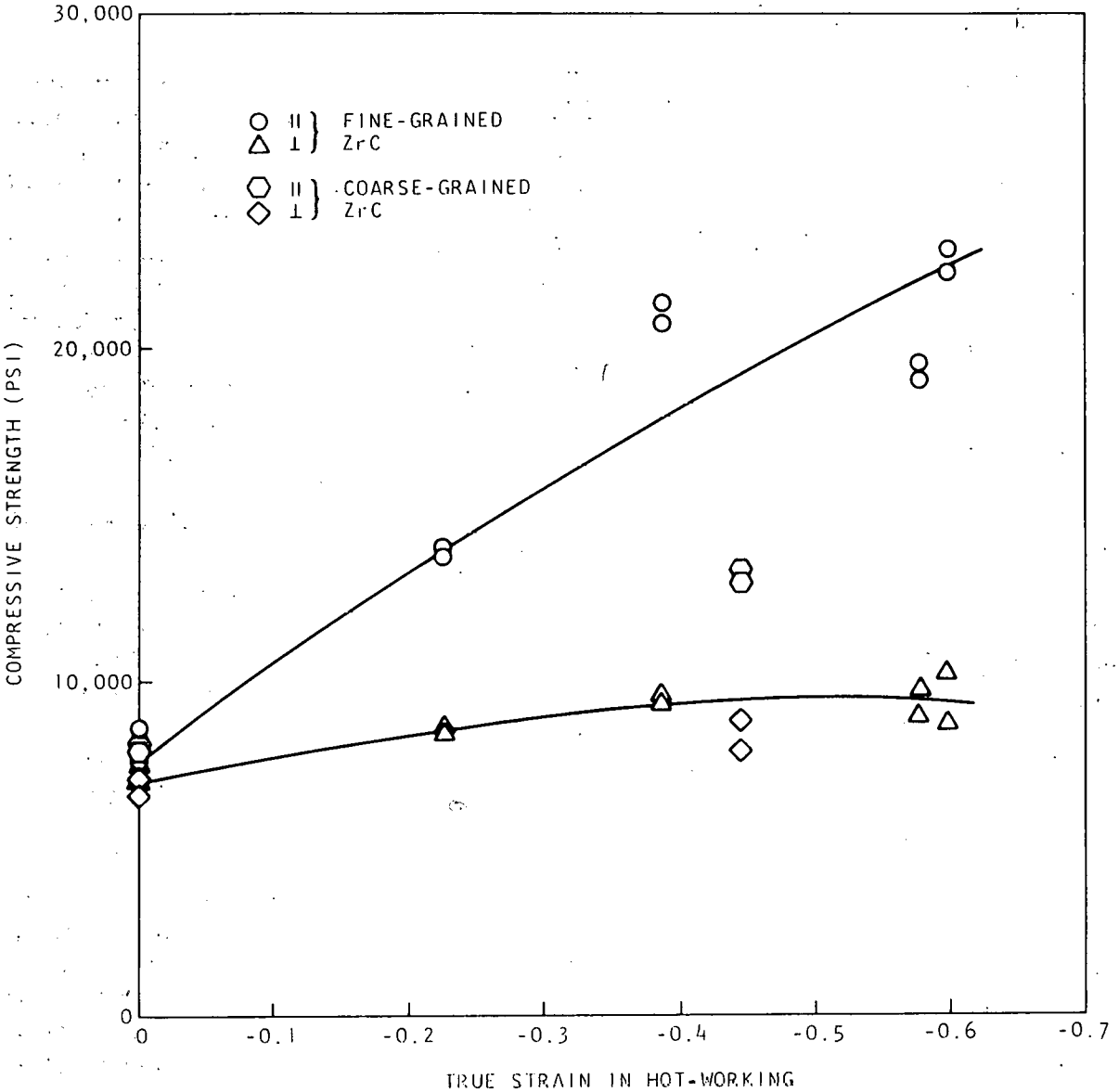

Fig. 14--Compressive strength of hot-worked graphite containing zirconium carbide.

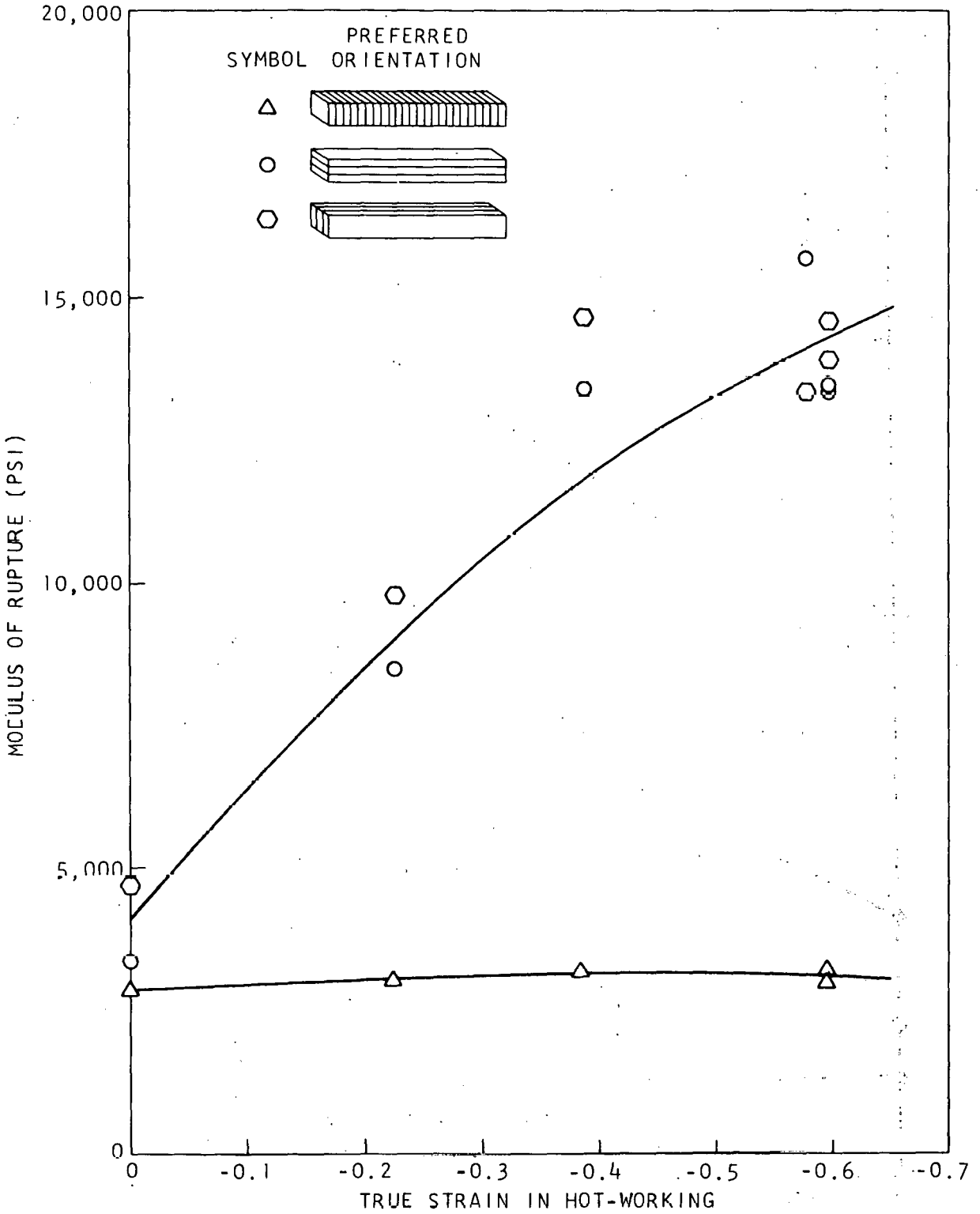

Fig. 15--Modulus of rupture of hot-worked graphite containing zirconium carbide.

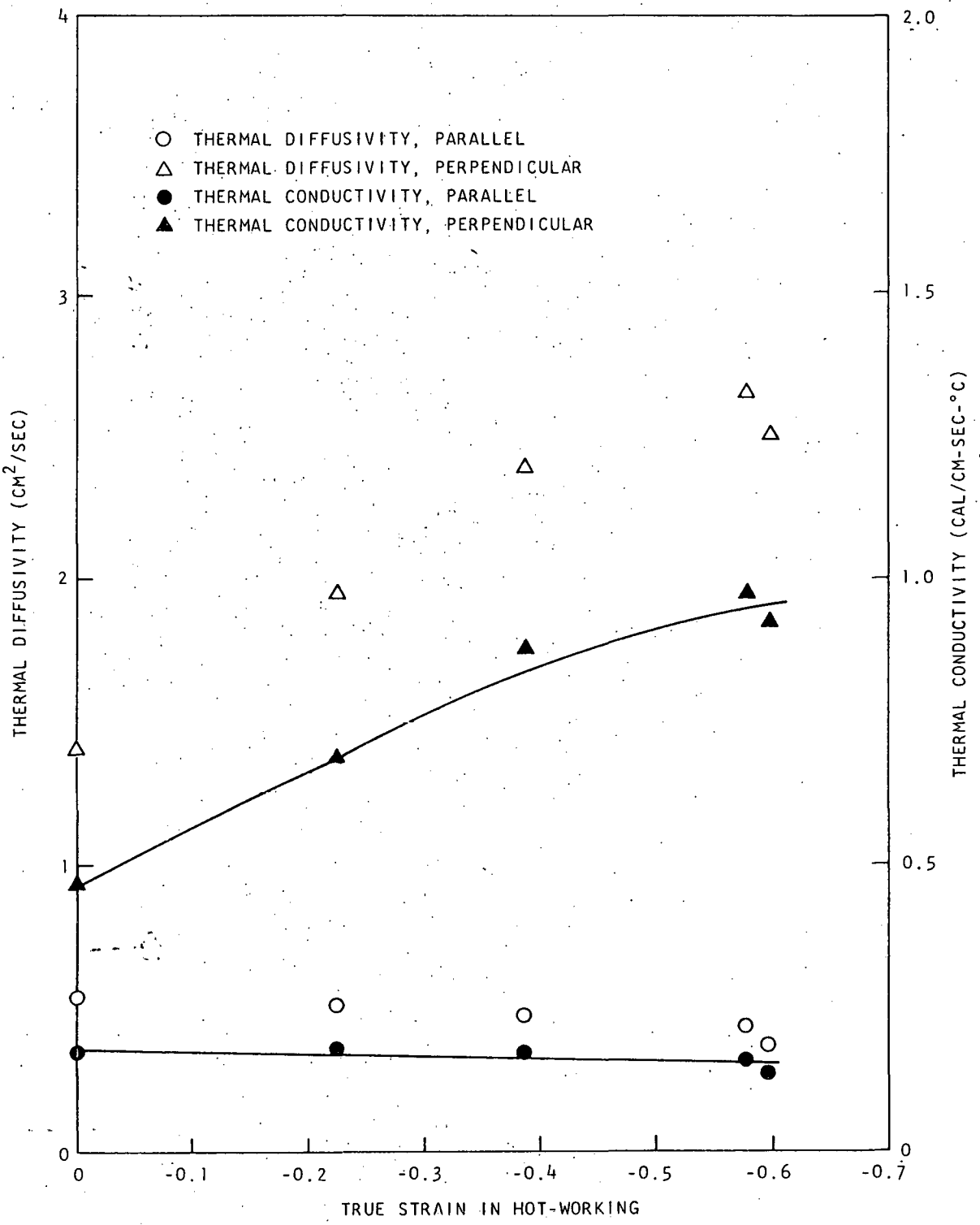

Fig. 16--Thermal diffusivity and thermal conductivity of hot-worked graphite containing zirconium carbide

The materials were prepared in essentially the same manner as for the ZrC-bearing bodies described previously. The particles of commercial molybdenum carbide were screened to less than 38 μ, and the pitch content of the graphite matrix was 20 wt-%.

The hot-pressed bodies were hot-worked at temperatures in the neighborhood of 2750°C, using loads generally less than 6000 lb for the 1-in.-diameter specimens. The hot-working behavior was similar to that of the ZrC-bearing bodies; in general, the liquid-carbide-bearing bodies are more readily hot-worked than the matrix graphite without an additive or with a solid-state additive. A photograph of a specimen at approximately 25% strain is shown in Fig. 17.

The results of chemical analysis of the hot-worked specimens (Fig. 18) show that the molybdenum content drops somewhat less abruptly with increasing strain than noted for zirconium. In view of uncertainties as to the structure of the carbide when cooled to room temperature (the most recent phase diagram[10] indicates that MoC is unstable below about 1650°C), no attempt has been made to calculate the volume fraction of carbide (or other properties which depend on knowledge of carbide structure, e.g., graphite density and theoretical porosity).

Photomicrographs of the matrix graphite containing molybdenum carbide particles are shown in Figs. 19 through 22 for four levels of hot-working strain and for both longitudinal and transverse sections. The progressive reduction in porosity and increasing uniformity of structure are illustrated by these photomicrographs. The carbide particles appear as a uniform dispersion with a particle size generally less than 4 μ. The particles show little tendency to depart from an equiaxed geometry even in the highly hot-worked specimens.

Techniques of replication electron micrography are being developed to study the structures of the graphite bodies hot-worked with a dispersed liquid carbide phase. Some electron micrographs of the molybdenum-bearing specimen of Fig. 21 are given in Section VI of this report.

Measurements of the porosity and bulk density are given in Fig. 23. Measurements of the helium permeability (see Fig. 24) showed the same drop when the sample was hot-worked, to values at or below the limit of detection with the existing apparatus, as noted for the ZrC-bearing bodies.

The compressive strength (Fig. 25) and modulus of rupture (Fig. 26) show greater increases in strength in the strong directions with increasing hot-work than those observed with the ZrC-bearing bodies. Compressive strengths in excess of 40,000 psi and moduli of rupture in excess of 20,000 psi are competitive with current production pyrolytic graphite.[11]

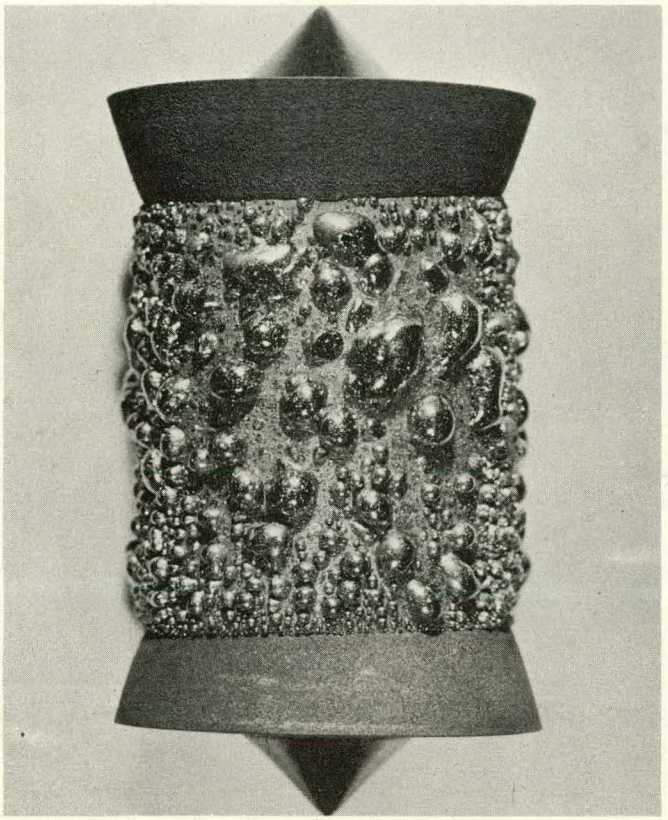

M-10556-1 (1.85×)

Fig. 17--Photograph of carbide-containing specimen after hot-working to a compressive strain of approximately 25%. Original specimen was 2 in. in length and 1 in. in diameter.

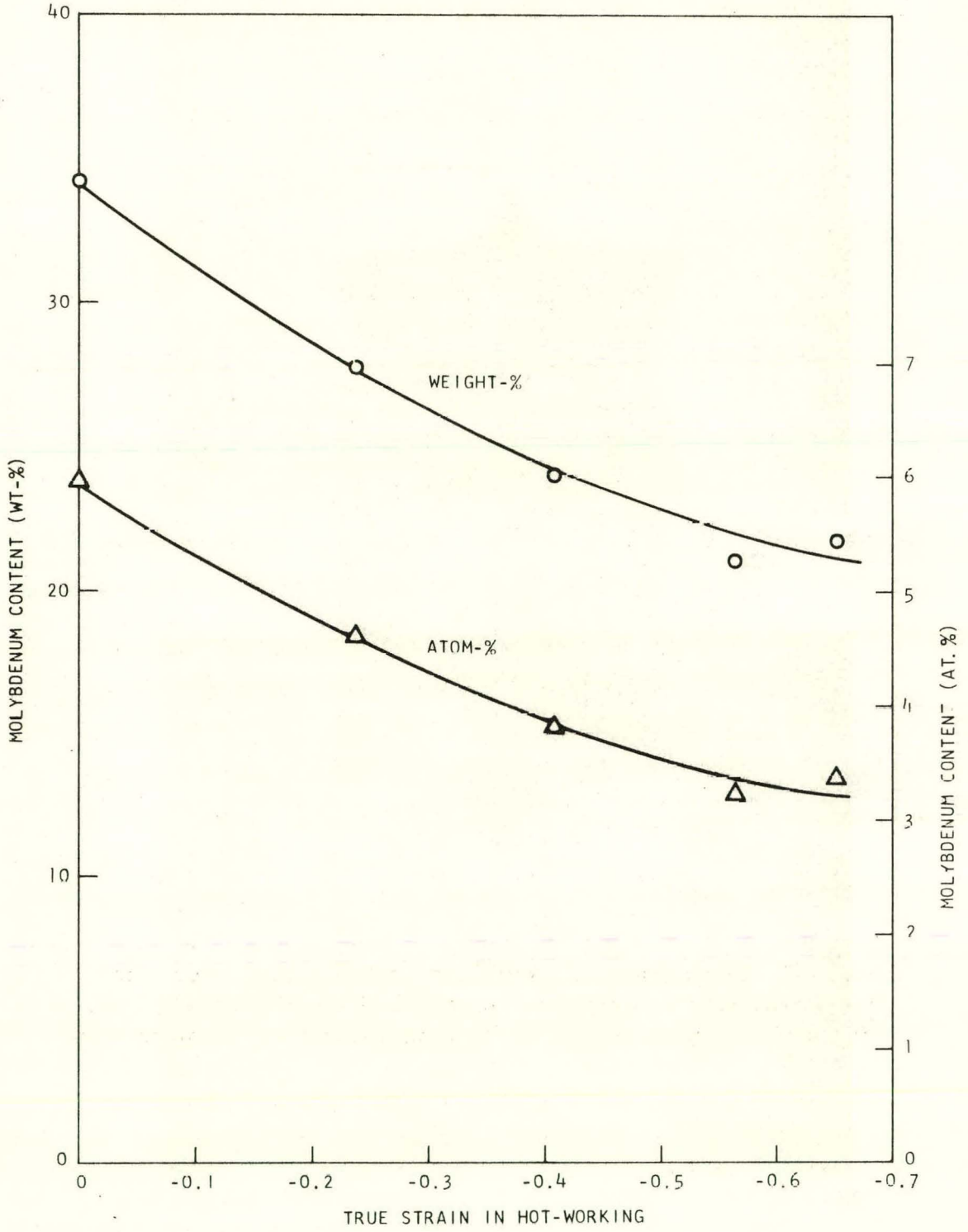

Fig. 18--Results of chemical analysis of hot-worked matrix graphite containing molybdenum carbide.

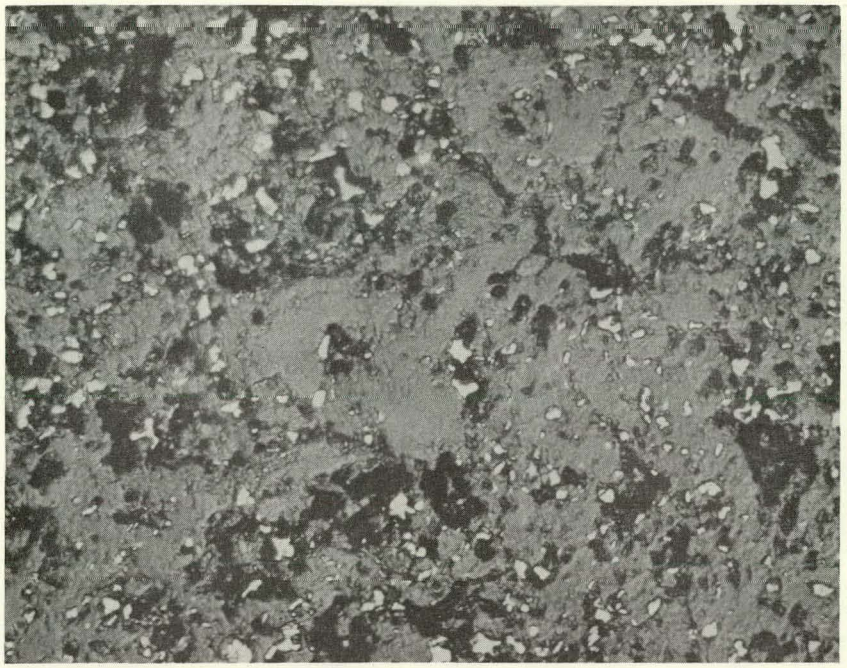

M-10357-12 (400×)

(a)

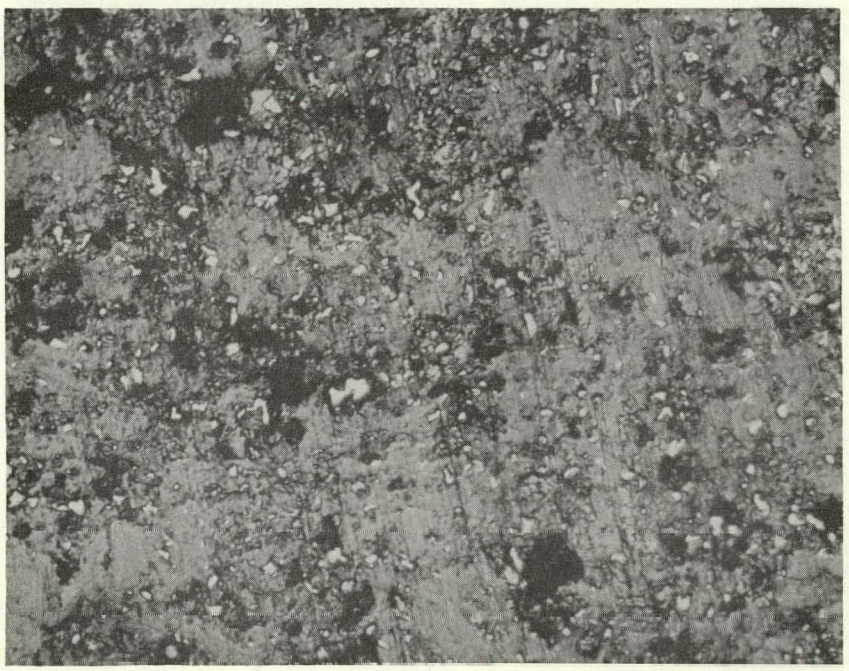

M-10530-1 (400×)

(b)

Fig. 19--Photomicrographs of graphite matrix containing molybdenum carbide particles. Specimen annealed at 2700°C; no hot-work.
(a) longitudinal section; (b) transverse section.

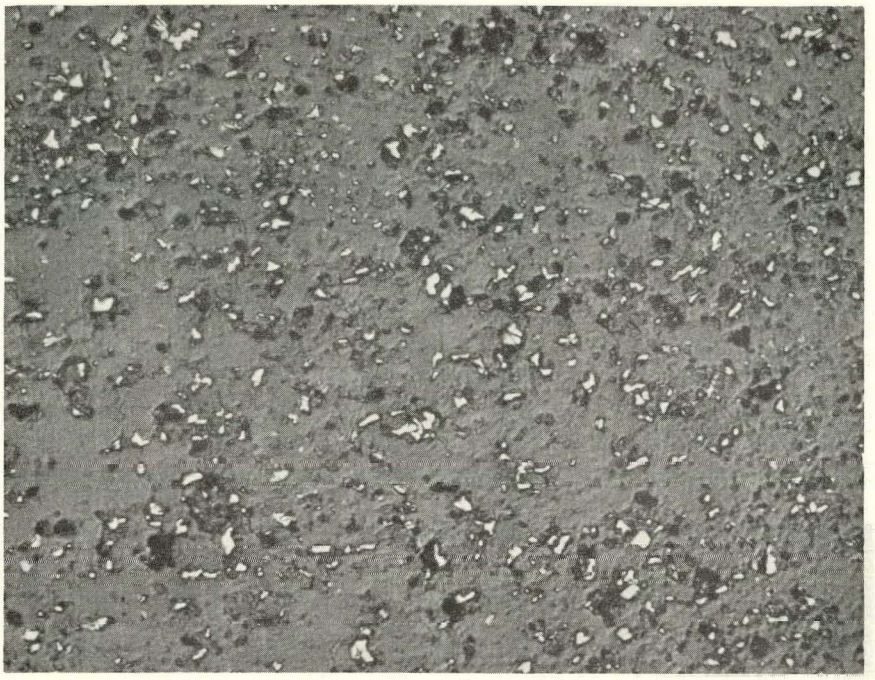

M-10358-10 (400×)

(a)

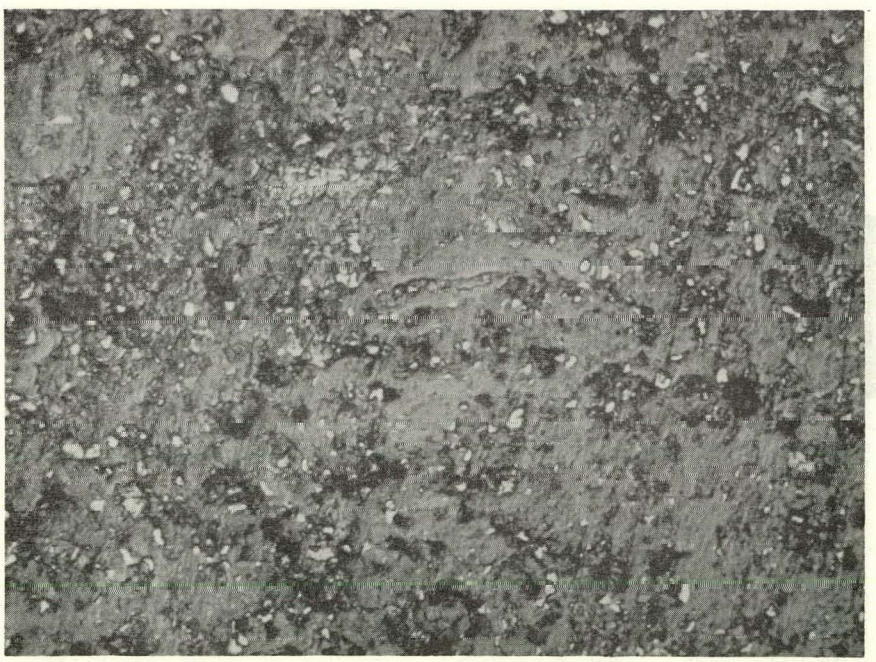

M-10531-1 (400×)

(b)

Fig. 20--Photomicrographs of graphite matrix containing molybdenum carbide particles. Specimen hot-worked at 2720°C to true strain of 24%. (a) longitudinal section, (b) transverse section.

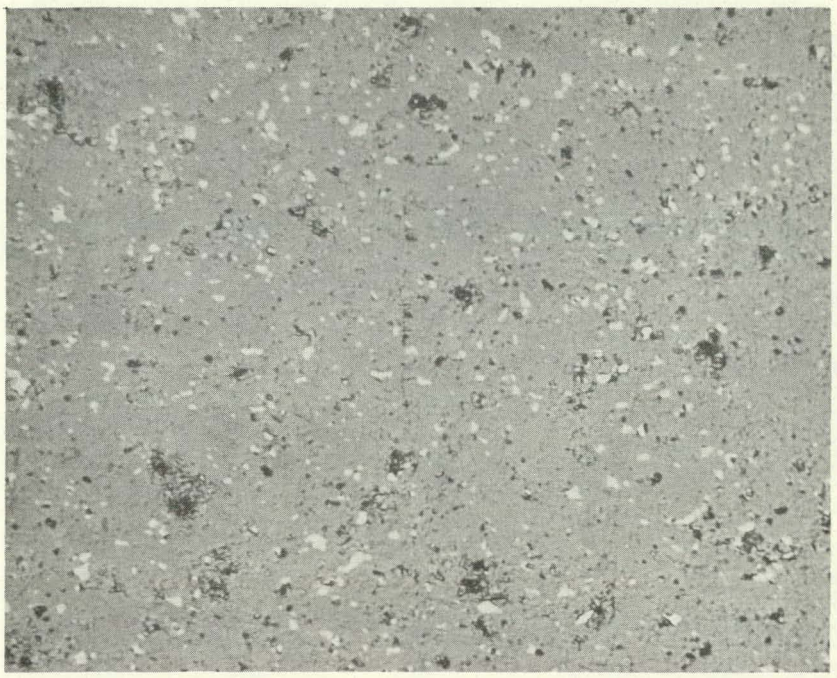

M-9924-10 (400×)

(a)

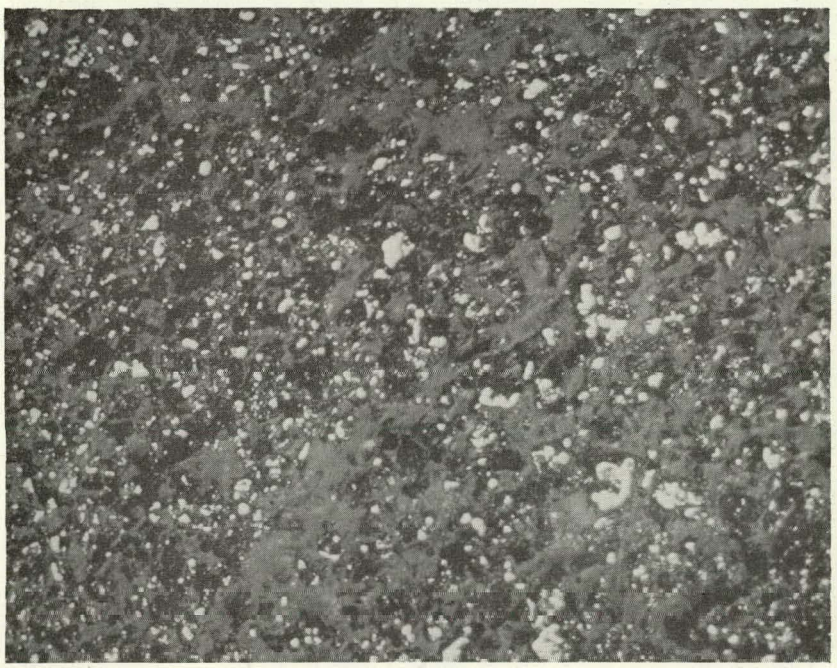

M-10532-1 (400×)

Fig. 21--Photomicrographs of graphite matrix containing molybdenum carbide particles. Specimen hot-worked at 2720°C to true strain of 41%. (a) longitudinal section, (b) transverse section.

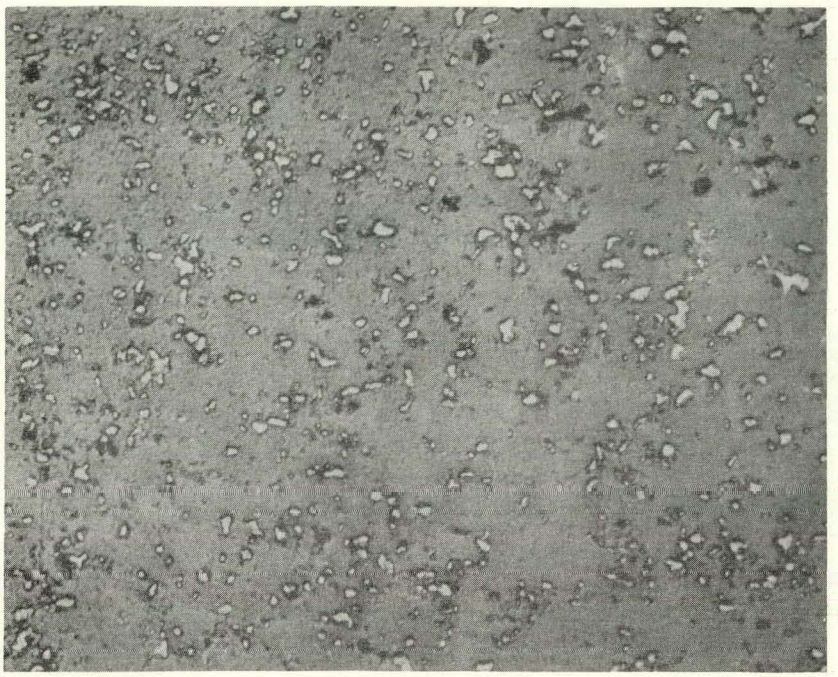

M-10359-10 (400×)

(a)

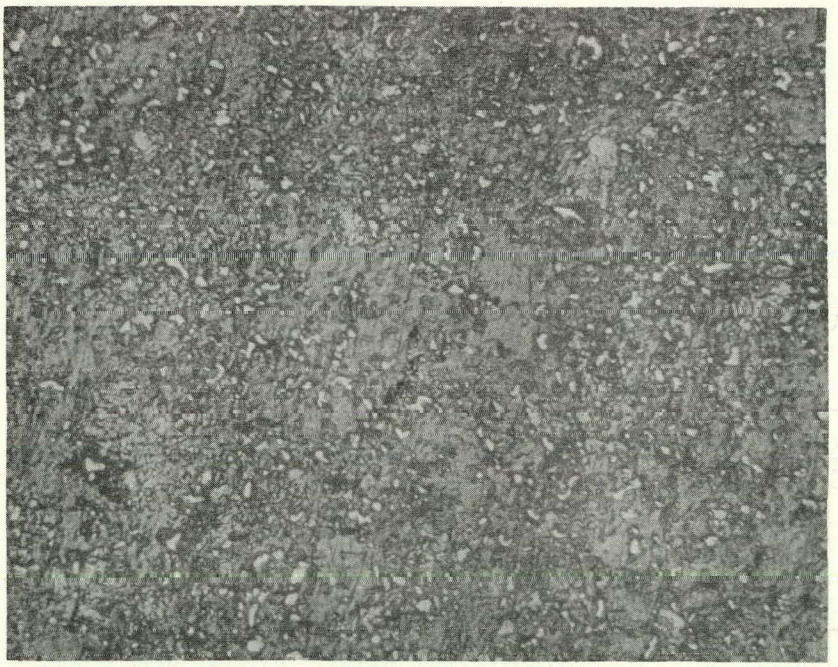

M-10533-1 (400×)

(b)

Fig. 22--Photomicrographs of graphite matrix containing molybdenum carbide particles. Specimen hot-worked at 2720°C to true strain of 56%. (a) longitudinal section, (b) transverse section.

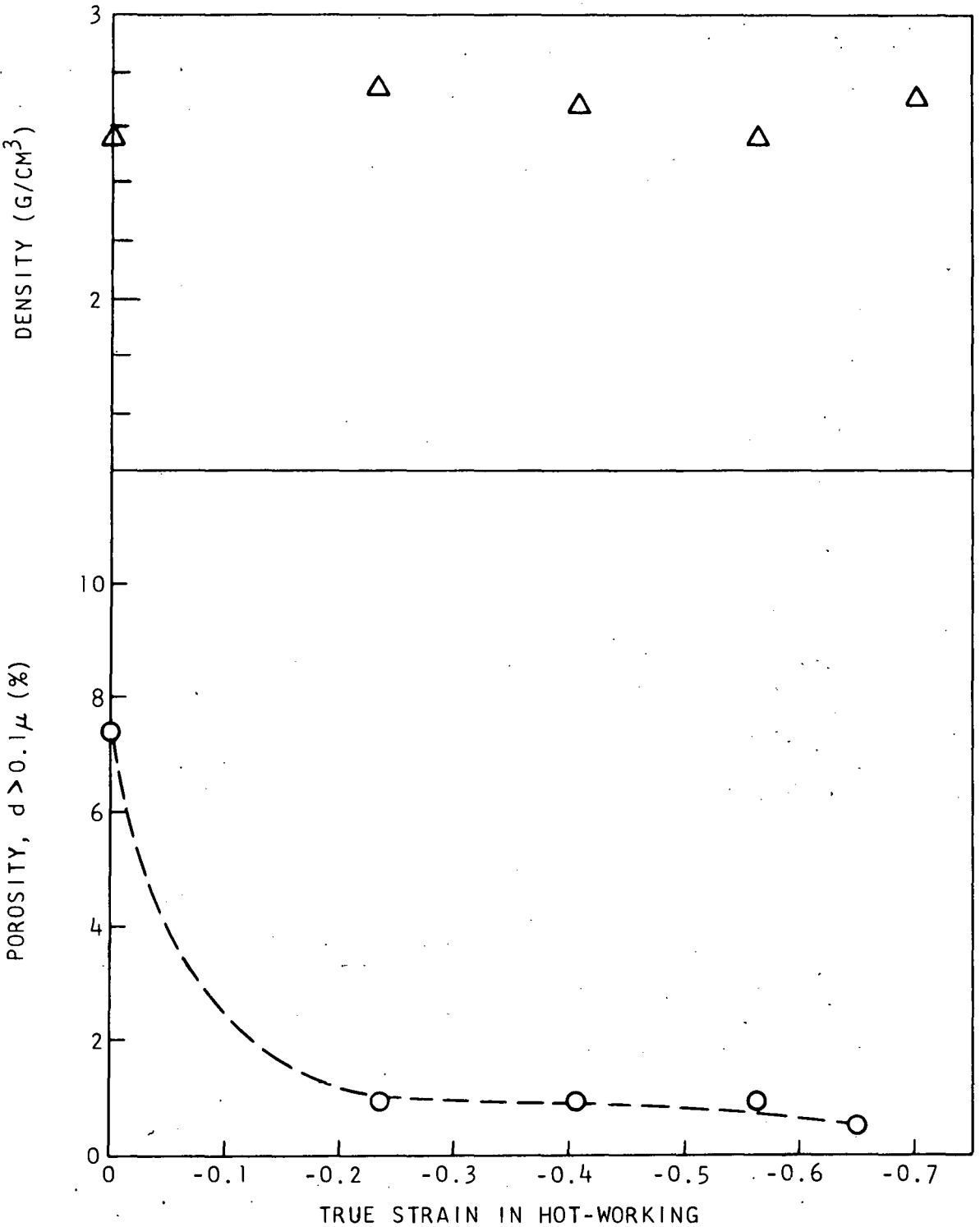

Fig. 23--Bulk density and porosity (d > 0.1 micron) of hot-worked graphite containing molybdenum carbide.

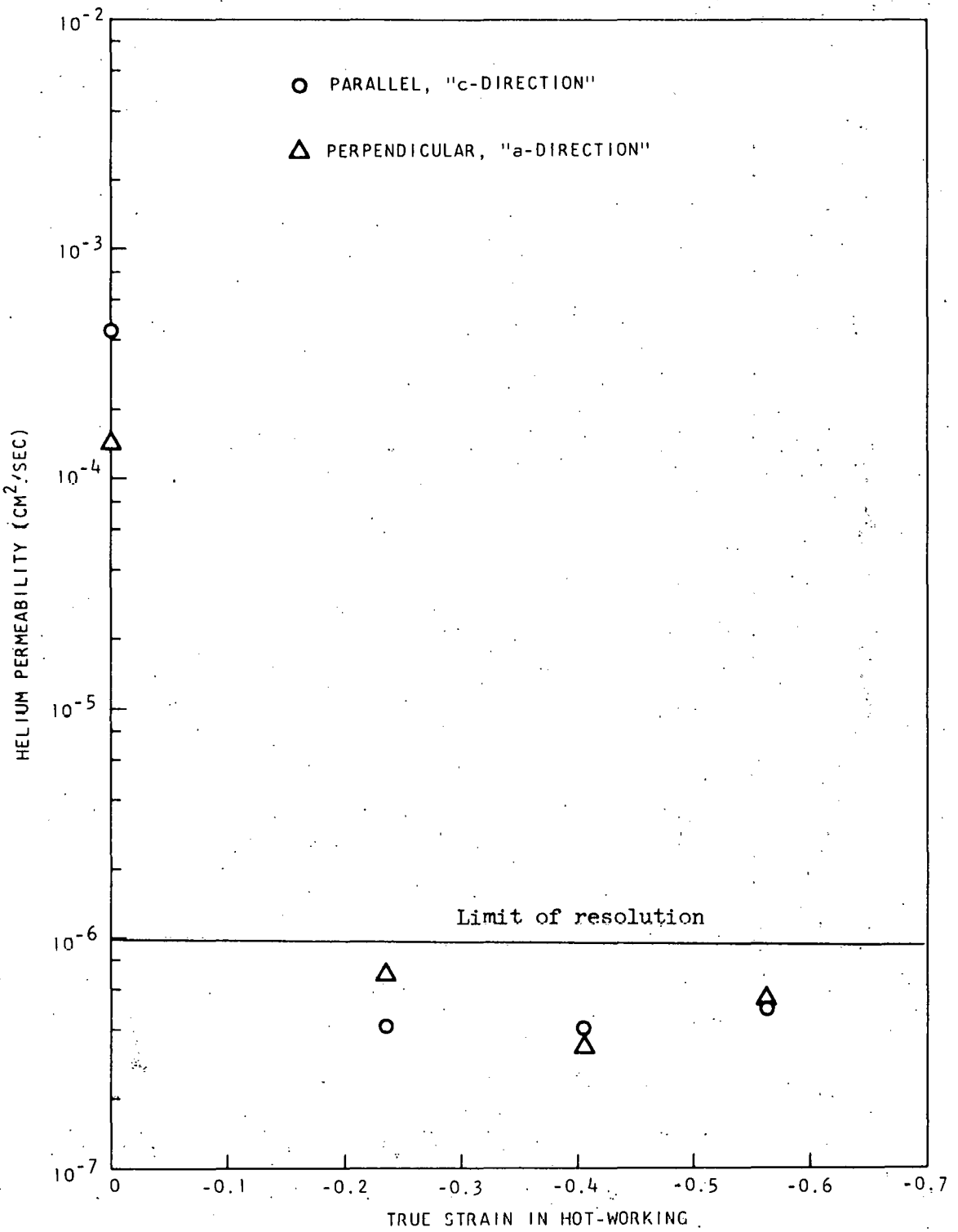

Fig. 24--Helium permeability of hot-worked graphite containing molybdenum carbide.

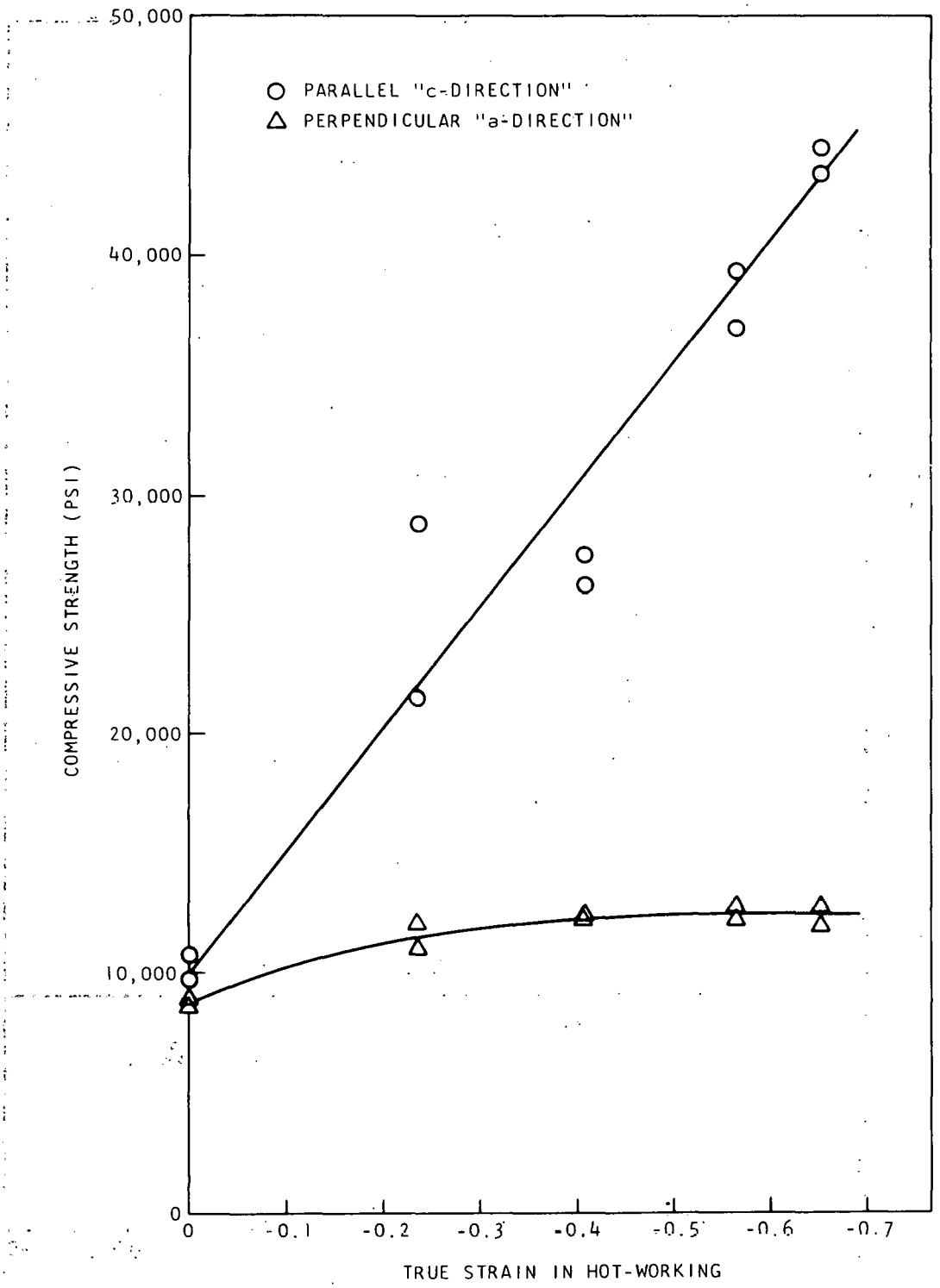

Fig. 25--Compressive strength of hot-worked graphite containing molybdenum carbide.

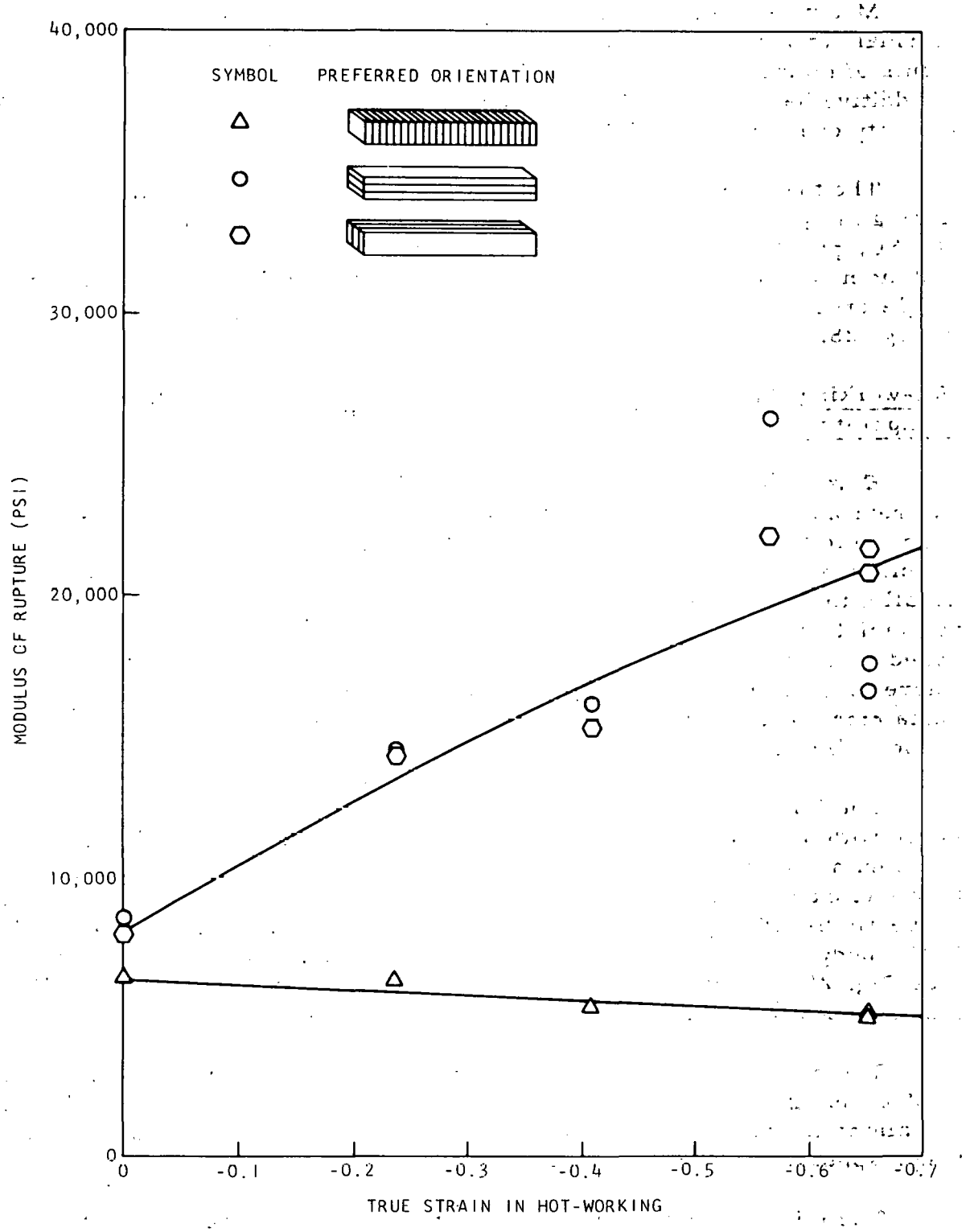

Fig. 26--Moduli of rupture of hot-worked graphite containing molybdenum carbide.

Measurements of the thermal diffusivity are given in Figure 27. The thermal conductivity has been calculated using the experimental measurements of molybdenum content and bulk density and by making the assumption of additive heat capacities[12] in the absence of measurements of the heat capacity of molybdenum carbides.

The thermal expansion of the series of hot-worked specimens containing molybdenum carbide has been measured from room temperature to 1000°C, parallel and perpendicular to the direction of hot-working. The instantaneous thermal expansions for 400°C (where the a-direction of the single crystal shows zero thermal expansion) were derived and are shown in Fig. 28.

Hot-working Extruded Graphite-Carbide Bodies Above Eutectic Temperature

Extruded graphite bodies are attractive as starting materials for two reasons: (1) since the preferred orientation of extruded bodies is opposite to that resulting from hot-working, a wide range of preferred orientations should be attainable by deforming the body in compression parallel to the extrusion axis; (2) extruded bodies are relatively free from the variations in density of hot-pressed bodies and the material can be prepared with a more uniform structure for a series of hot-worked specimens. Therefore, attempts are being made to hot-work extruded graphite bodies containing molybdenum carbide at temperatures such that the carbide phase is liquid.

The initial experiments are being made with an extruded body prepared with approximately 8 vol-% molybdenum metal, 54 vol-% graphitized petroleum coke as the filler, and 38 vol-% pitch as the binder. This mixture was extruded at 220°C to form a 1-in.-diameter body, which was subsequently baked to 900°C and sintered in vacuum at 1750°C. Although this initial body was found to contain voids owing to incomplete pitch distribution (see Fig. 29), a preliminary hot-working run was conducted to learn if the material could be satisfactorily hot-worked despite these defects.

The body was hot-worked at approximately 2700°C to a strain level of 35%, using loads no greater than 3000 lb. As for the hot-pressed graphites containing molybdenum carbide, the liquid carbide was squeezed from the body, appearing as beads on the cylindrical surface.

The microstructure of the hot-worked body is dense and uniform with no evidence of the voids found in the starting material. A few property measurements have been made and are summarized in Table 4. In view of these promising results further work is being undertaken, and extruded bodies are being prepared free from shrinkage voids to improve the quality of the starting material.

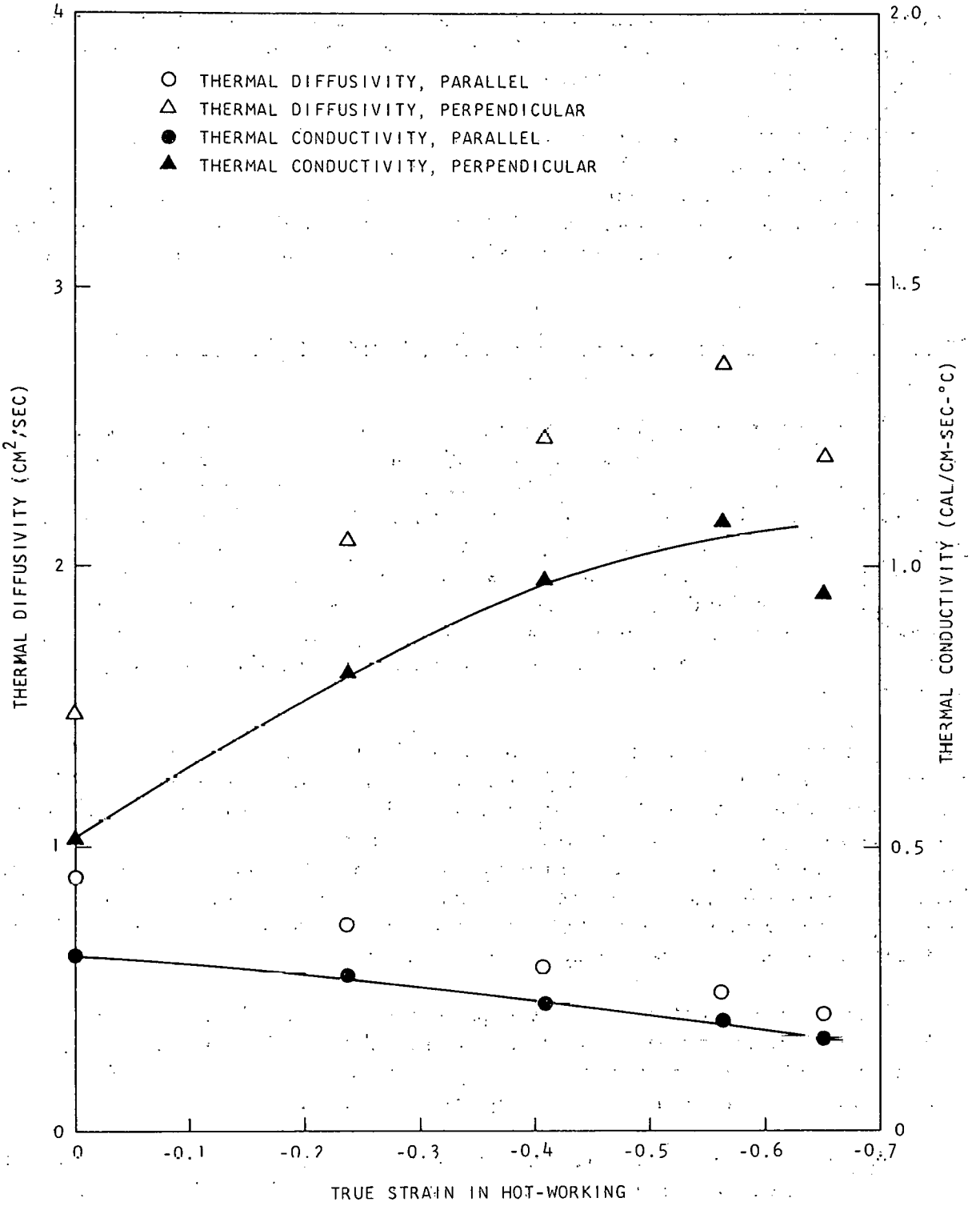

Fig. 27--The thermal diffusivity of hot-worked graphite containing molybdenum carbide

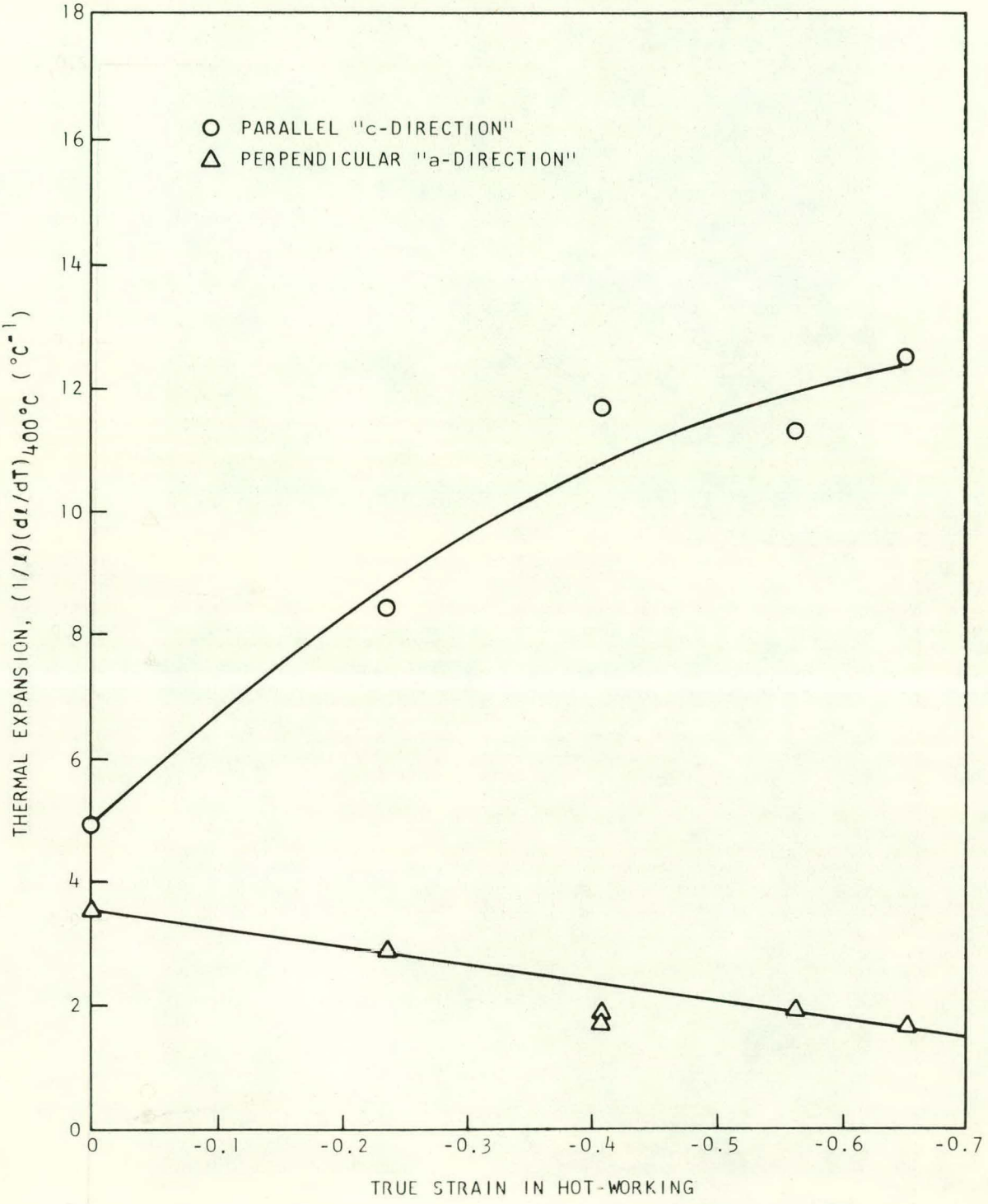

Fig. 28--Instantaneous thermal expansion at 400°C of hot-worked graphite containing molybdenum carbide.

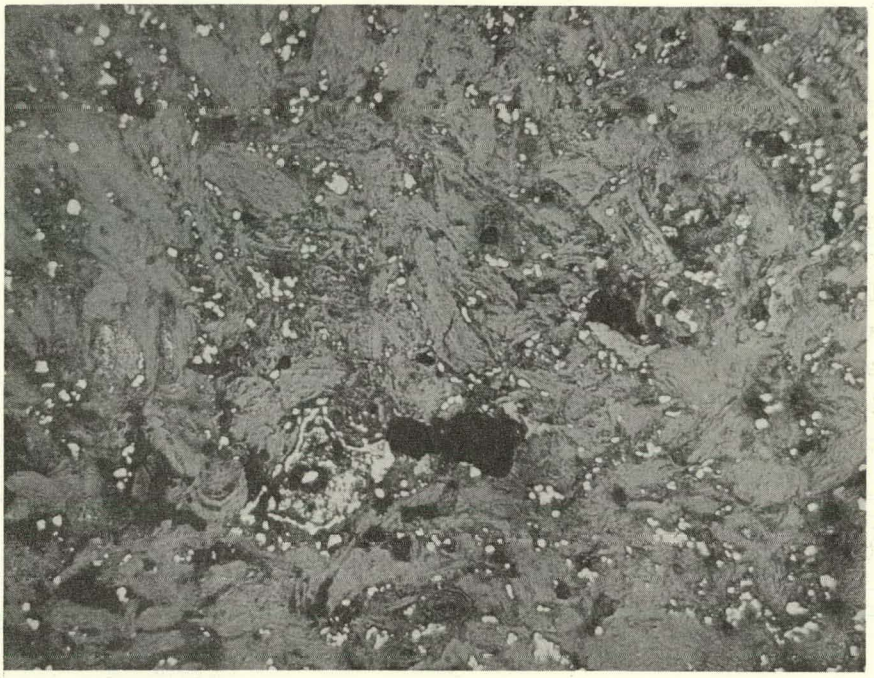

M-10708-2 200x

(a)

M-10713-2 200x

(b)

Fig. 29--The microstructure of extruded graphite bodies containing molybdenum: (a) after sintering at 1750°C, (b) after hot-working to approximately 35% true strain at 2700°C.

Table 4

PROPERTIES OF EXTRUDED GRAPHITE-CARBIDE BODY AFTER HOT-WORKING

Compressive strain in hot-working	-0.35
Instantaneous thermal expansion at 400°C	
Parallel to direction of hot-working	$5.8 \times 10^{-6} {}^{o}C^{-1}$
Perpendicular to direction of hot-working	$1.8 \times 10^{-6} {}^{o}C^{-1}$
Compressive strength	
Parallel to direction of hot-working	18,400 psi
Perpendicular to direction of hot-working	12,200 psi
Modulus of rupture	
Strong test orientation (average)	9600 psi
Weak test orientation	5350 psi

REFERENCES

1. Anderson, E. E., et al., "Advanced, Graphite-matrix, Dispersion-type Systems, Annual Report, April 1, 1962, through March 31, 1963," USAEC Report GA-4022 (Part 1), General Atomic Division, General Dynamics Corporation, May 1, 1963.

2. Price, R. J., and J. L. White, "Research on Graphite, Annual Report, April 1, 1963, through March 31, 1964," USAEC Report GA-5033, General Atomic Division, General Dynamics Corporation.

3. White, J. L., and R. J. Price, "Hot-working of Graphite for Graphite-matrix Nuclear Fuels," Carbon 2, 327 (1965).

4. Goeddel, W. V., G. R. Tully, Jr., and R. A. Meyer, Proc. Fifth Carbon Conf. 2, 347 (1963).

5. White, J. L., and J. M. Pontelandolfo, "Graphite-Carbide Materials Prepared for Hot-Working," USAEC Report GA-6052, General Atomic Division, General Dynamics Corporation, February 3, 1965.

6. Sara, R. V., "The System Zirconium-Carbon," J. Am. Ceram. Soc. 48, 243 (1965).

7. Turner, J. H., and M. B. Carter, "Investigation of Hot-worked Recrystallized Graphites," Union Carbide Corporation Report WADD-TR-61-72, Vol. XXXIII, June, 1964.

8. Stull, D. R., and G. C. Sinke, Thermodynamic Properties of the Elements, American Chemical Society, New York, 1956.

9. Storms, E. K., "A Critical Review of Refractories," Los Alamos Scientific Laboratory Report LA-2942, March, 1964.

10. Rudy, E., St. Windisch, and Y. A. Chang, "Ternary Phase Equilibria in Transition Metal-Boron-Carbon-Silicon Systems. Part I. Related Binary Systems. Volume I. Mo-C System," Aerojet-General Corporation Report AFML-TR-65-2, Part I, Vol. I, January, 1965.

11. Gebhardt, J. J., and J.M. Berry, "Mechanical Properties of Pyrolytic Graphite," AIAA J. 3, 302 (1965).

IX. APPLICATION OF HOT-WORKING PROCESSES TO FABRICATION OF GRAPHITE-MATRIX FUEL BODIES

J. L. White, J. M. Pontelandolfo

The feasibility of using hot-working processes to fabricate a graphite-matrix fuel body has been investigated, and this work has been summarized in a classified topical report, "Hot-Worked Graphite-Matrix Fuel Bodies (U)."[1]

It is concluded that although it is technically feasible to prepare hot-worked graphite-matrix fuel bodies, the process conditions require stringent control and only modest improvements in the properties of the fuel body are accomplished by hot-working. Accordingly, attention has been shifted to the development of methods for the attainment of substantial improvements in the graphite matrix, and the results obtained in hot-working graphite containing liquid carbide additives have been presented in Section VIII of this report.

REFERENCE

1. White, J. L., and J. M. Pontelandolfo, "Hot-Worked Graphite-Matrix Fuel Bodies (U);" General Atomic Report GA-5882 (C/RD), January, 1965.